

**Microheterogeneous Solid Polymer Electrolyte
(SPE) membranes for electrocatalysis**

by

WYNOMA CHANTAL MICHAELS



Dissertation presented for the degree of
Doctor of Philosophy (Polymer Science)

at the

University of Stellenbosch

Promoter: **Dr D.G. Bessarabov**
Co-promoter: **Prof. R.D. Sanderson**

Stellenbosch
March 2002

DECLARATION

I, the undersigned hereby declare that the work contained in this dissertation is my own original work and has not previously in its entirety or in part been submitted at any university for a degree.

Signature

Date

Abstract

The deposition of platinum catalyst on cation-exchange membranes was achieved by a counter diffusion deposition method known as the Takenaka-Torikai method. The morphology of the platinum catalyst on the membranes were controlled by varying the conditions of the platinum deposition process, such as, temperature, type of reducing agent and concentration of the platinic acid solution. The effect of the sonication of platinic acid solution and the pre-treatment of membranes on the morphology of a platinum catalyst was also investigated.

Platinum loading on cation-exchange membranes was determined by UV spectrophotometric and gravimetric analyses. Suitable conditions for the quantitative determination of the platinum loading on membranes by UV spectrophotometric analysis was established through the development of a protocol.

Membranes were characterised using different techniques such as, Atomic Force Microscopy (AFM), Scanning Electron Microscopy (SEM), Infrared spectrometry (IR), Dielectric analysis (DEA) and Brunauer Emmett Teller adsorption (BET).

The roughness profile of a platinum catalyst embedded on a membrane was explored by various statistical methods. The statistical analysis of various data sets for a surface of a platinum-containing membrane was investigated using the Hurst exponent.

The effect of surface modification of membranes on the deposition process, as well as the morphology of the platinum catalyst, was investigated. Membranes were modified with ethylene diamine (EDA) and cetyltrimethylammonium bromide surfactant. Modification of membranes with cetyltrimethylammonium bromide surfactant resulted in a unique textured platinum catalyst.

The electrochemical “switching” phenomenon was investigated for EDA-modified membranes and EDA-modified membranes embedded with platinum catalyst. The “switching” phenomenon was observed in *i*-V cyclic curves, which were obtained by galvanodynamic measurements.

The application of electrocatalytic membrane systems in the anodic oxidation of water was investigated by electrochemical techniques such as galvanostatic and cyclic voltammetric measurements.

Opsomming

Die deponering van 'n platinum katalis op kation-uitruil membrane is suksesvol gedoen d.m.v. die Takenaka-Torikai metode. Die morfologie van die platinum katalis op die membrane is gekontroleer deur variasie van die kondisies van die platinum deponeringsproses, bv. temperatuur, tipe reduseermiddel gebruik en konsentrasie van die platiensuuroplossing, asook die ultrasonifikasie van die platiensuuroplossing en voorafbehandeling van die membrane.

UV spektrofotometriese asook gravimetriese analitiese metodes is gebruik om die platynumlading op kation-uitruil membrane te bepaal. Geskikte kondisies vir die kwantitatiewe bepaling van die platynumlading op membrane d.m.v. UV spektrofotometriese analise is ontwikkel deur die skep van 'n protokol.

Membrane is gekarakteriseer d.m.v. die volgende tegnieke: Atoomkrag Mikroskopie, Skanderingselektron Mikroskopie, Infrarooi Spektrometrie, di-elektriese analise en Brunauer Emmett Teller adsorpsie.

Die skurfheidsprofiel van 'n platinum katalis op 'n membraan is ondersoek deur gebruik te maak van verskeie statistiese metodes. Statistiese analises van verskeie data stelsels van 'n platinum-bevattende membraan is ondersoek deur gebruik te maak van die Hurst eksponent.

Die effek van oppervlakmodifikasie op membrane sowel as die deponeringsproses en morfologie van die platinum katalis is ondersoek deur die modifikasie van membrane met etileen diamien (EDA) en setieltrimetielammonium bromied as versepingsmiddel

Die elektrochemiese omswaai van EDA-gemodifiseerde membrane sowel as gemodifiseerde platinum bevattende membrane is ondersoek d.m.v. galvanodinamiese metings.

Die gebruik van elektro-katalitiese membraansisteme in die anodiese oksidasie van water is ondersoek deur gebruik te maak van elektrochemiese tegnieke, bv. galvanostatiese en sikliese voltammetriese metings.

*The endless cycle of idea and action,
Endless invention, endless experiment,
Brings knowledge of motion, but not of stillness;
Knowledge of speech, but not of silence;
Knowledge of words, and ignorance of the Word.
All our knowledge brings us nearer to our ignorance,
All our ignorance brings us nearer to death,
But nearness to death no nearer to God.
Where is the Life we have lost in living?
Where is the wisdom we have lost in knowledge?
Where is the knowledge we have lost in information?*

T.S. Elliot

Acknowledgements

Dr. Dmitri Bessarabov for teaching me so much about Science, discipline, dedication and hard work. Thank you for your patience and continual understanding throughout this study. It is a privilege to work with an academic of your stature.

Prof. R.D. Sanderson for believing in me when others doubted my ability. Your continuous support, encouragement and concern have been tremendous.

Dr. Yu. M. Popkov for assistance with membrane preparation. It was a privilege to work with you.

Dr. Margie Hurndall for ensuring that the language of this thesis is readable. Also, for encouraging and assisting me through some of the darkest times in my journey through this study.

Jerry Vermeulen, Sue Marais and Ms. M. Waldron for use of DEA, AFM and SEM, respectively.

Aneli Fourie, Erinda Cooper and Johan Bonthuys for all their assistance.

The **Water Research Commission** and the **NRF** for financial support.

Pastors Glenn and Michelle Robertson, as well as **Pastors Nils and Maureen Hinrichsen**, for their love and support.

Dad and Mom for your endless sacrifices.

LIST OF CONTENTS

	Page
<u>Abstract</u>	iii
<u>Opsomming</u>	iv
<u>Acknowledgements</u>	vi
<u>List of contents</u>	xx
<u>List of figures</u>	xl
<u>List of tables</u>	1
<u>Introduction and objectives</u>	
 Chapter 1	 10
<u>1. Solid polymer electrolyte-based membrane catalytic systems</u>	10
1.1. Solid polymer electrolytes	11
1.1.1. Polymers in which nitrogen acts as a mediator for proton conduction	12
1.1.2. Organically modified ceramics-type polymers	12
1.1.3. Sulphonated ion-conducting polymers	15
1.2. Perfluorinated carbon chain polymers	15
1.3. Nafion as SPE material	15
1.3.1. Chemical structure	18
1.3.2. Properties	19
1.3.3. Applications	19
1.3.3.1. Chloralkali cells	22
1.3.3.2. Chromic acid regeneration	22
1.3.3.3. Synthesis of dinitrogen pentoxide	23
1.3.4. Advantages and disadvantages of using Nafion as a SPE	24
1.4. Techniques for deposition of platinum catalyst on Nafion membranes	24
1.4.1. Mechanical deposition	25
1.4.2. Electroless deposition	25
1.4.2.1. Counter diffusion deposition (Takenaka-Torikai method)	27
1.4.2.2. Impregnation reduction deposition (Fedkiw and Her method)	27
1.4.3. General mechanisms of chemical deposition reactions	27

1.4.3.2. Unified mechanism of electroless deposition	28
1.5. Electrocatalytic syntheses using solid polymer electrolyte (SPE)-based membrane catalytic systems	29
1.5.1. Advantages of using SPE in catalytic membrane systems	29
1.5.2. Generation of hydrogen and oxygen	29
1.5.2.1. Examples of recent industrial applications	30
1.5.3. Fuel cell technology	30
1.5.3.1. Examples of recent industrial applications	31
1.5.4. Generation of ozone	31
1.5.4.1. Examples of recent industrial applications	32
1.5.5. Separation of isotopes: hydrogen and deuterium	33
1.5.6. Water treatment using SPE membrane electrocatalytic systems	33
1.5.7. Hydrogen absorber	33
1.5.8. Electroinduced membrane gas separation	34
1.5.9. Oxidation of cyclohexanol to cyclohexanone	34
1.5.10. Electrochemical hydrogenation of olefinic double bonds	35
1.5.11. Electrochemical coupling of SPE-based water electrolysis and benzene hydrogenation	36
1.5.12. Methoxylation of furane	39
1.5.13. Alkoxylation of N-alkyl-amides	39
1.5.14. Oxidation of alcohols	40
1.5.15. Electrochemical reduction of benzaldehyde	41
1.6. Current trends in research using SPE-based membrane catalytic systems	41
1.6.1. Methods to optimise the morphology of platinum catalyst	42
1.6.2. Methods to optimise the chemical structure of the platinum catalyst	43
1.7. Chemical modification of cation-exchange membranes	45
1.8. Conclusions	46
References	

Chapter 2

<u>2. Preparation of platinum-containing perfluorinated cation-exchange membranes: experimental procedure for non-modified membranes</u>	53
2.1. Introduction	53

2.2. Materials	53
2.3. Hydrolysis of flat sheet cation-exchange membranes	54
2.3.1. Hydrolysis of cation-exchange membranes in 6N NaOH solution	54
2.3.2. Hydrolysis of cation-exchange membranes in a solution of 6N NaOH (70 vol. %) and MeOH (30 vol. %)	54
2.3.3. Conversion of membranes to the H ⁺ -ionic form	54
2.4. Determination of the ion-exchange capacities of cation-exchange flat sheet membranes	55
2.4.1. Determination of the ion-exchange capacities of hydrolysed membranes	55
2.5. Chemical deposition of platinum on cation-exchange membranes	56
2.5.1. Pre-treatment of hydrolysed membranes	56
2.5.2. Preparation of “working” solutions for chemical deposition of platinum on membranes by counter diffusion (Takenaka-Torikai) method	57
2.5.3. Deposition of platinum catalyst on flat-sheet cation-exchange membranes by counter diffusion method	57
2.5.4. Chemical deposition of platinum catalyst on membranes at room temperature	58
2.5.5. Chemical deposition of platinum catalyst on membranes at 40 °C	58
2.5.5.1. Chemical deposition using 0.05M platonic acid solution	58
a. Chemical deposition using hydrazine	59
b. Chemical deposition using sodium borohydride	59
2.5.5.2. Chemical deposition using 0.03M platonic acid solution	59
a. Chemical deposition using sodium borohydride	59
2.5.6. Chemical deposition process with sonication of platonic acid solution	60
2.6. Conclusions	61
References	61

Chapter 3

<u>3. Quantitative determination of the platinum loading on cation-exchange membranes</u>	62
3.1. Development of a protocol for the quantitative determination of platinum loading on cation-exchange membranes by UV spectrophotometric	

analysis	62
3.1.1. Preparation of a tin chloride solution for quantitative analysis	65
3.1.2. Determination of platinum ions within solutions by UV spectrophotometric analysis: Time-drive spectrum	65
3.1.2.1. UV spectrophotometric analysis of solutions containing platinum ions without aqua regia	65
3.1.2.2. UV spectrophotometric analysis of solutions containing platinum ions with low concentration of aqua regia	66
3.1.2.3. UV spectrophotometric analysis of solutions containing platinum ions with high concentration of aqua regia	66
3.1.3. UV spectrophotometric results of solutions containing platinum ions	66
3.1.4. Discussion	70
3.1.5. Final remarks and recommendations	72
3.2. Quantitative determination of the platinum loading on cation-exchange membranes by UV spectrophotometric and gravimetric analyses	74
3.2.1. Preparation of standard solutions for UV spectrophotometric analysis	74
3.2.2. Determination of platinum loading on membranes by UV spectrophotometric analysis	75
3.2.2.1. Removal of platinum catalyst from platinum-containing membranes	75
3.2.2.2. Preparation of solutions containing platinum ions for UV spectrophotometric analysis	76
3.2.3. Determination of platinum loading on membranes by gravimetric method	76
3.2.4. Quantitative determination of the platinum embedded on cation- exchange membranes by the reduction of 0.05M platinic acid solution with sodium borohydride at 40 °C (see section 2.5.5.1.b)	76
3.2.4.1. Quantitative determination of the platinum loading on cation- exchange membranes by UV spectrophotometric analysis	76
3.2.4.2. Quantitative determination of the platinum loading on cation- exchange membranes by gravimetric analysis	78
3.2.5. Quantitative determination of the platinum embedded on cation- exchange membranes by the reduction of 0.03M platinic acid solution	

with sodium borohydride at 40 °C (see section 2.5.5.2.a)	80
3.2.5.1. Quantitative determination of the platinum loading on cation-exchange membranes by UV spectrophotometric analysis	80
3.2.5.2. Quantitative determination of the platinum loading on cation-exchange membranes by gravimetric analysis	82
3.2.6. Quantitative determination of the platinum embedded on cation-exchange membranes by the reduction of 0.05M platonic acid solution with hydrazine at 40 °C (see section 2.5.5.1.a)	83
3.2.6.1. Quantitative determination of the platinum loading on cation-exchange membranes by UV spectrophotometric analysis	83
3.2.6.2. Quantitative determination of the platinum loading on cation-exchange membranes by gravimetric analysis	85
3.2.7. Quantitative determination of the platinum embedded on pre-treated cation-exchange membranes by the reduction of 0.05M platonic acid solution with hydrazine at room temperature	87
3.2.7.1. Quantitative determination of the platinum loading on cation-exchange membranes by UV spectrophotometric analysis	87
3.2.7.2. Quantitative determination of the platinum loading on cation-exchange membranes by gravimetric analysis	88
3.2.8. Discussion	89
3.3. Conclusions	93
References	94

Chapter 4

<u>4. Characterisation of electrocatalytic solid polymer electrolyte membranes</u>	96
4.1. Characterisation of the morphology of the platinum catalyst embedded on the cation-exchange membrane by Atomic Force Microscopy (AFM)	96
4.1.1. Surface roughness analysis of platinum catalyst embedded on cation-exchange membranes by the reduction of platonic acid solution at 40 °C	99
4.1.1.1. AFM imaging of membranes embedded with platinum catalyst by the reduction of 0.05M platonic acid solution with hydrazine at 40 °C.	99

4.1.1.2. AFM imaging of membranes embedded with platinum catalyst by reduction of 0.03M platinic acid solution with hydrazine at 40 °C	114
4.1.1.3. AFM imaging of membranes embedded with platinum catalyst by the reduction of 0.05M platinic acid solution with sodium borohydride at 40 °C.	121
4.1.1.4. AFM imaging of membranes embedded with platinum catalyst by the reduction of 0.03M platinic acid solution with sodium borohydride at 40 °C.	131
4.1.2. Surface roughness analysis of platinum catalyst embedded on cation-exchange membranes by the reduction of platinic acid solution with hydrazine at room temperature	143
4.1.3. Surface roughness analysis of platinum catalyst embedded on pre-treated cation-exchange membranes by the reduction of platinic acid solution with hydrazine at room temperature	144
4.1.4. Final remarks	150
4.2. Characterisation with scanning electron microscopy (SEM) of the surface profile of the platinum catalyst embedded on a cation-exchange membrane	152
4.2.1. Surface profile analysis of the platinum catalyst embedded on cation-exchange membranes by the reduction of platinic acid solution at 40 °C	153
4.2.1.1. SEM imaging of membranes embedded with platinum catalyst by the reduction of 0.05M platinic acid solution with hydrazine at 40 °C	153
4.2.1.2. SEM imaging of membranes embedded with platinum catalyst by the reduction of the sonicated 0.03M platinic acid solution with hydrazine at 40 °C	158
4.2.1.3. SEM imaging of membranes embedded with platinum catalyst by the reduction of 0.05M platinic acid solution with sodium borohydride at 40 °C	161
4.2.1.4. SEM imaging of membranes embedded with platinum catalyst by the reduction of 0.03M platinic acid solution with sodium borohydride at 40 °C	166
4.2.2. Surface roughness analysis of platinum catalyst embedded on cation-	

exchange membranes by the reduction of 0.05M platonic acid solution with hydrazine at room temperature	171
4.2.3. Surface profile analysis of the platinum catalyst embedded on pre-treated cation-exchange membranes by the reduction of 0.05M platonic acid solution with hydrazine at room temperature	172
4.2.4. Final remarks	175
4.3. Porosity determination of cation-exchange membranes by BET analysis	178
4.3.1. Preparation of membranes for characterisation by BET analysis	179
4.3.1.1. Hydrolysis of cation-exchange membranes	179
4.3.1.2. Pre-treatment of hydrolysed membranes	179
4.3.1.3. Chemical deposition of platinum catalyst onto membranes at room temperature	179
4.3.2. Results of the BET analysis of cation-exchange membranes	179
4.3.3. Final remarks	181
4.4. Conclusion	182
References	183

Chapter 5

<u>5. Surface modification of flat sheet cation-exchange membranes</u>	184
5.1. Chemical modification of the surface of a cation-exchange membrane with ethylene diamine (EDA)	184
5.1.1. Modification of cation-exchange membranes with EDA	185
5.1.1.1. Modification of both sides of a non-hydrolysed membrane with ethylene diamine (EDA)	185
5.1.1.2. Modification of one side of a non-hydrolysed membrane with ethylene diamine (EDA)	186
5.1.2. Deposition of platinum catalyst on membranes modified with EDA	186
5.1.2.1. Hydrolysis of membranes modified with EDA	186
5.1.2.2. Chemical deposition of platinum on membranes modified with EDA	186
5.1.2.3. Deposition of platinum on a membrane modified with EDA for 20 seconds	187
5.1.2.4. Deposition of platinum on a membrane modified with EDA for 45	

seconds	187
5.1.2.5. Deposition of platinum on a membrane modified with EDA for 1 minute	187
5.1.2.6. Deposition of platinum on a membrane modified with EDA for 1 minute 25 seconds	187
5.1.2.7. Deposition of platinum on a membrane modified with EDA for 2 minutes	187
5.1.3. SEM characterisation of membranes modified on one-side with EDA with an embedded platinum catalyst	188
5.1.4. Infra-red spectrometry characterisation of membranes modified with ethylene diamine	189
5.1.4.1. IR characterisation of unmodified membranes	189
5.1.4.2. IR characterisation of membranes modified with EDA	189
5.1.4.3. IR characterisation of membranes modified with EDA for 5 days	190
5.1.4.4. Discussion	191
5.1.5. Characterisation of membranes modified with EDA by dielectric analysis	193
5.1.5.1. Tan δ of a membrane modified with EDA	193
5.1.5.2. Loss factor at frequency of 60 Hz for membranes modified on one-side with EDA	193
5.1.5.3. DEA of the loss factor at high frequency of 100 kHz for membranes modified on one-side with EDA	194
5.1.5.4. Discussion	195
5.1.6. Resistance measurements of cation-exchange membranes modified with EDA	196
5.1.6.1. Electromembrane cell for resistance measurements of membranes modified with EDA	196
5.1.6.2. Characterisation of membranes modified with EDA by resistance measurements	196
5.1.6.3. Discussion	199
5.1.7. The sorption of water by cation-exchange membranes modified with ethylene diamine	201
5.1.7.1. Preparation of membranes modified with ethylene diamine	201

5.1.7.2. Results of the sorption of water by modified membranes	201
5.1.7.3. Discussion	202
5.1.8. Final remarks	203
5.2. Development of unique textured platinum particles by modification of the surface of the membrane	204
5.2.1. Surface modification of flat-sheet cation-exchange membranes with surfactant	204
5.2.2. Chemical deposition of platinum catalyst onto cation exchange membranes modified with surfactant	205
5.2.3. Characterisation of platinum catalyst deposited on surfactant-treated membranes by Atomic Force Microscopy (AFM)	205
5.2.3.1. AFM imaging of platinum particles on the surface of the membrane modified with 1% CH ₃ (CH ₂) ₁₅ N(CH ₃) ₃ Br surfactant	205
5.2.3.2. Discussion	209
5.2.4. Characterisation of the modification of membranes with surfactant by infrared spectrometry	210
5.2.4.1. Preparation of cation-exchange membranes for modification with surfactant	210
5.2.4.2. Removal of surfactant from modified membranes with base solution by ion-exchange	210
5.2.4.3. Removal of surfactant from modified membranes with acid solution by ion-exchange	210
5.2.4.4. Characterisation of membranes modified with surfactant by IR spectrometry	210
5.2.4.5. IR spectrometry of the removal of surfactant from modified membranes with sodium hydroxide by ion-exchange process	211
5.2.4.6. IR spectrometry of the removal of surfactant from modified membranes with nitric acid by ion-exchange process	213
5.2.4.7. Discussion	213
5.2.5. The effect of electrical resistance on surfactant-treated cation-exchange membranes	214
5.2.5.1. Preparation of membranes for electrical resistance measurements in electromembrane cell	214

5.2.5.2. Electrical resistance measurements of surfactant-treated membranes	215
5.2.5.3. Discussion	219
5.2.6. The sorption of water by cation-exchange membranes modified with surfactant	220
5.2.6.1. Preparation of membranes modified with surfactant	220
5.2.6.2. Results of the sorption of water by modified membranes	220
5.2.6.3. Discussion	221
5.2.7. Final remarks	221
5.3. Conclusion	224
References	225

Chapter 6

6. Galvanodynamic study of the electrochemical switching effect in

perfluorinated cation-exchange membranes modified with ethylene

diamine

	228
6.1. Introduction	228
6.2. Switching effect in modified perfluorinated membranes	228
6.3. Galvanodynamic characterisation of modified membranes	229
6.3.1. Galvanodynamic characterisation of membranes modified on one side with EDA	229
6.3.2. Results of galvanodynamic cycling of aminated membranes without platinum particles	230
6.3.2.1. Unmodified hydrolysed membranes without platinum catalyst	230
6.3.2.2. Membranes modified with EDA for 85 seconds without platinum catalyst	231
6.3.2.3. Membranes modified for 85 and 120 seconds with embedded platinum catalyst	233
6.4. Discussion	234
6.5. Conclusions	238
References	239

Chapter 7

<u>7. Anodic oxidation of water by electrocatalysis using electrocatalytic membrane system</u>	241
7.1. Theory of water electrolysis in a electrocatalytic cell	241
7.1.1. Determination of cell potential of hydrolysed membranes without platinum catalyst by galvanostatic measurements	243
7.1.1.1. Experimental set-up for galvanostatic measurements	243
7.1.2. Determination of the effect of temperature on the anodic oxidation of water by galvanostatic measurements	244
7.1.2.1. Preparation of platinum-containing membranes for use in anodic oxidation of water	244
7.1.2.2. Galvanostatic experimental conditions for anodic oxidation of water	245
7.1.2.3. Results of the anodic oxidation of water with platinum-containing membranes	245
7.1.3. Final remarks	246
7.2. Development and validation of a method to study electrocatalytic reactions on a platinised membrane	248
7.2.1. Cyclic voltammetry of the anodic oxidation of water on flat platinum electrodes: spatial separation of the reference electrode from the working electrode	248
7.2.2. Final remarks	249
7.2.3. Characterisation of water electrolysis at different temperatures by cyclic voltammetry	250
7.2.4. Final remarks	253
7.3. Conclusion	253
References	254

Chapter 8

<u>8. Quantification of Atomic Force Microscopy images of membranes embedded with platinum catalyst by statistical method</u>	255
8.1. Introduction	255
8.2. Regular and irregular solid surfaces	256

8.3. Development of irregular surfaces	256
8.4. Surface growth models	257
8.5. Experimental methods for the characterisation of irregular surfaces	257
8.6. Different statistical methods for surface roughness characterisation	258
8.6.1. Hurst exponent and its significance in the statistical analysis of various data sets	258
8.6.2. Fractal description of surface disorders	262
8.6.3. Power spectrum	264
8.6.4. Variograms	266
8.6.5. Wavelets	268
8.6.5.1. Description of Benoit algorithm for calculation of Hurst exponent	269
8.6.6. Standard roughness average (R_a)	269
8.6.7. Root-mean-square surface roughness (R_{rms})	270
8.7. Quantification of the surface roughness profile of platinum-containing membranes	270
8.7.1. Protocol for the determination of the roughness profile of a platinum-containing membrane	270
8.7.2. Results of surface roughness quantification of platinum-containing membranes	271
8.8. Discussion	276
8.9. Conclusions	278
References	279

Chapter 9

<u>9. Considerations for future research into the use of solid polymer electrocatalytic membrane systems</u>	282
9.1. Electrocatalytic immobilised phosphoric liquid membranes (ILM)	282
9.1.1. Wacker-type catalytic systems	283
9.1.2. Selective hydrogenation of nitric oxide	284
9.1.3. Partial oxidation of light alkanes	285
9.1.4. Partial oxidation of olefins	287
9.1.5. Epoxidation of olefins during water electrolysis	288
9.2. Further application of electrocatalytic membrane systems	290

9.3. Binary catalyst systems	291
9.4. Conclusions	291
References	292

<u>Conclusions</u>	294
---------------------------	-----

	Appendix A
List of publications	298

	Appendix B
List of scientific communications	299

List of Figures

Chapter 1

Figure 1.1. *Proposed cluster-network model for Nafion perfluorinated membranes (Gierke and Hsu, 1982).*

Figure 1.2. *Schematic representation of the phase inversion of Nafion (Du Pont information release).*

Figure 1.3. *Schematic representation of the synthesis of dinitrogen pentoxide with SPE-based membrane technology (Scott and Hughes, 1996).*

Figure 1.4. *The principle of metal deposition using counter diffusion method, in which one surface of the membrane is in contact with an anionic metal ion solution, while the other is in contact with a reducing agent (Enea, 1995).*

Figure 1.5. *Catalytic activities of metals during anodic oxidation of different reducing agents listed in decreasing order of catalytic activity (Ohno et al., 1985).*

Figure 1.6. *Schematic representation of Nafion embedded with a catalyst for the electrolysis of water (Bessarabov, 1998).*

Figure 1.7. *Schematic representation of the production of ozone using SPE technology (www.lynnotech.com/licensing/ozone/index.shtml).*

Figure 1.8. *The oxidation of cyclohexanol to cyclohexanone using platinum-SPE in the presence of mediators (Ogumi et al., 1985).*

Figure 1.9. *The electrochemical hydrogenation of olefinic double bonds, without the use of supporting electrolytes, can be achieved with a cationic membrane with electrocatalytic metal electrodes on each side of the membrane (Ogumi et al., 1981).*

Figure 1.10. *Schematic model of the electrochemical hydrogenation of olefinic compounds on a SPE composite (Ogumi et al., 1981).*

Figure 1.11. *Hydrogenation of benzene by the electrolysis of water, using solid polymer electrolyte (Itoh et al., 2000).*

Figure 1.12. *Proposed reaction of the methoxylation of furane using a SPE (Behr et al., 1997).*

Figure 1.13. *Several alkoxylation reactions of N-alkyl-amides using Nafion cation-exchange membranes in a non-aqueous medium (Jörissen, 1996).*

Figure 1.14. *An SPE cell for the anodic oxidation of alcohol using a cation-exchange membrane (Jörissen, 1996).*

Chapter 2

Figure 2.1. Schematic representation of the determination of the ion-exchange capacity of a cation-exchange membrane.

Figure 2.2. Membrane holder and bath used for deposition of thin layer of platinum on membrane. 1. Chamber to hold flat membranes; 2. Ion-exchange membrane; 3. Bath containing solution of reducing agent; 4. Magnetic stirrer; 5. Solution of platinic acid.

Figure 2.3. Membrane holder and bath used for deposition of thin layer of platinum on membrane with the sonication of the platinic acid solution. 1. Chamber to hold flat membranes; 2. Ion-exchange membrane; 3. Bath containing solution of reducing agent; 4. Magnetic stirrer; 5. Solution of platinic acid and 6. Heat Systems Ultrasonics Inc., model H-I 50-4 sonicator.

Chapter 3

Figure 3.1. Typical UV absorption spectrum with peaks at 403 nm and 310 nm of a solution containing 0.5 ml 0.5M platinic acid solution, 2 ml aqua regia and 2 ml tin chloride solution.

Figure 3.2. UV absorption spectrum of a solution containing platinum ions without aqua regia after 180 min.

Figure 3.3. Time-drive spectrum of the absorbance of a solution containing platinum ions without aqua regia, over a time period of 1800 min at a wavelength of 402.23nm. It is seen that the first 150 min of the time-drive spectrum is considerably inconsistent.

Figure 3.4. UV absorption spectrum of a solution containing platinum ions with a low concentration of aqua regia after 180 min.

Figure 3.5. UV absorption spectrum of a solution containing platinum ions with a low concentration of aqua regia after 180 min between the wavelengths of 600 nm and 190 nm.

Figure 3.6. Time-drive spectrum for the absorbance of a solution containing platinum ions with a low concentration of aqua regia over a time period of 1425 min at a wavelength of 402.27 nm.

Figure 3.7. Time-drive spectrum for the absorbance of a solution containing platinum ions with a high concentration of aqua regia over a time period of 1800 min at a wavelength of 402.27 nm.

Figure 3.8. UV absorption spectrum of a solution containing platinum ions with a high concentration of aqua regia after 1800 min.

Figure 3.9. Time-drive spectrum at a wavelength of 402.27nm of platinum solutions without aqua regia (A), with a low concentration of aqua regia (B) and with a high concentration of aqua regia (C).

Figure 3.10. UV absorption spectrum of standard solutions containing platinum solution, SnCl_3^- and aqua regia of concentrations 1×10^{-5} (1), 2×10^{-5} (2), 4×10^{-5} (3) and 8×10^{-5} (4) mol/L.

Figure 3.11. Calibration curve of standard solutions containing platinum solution, SnCl_3^- and aqua regia of the concentrations 1×10^{-5} , 2×10^{-5} , 4×10^{-5} and 8×10^{-5} mol/L.

Figure 3.12. UV absorption spectrum of solutions containing platinum ions of unknown concentrations. The platinum catalyst was deposited by the reduction of 0.05M platinum acid solution with NaBH_4 . The total time of platinisation was 4.5(A), 6.5(B), 10.5(C), 12.5(D) and 16.5(E) minutes.

Figure 3.13. Plot of total platinum loading on membranes achieved by the reduction of 0.05M platinum acid solution with NaBH_4 for the total time of platinisation of 4.5, 6.5, 10.5, 12.5 and 16.5 minutes, as determined by gravimetric and spectrophotometric (spec) analysis.

Figure 3.14. UV absorption spectrum of solutions containing platinum ions of unknown concentrations. The platinum catalyst was deposited by the reduction of 0.03M platinum acid solution with NaBH_4 for the total time of platinisation of 4.5(A), 12.5(B), 16.5(C), 26.5(D) and 36.5(E) minutes.

Figure 3.15. Plot of total platinum loading on membranes achieved by the reduction of 0.03M platinum acid solution with NaBH_4 for the total time of platinisation of 4.5, 12.5, 16.5, 26.5 and 36.5 minutes, as determined by gravimetric and spectrophotometric (spec) analysis.

Figure 3.16. UV absorption spectrum of solutions containing platinum ions of unknown concentrations. The platinum catalyst was deposited by the reduction of 0.05M platinum acid solution with hydrazine. The total time of platinisation was 16.5(1), 12.5(2), 10.5(3), 8.5(4), 6.5(5) and 4.5(6) minutes.

Figure 3.17. Plot of total platinum loading on membranes achieved by the reduction of 0.05M platinum acid solution with N_2H_4 for the total time of platinisation of 4.5, 6.5, 8.5, 10.5, 12.5 and 16.5 minutes, as determined by gravimetric and spectrophotometric (spec) analysis.

Figure 3.18. UV absorption spectrum of solutions containing platinum ions of unknown concentrations. The platinum catalyst was deposited on membranes (A) pre-treated with $\text{H}_2\text{O}/\text{MeOH}$ and (B) pre-treated with boiling water.

Figure 3.19. Results of UV spectrophotometric analysis of the total platinum loading on a membrane when (A) 0.05M platonic acid solution was reduced by NaBH₄, (B) 0.05M platonic acid solution was reduced by N₂H₄ and (C) 0.03M platonic acid solution was reduced by NaBH₄.

Figure 3.20. Plot of the total platinum loading on membranes achieved with the reduction of 0.05M platonic acid solution by hydrazine (N₂H₄) and sodium borohydride (NaBH₄), as determined by UV spectrophotometric analysis.

Chapter 4

Figure 4.1. AFM surface image (20µm×20µm) of a cation-exchange membrane embedded with platinum catalyst by the reduction of 0.05M platonic acid solution with hydrazine for 3.5 minutes at 40 °C.

Figure 4.2. Three-dimensional AFM surface image (20µm×20µm) of a cation-exchange membrane embedded with platinum catalyst by the reduction of 0.05M platonic acid solution with hydrazine for 3.5 minutes at 40 °C.

Figure 4.3. Line analysis plot of the surface roughness of a cation-exchange membrane embedded with platinum catalyst by the reduction of 0.05M platonic acid solution with hydrazine for 3.5 minutes at 40 °C.

Figure 4.4. AFM surface image (130µm×130µm) of a cation-exchange membrane embedded with platinum catalyst by the reduction of 0.05M platonic acid solution with hydrazine for 3.5 minutes at 40 °C.

Figure 4.5. Three-dimensional AFM surface image (130µm×130µm) of a cation-exchange membrane embedded with platinum catalyst by the reduction of 0.05M platonic acid solution with hydrazine for 3.5 minutes at 40 °C.

Figure 4.6. Line analysis plot of the surface roughness of a cation-exchange membrane embedded with platinum catalyst by the reduction of 0.05M platonic acid solution with hydrazine for 3.5 minutes at 40 °C.

Figure 4.7. AFM surface image (20µm×20µm) of a cation-exchange membrane embedded with platinum catalyst by the reduction of 0.05M platonic acid solution with hydrazine for 5.5 minutes at 40 °C.

Figure 4.8. Three-dimensional AFM surface image (20µm×20µm) of a cation-exchange membrane embedded with platinum catalyst by the reduction of 0.05M platonic acid solution with hydrazine for 5.5 minutes at 40 °C.

Figure 4.9. *Line analysis plot of the surface roughness of a cation-exchange membrane embedded with platinum catalyst by the reduction of 0.05M platinic acid solution with hydrazine for 5.5 minutes at 40 °C.*

Figure 4.10. *AFM surface image (130 μ m \times 130 μ m) of a cation-exchange membrane embedded with platinum catalyst by the reduction of 0.05M platinic acid solution with hydrazine for 5.5 minutes at 40 °C.*

Figure 4.11. *Three-dimensional AFM surface image (130 μ m \times 130 μ m) of a cation-exchange membrane embedded with platinum catalyst by the reduction of 0.05M platinic acid solution with hydrazine for 5.5 minutes at 40 °C.*

Figure 4.12. *Line analysis plot of the surface roughness of a cation-exchange membrane embedded with platinum catalyst by the reduction of 0.05M platinic acid solution with hydrazine for 5.5 minutes at 40 °C.*

Figure 4.13. *AFM surface image (20 μ m \times 20 μ m) of a cation-exchange membrane embedded with platinum catalyst by the reduction of 0.05M platinic acid solution with hydrazine for 7.5 minutes at 40 °C.*

Figure 4.14. *Three-dimensional AFM surface image (20 μ m \times 20 μ m) of a cation-exchange membrane embedded with platinum catalyst by the reduction of 0.05M platinic acid solution with hydrazine for 7.5 minutes at 40 °C.*

Figure 4.15. *Line analysis plot of the surface roughness of a cation-exchange membrane embedded with platinum by the reduction of 0.05M platinic acid solution with hydrazine for 7.5 minutes at 40 °C.*

Figure 4.16. *AFM surface image (130 μ m \times 130 μ m) of a cation-exchange membrane embedded with platinum catalyst by the reduction of 0.05M platinic acid solution with hydrazine for 7.5 minutes at 40 °C.*

Figure 4.17. *Three-dimensional AFM surface image (130 μ m \times 130 μ m) of a cation-exchange membrane embedded with platinum catalyst by the reduction of 0.05M platinic acid solution with hydrazine for 7.5 minutes at 40 °C.*

Figure 4.18. *Line analysis plot of the surface roughness of a cation-exchange membrane embedded with platinum catalyst by the reduction of 0.05M platinic acid solution with hydrazine for 7.5 minutes at 40 °C.*

Figure 4.19. *AFM surface image (20 μ m \times 20 μ m) of a cation-exchange membrane embedded with platinum catalyst by the reduction of 0.05M platinic acid solution with hydrazine for 9.5 minutes at 40 °C.*

Figure 4.20. *Three-dimensional AFM surface image (20 μ m \times 20 μ m) of a cation-exchange membrane embedded with platinum catalyst by the reduction of 0.05M platinic acid solution with hydrazine for 9.5 minutes at 40 °C.*

Figure 4.21. *Line analysis plot of the surface roughness of a cation-exchange membrane embedded with platinum catalyst by the reduction of 0.05M platinic acid solution with hydrazine for 9.5 minutes at 40 °C.*

Figure 4.22. *AFM surface image (20 μ m \times 20 μ m) of a cation-exchange membrane embedded with a platinum catalyst by the reduction of 0.05M platinic acid solution with hydrazine for 11.5 minutes at 40 °C.*

Figure 4.23. *Three-dimensional AFM surface image (20 μ m \times 20 μ m) of a cation-exchange membrane embedded with platinum catalyst by the reduction of 0.05M platinic acid solution with hydrazine for 11.5 minutes at 40 °C.*

Figure 4.24. *Line analysis plot of the surface roughness of a cation-exchange membrane embedded with platinum catalyst by the reduction of 0.05M platinic acid solution with hydrazine for 11.5 minutes at 40 °C.*

Figure 4.25. *AFM surface image (20 μ m \times 20 μ m) of a cation-exchange membrane embedded with platinum by the reduction of 0.05M platinic acid solution with hydrazine for 15.5 minutes at 40 °C.*

Figure 4.26. *Three-dimensional AFM surface image (20 μ m \times 20 μ m) of a cation-exchange membrane embedded with platinum catalyst by the reduction of 0.05M platinic acid solution with hydrazine for 15.5 minutes at 40 °C.*

Figure 4.27. *Line analysis plot of the surface roughness of a cation-exchange membrane embedded with platinum catalyst by the reduction of 0.05M platinic acid solution with hydrazine for 15.5 minutes at 40 °C.*

Figure 4.28. *AFM surface image (20 μ m \times 20 μ m) of a cation-exchange membrane embedded with platinum catalyst by the reduction of 0.03M platinic acid solution with hydrazine for 7 minutes at 40 °C.*

Figure 4.29. *Three-dimensional AFM surface image (20 μ m \times 20 μ m) of a cation-exchange membrane embedded with platinum catalyst by the reduction of 0.03M platinic acid solution with hydrazine for 7 minutes at 40 °C.*

Figure 4.30. *Line analysis plot of the surface roughness of a cation-exchange membrane embedded with platinum catalyst by the reduction of 0.03M platinic acid solution with hydrazine for 7 minutes at 40 °C.*

Figure 4.31. *AFM surface image (20 μ m \times 20 μ m) of a cation-exchange membrane embedded with platinum by the reduction of 0.03M platonic acid with hydrazine for 7 minutes at 40 °C, while pulses between 20 and 40 kHz were rippled through the platonic acid solution.*

Figure 4.32. *Three-dimensional AFM surface image (20 μ m \times 20 μ m) of a cation-exchange membrane embedded with platinum catalyst by the reduction of 0.03M platonic acid solution with hydrazine for 7 minutes at 40 °C, while pulses between 20 and 40 kHz were rippled through the platonic acid solution.*

Figure 4.33. *Line analysis plot of the surface roughness of a cation-exchange membrane embedded with platinum catalyst by the reduction of 0.03M platonic acid solution with hydrazine for 7 minutes at 40 °C, while pulses between 20 and 40 kHz were rippled through the platonic acid solution.*

Figure 4.34. *AFM surface image (130 μ m \times 130 μ m) of a cation-exchange membrane embedded with platinum catalyst by the reduction of 0.03M platonic acid solution with hydrazine for 7 minutes at 40 °C, while pulses between 20 and 40 kHz were rippled through the platonic acid solution.*

Figure 4.35. *Three-dimensional AFM surface image (130 μ m \times 130 μ m) of a cation-exchange membrane embedded with platinum catalyst by the reduction of 0.03M platonic acid solution with hydrazine for 7 minutes at 40 °C, while pulses between 20 and 40 kHz were rippled through the platonic acid solution.*

Figure 4.36. *Line analysis plot of the surface roughness of a cation-exchange membrane embedded with platinum catalyst by the reduction of 0.03M platonic acid solution with hydrazine for 7 minutes at 40 °C, while pulses between 20 and 40 kHz were rippled through the platonic acid solution.*

Figure 4.37. *AFM surface image (130 μ m \times 130 μ m) of a cation-exchange membrane embedded with platinum by the reduction of 0.05M platonic acid solution with sodium borohydride for 3.5 minutes at 40 °C.*

Figure 4.38. *Three-dimensional AFM surface image (130 μ m \times 130 μ m) of a cation-exchange membrane embedded with platinum by the reduction of 0.05M platonic acid solution with sodium borohydride for 3.5 minutes at 40 °C.*

Figure 4.39. *Line analysis plot of the surface roughness of a cation-exchange membrane embedded with platinum by the reduction of 0.05M platonic acid solution with sodium borohydride for 3.5 minutes at 40 °C.*

Figure 4.40. *AFM surface image (130 μ m \times 130 μ m) of a cation-exchange membrane embedded with platinum catalyst by the reduction of 0.05M platonic acid with sodium borohydride for 5.5 minutes at 40 °C.*

Figure 4.41. *Three-dimensional AFM surface image (130 μ m \times 130 μ m) of a cation-exchange membrane embedded with platinum catalyst by the reduction of 0.05M platinic acid solution with sodium borohydride for 5.5 minutes at 40 °C.*

Figure 4.42. *Line analysis plot of the surface roughness of a cation-exchange membrane embedded with platinum catalyst by the reduction of 0.05M platinic acid solution with sodium borohydride for 5.5 minutes at 40 °C.*

Figure 4.43. *AFM surface image (130 μ m \times 130 μ m) of a cation-exchange membrane embedded with platinum catalyst by the reduction of 0.05M platinic acid solution with sodium borohydride for 7.5 minutes at 40 °C.*

Figure 4.44. *Three-dimensional AFM surface image (130 μ m \times 130 μ m) of a cation-exchange membrane embedded with platinum catalyst by the reduction of 0.05M platinic acid solution with sodium borohydride for 7.5 minutes at 40 °C.*

Figure 4.45. *Line analysis plot of the surface roughness of a cation-exchange membrane embedded with platinum catalyst by the reduction of 0.05M platinic acid solution with sodium borohydride for 7.5 minutes at 40 °C.*

Figure 4.46. *AFM surface image (130 μ m \times 130 μ m) of a cation-exchange membrane embedded with platinum catalyst by the reduction of 0.05M platinic acid solution with sodium borohydride for 9.5 minutes at 40 °C.*

Figure 4.47. *Three-dimensional AFM surface image (130 μ m \times 130 μ m) of a cation-exchange membrane embedded with platinum catalyst by the reduction of 0.05M platinic acid solution with sodium borohydride for 9.5 minutes at 40 °C.*

Figure 4.48. *Line analysis plot of the surface roughness of a cation-exchange membrane embedded with platinum by the reduction of 0.05M platinic acid solution with sodium borohydride for 9.5 minutes at 40 °C.*

Figure 4.49. *AFM surface image (130 μ m \times 130 μ m) of a cation-exchange membrane embedded with platinum by the reduction of 0.05M platinic acid solution with sodium borohydride for 12.5 minutes at 40 °C.*

Figure 4.50. *Three-dimensional AFM surface image (130 μ m \times 130 μ m) of a cation-exchange membrane embedded with platinum catalyst by the reduction of 0.05M platinic acid solution with sodium borohydride for 12.5 minutes at 40 °C.*

Figure 4.51. *Line analysis plot of the surface roughness of a cation-exchange membrane embedded with platinum catalyst by the reduction of 0.05M platinic acid solution with sodium borohydride for 12.5 minutes at 40 °C.*

Figure 4.52. *AFM surface image (130 μ m \times 130 μ m) of a cation-exchange membrane embedded with platinum catalyst by the reduction of 0.05M platinic acid solution with sodium borohydride for 15.5 minutes at 40 °C.*

Figure 4.53. *Three-dimensional AFM surface image (130 μ m \times 130 μ m) of a cation-exchange membrane embedded with platinum catalyst by the reduction of 0.05M platinic acid solution with sodium borohydride for 15.5 minutes at 40 °C.*

Figure 4.54. *Line analysis plot of the surface roughness of a cation-exchange membrane embedded with platinum catalyst by the reduction of 0.05M platinic acid solution with sodium borohydride for 15.5 minutes at 40 °C.*

Figure 4.55. *AFM surface image (20 μ m \times 20 μ m) of a cation-exchange membrane embedded with platinum catalyst by the reduction of 0.03M platinic acid solution with sodium borohydride for 3.5 minutes at 40 °C.*

Figure 4.56. *Three-dimensional AFM surface image (20 μ m \times 20 μ m) of a cation-exchange membrane embedded with platinum catalyst by the reduction of 0.03M platinic acid solution with sodium borohydride for 3.5 minutes at 40 °C.*

Figure 4.57. *Line analysis plot of the surface roughness of a cation-exchange membrane embedded with platinum catalyst by the reduction of 0.03M platinic acid solution with sodium borohydride for 3.5 minutes at 40 °C.*

Figure 4.58. *AFM surface image (130 μ m \times 130 μ m) of a cation-exchange membrane embedded with platinum catalyst by the reduction of 0.03M platinic acid solution with sodium borohydride for 3.5 minutes at 40 °C.*

Figure 4.59. *Three-dimensional AFM surface image (130 μ m \times 130 μ m) of a cation-exchange membrane embedded with platinum catalyst by the reduction of 0.03M platinic acid solution with sodium borohydride for 3.5 minutes at 40 °C.*

Figure 4.60. *Line analysis plot of the surface roughness of a cation-exchange membrane embedded with platinum catalyst by the reduction of 0.03M platinic acid solution with sodium borohydride for 3.5 minutes at 40 °C.*

Figure 4.61. *AFM surface image (20 μ m \times 20 μ m) of a cation-exchange membrane embedded with platinum catalyst by the reduction of 0.03M platinic acid solution with sodium borohydride for 11.5 minutes at 40 °C.*

Figure 4.62. *Three-dimensional AFM surface image (20 μ m \times 20 μ m) of a cation-exchange membrane embedded with platinum catalyst by the reduction of 0.03M platinic acid solution with sodium borohydride for 11.5 minutes at 40 °C.*

Figure 4.63. *Line analysis plot of the surface roughness of a cation-exchange membrane embedded with platinum catalyst by the reduction of 0.03M platinic acid solution with sodium borohydride for 11.5 minutes at 40 °C.*

Figure 4.64. *AFM surface image (130µm×130µm) of a cation-exchange membrane embedded with platinum catalyst by the reduction of 0.03M platinic acid solution with sodium borohydride for 11.5 minutes at 40 °C.*

Figure 4.65. *Three-dimensional AFM surface image (130µm×130µm) of a cation-exchange membrane embedded with platinum catalyst by the reduction of 0.03M platinic acid solution with sodium borohydride for 11.5 minutes at 40 °C.*

Figure 4.66. *Line analysis plot of the surface roughness of a cation-exchange membrane embedded with platinum by the reduction of 0.03M platinic acid solution with sodium borohydride for 11.5 minutes at 40 °C.*

Figure 4.67. *AFM surface image (130µm×130µm) of a cation-exchange membrane embedded with platinum catalyst by the reduction of 0.03M platinic acid solution with sodium borohydride for 15.5 minutes at 40 °C.*

Figure 4.68. *Three-dimensional AFM surface image (130µm×130µm) of a cation-exchange membrane embedded with platinum catalyst by the reduction of 0.03M platinic acid with sodium borohydride for 15.5 minutes at 40 °C.*

Figure 4.69. *Line analysis plot of the surface roughness of a cation-exchange membrane embedded with platinum catalyst by the reduction of 0.03M platinic acid solution with sodium borohydride for 15.5 minutes at 40 °C.*

Figure 4.70. *AFM surface image (130µm×130µm) of a cation-exchange membrane embedded with platinum catalyst by the reduction of 0.03M platinic acid solution with sodium borohydride for 25.5 minutes at 40 °C.*

Figure 4.71. *Three-dimensional AFM surface image (130µm×130µm) of a cation-exchange membrane embedded with platinum catalyst by the reduction of 0.03M platinic acid solution with sodium borohydride for 25.5 minutes at 40 °C.*

Figure 4.72. *Line analysis plot of the surface roughness of a cation-exchange membrane embedded with platinum catalyst by the reduction of 0.03M platinic acid solution with sodium borohydride for 25.5 minutes at 40 °C.*

Figure 4.73. *AFM surface image (130µm×130µm) of a cation-exchange membrane embedded with platinum catalyst by the reduction of 0.03M platinic acid solution with sodium borohydride for 35.5 minutes at 40 °C.*

Figure 4.74. *Three-dimensional AFM surface image (130 μ m \times 130 μ m) of a cation-exchange membrane embedded with platinum catalyst by the reduction of 0.03M platinic acid solution with sodium borohydride for 35.5 minutes at 40 °C.*

Figure 4.75. *Line analysis plot of the surface roughness of a cation-exchange membrane embedded with platinum by the reduction of 0.03M platinic acid with sodium borohydride for 35.5 minutes at 40 °C.*

Figure 4.76. *AFM surface image (20 μ m \times 20 μ m) of a cation-exchange membrane embedded with platinum by the reduction of 0.05M platinic acid solution with hydrazine for 10 minutes at room temperature.*

Figure 4.77. *Three-dimensional AFM image (20 μ m \times 20 μ m) of a cation-exchange membrane embedded with platinum by the reduction of 0.05M platinic acid solution with hydrazine for 10 minutes at room temperature.*

Figure 4.78. *Line analysis plot of the surface roughness of a cation-exchange membrane embedded with platinum by the reduction of 0.05M platinic acid solution with hydrazine for 10 minutes at room temperature.*

Figure 4.79. *AFM surface image (20 μ m \times 20 μ m) of a cation-exchange membrane embedded with platinum catalyst after membrane was pre-treated with a solution of H₂O (70 vol. %) and MeOH (30 vol. %) and hydrolysed with NaOH.*

Figure 4.80. *Three-dimensional AFM image (20 μ m \times 20 μ m) of a cation-exchange membrane embedded with platinum catalyst after membrane was pre-treated with a solution of H₂O (70 vol. %) and MeOH (30 vol. %) and hydrolysed with NaOH.*

Figure 4.81. *Line analysis plot of the surface roughness of a cation-exchange membrane embedded with platinum catalyst after membrane was pre-treated with a solution of H₂O (70 vol. %) and MeOH (30 vol. %) and hydrolysed with NaOH.*

Figure 4.82. *AFM surface image (20 μ m \times 20 μ m) of a cation-exchange membrane embedded with platinum catalyst after membrane was pre-treated with a solution of H₂O (70 vol. %) and MeOH (30 vol. %) and hydrolysed with a solution of NaOH (70 vol. %) and MeOH (30 vol. %).*

Figure 4.83. *Three-dimensional AFM image (20 μ m \times 20 μ m) of a cation-exchange membrane embedded with platinum catalyst after membrane was pre-treated with a solution of H₂O (70 vol. %) and MeOH (30 vol. %) and hydrolysed with a solution of NaOH (70 vol. %) and MeOH (30 vol. %).*

Figure 4.84. *Line analysis plot of the surface roughness of a cation-exchange membrane embedded with platinum catalyst after membrane was pre-treated with a solution of H₂O (70 vol. %) and MeOH (30 vol. %) and hydrolysed with a solution of NaOH (70 vol. %) and MeOH (30 vol. %).*

Figure 4.85. *AFM surface image (20 μ m \times 20 μ m) of a cation-exchange membrane embedded with platinum catalyst after membrane was pre-treated with H₂O and hydrolysed with a solution of NaOH (70 vol. %) and MeOH (30 vol. %).*

Figure 4.86. *Three-dimensional AFM image (20 μ m \times 20 μ m) of a cation-exchange membrane embedded with platinum catalyst after membrane was pre-treated with H₂O and hydrolysed with a solution of NaOH (70 vol. %) and MeOH (30 vol. %).*

Figure 4.87. *Line analysis plot of the surface roughness of a cation-exchange membrane embedded with platinum catalyst after membrane was pre-treated with H₂O and hydrolysed with a solution of NaOH (70 vol. %) and MeOH (30 vol. %).*

Figure 4.88. *SEM image (using a backscattering detector) of a cation-exchange membrane embedded with platinum catalyst by the reduction of 0.05M platonic acid solution with hydrazine for 3.5 minutes at 40 °C.*

Figure 4.89. *High-magnification SEM image (using a backscattering detector) of a cation-exchange membrane embedded with platinum catalyst by the reduction of 0.05M platonic acid solution with hydrazine for 3.5 minutes at 40 °C.*

Figure 4.90. *SEM image (using a backscattering detector) of a cation-exchange membrane embedded with platinum catalyst by the reduction of 0.05M platonic acid solution with hydrazine for 5.5 minutes at 40 °C.*

Figure 4.91. *SEM image (using a backscattering detector) of a cation-exchange membrane embedded with platinum catalyst by the reduction of 0.05M platonic acid solution with hydrazine for 7.5 minutes at 40 °C.*

Figure 4.92. *SEM image (using a backscattering detector) of a cation-exchange membrane embedded with platinum catalyst by the reduction of 0.05M platonic acid solution with hydrazine for 9.5 minutes at 40 °C.*

Figure 4.93. *High-magnification SEM image (using a backscattering detector) of a cation-exchange membrane embedded with platinum catalyst by the reduction of 0.05M platonic acid solution with hydrazine for 9.5 minutes at 40 °C.*

Figure 4.94. *SEM image (using a backscattering detector) of a cation-exchange membrane embedded with platinum by the reduction of 0.05M platonic acid solution with hydrazine for 11.5 minutes at 40 °C.*

Figure 4.95. *SEM image (using a backscattering detector) of a cation-exchange membrane embedded with platinum catalyst by the reduction of 0.05M platonic acid solution with hydrazine for 15.5 minutes at 40 °C.*

Figure 4.96. *High-magnification SEM image (using a backscattering detector) of a cation-exchange membrane embedded with platinum catalyst by the reduction of 0.05M platinic acid solution with hydrazine for 15.5 minutes at 40 °C.*

Figure 4.97. *SEM image of a cation-exchange membrane embedded with platinum catalyst by the reduction of 0.03M platinic acid solution with hydrazine for 7 minutes at 40 °C, while the platinic acid solution underwent sonication*

Figure 4.98. *High-magnification SEM image of a cation-exchange membrane embedded with platinum catalyst by the reduction of 0.03M platinic acid solution with hydrazine for 7 minutes at 40 °C, while the platinic acid solution underwent sonication*

Figure 4.99. *SEM image (using a backscattering detector) of a cation-exchange membrane embedded with platinum catalyst by the reduction of 0.03M platinic acid solution with hydrazine for 7 minutes at 40 °C.*

Figure 4.100. *High-magnification SEM image (using a backscattering detector) of a cation-exchange membrane embedded with platinum catalyst by the reduction of 0.03M platinic acid solution with hydrazine for 7 minutes at 40 °C.*

Figure 4.101. *SEM image (using a backscattering detector) of a cation-exchange membrane embedded with platinum catalyst by the reduction of 0.05M platinic acid solution with sodium borohydride for 3.5 minutes at 40 °C.*

Figure 4.102. *High-magnification SEM image (using a backscattering detector) of a cation-exchange membrane embedded with platinum catalyst by the reduction of 0.05M platinic acid solution with sodium borohydride for 3.5 minutes at 40 °C.*

Figure 4.103. *SEM image of a cation-exchange membrane (using a backscattering detector) embedded with platinum catalyst by the reduction of 0.05M platinic acid solution with sodium borohydride for 5.5 minutes at 40 °C.*

Figure 4.104. *SEM image (using a backscattering detector) of a cation-exchange membrane embedded with platinum catalyst by reduction of 0.05M platinic acid solution with sodium borohydride for 7.5 minutes at 40 °C.*

Figure 4.105. *SEM image (using a backscattering detector) of a cation-exchange membrane embedded with platinum by the reduction of 0.05M platinic acid solution with sodium borohydride for 9.5 minutes at 40 °C.*

Figure 4.106. *High-magnification SEM image (using a backscattering detector) of a cation-exchange membrane embedded with platinum catalyst by the reduction of 0.05M platinic acid solution with sodium borohydride for 9.5 minutes at 40 °C.*

Figure 4.107. SEM image (using a backscattering detector) of a cation-exchange membrane embedded with platinum catalyst by the reduction of 0.05M platonic acid solution with sodium borohydride for 11.5 minutes at 40 °C.

Figure 4.108. SEM image (using a backscattering detector) of a cation-exchange membrane embedded with platinum by the reduction of 0.05M platonic acid solution with sodium borohydride for 15.5 minutes at 40 °C.

Figure 4.109. High-magnification SEM image (using a backscattering detector) of a cation-exchange membrane embedded with platinum catalyst by the reduction of 0.05M platonic acid solution with sodium borohydride for 15.5 minutes at 40 °C.

Figure 4.110. SEM image (using a backscattering detector) of a cation-exchange membrane embedded with platinum catalyst by the reduction of 0.03M platonic acid solution with sodium borohydride for 3.5 minutes at 40 °C.

Figure 4.111. SEM image (using a backscattering detector) of a cation-exchange membrane embedded with platinum catalyst by the reduction of 0.03M platonic acid solution with sodium borohydride for 11.5 minutes at 40 °C.

Figure 4.112. SEM image (using a backscattering detector) of a cation-exchange membrane embedded with platinum catalyst by the reduction of 0.03M platonic acid solution with sodium borohydride for 15.5 minutes at 40 °C.

Figure 4.113. High-magnification SEM image (using a backscattering detector) of a cation-exchange membrane embedded with platinum catalyst by the reduction of 0.03M platonic acid solution with sodium borohydride for 15.5 minutes at 40 °C.

Figure 4.114. SEM image (using a backscattering detector) of a cation-exchange membrane embedded with platinum catalyst by the reduction of 0.03M platonic acid solution with sodium borohydride for 25.5 minutes at 40 °C.

Figure 4.115. High-magnification SEM image (using a backscattering detector) of a cation-exchange membrane embedded with platinum catalyst by the reduction of 0.03M platonic acid solution with sodium borohydride for 25.5 minutes at 40 °C.

Figure 4.116. SEM image (using a backscattering detector) of a cation-exchange membrane embedded with platinum catalyst by the reduction of 0.03M platonic acid solution with sodium borohydride for 35.5 minutes at 40 °C.

Figure 4.117. High-magnification SEM image (using a backscattering detector) of a cation-exchange membrane embedded with platinum catalyst by the reduction of 0.03M platonic acid solution with sodium borohydride for 35.5 minutes at 40 °C.

Figure 4.118. SEM image (using a backscattering detector) of the profile of the layer of platinum catalyst on a cation-exchange membrane

Figure 4.119. *High-magnification SEM image (using a backscattering detector) of the profile of the layer of platinum on a cation-exchange membrane*

Figure 4.120. *SEM image (using a backscattering detector) of the profile of the layer of platinum catalyst on a membrane hydrolysed with NaOH and pre-treated with a solution of H₂O (70 vol. %) and MeOH (30 vol. %).*

Figure 4.121. *High-magnification SEM image (using a backscattering detector) of the profile of the layer of platinum catalyst on a membrane hydrolysed with NaOH and pre-treated with a solution of H₂O (70 vol. %) and MeOH (30 vol. %)*

Figure 4.122. *SEM image (using a backscattering detector) of the profile of the layer of platinum catalyst on a membrane hydrolysed with a solution of NaOH (70 vol. %) and MeOH (30 vol. %) and pre-treated with a solution of H₂O (70 vol. %) and MeOH (30 vol. %).*

Figure 4.123. *High-magnification SEM image (using a backscattering detector) of the profile of the layer of platinum catalyst on a membrane hydrolysed with a solution of NaOH (70 vol. %) and MeOH (30 vol. %) and pre-treated with a solution of H₂O (70 vol. %) and MeOH (30 vol. %).*

Figure 4.124. *SEM image (using a backscattering detector) of the profile of the platinum catalyst on a cation-exchange membrane, which was hydrolysed with NaOH (70 vol. %) and MeOH (30 vol. %) and pre-treated with H₂O.*

Figure 4.125. *High-magnification SEM image (using a backscattering detector) of the profile of the platinum catalyst on a cation-exchange membrane, which was hydrolysed with NaOH (70 vol. %) and MeOH (30 vol. %) and pre-treated with H₂O.*

Figure 4.126. *Plot of the thickness of the layer of platinum catalyst on a membrane under various conditions of the deposition process*

Figure 4.127. *Adsorption isotherm of the adsorption (+) and desorption (*) of nitrogen gas on a hydrolysed membrane without platinum catalyst.*

Figure 4.128. *Adsorption isotherm of the adsorption (+) and desorption (*) of nitrogen gas on a pre-treated membrane embedded with platinum catalyst.*

Chapter 5

Figure 5.1. *Magnified SEM image (using a backscattering detector) of a profile of a layer of platinum on a membrane modified on one-side with EDA for one minute.*

Figure 5.2. *IR spectra of hydrolysed and non-hydrolysed cation-exchange membranes not modified with EDA*

Figure 5.3. IR spectra of EDA-modified (5 min and 30 min) and unmodified (0 min) hydrolysed membranes

Figure 5.4. IR spectra of membranes modified for 5 days with EDA in the Na^+ -ionic form and the H^+ -ionic form

Figure 5.5. Dependence of the $\tan \delta$ upon temperature at frequency of 100 kHz for membranes modified with EDA on one side for 1, 5 and 60 minutes (curves 1, 2 and 3 respectively).

Figure 5.6. Dependence of the loss factor upon temperature at frequency of 60 Hz for membranes exposed to EDA treatment for various times: curve 1 reflects no treatment, curve 2 - 1 minute, curve 3 - 5 minutes and curve 4 - 60 minutes of treatment.

Figure 5.7. Dependence of the loss factor upon temperature at frequency of 100 kHz for membranes modified on one side for 1 minute with EDA (curve 1), for 5 minutes (curve 2) and for 60 minutes (curve 3).

Figure 5.8. Schematic representation of a two-compartment cell used to measure resistance of cation-exchange membranes modified with EDA. 1-conductivity meter, 2-Pt electrodes, 3-water jacket for thermal stability, 4-membrane, 5-inlet for water from thermostat, 6-vessel with NaCl solution, 7-O-rings, 8-inlet for NaCl solution.

Figure 5.9. Dependence of membrane resistance (R_m) on the time of treatment of one-side of the membrane with EDA. Membranes were equilibrated with 0.1N NaCl solution at pH=6.0 and pH=9.0.

Figure 5.10. Dependence of membrane resistance on the time of treatment of the membrane with EDA

Figure 5.11. AFM surface image ($5\mu\text{m}\times 5\mu\text{m}$) of platinum catalyst embedded on a cation-exchange membrane that was treated with 1% $\text{CH}_3(\text{CH}_2)_{15}\text{N}(\text{CH}_3)_3\text{Br}$ surfactant

Figure 5.12. Three-dimensional AFM surface image ($5\mu\text{m}\times 5\mu\text{m}$) of platinum catalyst embedded on a cation-exchange membrane that was treated with 1% $\text{CH}_3(\text{CH}_2)_{15}\text{N}(\text{CH}_3)_3\text{Br}$ surfactant

Figure 5.13. Line analysis of the surface profile of the platinum catalyst embedded on a cation-exchange membrane that was treated with 1% $\text{CH}_3(\text{CH}_2)_{15}\text{N}(\text{CH}_3)_3\text{Br}$ surfactant

Figure 5.14. *AFM surface image ($10\mu\text{m}\times 10\mu\text{m}$) of platinum catalyst embedded on a cation-exchange membrane that was treated with 1% $\text{CH}_3(\text{CH}_2)_{15}\text{N}(\text{CH}_3)_3\text{Br}$ surfactant*

Figure 5.15. *Three-dimensional AFM surface image ($10\mu\text{m}\times 10\mu\text{m}$) of platinum catalyst embedded on a cation-exchange membrane that was treated with 1% $\text{CH}_3(\text{CH}_2)_{15}\text{N}(\text{CH}_3)_3\text{Br}$ surfactant*

Figure 5.16. *Line analysis of the surface profile of the platinum catalyst embedded on a cation-exchange membrane that was treated with 1% $\text{CH}_3(\text{CH}_2)_{15}\text{N}(\text{CH}_3)_3\text{Br}$ surfactant*

Figure 5.17. *AFM surface image ($20\mu\text{m}\times 20\mu\text{m}$) of platinum catalyst embedded on a cation-exchange membrane that was treated with 1% $\text{CH}_3(\text{CH}_2)_{15}\text{N}(\text{CH}_3)_3\text{Br}$ surfactant*

Figure 5.18. *Three-dimensional AFM surface image ($20\mu\text{m}\times 20\mu\text{m}$) of platinum catalyst embedded on a cation-exchange membrane that was treated with 1% $\text{CH}_3(\text{CH}_2)_{15}\text{N}(\text{CH}_3)_3\text{Br}$ surfactant*

Figure 5.19. *Line analysis of the surface profile of the platinum catalyst embedded on a cation-exchange membrane that was treated with 1% $\text{CH}_3(\text{CH}_2)_{15}\text{N}(\text{CH}_3)_3\text{Br}$ surfactant*

Figure 5.20. *IR spectra of unmodified and surfactant-modified hydrolysed membranes*

Figure 5.21. *IR spectra of a modified membrane (1), modified membrane placed in 6N NaOH for 48 hours (2) and modified membrane boiled in 6N NaOH for 5 hours (3)*

Figure 5.22. *IR spectra of modified membranes after treatment with 3N NaCl and 6N NaOH*

Figure 5.23. *IR spectra of modified membranes after treatment with 5%, 30% and 50% HNO_3*

Figure 5.24. *Plot of the resistance of membranes ($\log R_{\text{membrane}}$) treated with surfactant solutions of concentrations 0.05%, 0.5% and 7.5% at time intervals of 1 minute*

Figure 5.25. *Typical three-dimensional AFM image of a textured Pt catalyst embedded on a membrane. The platinum particles are small in size and pyramidally textured.*

Figure 5.26. Typical AFM image (three-dimensional mesh view) of the surface of a membrane with platinum catalyst (seen as “flakes”).

Figure 5.27. Typical AFM image (three-dimensional mesh view) of the surface of a membrane with platinum catalyst (seen as unevenly distributed, semi-spherical particles).

Figure 5.28. Structural arrangement of micelles on a membrane that contribute to the pyramidal shape of the platinum particles

Chapter 6

Figure 6.1. Schematic representation of a four-compartment cell used in resistance measurements of the cation-exchange membranes modified with EDA. (1) Platinum electrodes; (2) water jacket for thermal stability; (3) Luggin capillaries; (4) Ag/AgCl/KCl reference electrodes; (5) Cation-exchange membrane modified with EDA from the right side; (6) cation-exchange membranes. I, II, III and IV are the chambers of the cell.

Figure 6.2. A typical cyclic i - V curve of a unmodified perfluorinated membrane in 0.1M NaCl, equilibrated at pH=6.

Figure 6.3. Cyclic i - V curves of a membrane modified with EDA on one side for 85 seconds. Arrows on the curves indicate the direction of the current. Curve 1 corresponds to the first cycle and curve 5 corresponds to the last cycle. Curves 2, 3, and 4 show intermediate cycles.

Figure 6.4. Cyclic i - V curves of a membrane modified with EDA for 85 seconds. Anodic cycling was applied to the membrane only (curves 1 and 2). Curve 3 corresponds to the galvanodynamic cycle with both cathodic and anodic waves. Arrows on curve 3 indicate the direction of the current.

Figure 6.5. Cyclic i - V curves of EDA-treated membranes with the aminated layers containing embedded microparticles of platinum. Curve 1 corresponds to 85 sec of EDA treatment, and curve 2 corresponds to 120 seconds of EDA treatment, respectively.

Figure 6.6. Cyclic i - V curves of EDA-treated perfluorinated membranes. Times of modification: 45, 60 and 85 seconds (curves 1, 2, and 3, respectively). The slopes ($\alpha_1=0.166$, $\alpha_2=0.107$ and $\alpha_3=0.072$) of the initial parts of the i - V curves correspond to 45, 60 and 85 seconds of modification with EDA. Steady-state values U_1 , U_2 , and U_3 correspond to 3.5, 6.7 and 10.1 volts, respectively, when the potential of a modified membrane begins to decrease at a current density of approximately 0.01 amps/cm².

Figure 6.7. Schematic representation of the processes occurring in chambers II and chambers III of the electrochemical cell during anodic polarisation of the aminated layer of the membrane containing platinum particles

Chapter 7

Figure 7.1. Reactor used in galvanostatic measurements, which consists of titanium electrodes, gas and liquid distribution channels, inlets and outlets for water and gas.

Figure 7.2. Components of reactor: Gaskets and SPE platinum-containing membrane

Figure 7.3. Schematic representation of membrane cell used in anodic oxidation of water. Microporous Ti electrodes (1); proton-exchange membrane (PEM) (2); isolators between Ti electrodes (3) and reactor (5); outlet (for water and hydrogen) (4); cathode side of a reactor (5); cathodic inlet (for water) (6); gas and liquid distribution channels (7); anodic outlet (for water) (8); anode side of the reactor (9).

Figure 7.4. Typical plot for the anodic oxidation of water at a temperature of 33 °C for an applied current of 0.270A

Figure 7.5. The effect of temperature on the anodic oxidation of water at temperatures of 33 °C (T1), 45 °C (T2) and 60 °C (T3)

Figure 7.6. Anodic oxidation of water by galvanostatic measurements with an applied current of 1.9A for 800 seconds at a temperature of 33 °C. The peaks represent the bursts of oxygen evolution.

Figure 7.7. Schematic representation of experimental set-up used for cyclic voltammetry measurements in the electrolysis of water using a Ag/AgCl [KCl(sat)] electrode, working electrode (WE) and counter electrode (CE)

Figure 7.8. Cyclic voltammogram of the electrolysis of water at room temperature of a scan rate of 100mV/sec. Ag/AgCl/[KCl(sat)] was used as the reference electrode

Figure 7.9. Reactor used in galvanostatic measurements, which consists of pressure regulator, membrane cell, cooling chambers and gas and water inlets and outlets

Figure 7.10. Schematic representation of experimental set-up used in electrolysis of water using Nafion. The reaction was investigated by cyclic voltammetry using a Ag/AgCl [KCl(sat)] electrode, working electrode (WE) and counter electrode (CE)

Figure 7.11. Cyclic voltammograms for the electrolysis of water at temperatures of 33 °C (2) and 60 °C (1)

Chapter 8

Figure 8.1. *A typical curve showing the behaviour of a data set characterised by the Hurst exponent for $H=0.5$.*

Figure 8.2. *A typical curve showing the behaviour of a data set characterised by the Hurst exponent for $H<0.5$*

Figure 8.3. *A typical curve showing the behaviour of a data set characterised by the Hurst exponent for $H>0.5$*

Figure 8.4. *Schematic representation of surfaces with different fractal dimensions (F_d). F_d is 1.0 (A); F_d is 2.0 (B); F_d is between 1.0 and 2.0 (C); F_d is 2.0 (D); F_d is 3.0 (E); F_d is between 2.0 and 3.0 (F) (Marchese-Ragona et al., 1993).*

Figure 8.5. *Schematic representation of different types of fractals: surface fractal (A), mass fractal (B) and pore fractal (C) (Salvarezza et al., 1995).*

Figure 8.6. *Typical plot representing a power spectrum of a platinum-containing membrane*

Figure 8.7. *Curve representing a variogram of a series with relation to Hurst exponent (H)*

Figure 8.8. *Typical curve representing a variogram of a platinum-containing membrane*

Figure 8.9. *Typical vertical line profile of a membrane sample obtained from an AFM image*

Figure 8.10. *Schematic representation of the dependence of R_{RMS} on the measured length (scan area) of a surface (Kiely et al., 1997)*

Chapter 9

Figure 9.1. *Schematic reaction scheme for the Wacker-type oxidation of alkenes (Malleron et al., 1997)*

Figure 9.2. *Schematic representation of a cell used for the oxidation of light alkanes in the gas phase*

Figure 9.3. *Schematic diagram of a reactor for the epoxidation of olefins during water electrolysis*

Figure 9.4. *Schematic representation of the instrument used for potential measurements (Otsuka et al., 1995)*

List of Tables

Chapter 1

Table 1.1. *Typical chemical structures of some SPE membrane materials that are ionomeric in nature (Gottesfield et al., 1997).*

Table 1.2. *Physical and chemical properties of Nafion-120 membranes at 25°C (Eisenberg and Yeager, 1982).*

Table 1.3. *Membrane properties of perfluorinated ionomers classified by ion-exchange group and membrane structure (Eisenberg and Yeager, 1982).*

Table 1.4. *Composition and purpose of components in a typical electroless-deposition bath (Okinaka et al., 1990).*

Figure 1.5. *Catalytic activities of metals during anodic oxidation of different reducing agents listed in decreasing order of catalytic activity (Ohno et al., 1985).*

Chapter 2

Table 2.1. *Ion-exchange capacities of cation-exchange membranes with different conditions of hydrolysis.*

Chapter 3

Table 3.1. *Absorbance of standard solutions containing platonic acid solution, SnCl_3^- and aqua regia, which were measured at a wavelength of 402.27nm.*

Table 3.2. *Concentration of the solutions containing platinum ions, as determined from the calibration curve.*

Table 3.3. *UV spectrophotometric results of platinum loading on cation-exchange membranes by the reduction of 0.05M platonic acid solution with NaBH_4 for total times of platinisation of 4.5, 6.5, 10.5, 12.5 and 16.5 minutes for a membrane area of 2.26 cm^2 .*

Table 3.4. *Results of gravimetric and spectrophotometric analysis of the total platinum loading on membranes by the reduction of 0.05M platonic acid solution with NaBH_4 for the total times of platinisation of 4.5, 6.5, 10.5, 12.5 and 16.5 minutes.*

Table 3.5. *Concentration of the solutions containing platinum ions as determined from the calibration curve*

Table 3.6. *UV spectrophotometric results of platinum loading on cation-exchange membranes by the reduction of 0.03M platonic acid solution with NaBH_4 for total*

times of platinisation of 4.5, 12.5, 16.5, 26.5 and 36.5 minutes for a membrane area of 2.26 cm².

Table 3.7. *Results of gravimetric and spectrophotometric analysis of the total platinum loading on membranes by the reduction of 0.03M platonic acid solution with NaBH₄ for total times of platinisation of 4.5, 12.5, 16.5, 26.5 and 36.5 minutes.*

Table 3.8. *Concentration of the solutions containing platinum ions, as determined from the calibration curve*

Table 3.9. *UV spectrophotometric results of the platinum loading on cation-exchange membranes by the reduction of 0.05M platonic acid solution with hydrazine for the total times of platinisation of 4.5, 6.5, 8.5, 10.5, 12.5 and 16.5 minutes for a membrane area of 9 cm².*

Table 3.10. *Results of gravimetric and spectrophotometric analysis of the total platinum loading on membranes by the reduction of 0.05M platonic acid solution with hydrazine for the total times of platinisation of 4.5, 6.5, 8.5, 10.5, 12.5 and 16.5 minutes.*

Table 3.11. *UV spectrophotometric results of platinum loading on cation-exchange membranes by the reduction of 0.05M platonic acid solution with hydrazine for a total time of platinisation of 11 minutes.*

Table 3.12. *Results of gravimetric and spectrophotometric analysis of the total platinum loading on membranes by the reduction of 0.05M platonic acid solution with hydrazine for the total time of platinisation of 11 minutes at room temperature.*

Table 3.13. *Results of the reduction of platonic acid solution by hydrazine for 15.5 minutes at a temperature of 40 °C*

Chapter 4

Table 4.1. *Results of AFM images for the scan area 20µm×20µm of membranes embedded with platinum catalyst by the reduction of 0.05M platonic acid solution with hydrazine at 40 °C for varying lengths of time.*

Table 4.2. *Results of AFM images for the scan area 130µm×130µm of membranes embedded with platinum catalyst by the reduction of 0.05M platonic acid solution with hydrazine at 40 °C for varying lengths of time.*

Table 4.3. *Results of AFM images for the scan area 20µm×20µm of membranes embedded with platinum catalyst by the reduction of 0.03M platonic acid solution with hydrazine at 40 °C, while pulses between 20 and 40 kHz were rippled through platonic acid solution.*

Table 4.4. Results of AFM images for the scan area $130\mu\text{m}\times 130\mu\text{m}$ of membranes embedded with platinum catalyst by the reduction of 0.05M platinic acid solution with sodium borohydride at 40 °C for varying lengths of time.

Table 4.5. Results of AFM for the scan area $20\mu\text{m}\times 20\mu\text{m}$ of membranes embedded with platinum catalyst by the reduction of 0.03M platinic acid solution with sodium borohydride at 40 °C for varying lengths of time.

Table 4.6. Results of AFM for the scan area $130\mu\text{m}\times 130\mu\text{m}$ of membranes embedded with platinum catalyst by the reduction of 0.03M platinic acid solution with sodium borohydride at 40 °C for varying lengths of time.

Table 4.7. Surface analysis of platinum catalyst deposited on membranes by the reduction of 0.05M platinic acid solution with hydrazine

Table 4.8. Surface analysis of platinum catalyst that was deposited on membranes by the reduction of 0.03M platinic acid solution with hydrazine

Table 4.9. Surface analysis of platinum catalyst that was deposited on membranes by the reduction of 0.05M platinic acid solution with sodium borohydride

Table 4.10. Surface analysis of platinum catalyst that was deposited on membranes by the reduction of 0.03M platinic acid solution with sodium borohydride

Table 4.11. BET results of pre-treated membranes embedded with platinum catalyst and hydrolysed membranes without platinum catalyst.

Chapter 5

Table 5.1. Results of the resistance measurements of membranes modified with EDA for 0, 20, 45, 60, 85, 125, 300 and 600 seconds, which were equilibrated at pH=9

Table 5.2. Results of resistance measurements of membranes modified with EDA for 0, 20, 45, 60, 85, 125, 300 and 600 seconds, which were equilibrated at pH=6

Table 5.3. Results of water sorption of a membrane in the H^+ -ionic form, membrane modified with EDA and EDA-modified membrane that underwent heat treatment

Table 5.4. The electrical resistance of 0.05%, 0.5% and 7.5% surfactant solutions before and after electrical resistance measurements of cation-exchange membranes

Table 5.5. Results of electrical resistance measurements of cation-exchange membranes treated with 0.05% $\text{CH}_3(\text{CH}_2)_{15}\text{N}(\text{CH}_3)_3\text{Br}$ surfactant solution at time intervals of 1 minute

Table 5.6. *Results of electrical resistance measurements of cation-exchange membranes treated with 0.5% $\text{CH}_3(\text{CH}_2)_{15}\text{N}(\text{CH}_3)_3\text{Br}$ surfactant solution at time intervals of 1 minute*

Table 5.7. *Results of electrical resistance measurements of cation-exchange membranes treated with 7.5% $\text{CH}_3(\text{CH}_2)_{15}\text{N}(\text{CH}_3)_3\text{Br}$ surfactant solution at time intervals of 1 minute*

Table 5.8. *Results of the water sorption of a membrane modified with surfactant and a membrane in H^+ -ionic form*

Chapter 8

Table 8.1. *Hurst exponent of membranes embedded with platinum when 0.05M platinic acid solution was reduced by hydrazine at various time intervals.*

Table 8.2. *Percentage deviation of Hurst exponent (of 10 line profiles) of membranes embedded with platinum when 0.05M platinic acid solution was reduced by hydrazine at various time intervals*

Table 8.3. *Results of surface roughness characterisation of membranes embedded with platinum when 0.05M platinic acid solution was reduced by hydrazine at various time intervals.*

Table 8.4. *Hurst exponent of membranes embedded with platinum when 0.05M platinic acid solution was reduced by sodium borohydride at various time intervals*

Table 8.5. *Percentage deviation of Hurst exponent (of 10 line profiles) of membranes embedded with platinum when 0.05M platinic acid solution was reduced by sodium borohydride at various time intervals*

Table 8.6. *Results of surface roughness characterisation of membranes embedded with platinum when 0.05M platinic acid solution was reduced by sodium borohydride at various time intervals.*

Table 8.7. *Hurst exponent of membranes embedded with platinum when 0.03M platinic acid solution was reduced by sodium borohydride at various time intervals*

Table 8.8. *Percentage deviation of Hurst exponent (of 10 line profiles) of membranes embedded with platinum when 0.03M platinic acid solution was reduced by sodium borohydride at various time intervals*

Table 8.9. *Results of surface roughness characterisation of membranes embedded with platinum when 0.03M platinic acid solution was reduced by sodium borohydride at various time intervals.*

Introduction and objectives

Background

Heterogeneous electrocatalysis

Heterogeneous electrocatalysis has all the advantages of heterogeneous catalysis, such as enhancement of reaction rates by the surface structure of a catalyst. In addition, heterogeneous electrocatalysis offers further control of the reaction rates by varying the electrode potential with its resulting effect on heterogeneous electron transfer (Wieckowski et al., 2000).

Heterogeneous electrocatalysis involves the chemical reactions occurring in an electrochemical cell at the surface of an electrode, that is, at the electrochemical interface. Heterogeneous electrocatalytic processes are sensitive to the nature of the electrode material and its surface morphology. Heterogeneous catalytic reactions occur mainly in three environments, namely, metal/solution, solid/polymer (usually catalyst/solid polymer electrolyte (SPE) membrane) and gas/solid interfaces (Fig. 1) (Wieckowski et al., 2000).

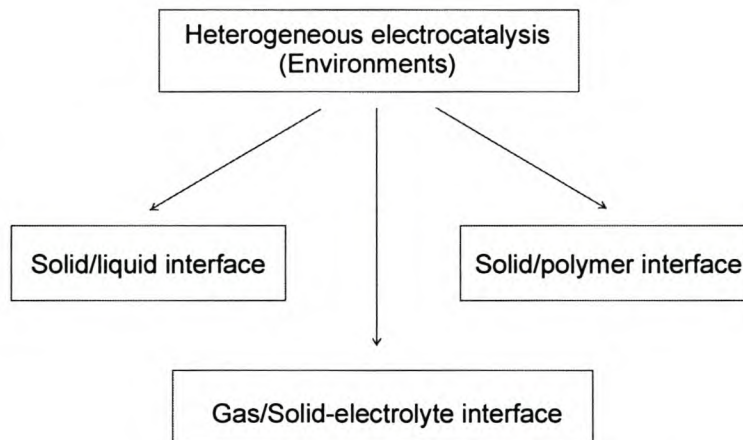


Figure 1. Schematic representation showing the three environments in which heterogeneous electrocatalytic reactions occur: metal/solution, solid/polymer and gas/solid interfaces.

The present study will focus on the preparation and characterisation of SPE/platinum catalyst membranes and on the reactions that occur in solid/polymer environments.

Solid polymer electrolyte technology

Solid polymeric materials that exhibit ionic conductivity are regarded as a solid polymer electrolyte (SPE). SPE technology is a new and fast growing area of material and polymer science (see, for example, the special issue of *J. Electrochimica Acta*, Vol. 46, Iss. 10-11, 2001). SPE technology has demonstrated outstanding advantages and operation characteristics in fields such as aerospace and military application (Bessarabov, 1998). SPE technology has many advantages over conventional electrochemical devices, including: (i) significantly higher electrochemical efficiency than achievable with conventional electrochemical devices at comparable current densities, resulting in lower power consumption per unit of a chemical processed, (ii) higher current density capability, resulting in lower capital costs, size and weight of the electrochemical modules, and (iii) chemical binding of an electrolyte in a polymer chain, resulting in a system that requires no corrosive liquids in the design, assembly, operation and maintenance of the system (Bessarabov, 1998).

SPE electrocatalytic membrane technology

SPE electrocatalytic membrane systems offer a wide range of applications and potential processes, as shown in Figure 2. Figure 2 is a schematic representation of a perfluorinated cation-exchange SPE matrix embedded with a catalyst on the anode and cathode sides. Electrolysis of water occurs under electrical polarisation conditions on the surface of the membrane. Examples of SPE-based electrocatalytic membrane processes, as shown in Figure 2, include (excluding fuel cell application):

- the generation of hydrogen and oxygen (process 1) (Nutall, 1977),
- production of ozone (process 2) (Tatapudi et al., 1993; Bessarabov, 1999),
- electrocatalytic membrane sensors (process 3) (Heitner-Wirguin, 1996),
- separation of isotopes: hydrogen and deuterium (process 4) (Bessarabov, 1998),
- hydrogen “absorber” (process 5) (Bessarabov, 1998),
- electrocatalytic syntheses based on SPE membranes (process 6) (Ogumi et al., 1981; Jörissen, 1996; Itoh et al., 2000),
- water treatment by SPE membrane electrocatalytic systems (process 7) (Grimm et al., 2000) and

- electroinduced gas separation (process 8) (Bessarabov, 1997; Bessarabov et al., 1998).

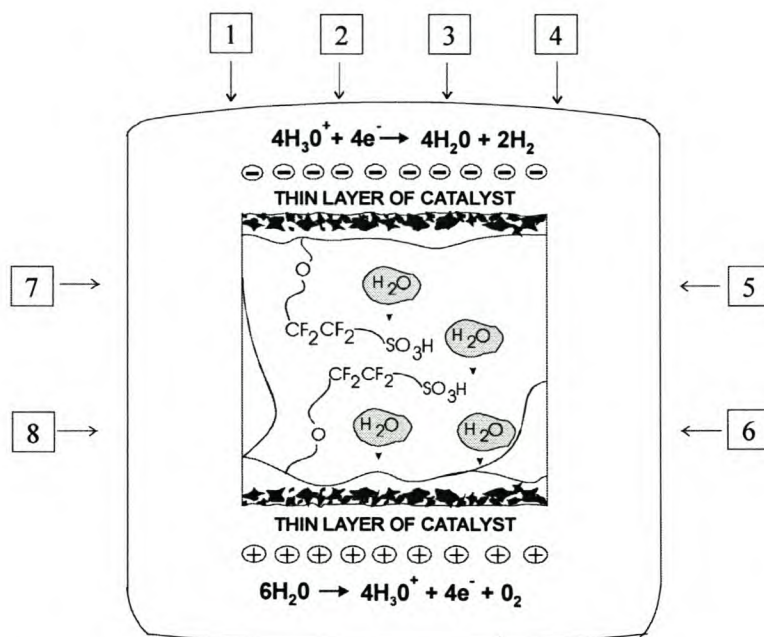


Figure 2. Schematic representation of a SPE membrane/catalyst composite system, showing the existing and potential related technologies in the field of SPE-based electrocatalysis.

Considerations of future research

Despite recent progress made in SPE-based electrocatalytic membrane technology there are several aspects that require further detailed studies. Firstly, for example, i) how does the catalytic activity of both the catalyst particles and the functional groups of a SPE polymeric matrix determine the resulting catalytic properties of the entire system, and ii) how does membrane surface modification effect the morphology of a catalyst deposited on the surface of a SPE membrane. The chemical modification of ion-exchange membrane surfaces is a powerful method by which to change membrane surface properties, as well as conditions and results of the electroless deposition of catalysts. These include the size, shape and distribution of catalyst particles in membranes, membrane electrical properties, etc. (Bessarabov et al., 2000).

Secondly, another important area of research in the field of SPE-based electrocatalytic membrane science and technology is the preparation, characterisation, optimisation and improved adhesion of the thin porous catalytic layer to a membrane

polymeric matrix that consists of clusters of metal or particles of metal oxides (Bessarabov, 1998).

Thirdly, the development of membrane-based SPE composite catalysts for optimal performance in heterogeneous reactions occurring under conditions of electrical polarisation requires knowledge and understanding of the structure, morphology, concentration and energy distribution of the active sites on the surface of a membrane.

Fourthly, in addition to its good stability, a metal catalyst deposited on an SPE membrane should also provide large active areas and a suitable structure to ensure the best possible performance of the entire system (Bessarabov, 1998).

In the present study, focus was placed on the preparation and characterisation of SPE/Pt membrane systems, and the evaluation of these SPE/Pt membrane composites for the anodic oxidation of water. Different techniques by which to prepare SPE/Pt membrane systems were considered. Much attention was given to the investigation of the chemical surface modification of SPE membranes.

Results of these studies in the field of SPE catalytic membrane systems should lead to new catalytic systems with not only favourable chemical compositions of a catalyst and electrical properties of SPE membranes, but also the pre-determined orientation of catalyst particles on SPE membranes to achieve maximum catalytic activity from catalytic systems with optimal catalyst loading.

It can be expected that heterogeneous membrane electrocatalysis will display further unsuppressed growth because of the outstanding challenges, both experimental and theoretical, and as a part of the global effort to develop clean and renewable energy resources. Such growth should be expected in the designing of new catalytic and electrolyte membrane materials, and the focussing on new processes (e.g. methane and ethanol activation by membrane electrocatalysis). Progress in the theories of electrocatalytic reactions and surface dynamics could possibly be the main driving force to cause further growth of SPE electrocatalytic membrane technology.

It was for the above reasons that the present study was undertaken.

Objectives

The objectives of the study were the following:

1. Preparation of platinum-containing perfluorinated cation-exchange membranes, with varying characteristics of the platinum catalyst

Although patents and the open literature provide some information on deposition procedures for the preparation of platinum-containing cation-exchange membranes, this information was considered insufficient for successful manufacturing of platinum-containing membranes. Hence, the successful preparation of platinum-containing membranes was the first, and one of the main objectives of this study. The preparation of these membranes involved the electroless deposition of a thin layer of platinum catalyst on perfluorinated cation-exchange membranes as developed by Takenaka (1982).

The characteristics of the platinum catalyst on a membrane were influenced by varying the variables in the electroless deposition process, such as: temperature of reducing agent, type of reducing agent, concentration of the platonic acid solution, applied external activation and the pre-treatment of the membranes.

2. Characterisation of cation-exchange membranes and platinum catalyst

The characterisation of cation-exchange membranes and platinum catalyst provides information on the morphological characteristics of the platinum catalyst on the membrane, as well as the chemical characteristics of modified and non-modified membranes. Characterisation of membranes and catalyst morphology was determined by various physical-chemical characterisation techniques, such as: infrared spectrometry (IR), Brunauer, Emmett and Teller adsorption (BET), dielectric analysis (DEA); Electrochemical characterisation methods, such as: galvanodynamic and galvanostatic measurements; and microscopy characterisation methods, such as: Atomic Force Microscopy (AFM) and Scanning Electron Microscopy (SEM).

3. Surface modification of cation-exchange perfluorinated membranes

The surface chemical modification of cation-exchange perfluorinated membranes was carried out to change membrane electrical properties and morphology of platinum catalyst deposited on a membrane. The effect of modification on the morphology of a platinum catalyst on a membrane was investigated as the modification of a membrane

can vary the profile of the platinum catalyst embedded on a membrane, the platinum particle shape and size, and the distribution of the platinum throughout the membrane.

4. Development of a protocol for the quantitative determination of platinum loading on a cation-exchange membrane by UV spectrophotometric analysis

Knowledge of platinum loading density on a cation-exchange membrane can be used to determine suitable conditions for the deposition of the platinum catalyst on a cation-exchange membrane. An objective of this study was to develop a protocol for the quantitative determination of platinum loading on a cation-exchange membrane. This was to be done by UV spectrophotometric analysis, since the gravimetric method has many limitations. The platinum loading of the membrane was to be determined by colorimetric analysis with aqua regia (3HCl:HNO₃) and tin (II) chloride reagents.

5. Quantification of membrane surface roughness obtained by means of AFM measurements

Quantification of the surface roughness profile of membranes by AFM was attempted. The study aimed at obtaining a more accurate method of determining the surface roughness profile of a platinum-containing membrane other than by AFM.

6. Anodic oxidation of water with platinum-containing membranes

The application of platinum-containing SPE membranes in the anodic oxidation of water was investigated with galvanostatic and cyclic voltammetric measurements. The objective was to demonstrate the application of the anodic oxidation of water using platinum-containing membranes prepared in this study.

Outline of the present study

Chapter 1 is a literature survey of the design of various electrocatalytic SPE membrane systems and their different applications. Special focus was placed on their use in organic and inorganic electrocatalytic syntheses.

Chapter 2 describes the preparation of cation-exchange membranes and the deposition of platinum catalyst on cation-exchange membranes. The platinum catalyst was embedded on the membrane by the autocatalytic electroless reduction of [PtCl₆]²⁻ complex anions (Counter-diffusion method) (Takenaka et al., 1982).

Chapter 3 describes the development of a protocol for the quantitative determination of platinum loading on a cation-exchange membrane by UV spectrophotometric analysis.

Chapter 4 describes the characterisation techniques used to determine the chemical characteristics of the cation-exchange membrane and the morphological characteristics of the platinum catalyst on the membrane. These techniques include: UV spectrophotometric analysis, scanning electron microscopy (SEM), atomic force microscopy (AFM), and BET adsorption. The morphological characteristics of the platinum catalyst on the membrane were explored with scanning electron microscopy (SEM) and atomic force microscopy (AFM). Results of these characterisation techniques provide information on the size and shape of platinum particles, thickness of the platinum layer, distribution of platinum particles within the membrane and surface roughness of the layer of platinum on membrane.

Chapter 5 describes the chemical modification of the surface of a cation-exchange membrane and the deposition of platinum on these modified membranes. In the present study, two methods were explored to achieve surface modification of the cation-exchange membranes, namely: membrane modification with ethylene diamine (EDA) and membrane modification with a cationic surfactant, cetyltrimethylammonium bromide.

The membranes modified with ethylene diamine (EDA) were characterised with techniques such as, infrared spectrometry (IR), scanning electron microscopy (SEM), electrical conductivity measurements and dielectric analysis (DEA). The degree of modification of the membranes modified with EDA was investigated with electrical resistance measurements. The membranes modified with a cationic surfactant were characterised with techniques such as, infrared spectrometry (IR), atomic force microscopy (AFM) and electrical conductivity measurements.

The morphology of the platinum catalyst embedded on the membrane modified with surfactant was also investigated. The zwitterionic nature of the layers of membrane modified with EDA was investigated.

Chapter 6 describes experimental details of the galvanodynamic study of the electrochemical switching effect in cation-exchange membranes modified with EDA and relevant discussion on the results. The influence of the surface treatment of the membranes with EDA and the effect of platinum catalyst on the electrochemical “switching” phenomenon were investigated.

Chapter 7 describes the experimental anodic oxidation of water as an example of the application of platinum-containing perfluorinated cation-exchange membranes.

Chapter 8 introduces various mathematical approaches for the quantification of the surface roughness of platinum catalyst on cation-exchange membranes.

Chapter 9 discusses the advances made in electrocatalytic membrane systems consisting of phosphoric acid-based immobilised liquid membranes (ILM) and the potential of extending similar application in SPE-based electrocatalytic membrane systems.

Approbation and presentation of the results

Significant non-confidential results of the study have already been published in 5 peer-reviewed articles, in the Journal of Membrane Science, Membrane Technology Newsletter and International Journal of Ionics. Other published material that has resulted from this study includes proceedings of local and international conferences. The complete list of the output of the study is given in the Appendices.

References

1. Bessarabov DG, Sanderson RD, Valuev VV, Popkov YM and Timashev SF, 1997, New possibilities of electroinduced membrane gas and vapor separation, *Ind. Eng. Chem. Res.*, 36, 2487-2489
2. Bessarabov DG, 1998, Electrochemically-aided membrane separation and catalytic processes, *Membranes Technology*, 93, 8-11
3. Bessarabov DG, Sanderson RD, Popkov YM and Timashev SF, 1998, Characterisation of membranes for electrochemically aided gas separation: Morphology of platinum deposition, *Separation and Purification Technology*, 14, 201-208
4. Bessarabov DG, 1999, Electrochemical ozone generator based on solid polyelectrolyte (SPE) membranes for water treatment, in: *Book of Abstracts, The Fifth International Conference on Advanced Oxidation Technologies for Water and Air Remediation, Albuquerque, New Mexico, USA, May 24-28*, pp 112-113
5. Bessarabov DG, Michaels W, Sanderson RD, 2000, Preparation and characterisation of chemically-modified perfluorinated cation-exchange platinum-containing membranes, *Journal of Membrane Science*, 179, 221-229

6. Forsyth M (ed), 2001, Polymer electrolytes, *Journal of Electrochimica Acta*, 46, 10-11, 1395-1766
7. Grimm JH, Bessarabov DG, Simon U, Sanderson RD, 2000, Characterisation of doped tin dioxide anodes prepared by a sol-gel technique and their application in an SPE-reactor, *Journal of Applied Electrochemistry*, 30, 293
8. Heitner-Wirguin C, 1996, Recent advantages in perfluorinated ionomer membranes: structure, properties and applications, *Journal of Membrane Science*, 120, 1
9. Itoh N, Xu WC, Hara S and Sakaki K, 2000, Electrochemical Coupling of Benzene Hydrogenation and Water Electrolysis, *Catalysis Today*, 56, 307-314
10. Jorissen J, 1996, Ion exchange membranes as solid polymer electrolytes (SPE) in electro-organic synthesis without supporting electrolytes, *Electrochimica Acta*, 41, 553
11. Nuttall LJ, 1977, Conceptual design of large scale water electrolysis plant using solid polymer electrolyte technology, *International Journal of Hydrogen Energy*, 2, 395
12. Ogumi Z, Nishio K, Yoshizana S, 1981, Application of the SPE method to organic electrochemistry-II. Electrochemical hydrogenation of olefinic double bonds, *Electrochimica Acta*, 26, 1779
13. Takenaka H, Torikai E, Kawami Y, Wakabayashi N, 1982, Solid polymer electrolytes water electrolysis, *International Journal of Hydrogen Energy*, 7, 397
14. Takenaka H, 1982, Method for the manufacture of ion-exchange membrane-catalytic metal composites, U.S patent 4,328,086
15. Tatapudi P and Fenton JM, 1993, Synthesis of ozone in a proton exchange membrane electrochemical reactor, *Journal of Electrochemical Society*, 140, 3527

Solid Polymer Electrolyte (SPE)-based membrane catalytic systems**Abstract**

In this chapter, different types of solid polymer electrolytes are discussed. These include: ionically-conducting phases, organically-modified ceramic polymers, polymers in which nitrogen acts as a mediator for proton conduction and sulphonated polymers. Emphasis is placed on sulphonic-containing perfluorinated ionomers, such as Nafion. Various pre-treatment methods and methods for the preparation of perfluorinated cation-exchange membranes, and the deposition of a platinum catalyst on these membranes by electroless deposition methods, are considered. An overview is given of the numerous diverse fields of application of these microheterogenous SPE-based membrane catalytic systems. The chapter is concluded with mention of current trends in research in terms of the optimisation of the morphology and chemical composition of catalyst deposition on SPE membranes.

1.1. Solid Polymer Electrolytes

Over the past few years there has been a growing interest in the development of polymers that have the unique property of acting as solvents for salts (Vincent, 1989). In this case, polymer electrolytes are ionically-conducting phases formed by dissolving salts in polar polymers which are able to co-ordinate ions. An example of a polymer electrolyte is a solution of an alkali metal salt in poly(ethylene oxide) (PEO), the ionic conductivity of which is achieved by the presence of metal ions coordinated with a polar polymer (e.g., PEO) (Vincent, 1989).

The driving force behind this current interest in polymer electrolytes is the advantages that these ionically-conducting polymers have over conventional electrolytes for a range of practical applications, in terms of both fabrication and subsequent use (Vincent, 1989). One attractive application of ionically-conducting polymers is their use in high-energy density batteries, in which a thin-film electrolyte acts as the electrode separator and permits cells to be made with high electrode-electrolyte interfacial areas (Vincent, 1989). Further research into redox-active metal

lipoproteins, in which there is great interest as biosensors and biodevices, are expected to show their activity in PEO oligomers (Nakamura et al., 2001).

The formation of polymer salt complexes depends on the polymer having certain characteristics, including: the presence of groups with sufficient electron-donor ability to solvate the cations, low barriers to polymer-bond rotation so that segmental motion of the polymer can occur, and suitable distances between co-ordinating centres for the formation of multiple intrapolymer ion bonds.

Polymers that can form complexes with metal salts, poly(organophosphazenes), were recently investigated by Allcock et al. (1996), who showed that various poly(organophosphazenes) are polymer electrolytes.

Three requirements for an improved solid polymer electrolyte matrix are: (1) the polymer should be amorphous at room temperature and below, (2) it should possess coordination and solvation sites for ions that will assist ion-pair separation, and (3) the polymer molecules should be sufficiently mobile at room temperature so that facile ion migration can occur through the free volume (Allcock et al., 1998). For example, the polymer "MEEP" (methoxy-ethoxy-ethoxy-phosphazene) was developed in an attempt to achieve all three of these requirements in one polymer. The six oxygen atoms per repeat unit in the side groups of MEEP provide a high level of co-ordination and solvation power for cations which should favour ion pair separation and maximize the amount of salt that can be dissolved in the polymer (Allcock et al., 1998).

Many other polymeric materials exhibit ionic conductivity. These include polymers in which nitrogen acts as a mediator for proton conduction (Kreuer et al., 1998), organically modified ceramics-type polymers (ORMOCERs) (Popall et al., 1998) and sulphonated polymers (Gottesfield and Zawodzinski, 1997).

1.1.1. Polymers in which nitrogen acts as a mediator for proton conduction

An example of polymers in which nitrogen acts as a mediator for protons is blends of polymers with oxoacids such as polybenzimidazole and H_3PO_4 . Their nitrogen sites act as strong proton acceptors with respect to the sulphonic acid group, thus forming strong protonic charge carriers $(C_3H_3NH_2)^+$. Furthermore, the protonated and unprotonated nitrogen functions may act as donors and acceptors in proton transfer reactions, while the ring itself is non-polar. Nitrogen as a mediator for proton conduction in polymers is currently still being investigated (Kreuer et al., 1998)

Acid-doped polybenzimidazole (PBI) is an attractive alternative to Nafion (a brand of perfluorosulphonate polymer) for use in fuel cells, since it exhibits good conductivity at temperatures up to 200 °C. Wallgren et al. (2001) used PBI as an electrolyte for testing in sensor technology. Their study was aimed at investigating whether PBI reduces the strong humidity effects on sensor behaviour as observed with Nafion (Wallgren et al., 2001).

1.1.2. Organically modified ceramics-type polymers

ORMOCERs are generally hybrid polymeric materials consisting of interconnected inorganic oxidic units (Si, Al, Zr, etc.) and organic (polyethylene, polymethacrylate, polyethylene oxide, etc.) components (Popall et al., 1998). The characteristics of ORMOCERs depend on the inorganic polymer backbone, the organic side chain, and on the degree and nature of cross-linking (Skaarup et al., 1998). Grafted groups such as $-SO_3H$ can introduce proton conductivity into an ORMOCER network. The transport of a proton through the solid can be described as a vehicular mechanism, where the proton rides on a carrier molecule (NH_4^+ or H_3O^+ ion), or a Grothus type mechanism, in which the proton jumps from a donor to an acceptor molecule (Depre et al., 1998).

In contrast to the difficulty encountered in reproducing the filling of polymer electrolytes with nanoparticles (for example, metal catalyst), the polycondensation of alkoxy-silanes enables an extremely homogenised and reproducible distribution of the nano-sized oxidic units in ORMOCERs (Popall et al., 2001). This can be attributed to the high conductivity exhibited by ORMOCERs. Popall et al. (2001) investigated characterisation techniques of ORMOCERs and the behaviour of batteries in which ORMOCERs were used as a polymer separator and binder for electrodes.

1.1.3. Sulphonated ion-conducting polymers

In sulphonated ion-conducting polymers, charged groups are chemically bound to a polymer chain and the counterions, solvated by water, are free to migrate in the aqueous medium that surrounds the polymer matrix. Table 1.1 shows typical chemical structures of various sulphonated-based solid polymer electrolytes (SPE) materials (Gottesfield et al., 1997). These include: poly(styrenesulphonic acid) (PSSA), Nafion, a Dow perfluorosulphonic acid (PFSA) membrane, poly(ethylenesulphonic acid) (PESA), poly(2-acrylamido-2-methylpropanesulphonic acid) (poly-AMPS) and

α, β, β -Trifluorostyrene grafted onto poly(tetrafluoroethylene-ethylene) copolymers and post-sulphonated. The main focus in this chapter is on the perfluorinated solid polymer electrolytes, such as Nafion.

Table 1.1. Typical chemical structures of some SPE membrane materials that are ionomeric in nature (Gottesfield et al., 1997).

Membranes	Structures
PSSA	$ \begin{array}{c} (\text{H}_2\text{CfCH}_2)_m \\ \\ \text{C}_6\text{H}_4 \\ \\ \text{SO}_3\text{H} \end{array} $
Nafion	$ \begin{array}{c} (\text{CF}_2\text{CF}_2)_n(\text{CF}_2\text{CF})_m \\ \\ \text{O} \\ \\ \text{CF}_2 \\ \\ \text{CFfCF}_2 \\ \\ \text{O} \\ \\ \text{CF}_2\text{CF}_2\text{SO}_3\text{H} \end{array} $
Dow	$ \begin{array}{c} (\text{CF}_2\text{CF}_2)_n(\text{CF}_2\text{CF})_m \\ \\ \text{CF}_2 \\ \\ \text{CF} \\ \\ \text{SO}_3\text{H} \end{array} $
PESA	$ \begin{array}{c} (\text{CH}_2\text{CH})_n \\ \\ \text{SO}_3\text{H} \end{array} $
α , β , β -Trifluorostyrene grafted onto poly(tetrafluoroethylene-ethylene) with post-sulphonation	$ \begin{array}{c} (\text{CH}_2\text{CH}_2)_p(\text{CF}_2\text{CF}_2)_n(\text{CF}_2\text{CF})_m \\ \\ \text{CFfCF}_2 \\ \\ \text{C}_6\text{H}_4 \\ \\ \text{SO}_3\text{H} \end{array} $
Poly-AMPS	$ \begin{array}{c} \text{CH}_3 \\ \\ (\text{CH}_2\text{CH}\{\text{CONHfC}\text{CCH}_2\text{SO}_3\text{H}\})_n \\ \\ \text{CH}_3 \end{array} $

1.2. Perfluorinated carbon chain polymers

Perfluorinated carbon chain polymers are an important group of polymers in the wide range of carbon chain polymers (Kirsh et al., 1990). Properties of perfluorinated polymers such as chemical stability and thermal stability are attributed to the presence of fluorine atoms in the main chain of these polymers. The combination of such properties has resulted in the wide use of perfluorinated polymers. The creation of ion-exchange materials based on copolymers of tetrafluoroethylene (TFE) with perfluorovinyl ethers containing different functional groups has extended the field of application of perfluorinated polymers even further (Eisenberg and Yeager, 1982).

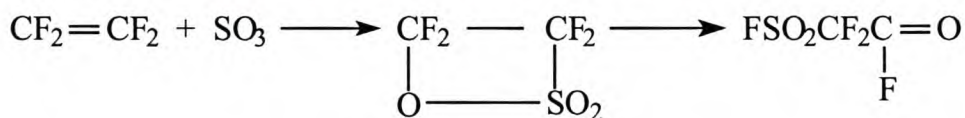
1.3. Nafion^{TM1} as SPE material

Sulphonic-containing perfluorocarbon polymers are ideal for cation transport because of their good chemical stability in corrosive environments (Eisenberg, 1974). Earlier work attempted to prepare sulphonic-containing perfluorinated polymers by grafting vinyl sulphonic acids onto the backbone of polytrifluoroethylene. Attempts were also made to graft styrene onto a fluorocarbon backbone. This was followed by the sulphonation of the styrene moiety. However, the latter two attempts were unsuccessful in producing useful material that resulted in the copolymer approach being preferred (Eisenberg, 1974).

1.3.1. Chemical Structure

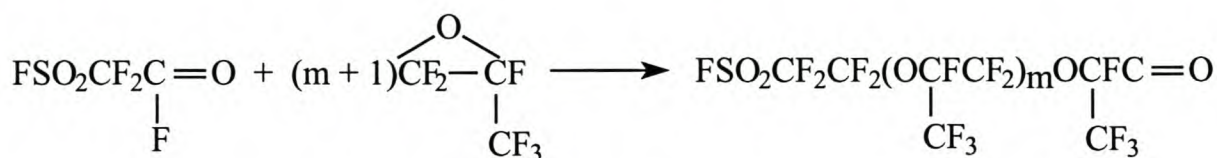
Du Pont manufactured Nafion, a brand of perfluorosulphonate polymer, in the mid 1960s (Grot, 1972). The synthesis pathway for Nafion is represented below (Eisenberg, 1974 and, Appleby and Yeager, 1986).

Tetrafluoroethylene reacts with SO₃ to form a cyclic sultone.

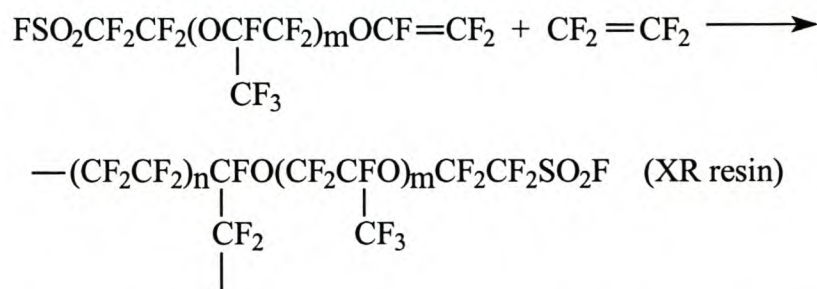


After rearrangement, the sultone can react with hexafluoropropylene epoxide to produce sulphonyl fluoride adducts, where $m \geq 1$.

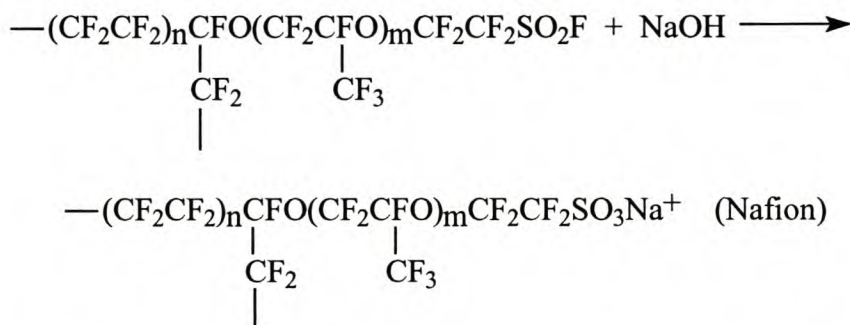
¹ A trade mark of Du Pont



When these adducts are heated with sodium carbonate, a sulphonyl fluoride vinyl ether is formed. This vinyl ether is then copolymerized with tetrafluoroethylene to form a resin referred to as an XR resin:



This resin is converted by base hydrolysis into the Nafion perfluorosulfonate polymer:



The hydrophobic fluorocarbon component and the hydrophilic ionic groups are incompatible. However, the hydrophilic hydrated $\sim\text{SO}_3\text{H}$ groups tend to be attracted to each other. As a result, there is a degree of phase separation between the fluorocarbon component and the hydrated $\sim\text{SO}_3\text{H}$ groups. This leads to the formation of interconnected hydrated ionic clusters (Appleby and Yeager, 1986). Gierke and Hsu (1982) proposed that these spherical symmetric clusters, connected by small transport tubes, could be used to describe the flux of ions through Nafion. The polymeric charges are most likely embedded in the solution near the interface between the electrolyte and the fluorocarbon backbone. This interaction minimises both the hydrophobic interaction of water with the backbone and the electrostatic repulsion of adjacent sulphonate groups. These hydrated ionic clusters determine the electrochemical properties of the polymer. Figure 1.1 shows the proposed structure of

the cluster-network model for Nafion perfluorinated membranes (Gierke and Hsu, 1982).

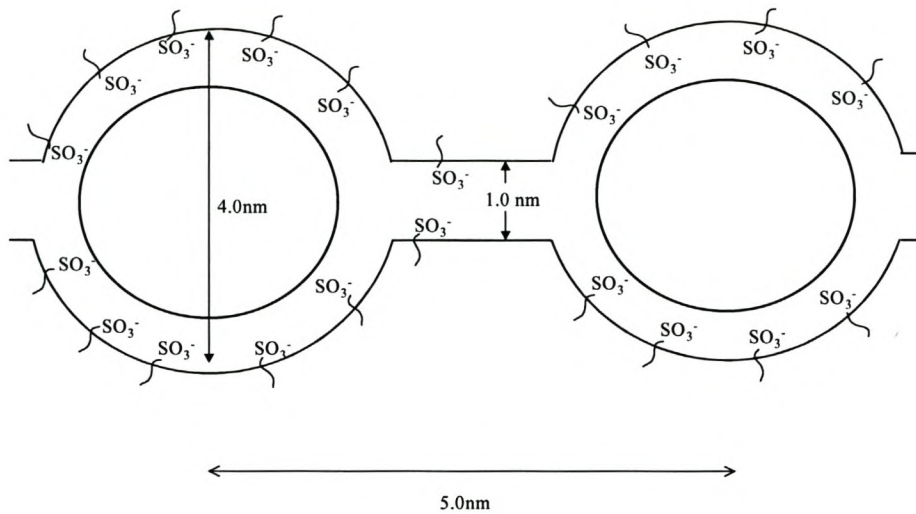


Figure 1.1. Proposed cluster-network model for Nafion perfluorinated membranes (Gierke and Hsu, 1982).

The function of the fluorocarbon phase is to prevent the ionic phase from dissolving. However, at temperatures higher than 200°C these restraining forces are weakened, and the fluorocarbon phase melts and permits the ionic phase to dissolve in a mixture of alcohol and water. This phase inversion is represented in Fig. 1.2 (Du Pont information brochure).

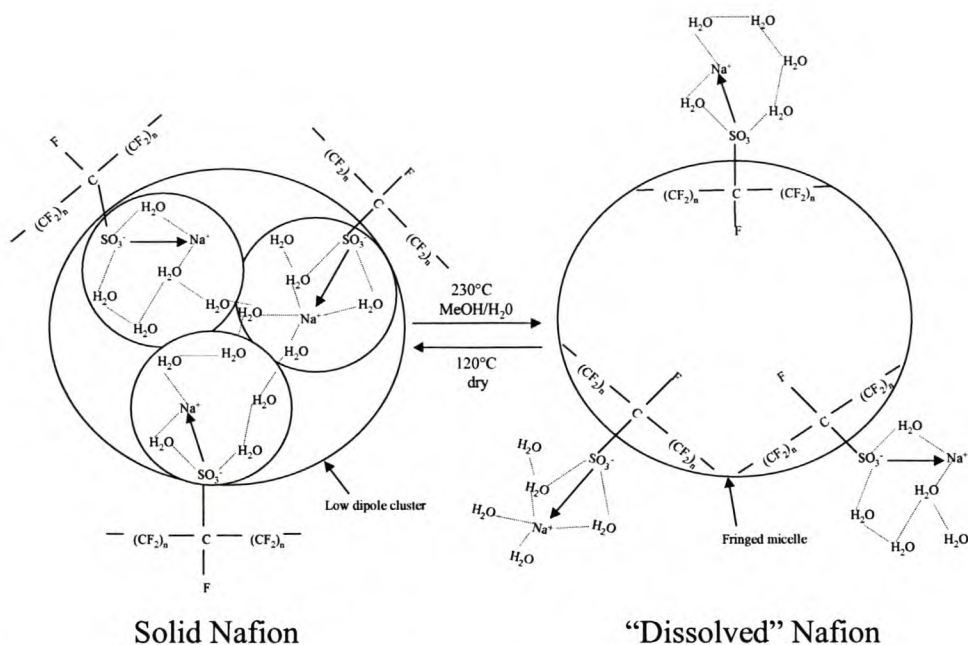


Figure 1.2. Schematic representation of the phase inversion of Nafion (Du Pont information release).

1.3.2. Properties

Ion-exchange polymers have many ionisable groups in their polymeric structures. One ionic component of these groups is fixed into or retained by the polymeric matrix whereas the other ionic component is a mobile, replaceable ion. The ability of these mobile ions to be replaced under appropriate conditions by other ions imparts ion-exchange characteristics to these materials (Table 1.2). It is for this reason that ion-exchange membranes are outstanding separators for use in electrochemical cells. They are permeable to one species of ion but resist the passage of ions of opposite charge (Heitner-Wirguin, 1996).

Chemically, Nafion is quite unreactive. It is stable in strong bases, strong oxidising and reducing acids, chlorine, oxygen, hydrogen and hydrogen peroxide, at temperatures of up to 125°C. The thermal stability of Nafion is excellent at temperatures of 200°C and higher, as evidenced by its glass-transition temperature being higher than its respective non-fluorinated analogues (Liu et al., 1992).

Since Nafion has high proton conductivity, it can be used at elevated temperatures to increase efficiency of proton-conducting devices (e.g., fuel cells). Nafion has good mechanical and structural strength in corrosive and oxidising environments (Liu et al., 1992).

Table 1.2. *Physical and chemical properties of Nafion-120 membranes at 25°C (Eisenberg and Yeager, 1982).*

Equivalent weight (EW) ²	1200
Ion exchange capacity ³	0.83 meq/g dry polymer
Ionic (H ₃ O ⁺) resistance	0.46 Ω cm ²
Tensile at break	2500 psi
Elongation at break	150 %
Mullen burst strength	150 psi
H ₂ permeability	5.6x10 ⁻⁴ cm ³ cm/cm ² .hr.atm
O ₂ permeability	3.0x10 ⁻⁴ cm ³ cm/cm ² .hr.atm
H ₂ O permeability	2.7x10 ⁻⁵ cm ³ cm/cm ² .hr.atm

1.3.3. Applications

One can distinguish between two types of applications based on SPE membranes, namely:

1. the traditional applications without the use of catalytic metal impregnated into the surface of SPE membranes, and
2. applications based on SPE with an embedded catalytic metal (e.g. Pt or Pd)

Here the focus is on traditional, but industrially important SPE systems, such as those used for chlorine production and chromic acid regeneration (Eisenberg and Yeager, 1982).

1.3.3.1. Chloralkali cells

In recent years, a number of electrolytic processes have used membranes to produce both anodic and cathodic products. The most important application of this technology has been in the chloralkali industry. Ion-exchange membranes for use in chloralkali processes should have the following properties:

- chemical stability
- physical stability

² EW is defined as the weight of acid polymer which neutralises one equivalent of base.

- uniform strength and flexibility
- high current efficiency
- low electric resistance
- low electrolyte diffusion

Perfluorinated ionomer membranes suitable for chloralkali processes are classified by the chemical structure of the ion-exchange group, number and type of membrane layers and polymer structure. The following types of ion-exchange membranes have been reported (Kirsh et al., 1990), namely those with a:

- sulphonic acid group $-\text{SO}_3\text{H}$
- sulphonamide group $-\text{SO}_2\text{NHR}$
- carboxylic acid group $-\text{COOH}$
- phosphoric acid group $-\text{PO}_3\text{H}_2$
- quaternary alcohol group $-\text{C-OH}$

Membranes that are currently used, which contain either a sulphonic acid, sulphonamide, carboxylic acid or both a carboxylic acid and a sulphonic acid group, have been tabulated in Table 1.3 (section 1.2).

³ IEC is defined as $\text{IEC} = 1000/\text{EW}$. IEC is expressed in milliequivalents per gram of dry H^+ form polymer.

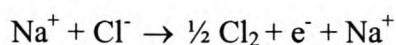
Table 1.3. Membrane properties of perfluorinated ionomers classified by ion-exchange group and membrane structure (Eisenberg and Yeager, 1982).

Ion-exchange group	R _f .SO ₃ H	R _f -SO ₂ NHR	R _f -COOH	R _f -COOH/ R _f -SO ₃ H
Hydrophilicity	high	very low	low	low/high
Water content	high	very low	low	low/high
Electric resistance	low	very high	high	low
Chemical stability	very high	low	high	high
Neutralisation of OH ⁻ by HCl	applicable	impossible	impossible	applicable
O ₂ in product Cl ₂	<0.5%	>2%	>2%	<0.5%
Current density	high	low	low	high

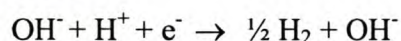
The industrial applications of chlor-alkali electrochemistry are found in the production of chlorine, caustic soda and potash, hydrogen and hypochlorite. The three general types of chlor-alkali electrolyzers in use today are mercury, diaphragm and membrane cells (Eisenberg and Yeager, 1982).

Metal anodes and fluorinated ion exchange membranes are used as separators in membrane cells to produce high quality caustic and chlorine in a two-chambered cell. Chlorine, with low oxygen content, is discharged from the anode in a relatively pure form. Pure hydrogen is evolved at the cathode and is separated from the chlorine by the ion-exchange membrane. The cation permselectivity of the membrane permits the passage of positively charged sodium ions and water, while simultaneously rejecting the passage of negatively charged ions, such as chloride (Cl⁻) and hydroxyl ions (OH⁻) in both directions. The electrode reactions are:

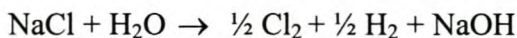
Anode:



Cathode:



Overall reaction:

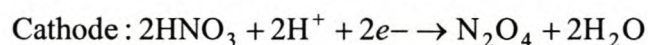
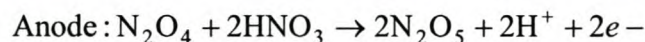


1.3.3.2. Chromic acid regeneration

The regeneration of chromic acid solutions is possible because of Nafion's excellent chemical stability. Chromic acid must be regenerated after it has been used in the oxidation of an organic material, for example in the etching of plastic parts prior to metallising. The solution that must be regenerated to chromic acid contains trivalent chromium (Cr^{3+}) and sulphuric acid. Cr^{3+} is readily converted to chromic acid by anodic oxidation. Other cations are removed by electro dialysis through the membrane.

1.3.3.3. Synthesis of dinitrogen pentoxide

In the synthesis of dinitrogen pentoxide, the versatility of the ion-exchange membrane is demonstrated by the transport of N_2O_4 and H_2O under severe oxidising conditions (Fig. 1.3). The following reactions occur in the synthesis of dinitrogen pentoxide (Scott and Hughes, 1996):



The N_2O_4 generated at the cathode assists in the splitting of nitric acid into N_2O_5 and H_2O (Scott and Hughes, 1996). The water that is formed is separated from the anolyte by the membrane. Since water present in the anolyte will be converted to nitric acid, the product formed at the cathode must first be purified of water before it is fed to the anode (Scott and Hughes, 1996).

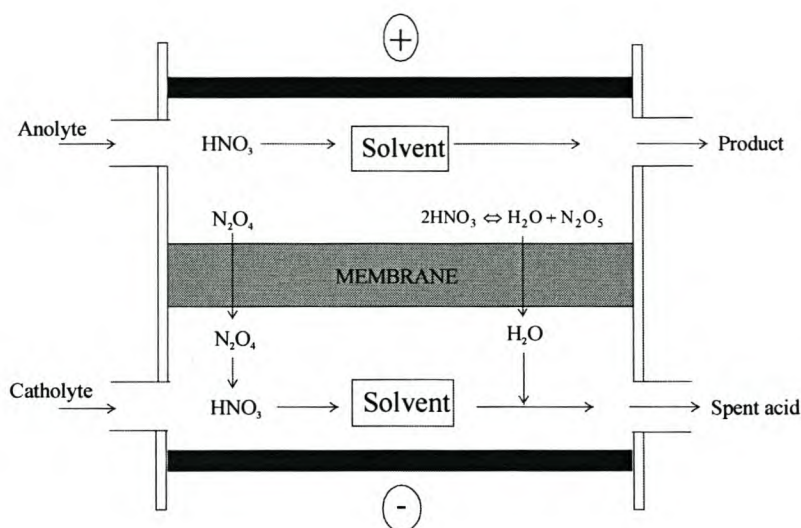


Figure 1.3. Schematic representation of the synthesis of dinitrogen pentoxide with SPE-based membrane technology (Scott and Hughes, 1996)

1.3.4. Advantages and disadvantages of using Nafion as a SPE

Nafion is used widely as an ion-exchange membrane because of the many advantages it offers over other electrolytes (Holze et al., 1992). Nafion, as an electrolyte, is preferred to aqueous solutions, molten salts and solid oxides, because all electrolytes other than Nafion must be operated at significantly elevated temperatures. Nafion can be used at pressures of up to 30 bar because of its mechanical stability. Nafion can therefore be used in processes that require considerable pressure.

SPE materials offer many advantages, namely:

- significantly higher electrochemical efficiency compared with conventional electrochemical devices at comparable current densities, which result in lower power consumption per unit of a chemical processed;
- higher current density capability that results in lower capital costs, and size and weight of the electrochemical modules;
- chemical binding of an electrolyte in a polymer chain, offering a system that requires no corrosive liquids in the design, assembly, operation or maintenance of the system.

Although the use of Nafion offers many advantages, there are disadvantages related to using Nafion as an ion-exchange membrane. The relatively high cost of perfluorinated

membranes limit their application when cost effectiveness is a concern. Nafion can sorb relatively large amounts of water and other solvents. The high water sorption results in a decrease in the electric resistance and tensile strength of Nafion (Eisenberg and Yeager, 1982).

Nafion has many applications, but its wide field of application is further increased when the membrane is metallised on one or both sides. Applications for these membranes include fuel cell technology, electrosynthesis and generators of oxygen and hydrogen, which will be discussed in Section 1.5.3. The techniques used for depositing a metal on Nafion are discussed in the following section.

1.4. Techniques for deposition of platinum catalyst on Nafion membranes

1.4.1. Mechanical deposition

Lawrence et al. (1981) used a mechanical deposition method to prepare an electrocatalytic membrane. The metal catalyst was deposited upon a roughened or abraded membrane surface and fixed to it by pressure or heat.

White et al. (1982) prepared a solid polymer electrolyte by co-depositing catalyst particles and a hydrophilic, thermoplastic ion-exchange material onto a solid polymer electrolyte permionic membrane. By this method, the application of the electrocatalyst particles to the thermoplastic, hydrophilic resin and the application of the hydrophilic resin and electrocatalyst particles to the membrane surface are carried out at elevated temperature and pressure. The temperature and pressure are maintained until the electrocatalyst particles are set in the resin and the resin and catalyst particles are able to adhere to the membrane.

Similar work by Watanabe et al. (1993) involved impregnating catalyst particles into an ion exchange membrane using an ion-exchange resin. A sheet-like catalyst layer is formed by means of hot-pressing or cold-pressing the resin. The catalyst layer is then thermally bonded to the ion-exchange membrane under pressure.

1.4.2. Electroless deposition

Electroless deposition is an autocatalytic method of metal deposition without a supply of external electrons. The composition and role of the components in a typical electroless deposition bath are given in Table 1.4.

Table 1.4. *Composition and purpose of components in a typical electroless-deposition bath (Okinaka et al., 1990).*

Component	Purpose
Metal salt	source of metal deposit
Reducing agent	reduction of metal ions
pH adjuster	pH adjustment
Complexing agent	form metal complex
Additives	improve the bath stability or the properties of the deposit

A characteristic aspect of the electroless-deposition bath is that it requires one of a number of reducing agents such as hydrazine, borohydride and dialkylamine borane. Although electroless deposition is very costly (compared to electrolytic deposition), its wide use is attributed to its many advantages, which include:

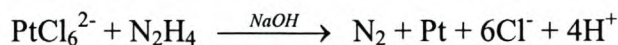
- uniform metal deposition thickness can be obtained on a substrate of any shape;
- strong adhesive bonding between metal film and substrate can be obtained;
- dense non-porous films can be obtained.

The counter diffusion deposition method (section 1.4.2.1) and the impregnation-reduction method (section 1.4.2.2) are both electroless deposition methods and will be discussed further below.

1.4.2.1. Counter diffusion deposition (Takenaka-Torikai method)

Takenaka et al. (1982) developed a method for depositing noble metals and their alloys onto a solid polymer electrolyte. This method did not involve the use of a binder or attempt to attach the metal directly to the solid polymer electrolyte. In counter diffusion deposition process, one-side of the cationic-exchange membrane is

in contact with the reducing agent, while the other is in contact with an anionic metal-ion solution (e.g., platinumic acid solution). The metal-ion solution is reduced by the reducing agent, resulting in a layer of the metal being deposited on the membrane surface (Fig. 1.4). The chemical reaction for the counter diffusion deposition process can be represented as follows (Bessarabov et al., 1997):



It is possible to deposit the metal on the other free surface of the membrane by the same procedure. Since the metal layer formed on the membrane has a microscopically porous structure, the reducing agent can diffuse through the metal layer and the membrane to reduce the metal-ion solution. This chemical deposition process was modified by Fedkiw et al. (1989) and is discussed in section 1.4.2.2.

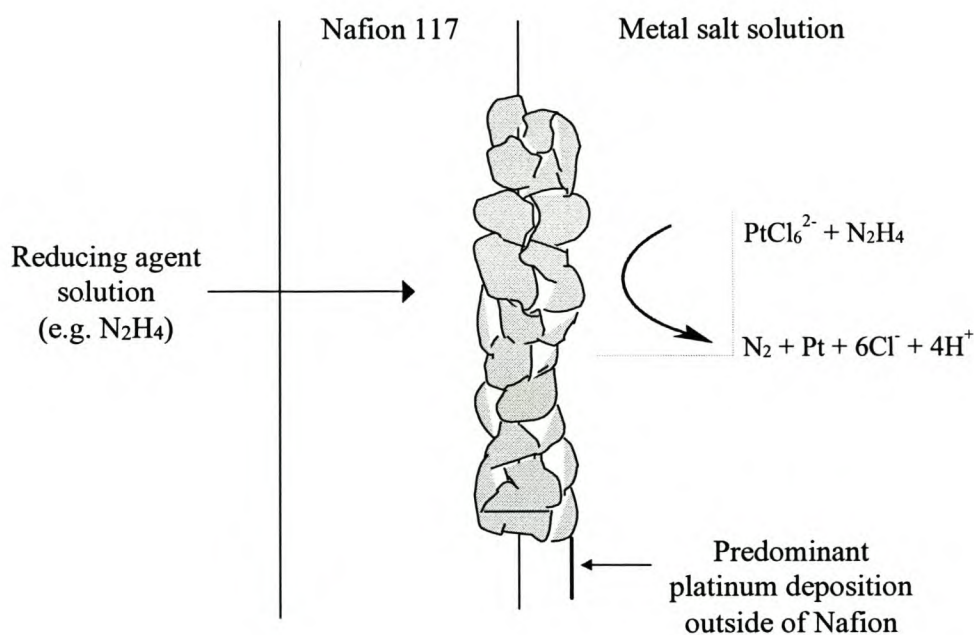


Figure 1.4. The principle of metal deposition using counter diffusion method, in which one surface of the membrane is in contact with an anionic metal ion solution, while the other is in contact with a reducing agent (Enea, 1995).

1.4.2.2. *Impregnation reduction deposition (Fedkiw and Her method)*

The impregnation-reduction method of Fedkiw and Her is a two-step procedure that involves the impregnation (ion-exchange) of a solid polymer electrolyte with a cationic metal complex, followed by the reduction of the cationic metal complex (Fedkiw et al., 1989). Fedkiw et al. (1989) impregnated (ion-exchanged) Nafion with $\text{Pt}(\text{NH}_3)_4\text{Cl}_2$ before reducing the metal salt with the reducing agent, NaBH_4 .

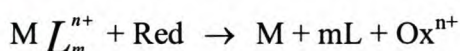
The advantage of using this method compared with the Takenaka-Torikai method is that greater deposition of platinum within the solid polymer electrolyte can be achieved (Enea, 1995). Fedkiw (1990) also showed that greater depth of platinum particles within the solid polymer electrolyte could be achieved with increasing time of impregnation.

1.4.3. General mechanisms of electroless-deposition reactions

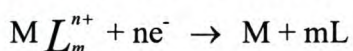
1.4.3.1. *Mixed-potential concept*

The cathodic and anodic partial reactions of electroless deposition reactions occur on the same substrate surface simultaneously. The potential of the electroless deposition, which is known as the mixed potential, is determined by anodic and cathodic partial reactions. These reactions are as follows (Okinaka et. al., 1990):

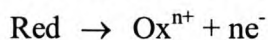
Overall reaction:



Cathodic partial reaction:



Anodic partial reaction:



The deposition rate of an electroless-deposition system is determined by the catalytic activity of the metal to be deposited. This activity affects the anodic oxidation of the reducing agent. Ohno et al. (1985) investigated the catalytic activity of metals for the anodic oxidation of different reducing agents in the electroless deposition process by evaluating the potentials at a reference current density. In Figure 1.5 the metals are

listed in decreasing order of catalytic activity for the anodic oxidation of each reducing agent (Ohno et al., 1985).

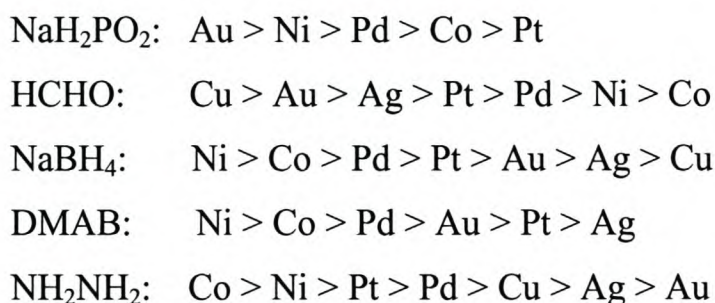


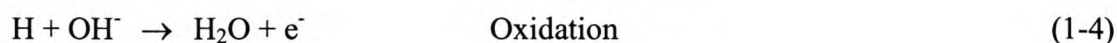
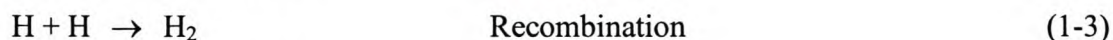
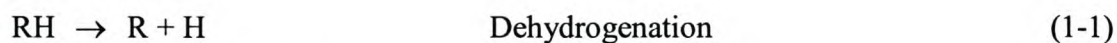
Figure 1.5. *Catalytic activities of metals during anodic oxidation of different reducing agents listed in decreasing order of catalytic activity (Ohno et al., 1985).*

It can be seen that the catalytic activity of a metal varies according to the nature of the reducing agents. This information can be used to choose a suitable reducing agent for the deposition of a particular metal.

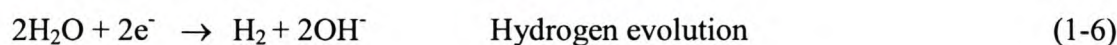
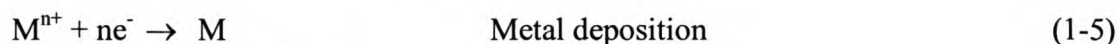
1.4.3.2. Unified mechanism of electroless deposition

Various mechanisms of different electroless deposition reactions with different reducing agents have been proposed. These mechanisms can explain most characteristics of the electroless solutions, but cannot describe electroless processes in general (Okinaka et al., 1990). Since all electroless processes are very similar, Van den Meerakker (1980) was able to propose a unified mechanism for all electroless systems, as follows:

Anodic:



Cathodic:



RH represents the reducing agent that dissociates to form the radical R and the atomic H upon adsorption at the surface of the deposited metal (1-1). The metal ions are reduced to the metal by electrons generated by R (1-2). Gaseous hydrogen results from the recombination of adsorbed atomic hydrogen, which is produced by the reducing agent (1-3). Gaseous hydrogen is formed cathodically (1-6).

The proposed mechanism confirms the validity of the mixed-potential theory, the catalytic nature and the high activation energy of the electroless processes. It also explains the influence of pH on the deposition rate.

1.5. Electrocatalytic syntheses using solid polymer electrolyte (SPE)-based membrane catalytic systems

1.5.1. Advantages of using SPE in catalytic membrane systems

There is an increasing interest in using SPE-based catalytic systems due to their many advantages, namely:

- embedded heterogeneous catalyst system offers a system that is free of corrosive liquids,
- sites of reduction and oxidation occur on the solid polymer electrolyte,
- no liquid electrolyte is required with the use of solid polymer electrolytes,
- less side reactions, which improves the purity of the product,
- proton-exchange membrane is the H⁺-conducting element, and
- catalytic reactions occur in the gaseous phase so separation of products and catalyst can easily be achieved.

The many advantages offered by solid polymer electrolytes justify their use in catalytic systems above those systems that rely on supporting electrolytes.

1.5.2. Generation of hydrogen and oxygen

Electrolysis of water can be achieved with the use of a suitable catalyst. During water electrolysis, oxygen is released at the anode side of the membrane and hydrogen at the cathode side of the membrane (Fig. 1.6). A solid polymer electrolyte acts as a proton-conducting material by allowing the diffusion of hydroxonium ions to the cathode to be discharged as hydrogen gas (Bessarabov, 1998; Nutall, 1977).

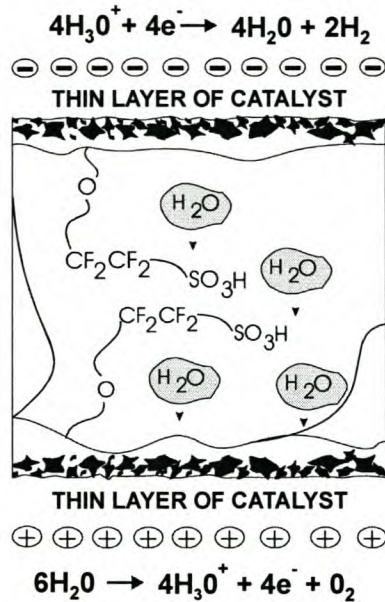


Figure 1.6. Schematic representation of Nafion embedded with a catalyst for the electrolysis of water (Bessarabov, 1998).

1.5.2.1. Examples of recent industrial applications

The ES Series of hydrogen generation systems of Hamilton Sundstrand represent a proven method in hydrogen production by water electrolysis (www.hsssi.com/Applications/Echem/Oxygen). The ES Series SPE water electrolysis cell offers on-site hydrogen generation without the danger of large volumes of stored high pressure hydrogen. This is because hydrogen is only produced as it is consumed.

The oxygen generating plant of Hamilton Sundstrand uses a proton exchange membrane (PEM)-based electrolyser to convert water into oxygen and hydrogen. This plant is used in nuclear submarines. The oxygen is generated at high pressure and regulated to a low pressure for the respiration of the crew on the nuclear submarine (www.hsssi.com/Applications/Echem/Oxygen).

1.5.3. Fuel cell technology

A fuel cell converts latent chemical energy into electricity when hydrogen and oxygen combine to form water. The important factor of a fuel cell is the SPE-based membrane with a suitable catalyst, such as platinum, palladium or iridium. Fuel cells have many possible applications, such as military power sources, in cars and space technology (Bessarabov, 1998).

1.5.3.1. Examples of recent industrial applications

Lynntech Inc (USA) has done extensive research and development in both hydrogen and methanol fuelled proton exchange membrane fuel cells (www.lynnotech.com/licensing/pem_fuelcell/index.shtml).

1.5.4. Generation of ozone

Ozone is playing an increasingly important role as an environmentally clean oxidant in water treatment, food processing, medical hygiene and several other processes in chemical and pulp industries. Ozone kills bacteria, decomposes organic molecules and removes coloration from aqueous systems (Bessarabov, 1998). Ozone does not result in harmful residues, as is the case when chlorine is used (Stucki et al., 1985).

Electrochemical SPE-based ozone generation can be achieved by the electrolysis of water. Stucki et al. (1985) investigated the application of solid polymer electrolyte with PbO₂ anodes for the anodic generation of ozone in electrolyte-free water. The excellent stability and performance of the cell are correlated with properties of the membrane and its interface with the anode (Stucki et al., 1985).

Tatapudi et al. (1993) was able to oxidise deionised water to ozone and oxygen at the anode in a proton exchange membrane electrochemical flow reactor. The optimum conditions for ozone generation were determined as a function of the applied voltage, electrode materials, catalyst loadings and reactant flow rates. Tatapudi et al. (1994) explored the simultaneous synthesis of ozone and hydrogen peroxide in a proton exchange membrane electrochemical flow reactor. The deionised water was oxidised at the anode while oxygen was reduced to hydrogen peroxide at the cathode. The research methodology for the paired synthesis was split into four reaction systems namely (Tatapudi et al., 1994):

- oxygen evolution at the anode and hydrogen evolution at the cathode (water electrolysis);
- ozone and oxygen evolution at the anode, and hydrogen evolution at the cathode;
- oxygen reduction at the cathode (hydrogen peroxide synthesis) and oxygen evolution at the anode; and
- simultaneous synthesis of ozone and hydrogen peroxide.

Tatapudi et al. (1994) obtained low ozone current efficiencies at high applied potentials. These low current efficiencies and high operating potentials for ozone evolution make the process uneconomical. Higher current efficiencies can be obtained through improvements in the electrode structure and cell design. Gold, activated carbon, carbon black and graphite were investigated as electrocatalysts for the synthesis of hydrogen peroxide and lead dioxide for ozone evolution (Tatapudi et al., 1994).

1.5.4.1. Examples of recent industrial applications

Water is split into hydrogen and oxygen atoms (Fig. 1.7). Hydrogen molecules are separated from the gas/water mixture and the oxygen is combined to form ozone (O_3) and diatomic oxygen (O_2) (www.lynnotech.com/licensing/ozone/index.shtml).

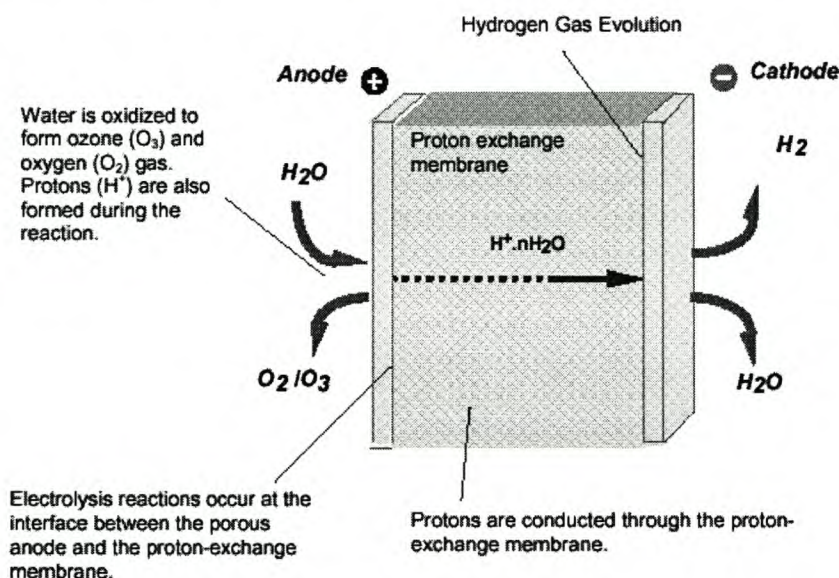


Figure 1.7. Schematic representation of the production of ozone using SPE technology (www.lynnotech.com/licensing/ozone/index.shtml)

The D-ozone generator of Cyclopss produces a continuous supply of highly concentrated ozonised water by an electrolytic process. No additional equipment, as required in ozone gas dissolving methods, is required (www.cyclopss.com/dozone.html). Tap water is passed through a pre-treatment unit that removes chlorine and organic matter and treats the water before it is introduced to the D-Ozone generator. A precious metal catalyst is used in the generator to ensure that clean ozonized water is provided (www.cyclopss.com/dozone.html).

It is possible to produce ozone from demineralised water for applications that require small quantities of ozone (www.ozonia.ch/products/membrel.htm). The demineralised water is electrolytically dissociated using an ion-exchange membrane, as the electrolyte and the ozone generated is simultaneously dissolved in water. The advantages of producing ozone with an electrolytic system, such as Membrel® electrolytic ozone generation systems, are (www.ozonia.ch/products/membrel.htm):

- there is no ionic contamination
- the ozone is dissolved in the process water as soon as it is formed

1.5.5. Separation of isotopes: hydrogen and deuterium

Hydrogen and deuterium can be separated by an SPE electrocatalytic membrane system (Bessarabov, 1998).

1.5.6. Water treatment using SPE membrane electrocatalytic systems

The advantages of SPE technology can be extended to water treatment, which include (Bessarabov, 1998):

- high contaminant removal,
- reduced fouling,
- the ability to treat a wide range of feeds polluted with organics, and
- the electrocatalytic elimination of nitrates.

Grimm et al. (2000) explored the anodic oxidation of hazardous organics in water with Sb-doped SnO₂ anodes coupled with a perfluorinated cation-exchange membrane system. Phenol was used as a standard contaminant. Results showed that the concentration of phenol could be reduced during galvanostatic electrolysis (Grimm et al., 2000).

1.5.7. Hydrogen absorber

An SPE system can be used for the highly selective removal and purification of hydrogen from gaseous mixtures. By the correct selection of catalyst and current density the selective transfer of protons to the cathode side of a membrane, to produce hydrogen gas through the reduction process, can be achieved (Bessarabov, 1998).

1.5.8. Electroinduced membrane gas separation

Bessarabov et al. (1997; 1998) explored a novel technique to effect electroinduced facilitated transport of neutral molecules in ion-exchange membranes. Their results showed that by applying an electric current to a platinum coated Nafion membrane in the $\text{Cu}^{2+}/\text{Cu}^+$ form, the permeability of ethylene increased 6-fold as compared to the permeability of the initial platinum-coated membrane without current.

1.5.9. Oxidation of cyclohexanol to cyclohexanone

Indirect electroorganic syntheses with mediatory systems have been used to oxidise primary and secondary alcohols to esters and ketones (Ogumi et al., 1985). Combining SPE and mediatory systems provide opportunities for the electrolysis of organic substances. Ogumi et al. (1985) used the oxidation of cyclohexanol to cyclohexanone to examine the feasibility of mediatory systems with SPE catalytic systems (Fig. 1.8). Iodine and potassium iodide were used as mediators to accelerate the oxidation of cyclohexanol and to improve the reaction efficiency for the oxidation of cyclohexanol. Unipositive iodine species, I^+ , produced on the anode of the SPE catalytic system reacts with cyclohexanol to form cyclohexanone, iodide ions and protons. The protons migrate to the cathode to form hydrogen gas. The iodide ion reacts at the anode of the SPE catalytic system to regenerate I^+ (Fig. 1.8) (Ogumi et al., 1985). The unipositive iodine is considered to be the oxidant in the mediatory system.

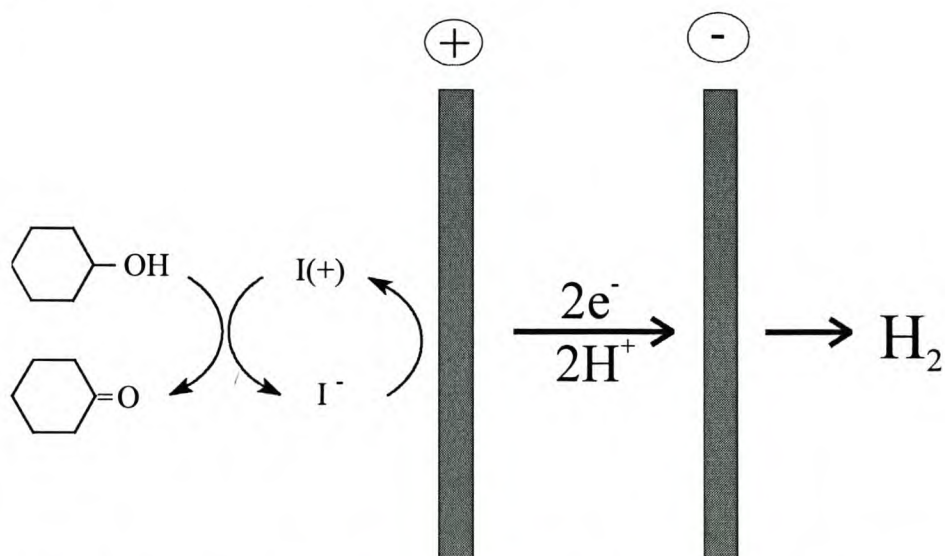
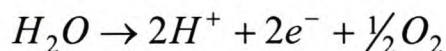


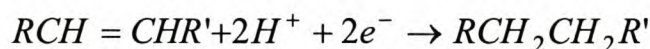
Figure 1.8. The oxidation of cyclohexanol to cyclohexanone using platinum-SPE in the presence of mediators (Ogumi et al., 1985).

1.5.10. Electrochemical hydrogenation of olefinic double bonds

The hydrogenation of olefinic double bonds occurs in a cell that is divided by a SPE cationic membrane (Fig. 1.9) (Ogumi et al., 1981). Electrocatalytic metal electrodes are deposited on each side of the cationic membrane. The water in the anodic compartment reacts electrochemically to produce oxygen gas and protons according to (Ogumi et al., 1981):



The protons migrate through the SPE cationic membrane to the cathode. The protons electrochemically hydrogenate the olefin in the catholyte as follows (Ogumi et al., 1981):



The overall reaction of the hydrogenation of the olefin can be represented as follows (Ogumi et al., 1981):

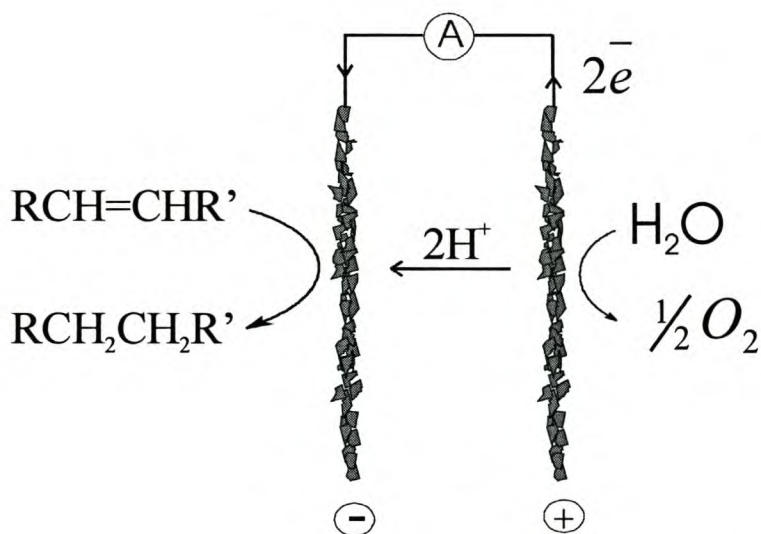
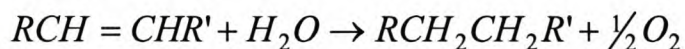


Figure 1.9. The electrochemical hydrogenation of olefinic double bonds, without the use of supporting electrolytes, can be achieved with a cationic membrane with electrocatalytic metal electrodes on each side of the membrane (Ogumi et al., 1981).

The olefinic double bonds of cyclo-octene, α -methyl styrene and diethyl maleate were electrochemically hydrogenated on SPE composite electrodes in *n*-hexane. Au-SPE, Au-Pt-SPE, Pt-SPE and Pt-Au-SPE composite electrodes were used in the

hydrogenation of olefins. The catalytic activity of gold for hydrogenation is very low, while it is high for platinum (Ogumi et al., 1981) Low current efficiencies for the hydrogenation of olefinic bonds was obtained with Au-SPE and Au-Pt-SPE, as compared with higher current efficiencies obtained with Pt-SPE and Pt-Au-SPE (Ogumi et al., 1981). In the case of Au-SPE and Au-Pt-SPE, gold is in contact with the solution containing the olefin, which results in a low reaction efficiency (Ogumi et al., 1981). In the case of Pt-SPE and Pt-Au-SPE, catalytically active platinum is in contact with the solution containing the olefin, which results in higher reaction efficiencies (Ogumi et al., 1981). Ogumi et al. (1981) suggests that the hydrogenation of the olefin occurs on the olefin solution side of the SPE composite, as opposed to inside the SPE membrane (Fig. 1.10).

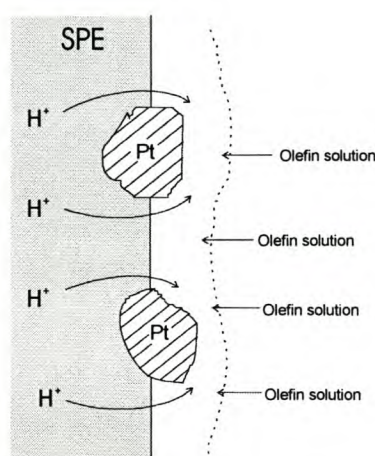
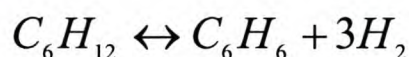


Figure 1.10. Schematic model of the electrochemical hydrogenation of olefinic compounds on a SPE composite (Ogumi et al., 1981)

1.5.11. Electrochemical coupling of SPE-based water electrolysis and benzene hydrogenation

Gaseous hydrogen, produced by water electrolysis, can be stored by being transformed to liquid hydrogen or liquid chemical carriers (Itoh et al., 2000). Examples of chemical hydrogen carriers are cyclohexane, methylcyclohexane, ammonia and methanol. These liquid chemical carriers can evolve hydrogen, as shown by the following reversible reaction for the hydrogenation of benzene to form cyclohexane (Itoh et al., 2000):



The hydrogenation of benzene, within a polymer electrolyte cell, was achieved with the combination of water electrolysis and the hydrogenation process (Fig. 1.11) (Itoh et al., 2000). This direct hydrogenation of benzene is more efficient as the hydrogen generated at the cathode, produced during water electrolysis, can be utilised in-situ.

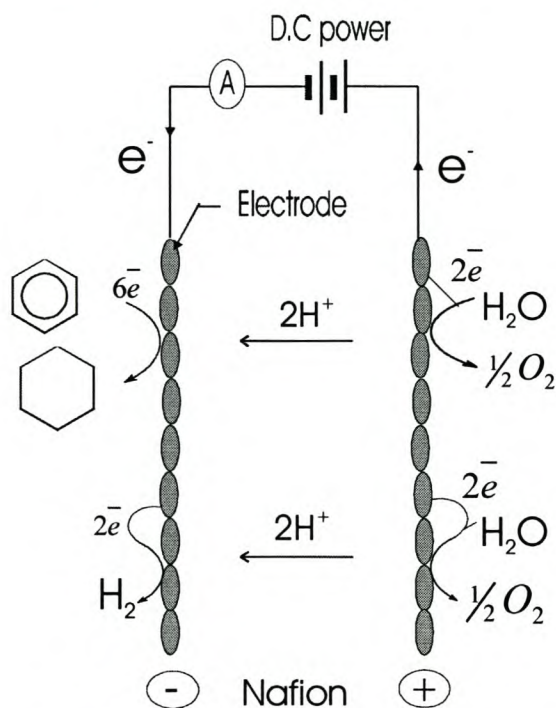
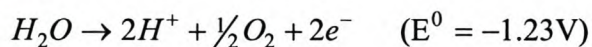


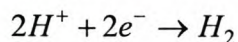
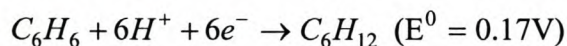
Figure 1.11. Hydrogenation of benzene by the electrolysis of water, using solid polymer electrolyte (Itoh et al., 2000).

The hydrogenation of benzene through the electrolysis of water using a solid polymer electrolyte, can be represented as follows (Itoh et al., 2000):

Anode



Cathode

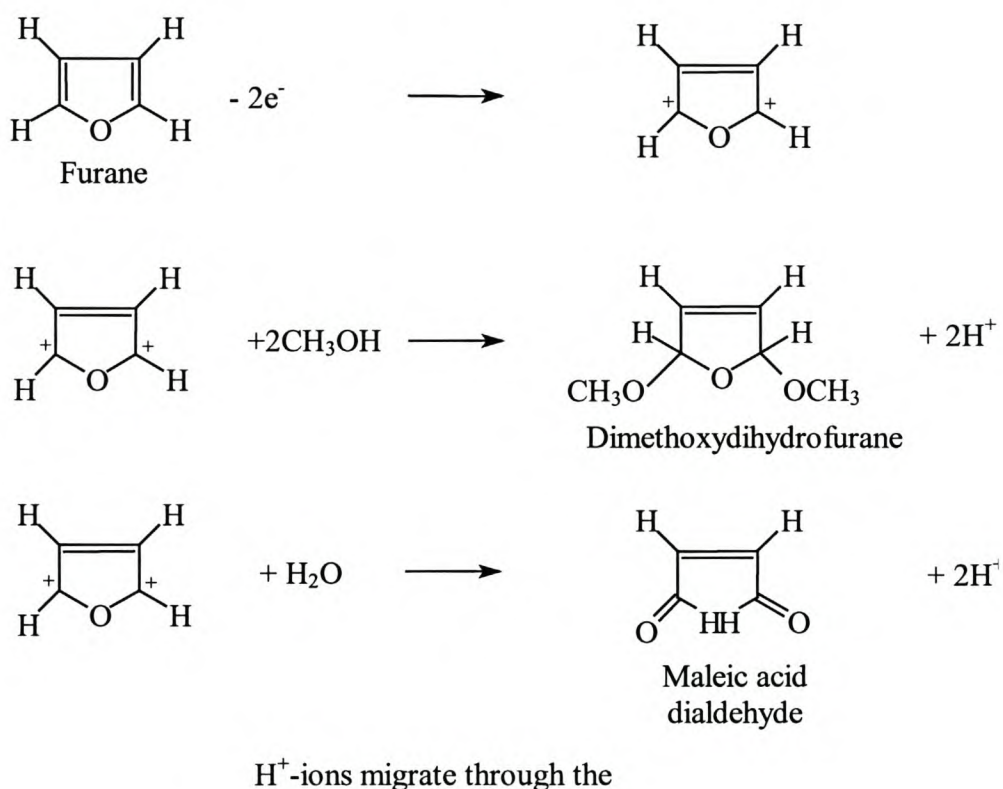


It was found that the Rh-Pt electrode is more active for the electrochemical hydrogenation of benzene than the Pt electrode is.

1.5.12. Methoxylation of furane

The conventional process for the anodic methoxylation of furane uses bromide as a mediator and supporting electrolyte. The methoxylation of furane is possible using Nafion cation-exchange membranes and Pt/Ir gauze anodes without supporting electrolyte (Fig. 1.12) (Jörissen, 1996). High current efficiencies of the product dimethoxy-dihydrofurane were achieved, but at high cell voltages (up to 50 V). Jörissen (1996) found that when using bromides as a mediator, high current efficiencies were obtained when the hydrogen bromide produced at the anode was instantly neutralised at the cathode by powerful mixing. However, when using SPE, high product concentrations can be achieved without a decrease of the current efficiency when using SPE (Jörissen, 1996).

Anode:



Cathode:

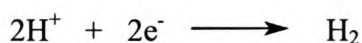
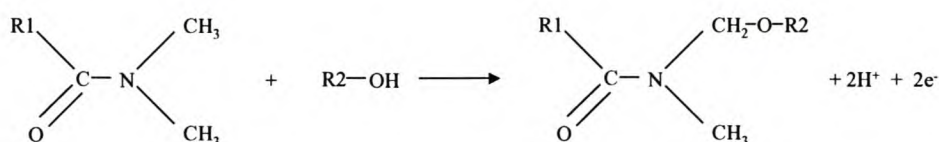


Figure 1.12. Proposed reaction of the methoxylation of furane using a SPE (Behr et al., 1997).

1.5.13. Alkoxylation of N-alkyl-amides

Jörissen (1996) showed that the alkoxylation of N-alkyl-amides with SPE could be achieved at low cell voltages, nearly 100% current efficiencies and selectivity of 30% amide conversion, and without additives.

The results of several alkoxylation reactions of N-alkylamides using Nafion cation exchange membranes in a non-aqueous medium are shown in Fig. 1.13 (Jörissen, 1996). Improved current efficiencies and cell voltages were obtained when using SPE as compared with the conventional butylammonium tetrafluoroborate supporting electrolyses (Jörissen, 1996).



Reactant	R1/R2	°C	Volt	Current efficiency	Conversion
Dimethylformamide (DMF) + methanol	H/CH ₃	60	5	98%	15%
Dimethylformamide (DMF) + isopropanol	H/CH(CH ₃) ₂	80	4	95%	10%
Dimethylacetamide + methanol	CH ₃ /CH ₃	80	6	98%	10%
N-methyl-2-pyrrolidinone + methanol		60	7	90%	10%

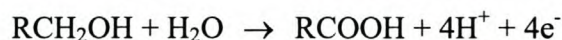
Figure 1.13. Several alkoxylation reactions of N-alkyl-amides using Nafion cation-exchange membranes in a non-aqueous medium⁴ (Jörissen, 1996).

1.5.14. Oxidation of alcohols

The electrode reactions for the oxidation of alcohols (e.g., 2-propanol and 2-propyne-1-ol) occur at electro-catalytic layers of the interfaces between the membrane and the permeable electrodes (Fig. 1.14) (Jörissen, 1996). These reactions are shown as:

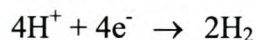
⁴ In the non-aqueous medium, the alcohol and amide reactants simultaneously act as the solvent.

Anode:



H^+ ions migrate through the membrane.

Cathode:



Hydrogen ions are formed at the anode during oxidation and migrate through the cation-exchange membrane together with a solvation shell of solvents, reactants and products (Jörissen, 1996).

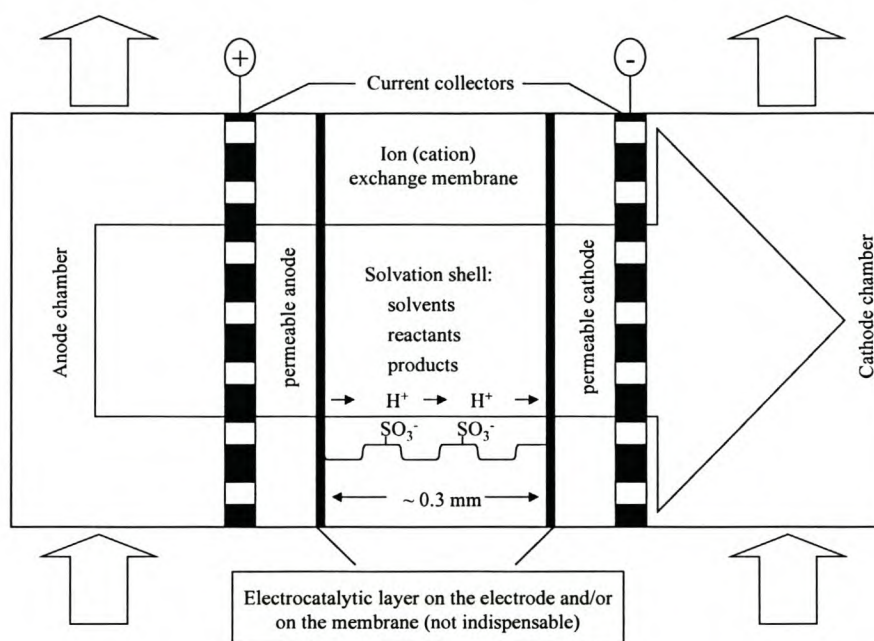
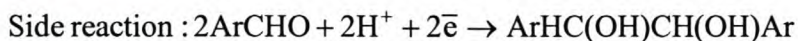
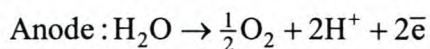


Figure 1.14. An SPE cell for the anodic oxidation of alcohol using a cation-exchange membrane (Jörissen, 1996).

Simond et al. (1997) investigated the anodic oxidation of methanol, ethanol, propanol and isopropanol in pure water using a Nafion cation-exchange membrane as a solid polymer electrolyte. The oxidation was carried out on an IrO_2 anode under conditions of simultaneous oxygen evolution (Simond et al., 1997a).

1.5.15. Electrochemical reduction of benzaldehyde

Chen et al. (1993) attempted the electrochemical reduction of benzaldehyde to benzyl alcohol. The mechanism of benzaldehyde reduction is as follows:



Chen et al. (1993) showed that the current efficiencies of benzyl alcohol production at various SPE electrodes decreased in the order of Pt+Pb-Nafion>Pb-Nafion>Ni-Nafion>Cu-Nafion>Ag+Cu-Nafion>Ag-Nafion>Pt-Nafion.

1.6. Current trends in research using SPE-based membrane catalytic systems

Due to the high cost of noble metals usually used in SPE-based membrane catalytic systems, it is important to achieve low catalyst loadings on the membranes for SPE technology to be economically viable. Thus, current trends in research are aimed at achieving the optimisation of a metal catalyst on a membrane and its chemical modification. Morphological and chemical optimisation methods used for achieving optimal catalyst loading on a cation-exchange membranes are described in this section.

1.6.1. Methods to optimise the morphology of the platinum catalyst

Various methods of achieving maximum catalytic activity of platinum catalyst with optimal catalyst loading on the membrane have been investigated (Fedkiw et al., 1990). The morphology of the platinum catalyst (size, shape, particle distribution, etc.) is related to the catalytic activity of the entire catalytic/membrane composite system (Mukerjee, 1990). Some of the experimental factors that pertain to electroless deposition have been investigated to determine the extent of their effect on the morphology of the platinum catalyst. These include: the concentration of the platinic acid, type of reducing agent, pH of the platinic acid solution, agitation of the platinic acid solution and modification of the deposition process.

Fedkiw et al. (1990) showed that the concentration of the platinic acid solution prior to electroless deposition influences the morphology of the platinum catalyst on the membranes. When using a lower concentration of platinic acid solution (0.02N), the platinum catalyst deposited on the membranes was less compact and more porous. When using a higher concentration of platinic acid solution (0.05N) the platinum

catalyst deposited on the membranes was thin and less porous with fewer and larger platinum particles (compared to where 0.02N platinic acid solution is used). The roughness factor of the platinum catalyst deposited on the membranes with 0.05N platinic acid solution increased as the platinum loading on the membranes increased. However, the roughness factor of the platinum catalyst deposited on the membranes with 0.05N platinic acid decreased as the platinum loading on the membranes increased.

The morphology of the platinum catalyst on the membranes is also affected by the concentration of the reducing agent used in the deposition process. Fedkiw et al. (1990) showed that the platinum deposition rate was linearly proportional to the concentration of the hydrazine (varied between 0.25M to 0.1M) when the conditions of the deposition process were kept constant (0.02N platinic acid, 2h reaction time). Thus, as the concentration of hydrazine increases, the platinum loading of the platinum catalyst on the membranes will increase.

Sheppard et al. (1998) showed that the agitation (stirring) of the platinic acid solution during the chemical deposition removes hydrogen gas bubbles from the surface of the membrane, which interferes with the electrolyte flow conditions and inhibits the nucleation of platinum. The removal of the inhibitors of platinum nucleation results in an increase in roughness and surface area of the platinum catalyst (Sheppard et al., 1998).

Delime et al. (1998) explored the possibility of modifying the impregnation-reduction method to enhance the roughness factor of the platinum catalyst on the membranes. The modification of the impregnation-reduction method included pre-treating the membrane with 0.5M $[\text{Pt}(\text{NH}_3)_4](\text{OH})_2$. Their results revealed an increase in roughness of the platinum catalyst on the membranes. Their method also reduced the quantity of platinum located deep within Nafion that was inaccessible to desired reactants.

1.6.2. Methods to optimise the chemical structure of the platinum catalyst

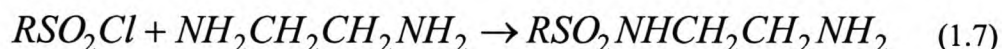
Since platinum is the most active metal of the platinum group metals for the oxidation of methanol, it has been extensively studied as a metal catalyst in SPE-based membrane catalytic systems. However, it does not exhibit the desired electrocatalytic activity for practical use in a methanol fuel cell (Aramata et al., 1988). It has been shown that the catalytic activity of a platinum catalyst can be improved by

modification of the structure of the platinum catalyst by the addition of a second or a third metal (Aramata et al., 1988; Chen et al., 1993; Delime et al., 1999). Binary electrodes, such as PtSn-SPE, PtPb-SPE, PtIr-SPE and PtRu-SPE, which have a higher catalytic activity than Pt-SPE, can provide optimal surface composition of a metal catalyst to promote a desired process (Napporn et al, 1996).

1.7. Chemical modification of cation-exchange membranes

Chemical surface modification (CSM) of various ion-exchange membranes for improved permselectivity for target ions has always been an important area of research in the field of membrane science and technology and has been considered as a very useful method by which to change membrane properties (Mizutani, 1990). The CSM of perfluorinated cation-exchange membranes has led to a considerable increase in cation selectivity of standard perfluorosulfonic acid membranes, achieved by amine modification of the sulfonyl halide groups with ethylene diamine (EDA) (Hora et al., 1977).

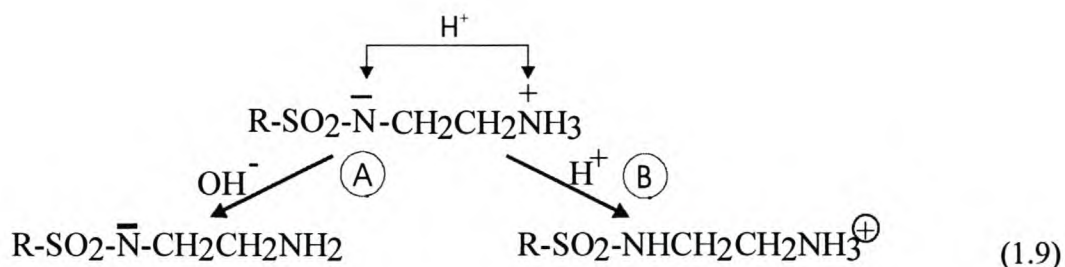
The kinetics of the reaction of EDA with sulfonyl chloride groups of the perfluorinated membranes was studied (Covitch et al., 1982; Covitch, 1983). The reaction of EDA with a perfluorinated membrane can be represented as follows (Covitch et al., 1982):



Covitch et al. (1982) showed that the terminal amino group of the EDA sulfonamide is a good leaving group and that the zwitterionic nature of this structure promotes displacement, even at neutral pH, as follows:



The zwitter ion in equation (1.8) may form various ionogenic groups, depending on whether the medium is acidic or alkaline (Timashev, 1991):



Thermal crosslinking of the membranes modified with EDA was also investigated (Covitch et al., 1982). It was shown that the reaction is controlled by the diffusion rate of EDA into the polymeric film and that the time of contact of EDA with a membrane surface determines the thickness of the resulting modified layer (Covitch et al., 1982).

Another interesting study of CSM of perfluorosulfonic polymeric membranes was aimed at the development of new membrane/catalyst composites for electrocatalytic applications (Nidola et al., 1982). Bessarabov et al. (2000) explored the electroless chemical deposition of platinum particles on perfluorinated membranes modified with EDA. It was found that the chemical modification of the membrane surface with EDA resulted in a change in the morphology of platinum deposition. In the same work IR spectroscopy and dielectric analysis (DEA) were used to study modified membranes.

An interesting effect of so-called “switching” membrane conductivity during the flow of electrical current through a perfluorinated cation-exchange membrane modified with EDA, was reported by Timashev (1991). It was reported that the phenomenon of switching conductivity consists of a jumpwise reversible transition of the system from a high-ohmic to a low-ohmic state and is induced by an electric field whose intensity exceeds some threshold value. A term “negative differential resistance” (NDR) was introduced when describing S-shaped cyclic i - V curves of the membranes. The switching effect could be related to the formation of additional fixed charged groups in the aminated layers of membranes and this is caused by heterolytic dissociation of water that could take place at the membrane-solution interface accompanied by formation of H^+ and OH^- ions (Timashev, 1991). Chapter 6 focuses on the galvanodynamic electrochemical investigation of the above-mentioned switching effect (Bessarabov et al., 2001).

1.8. Conclusions

In this chapter different types of solid polymer electrolytes have been discussed. Emphasis was placed on sulphonic-containing perfluorinated ionomers, such as Nafion. It has been shown that the platinum-containing SPE membranes have a wide field of application, such as in inorganic and organic electrocatalytic syntheses.

Current research of electrocatalytic SPE membranes is on the optimisation of the platinum catalyst on the membrane so as to provide a technology that is economically viable. The optimisation of platinum catalyst on the cation-exchange membranes also results in improved performance of SPE-based membrane catalytic systems. Roughness studies of platinum catalyst on a membrane (Timashev et al., 2000), modification of the process and conditions of deposition, and modification of the surface of the membrane are some factors that have been explored in an attempt to achieve optimal catalyst loading on cation-exchange membranes.

It can be seen from the examples of electrocatalytic chemical processes using platinum-containing SPE systems in Section 1.5 that catalytic systems require at least four elements to achieve catalysis, namely, an oxidation site, reduction site, proton conducting element and electron conducting element. The SPE-based membrane catalytic system consists of the necessary components required for electrocatalytic syntheses, which are:

1. site for oxidation (anode): generation of nascent oxygen
2. site for reduction (cathode): generation of nascent hydrogen
3. proton-conductor: solid polymer electrolyte (Nafion)
4. electron-conductor: current (DC)

The following chapter will describe the pre-treatment methods and the methods for the preparation of perfluorinated membranes, and the deposition of a platinum catalyst on these membranes by counter-ion diffusion deposition. The varying of the conditions of the deposition process, such as temperature, type of reducing agent, concentration of platinic acid solution and the sonication of the platinic acid solution, was explored to investigate their effects on the morphology of the platinum catalyst on the membrane.

References

1. Otsuka K, Yamanaka I and Hagiwara M, 1994, Simultaneous Epoxidation of 1-Hexene and Hydroxylation of Benzene during Electrolysis of Water, *Chemistry Letters*, 1861-1864
2. Allcock HR, Kuliarcik SE, Reed CS and Napierala ME, 1996, Synthesis of polyphosphazenes with ethyleneoxy-containing side groups: New solid electrolyte materials, *Macromolecules*, 29, 3384-3389
3. Allcock HR, Napierala ME, Olmeijer DL, Cameron CG, Kuliarcik SE, Reed CS and O'Connor JM, 1998, New macromolecules for solid polymeric electrolytes, *Electrochimica Acta*, 43, 10-11, 1145-1150
4. Appelby and Yeager, Solid polymer electrolyte fuel cells, *Energy*, Du Pont: Du Pont information brochure on Nafion, 11, 137-151
5. Aramata A, Kodera T and Masuda M, 1988, Electrooxidation of methanol on platinum bonded to the solid polymer electrolyte, Nafion, *Journal of Applied Electrochemistry*, 18, 577-582
6. Bessarabov DG, 1998, Electrochemically-aided membrane separation and catalytic processes, *Membrane Technology (Elsevier)*, 93, 8-11
7. Bessarabov DG, Michaels W, Sanderson RD, 2000, Preparation and characterisation of chemically-modified perfluorinated cation-exchange platinum-containing membranes, *Journal of Membrane Science*, 179, 1-2, 221
8. Bessarabov DG, Michaels WC and Popkov Yu.M, 2001, Galvanodynamic study of the electrochemical switching effect in perfluorinated cation-exchange membranes modified by ethylene diamine, *Journal of Membrane Science*, 194, 1, 81-90
9. Bessarabov DG, Sanderson RD, Popkov YM and Timashev SF, 1998, Characterisation of membranes for electrochemically aided gas separation: Morphology of platinum deposition, *Separation and Purification Technology*, 14, 201-208
10. Bessarabov DG, Sanderson RD, Valuev VV, Popkov Yu M and Timashev SF, 1997, New possibilities of electroinduced membrane gas and vapour separation, *Ind. Eng. Chem. Res.* 36, 2487-2489
11. Chen YL and Chou TC, 1993, Metals and alloys bonded on solid polymer electrolyte for electrochemical reduction of pure benzaldehyde without liquid supporting electrolyte, *Journal of Electroanalytical Chemistry*, 360, 247-259

12. Covitch MJ, 1983, A review of synthetic efforts to improve the selectivity of perfluorinated cation-exchange membranes, in: Proceedings of the Electrochemical Society, 83-93 (Proc. Symp. Membr. Ionic Electron Conduct. Polym., 1982)
13. Covitch MJ, Lowry SR, Gray, CL and Blackford B, 1982, Thermal cross-linking of a chemically-modified ionomer, Polym. Sci. Technol. (Polym. Sep. Media), 16, 257
14. Crabtree RH, 1988, The Organometallic Chemistry of the Transition Metals, John Wiley and Sons, New York
15. Delime F, Léger JM and Lamy C, 1998, Optimization of platinum dispersion in Pt-PEM electrodes: application to the electrooxidation of ethanol, Journal of Applied Electrochemistry, 28, 27-35
16. Delime F, Leger JM and Lamy C, 1999, Enhancement of the electrooxidation of ethanol on a Pt-PEM electrode modified by tin. Part I: Half cell study, Journal of Applied Electrochemistry, 29, 11, 1249-1254
17. Depre L, Kappel J and Popall M, 1998, Inorganic-organic proton conductors based on alkylsulfone functionalities and their patterning by photoinduced methods, Electrochimica Acta, 43, 1301-1306
18. Du Pont, Information brochure released by Du Pont on Nafion
19. Eisenberg A and Yeager HL, 1982, Perfluorinated ionomer membranes, ACS symposium series 180, American Chemical Society, Washington DC
20. Eisenberg A, 1974, Ion-containing polymers, John Wiley and Sons, New York, 230 pages
21. Enea O. Dupre Z and Amadelli R, 1995, Gas phase electrocatalysis on metal/Nafion membranes, Catalysis Today, 25, 271-276
22. Fedkiw PS and Her W, 1989, An impregnation-reduction method to prepare electrodes on Nafion SPE, Journal of the Electrochemical Society, 136, 3, 899-900
23. Fedkiw PS, 1990, Preparing in situ electrocatalytic films in solid polymer electrolyte membranes, composite microelectrode structures produced thereby and chloralkali process utilizing the same, U.S Patent 4,959,132
24. Fedkiw PS, Potente JM and Her WH, 1990, Electroreduction of gaseous ethylene on a platinized Nafion membrane, J. Electrochem. Soc., Vol. 137, No. 5, 1451-1460

25. Gierke TD and Hsu WS, 1982, The cluster-network model of ion-clustering in perfluorosulfonated membranes, in Eisenberg A and Yeager HL (Eds.), Perfluorinated Ionomer Membranes, ACS Symp. Ser., 180, American Chemical Society, Washington, DC
26. Gladkih SN, Shifrina RR, Popkov Yu.M, Timashev SF, 1987, On the electrical switching effects in the ion-exchange membranes (in Russian), *Elektrokhimiya*, 23, 4, 538
27. Gottesfield and Zawodzinski, 1997, Polymer electrolyte fuel cells, *Advances in Electrochemical Science and Technology*, 5, 4, 299-301
28. Grimm JH, Bessarabov DG, Simon U and Sanderson RD, 2000, Characterization of doped tin dioxide anodes prepared by a sol-gel technique and their application in an SPE-reactor, *Journal of Applied Electrochemistry*, 30, 293-302
29. Grot W, Munn GF, Walmsley PN, 1972, Paper presented at the 141st meeting of the Electrochemical Society, Houston
30. Hamed O, Thompson C and Henry P, 1997, Stereochemistry of the Wacker Reaction: Modes of Addition of Hydroxide, Methoxide and Phenyl at High and Low [Cl]. A Study using Chirality Transfer, *Journal of Organic Chemistry*, 62, 7082-7083
31. Heitner-Wirguin C, 1996, Recent advances in perfluorinated ionomer membranes: structure, properties and application, *Journal of Membrane Science*, 120, 1-33
32. Holze R and Ahn J, 1992, Advances in the use of perfluorinated cation-exchange membranes in integrated water electrolysis and hydrogen/oxygen fuel cell systems, *Journal of Membrane Science*, 73, 87-97
33. Itoh N, Xu WC, Hara S and Sakaki K, 2000, Electrochemical Coupling of Benzene Hydrogenation and Water Electrolysis, *Catalysis Today*, 56, 307-314
34. Jörissen J, 1996, Ion exchange membranes as solid polymer electrolytes (spe) in electro-organic synthesis without supporting electrolytes, *Electrochimica Acta*, 41, 4, 553-562
35. Kirsh Yu, Smirnov SA, Popkov Yu M and Timashev SF, 1990, Perfluorinated carbon-chain copolymers with functional groups and cation-exchange membranes based on them: Synthesis, structure and properties. *Russian Chemical Reviews*, 59, 6, 560-574

36. Kreuer KD, Fuchs A, Ise M, Spaeth M and Maier J, 1998, Imidazole and pyrazole-based proton conducting polymers and liquids, *Electrochimica Acta*, 43, 10-11, 1281-1288
37. Lawrence RH and Wood LD, 1981, Method of making solid polymer electrolyte catalytic electrodes and electrodes made thereby, U.S patent 4,272,353
38. Liu R, Her WH and Fedkiw PS, 1992, In situ electrode formation on a Nafion membrane by chemical platinization, *Journal of Electrochemical Society*, Vol. 139, No. 1, 15-23
39. Malleron J.-L, Fiaud J.-C and Legros J.-Y, 1997, *Handbook of palladium-catalyzed organic reactions: Synthetic aspects and catalytic cycles*, Academic Press, California
40. Mitzutani Y, 1990, Ion-exchange membranes with preferential permselectivity for monovalent ions, *Journal of Membrane Science*, 54, 233
41. Nakamura N, Nakamura Y, Tanimura R, Kawahara NY, Ohno H, Deligeer and Suzuki S, 2001, Electron transfer reaction of poly(ethylene oxide)-modified azurin in poly(ethylene oxide) oligomers, *Electrochimica Acta*, 46, 10-11, 1605-1608
42. Napporn WT, Laborde H, Leger JM and Lamy C, 1996, Electro-oxidation of C1 molecules at Pt-based catalysts highly dispersed into a polymeric matrix: Effect of the method of preparation, *Journal of Electroanalytical chemistry*, 404, 1, 153-159
43. Nidola A, Martelli GN, 1982, US Patent 4,364,803
44. Nutall LJ, 1977, Conceptual design of large scale water electrolysis plant using solid polymer electrolyte technology, *International Journal of Hydrogen Energy*, 2, 395
45. Ogumi Z, Nishio K and Yoshizana S, 1981, Application of the SPE Method to Organic Electrochemistry II. Electrochemical Hydrogenation of Olefinic Double Bonds, *Electrochimica Acta*, 26, 12, 1779-1782
46. Ogumi Z, Ohashi S and Takehara Z, 1985, Application of the SPE Method to Organic Electrochemistry IV. Oxidation of Cyclohexanol to Cyclohexanone on Pt-SPE in the Presence of Iodine and Iodide, *Electrochimica Acta*, 30, 1, 121-124
47. Ohno I, Wakabayashi O and Haruyama S, 1985, Anodic oxidation of reductants in electroless plating, *Journal of Electrochemical Society: Electrochemical Science and Technology*, 132, 10, 2323-2330

48. Okinaka Y and Osaka T, 1990, Electroless deposition processes: Fundamentals and applications, *Advances in Electrochemical Science and Engineering*, Gerischer H and Tobias CW, 3, 55-116
49. Otsuka K and Kobayashi A, 1991, Design of the Catalyst for Partial Oxidation of Ethylene by Applying an Electrochemical Device, *Chemistry Letters*, 1197-1200
50. Otsuka K and Yamanaka I, 1990(b), One step synthesis of hydrogen peroxide through fuel cell reaction, *Electrochimica Acta*, 35, 2, 319-322
51. Otsuka K, 1997(a), Design of Catalysts based on the Electrochemical Microcell Models, *Catalysis Surveys for Japan*, 195-203
52. Otsuka K, 1997(b), Reductive and Oxidative Activation of Oxygen for Selective Oxygenation of Hydrocarbons, 3rd World Congress on Oxidation Catalysis, 93-102
53. Otsuka K, Shimizu Y and Yamanaka I, 1990, Selective Synthesis of Acetaldehyde Applying a Fuel Cell System in the Gas Phase, *Journal of Electrochemical Society*, 137, 7, 2076-2081
54. Otsuka K, Ushiyama, Yamanaka I and Ebitani K, 1995, Electrocatalytic synthesis of propylene oxide during water electrolysis, *Journal of Catalysis*, 157, 450-460
55. Otsuka K, Yamanaka I and Wang Y, 1998, Reductive Activation of Oxygen for Partial Oxidation of Light Alkanes, *Natural Gas Conversion V: Studies in Surface Science and Catalysis*, 119, 15-24
56. Popall M, Andrei M, Kappel J, Kron J, Olma K and Olsowski B, ORMOCERs as inorganic-organic electrolytes for new solid state lithium batteries and supercapacitors, *Electrochimica Acta*, 43, 10-11, 1122-1166
57. Popall M, Buestrich R, Semrau G, Eichinger G, Andrei M, Parker WO, Skaarup S and West K, 2001, New polymer lithium secondary batteries based on ORMOCER electrolytes-inorganic-organic polymers, *Electrochimica Acta*, 46, 10-11, 1499-1508
58. Scott K and Hughes R (Eds.), 1996, *Industrial Membrane Separation Technology*, Chapman and Hall, UK
59. Siegbahn PEM, 1995, A Theoretical Study of Some Steps in the Wacker Process, *Structural Chemistry*, 6, 4/5, 271-279
60. Simond O and Comninellis Ch, 1997a, Anodic oxidation of organics on Ti/IrO₂ anodes using Nafion as electrolyte, *Electrochimica Acta*, 42, 13-14, 2013-2018

61. Simond O, Schaller V and Comninellis CH, 1997, Theoretical Model for the Anodic Oxidation of Organics on Metal Oxide Electrodes, *Electrochimica Acta*, 42, 13-142, 2009-2012
62. Skaarup S, West K, Zachua-Christiansen B, Popall M, Kappel J, Kron J, Eichinger G and Semrau G, 1998, Towards solid state lithium batteries based on ORMOCER electrolytes, 43, 10-11, 1589-1592
63. Smitd J, Hafner W, Jira R, Sieber R, Sedlmeier J and Sabel A, 1962, The Oxidation of Olefins with Palladium Chloride Catalysts, *Angewandte Chemie Intl.*, Edn Engl., 1, 2, 80-88
64. Stucki S, Theis G, Kötzt R, Devantay H and Christen HJ, 1985, In situ production of ozone in water using a membrel electrolyzer, *Journal of Electrochemical Society: Electrochemical Science and Technology*, 132, 2, 367-371
65. Takenaka H, Torikai E, Kawami Y and Wakabayashi N, 1982, Solid polymer electrolytes water electrolysis, *International Journal of Hydrogen Energy*, 7, 5, 397-403
66. Tammeveski K, Tenno T, Claret J and Ferrater C, Electrochemical Reduction of Oxygen on Thin-Film Pt Electrodes in 0.1M KOH, *Electrochimica Acta*, 1997, 42, 5, 893-897
67. Tatapudi P and Fenton JM, 1993, Synthesis of ozone in a proton exchange membrane electrochemical reactor, 140, 12, 3527-3530
68. Tatapudi P and Fenton JM, 1994, Simultaneous synthesis of ozone and hydrogen peroxide in a proton-exchange-membrane electrochemical reactor, 141, 5, 1174-1178
69. Timashev SF, 1991, *Physical Chemistry of Membrane Processes*, Ellis Horwood Series in Physical Chemistry, New York
70. Timashev SF, Bessarabov DG, Sanderson RD, Marais S, Lakeev SG, 2000, Description of non-regular membrane structures: A novel phenomenological approach, *Journal of Membrane Science*, 170, 2, 191-203
71. Van den Meerakker JEAM, 1981, On the mechanism of electroless plating. II. One mechanism for different reductants, *Journal of Applied Electrochemistry*, 11, 395-400
72. Vincent CA, 1989, Polymer electrolytes, *Chemistry in Britain*, 391-395

73. Wallgren K and Sotiropoulos S, 2001, Electrochemistry of planar solid-state amperometric devices based on Nafion and polybenzimidazole solid polymer electrolytes, *Electrochimica Acta*, 46, 10-11, 1523-1532
74. Wang Y and Otsuka K, 1997, Partial Oxidation of Ethane by Reductively Activated Oxygen over Iron Phosphate Catalyst, *Journal of Catalysis*, 171, 106-114
75. Watanabe M, 1993, Process of preparing electrode for fuel cell, U.S patent 5,186,877
76. White PS, 1982, Solid polymer electrolyte cell and electrode for same, U.S patent 4,272,353
77. Yamanaka I, Akimoto T, Nakagaki K and Otsuka K, 1996, Oxidation and Epoxidation of Hydrocarbons with O₂ Catalysed by EuCl₃, *Journal of Molecular Catalysis A: Chemical* 110, 119-128
78. Zhang Q and Otsuka K, 1997, Partial Oxidation of Light Alkanes during O₂-H₂ Cell Reactions at Room Temperature, *Chemistry Letters*, 363-364

Electronic references

79. Cyclopps: The ozone company, www.cyclopps.com/dozone.html
80. Hamilton Sundstrand, www.hsssi.com/Applications/Echem/Hydrogen
81. Lynntech Inc, www.lynnotech.com/licensing/pem_fuelcell/index.shtml
82. Ozonia, www.ch/products/membrel.htm

Preparation of platinum-containing perfluorinated cation-exchange membranes: experimental procedure for non-modified membranes

Abstract

The morphology of the platinum catalyst on a membrane was controlled by varying the deposition conditions, such as: temperature, type of reducing agent and concentration of the platinic acid solution. Preparation of platinum-containing membranes with the sonication of the platinic acid solution during the deposition process and the pre-treatment of membranes is also discussed.

2.1. Introduction

There is great interest in SPE electrocatalytic membrane systems as they offer a wide range of application and potential processes, such as fuel cell technology, water electrolysis, production of ozone, etc. Although patents and the open literature provide some information on deposition procedures for the preparation of platinum-containing cation-exchange membranes, this information was considered insufficient for successful manufacturing of platinum-containing membranes. Hence, the successful preparation of platinum-containing membranes was the objective of this chapter.

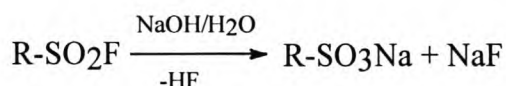
2.2. Materials

The following materials were used for the preparation of cation-exchange membranes: Sodium hydroxide (NaOH) pellets, Saarchem, 98%; methanol (MeOH), Waters, 99%; flat-sheet perfluorinated cation-exchange membranes made from a copolymer of tetrafluoroethylene and perfluoro-3,6-dioxa-5-methyl-1-octene-8-sulfonyl fluoride (“Plastpolymer”, Russia); flat-sheet cation-exchange made from the previously mentioned polymer, but in the form of perfluorosulphonic acid ($R-SO_3H^+$, ion-exchange capacity ranged from E=1120 to 1220) (“Plastpolymer”, Russia), phenol red indicator, Holpro, pH 6.4-8.2; hydrochloric acid (HCl), Anala R, 33%; methyl orange indicator; hydrogen hexachloroplatinate (IV) hydrate ($H_2PtCl_6 \cdot xH_2O$), 99.9% [26023-84-7: Aldrich]; hydrazine dihydrochloride ($N_2H_4 \cdot 2HCl$), Aldrich, 98%; tin

(II) chloride ($\text{SnCl}_2 \times 2\text{H}_2\text{O}$), PAL Chemicals AR; nitric acid, Aldrich, 65 wt. %; ethylene diamine (EDA), Unilab, 99% and sodium borohydride (NaBH_4), Aldrich, 99%.

2.3. Hydrolysis of flat-sheet cation-exchange membranes

Flat-sheet membrane samples were prepared from a copolymer of tetrafluoroethylene and perfluoro-3,6-dioxo-5-methyl-1-octene-8-sulfonyl fluoride by hot pressing.¹ The membranes were hydrolysed prior to the deposition of a thin layer of platinum catalyst on the membrane by counter-ion diffusion. Membrane samples were hydrolysed with a solution of 6N NaOH (70 vol. %) and MeOH (30 vol. %) or 6N NaOH. The hydrolysis reaction of a non-hydrolysed membrane can be expressed as follows (Timashev, 1991):



where R is a general description of a perfluorinated polymeric matrix.

2.3.1. Hydrolysis of cation-exchange membranes in 6N NaOH solution

Membrane samples were boiled in 6N NaOH solution for 7 hours. The membranes were washed with distilled water and placed in distilled water at a temperature of 60 °C for 10 minutes.

2.3.2. Hydrolysis of cation-exchange membranes in a solution of 6N NaOH (70 vol. %) and MeOH (30 vol. %)

Membrane samples were boiled in a solution of 6N NaOH (70 vol. %) and MeOH (30 vol. %) for 7 hours under reflux conditions. The membranes were washed with distilled water and placed in distilled water of a temperature of 60 °C for 10 minutes.

2.3.3. Conversion of membranes to H^+ -ionic form

The hydrolysed membranes were boiled in an excess of 0.4N HCl for 4 hours to convert membranes to the H^+ -ionic form. The membranes were then washed with distilled water to remove excess HCl.

¹ "Plastpolymer", Russia

2.4. Determination of the ion-exchange capacities of cation-exchange flat-sheet membranes

2.4.1. Determination of ion-exchange capacities of hydrolysed membranes

The hydrolysed membranes (as prepared in section 2.2) in the H^+ -ionic form were placed in separate 50 ml solutions of 0.1N NaOH solution for 24 hours. The NaOH solutions were titrated with 0.1N HCl, using phenol red indicator, to determine the concentration of the NaOH solution after the ion-exchange process.

The experimental steps for the determination of the ion-exchange capacity of a flat-sheet membrane sample are schematically summarised in Fig. 2.1.

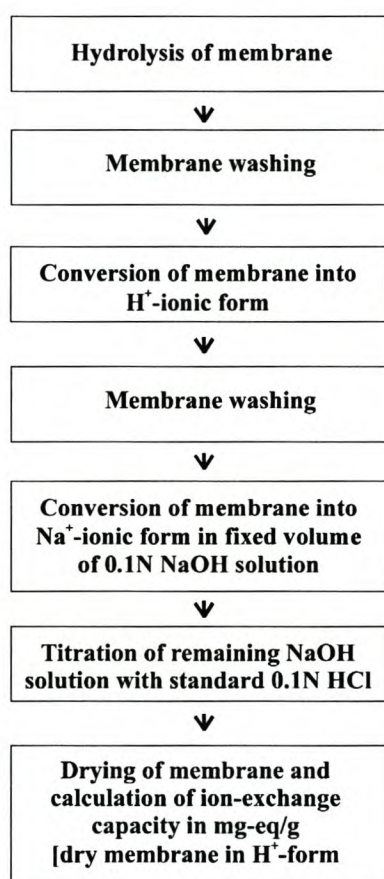


Figure 2.1. Schematic representation of the determination of the ion-exchange capacity of a cation-exchange membrane.

The ion-exchange capacity (E) of a hydrolysed membrane (as prepared in section 2.2) was calculated according to the following formula:

$$E = \frac{N_{st} \times \left(\frac{V_{sampl} - V_{HCl}}{V_{sampl}} \right) \times V_{total}}{M_{membr}}$$

where:

E = ion-exchange capacity of membrane (meq/g [dry membrane in H^+ -ionic form]),

V_{sampl} = volume of NaOH solution used for titration,

V_{HCl} = volume of titrated HCl solution,

V_{total} = total volume of NaOH solution used to convert membranes from the H^+ -ionic form into Na^+ -ionic form,

N_{st} = standard concentrations of HCl and NaOH used (in this case $N_{st} = 0.1N$), and

M_{membr} = mass (in grams) of the membrane in the H^+ -form.

The ion-exchange capacities of membranes hydrolysed under different conditions are tabulated in Table 2.1.

Table 2.1. Ion-exchange capacities of cation-exchange membranes with different conditions of hydrolysis.

Conditions of hydrolysis	Thickness of membrane (μm)	Mass of dry membrane [H^+ -form] (g)	Ion exchange capacity (E) (meq/g) [dry membrane, H^+ -form]	Equivalent weight (1000/E)
6N NaOH (70 vol. %) and MeOH (30 vol. %)	124	2.47	0.82	1220
6N NaOH	131	2.74	0.82	1220

2.5. Chemical deposition of platinum on cation-exchange membranes

2.5.1. Pre-treatment of hydrolysed membranes

Hydrolysed membranes in Na^+ -ionic form were pre-treated by either boiling in distilled water or in a solution of H_2O (70 vol. %) and MeOH (30 vol. %) for 2 hours prior to the chemical deposition process. The membranes were pre-treated to investigate the effect of the pre-treatment conditions on the morphology of the platinum catalyst on the membrane.

The equivalent weight of the pre-treated membranes was 1220 and 1120. These membranes were deposited with platinum at room temperature using hydrazine and 0.05M platonic acid solution by chemical deposition (total time of platinisation was 11 minutes).

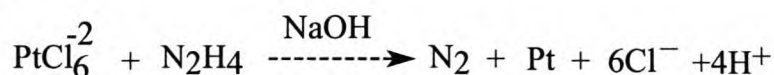
2.5.2. Preparation of “working” solutions for chemical deposition of platinum on membranes by counter diffusion (Takenaka-Torikai) method

0.05M $\text{H}_2\text{PtCl}_6 \times \text{XH}_2\text{O}^2$ and NaOH was prepared with 0.5M $\text{H}_2\text{PtCl}_6 \times \text{XH}_2\text{O}$. The pH of the 0.05M $\text{H}_2\text{PtCl}_6 \times \text{XH}_2\text{O}$ solution was increased from 3.5 to ~7 with the addition of small amounts of 1N NaOH. The pH meter was calibrated with pH=4 and pH=7 buffer solutions.

The reducing agents used in the chemical deposition process were either hydrazine or sodium borohydride. Hydrazine was prepared with 115g $\text{N}_2\text{H}_4 \times 2\text{HCl}$ and 130g of NaOH, dissolved in 2L of distilled water. Sodium borohydride was prepared with 23g NaBH_4 and 4g NaOH, dissolved in 1L of distilled water.

2.5.3. Deposition of platinum catalyst on flat-sheet cation-exchange membranes by counter diffusion method

The deposition of a thin metallic layer of platinum on a membrane was achieved by the autocatalytic reduction of $[\text{PtCl}_6]^{2-}$ complex anions with hydrazine through the Takenaka-Torikai method (Takenaka et al., 1981; Sheppard et al., 1998). The chemical reaction of the Takenaka-Torikai method can be represented as follows (Enea et al., 1995):



The deposition process was carried out in a membrane cell (Fig. 2.2). The membrane cell consisted of a chamber (1) to hold the flat-sheet cation-exchange membranes (2) and a metal-ion solution of platinum (5) in the upper section of the chamber (1). The

² $\text{H}_2\text{PtCl}_6 \times \text{XH}_2\text{O}$, containing 38-40 % of Pt, was purchased from Aldrich (catalogue # 26023-84-7). We chose to use an average value of 39 % Pt. This value (39 % Pt) formally corresponds to the following formula for the chemical: $\text{H}_2\text{PtCl}_6 \times 5\text{H}_2\text{O}$. (Although it is more appropriate to write $\text{H}_2\text{PtCl}_6 \times 6\text{H}_2\text{O}$, we will use the following formula: $\text{H}_2\text{PtCl}_6 \times 5\text{H}_2\text{O}$, because of the above mentioned reasons).

membrane chamber (1) was immersed in a solution of reducing reagent, hydrazine (3). The solution of reducing agent was well mixed by means of a magnetic stirrer (4).

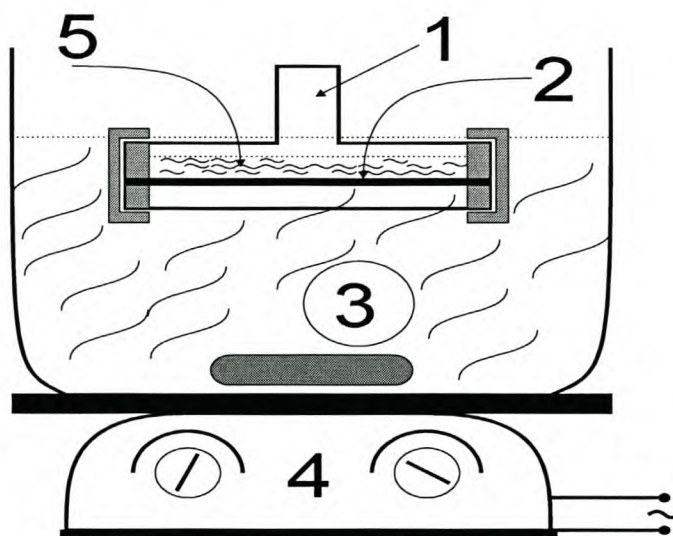


Figure 2.2. Membrane holder and bath used for deposition of thin layer of platinum on membrane. 1. Chamber to hold flat membranes; 2. Ion-exchange membrane; 3. Bath containing solution of reducing agent; 4. Magnetic stirrer; 5. Solution of platinic acid.

2.5.4. Chemical deposition of platinum catalyst on membranes at room temperature

15ml 0.05M platinic acid solution was poured onto each membrane in the membrane holder (chamber 1, Fig. 2.3). The time of contact of the platinic acid solution with the membrane was 1 minute. Thereafter, the membrane holder with the membrane and platinic acid solution was placed into a bath containing the reducing agent, hydrazine, for 10 minutes. The total time of the platinisation process was 11 minutes. The remaining platinic acid solution on the membrane after the deposition process was decanted into a beaker. The membrane was then washed with distilled water and boiled in distilled water for 2 hours.

2.5.5. Chemical deposition of platinum catalyst on membranes at 40 °C

2.5.5.1. Chemical deposition using 0.05M platinic acid solution

Chloroplatinic acid solution was prepared by dissolving platinum metal in boiling aqua regia, which consisted of one part nitric acid and three parts hydrochloric acid. An excess of hydrochloric acid was added on the formation of a platinum solution to

prevent the nitrates from complexing with the platinum. Upon crystallisation, the crystals of the chloroplatinic acid was dissolved in hydrochloric acid to form a solution of $8.1099 \times 10^{-2} \text{M}$ (Van Rensburg, 1995). 0.05M chloroplatinic acid solution was prepared from this solution for the deposition of platinum on membranes at a temperature of 40 °C.

a. Chemical deposition using hydrazine

5ml 0.05M platonic acid solution was poured onto each cation-exchange membrane in the membrane cell. The time of contact of the 0.05M platonic acid solutions with each membrane was 1 minute. Thereafter, the membrane holder with the membrane and platonic acid solution was placed into a bath containing hydrazine. The platonic acid solution was autocatalytically reduced in a bath of hydrazine on different membranes for 3.5, 5.5, 7.5, 9.5, 11.5 and 15.5 minutes respectively.

b. Chemical deposition using sodium borohydride

5ml 0.05M platonic acid solution was poured onto each cation-exchange membrane in the membrane cell. The time of contact of the 0.05M platonic acid solutions with each membrane was 1 minute. Thereafter, the membrane holder with the membrane and platonic acid solution was placed into a bath containing sodium borohydride. The platonic acid solution was autocatalytically reduced in a bath of sodium borohydride on different membranes for 3.5, 5.5, 7.5, 9.5, 11.5 and 15.5 minutes respectively.

2.5.5.2. Chemical deposition using 0.03M platonic acid solution

After the deposition of platinum on membranes with 0.05M platonic acid solution, the remaining platonic acid solution was further used in another chemical deposition process. This platonic acid solution that remained after the chemical deposition of platinum on membranes with 0.05M platonic acid solution was determined to be of the concentration of 0.03M. This 0.03M platonic acid solution was further used in the chemical deposition of platinum on membranes at a temperature of 40 °C.

a. Chemical deposition using sodium borohydride

5ml 0.03M platonic acid solution was poured onto each cation-exchange membrane in the membrane cell. The time of contact of the 0.03M platonic acid solutions with each membrane was 1 minute. Thereafter, the membrane holder with the membrane and platonic acid solution was placed into a bath containing sodium borohydride. The

platinic acid solution was autocatalytically reduced in a bath of sodium borohydride on different membranes for 3.5, 11.5, 25.5 and 35.5 minutes respectively.

2.5.6. Chemical deposition process with sonication of platinic acid solution

5ml 0.03M platinic acid solution was poured onto a cation-exchange membrane in the membrane cell. The time of contact of the 0.03M platinic acid solutions with each membrane was 1 minute. Thereafter, the membrane holder with the membrane and platinic acid solution was placed into a bath containing hydrazine. The platinic acid solution was autocatalytically reduced in a bath of hydrazine for 7 minutes with the sonication of the platinic acid solution. Pulses of 20-40kHz were rippled through the platinic acid with the Heat Systems Ultrasonics Inc., model H-I 50-4 sonicator.

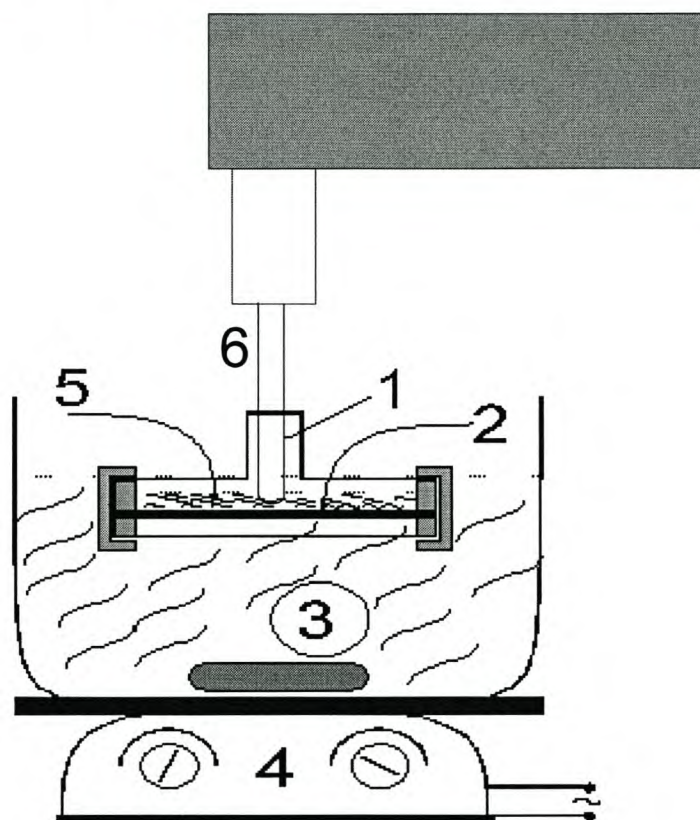


Figure 2.3. Membrane holder and bath used for deposition of thin layer of platinum on membrane with the sonication of the platinic acid solution. 1. Chamber to hold flat membranes; 2. Ion-exchange membrane; 3. Bath containing solution of reducing agent; 4. Magnetic stirrer; 5. Solution of platinic acid and 6. Heat Systems Ultrasonics Inc., model H-I 50-4 sonicator

2.6. Conclusions

The preparation of platinum-containing membranes by varying the conditions of counter diffusion method, such as temperature, type of reducing agent and concentration of the platinic acid solution was explored. The preparation of platinum-containing membranes, with the sonication of platinic acid solution and the pre-treatment of membranes, was also attempted.

The preparation of platinum-containing membranes by the counter diffusion method resulted in a very strong adhesion between the platinum catalyst and the membrane. This is desirable for a SPE electrocatalytic system that is strong and durable.

The following chapters on the characterisation of platinum-containing membranes investigate the morphology (shape, size, distribution profile) and loading of the platinum catalyst on the cation-exchange membrane with different characterisation techniques, such as Atomic Force Microscopy (AFM), Scanning Electron Microscopy (SEM), UV spectrophotometry and Brunauer, Emmett and Teller (BET) adsorption measurements.

References

1. Enea O, Dupre Z and Amadelli R, 1995, Gas phase electrocatalysis on metal/Nafion membranes, *Catal. Today*, 25, 271
2. Sheppard S.-A, Campbell SA, Smith JR, Lloyd GW, Ralph TR and Walsh FC, 1998, Electrochemical and microscopic characterisation of platinum-coated perfluorosulfonic acid (Nafion 117) materials, *Analyst*, 123, 1923
3. Takenaka H, Torikai E, Kawami Y and Wakabayashi N, 1982, Solid polymer electrolytes water electrolysis, *Int. J. Hydrogen Energy*, 7, 397
4. Timashev SF, 1991, *Physical Chemistry of Membrane Processes*, Ellis Horwood Series in Physical Chemistry, New York
5. Van Rensburg S, 1995, The use of hollow-fibre carbon membranes in the catalytic conversion of cyclohexane, MSc thesis, University of Stellenbosch

Quantitative determination of the platinum loading on cation-exchange membranes

Abstract

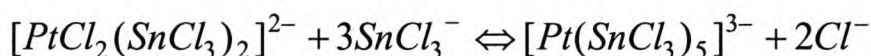
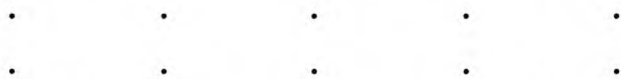
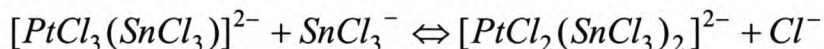
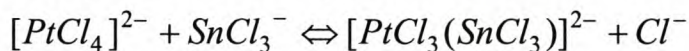
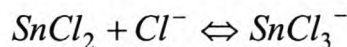
This chapter describes the quantitative determination of the platinum loading on cation-exchange membranes by UV spectrophotometric and gravimetric analyses. Suitable conditions for the quantitative determination of the platinum loading on membranes by UV spectrophotometric analysis were established through the development of a protocol. A comparison between results of UV spectrophotometric and gravimetric analysis for the quantitative determination of the platinum loading on membranes showed UV spectrophotometry was more accurate than gravimetric analysis.

3.1. Development of a protocol for the quantitative determination of platinum loading on cation-exchange membranes by UV spectrophotometric analysis

The interaction of stannous chloride with noble metals, in particular platinum, has been known for over a century. It was first reported that a red-brown colour was produced when an acid solution of platinum (II/IV) chloride was treated with excess tin (II) chloride (Sexton, 1892). This has resulted in stannous chloride being used as a colorimetric reagent for the quantitative determination of small amounts of platinum (Sexton, 1892). Wöhler et al. (1910) considered the red colour to be due to a colloidal suspension of finely dispersed metallic platinum. Ayres et al. (1951) disproved this postulate. They observed that this red suspension readily passed through semi-permeable membranes and was extractable into organic solvents.

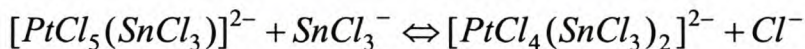
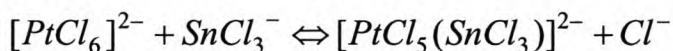
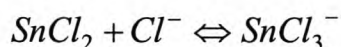
Extensive studies have investigated the platinum (II)-tin (II) complex (Koch et al., 1983; 1984; 1987). Ayres studied the interaction between platinum (II) and tin (II) chloride and proposed the existence of complexes in aqueous medium of tin:platinum ratios 1:4, 1:2, 1:1, 3:2, 2:1, 3:1 and 5:1 (Ayres et al, 1955). Precipitation of higher concentrations of tin with trimethylammonium resulted in the formation of red salts, which appeared to contain high ratios (up to 5:1) of tin:platinum (Young et al., 1964).

Young et al. (1964) proposed that several independent equilibria exist simultaneously in solutions containing tin (II) chloride and platinum (II) chloride, namely:



It was proposed that tin is coordinated to platinum to form a quinquedecacoordinate ion, $[\text{Pt}(\text{SnCl}_3)_5]^{3-}$ (Cramer et al., 1965). Determination of the configuration of the quinquedecacoordinate ion by x-ray diffraction showed the ion to be trigonal bipyramid. It consisted of a central platinum atom surrounded by five SnCl_3^- ligands attached through platinum-tin bonds (Cramer et al., 1965).

Fewer studies have focussed on the interaction of the platinum (IV)-tin (II) complex. However, it can be assumed that similar equilibria exist for platinum (IV) as proposed for platinum (II). The following is therefore assumed:



The proposed equilibria for platinum (II) and platinum (IV) complexes suggest that the platinum-tin system is very dynamic. The system will therefore be influenced by changes in temperature, the concentrations of tin chloride and platinum chloride and the pH of the solutions containing the platinum-tin system.

Ayres et al. (1951) investigated the reaction of tin (II) chloride and platinum (IV) by spectrophotometric analysis. They observed two absorbance maxima at 403nm and at 310 nm (Ayres et al., 1951; Berman, 1959). They succeeded in establishing conditions whereby the absorption peak at 310 nm could be used for the

quantitative determination of platinum. Berman and Goodhue (1959) showed that the absorbance at 310 nm was five times larger than at 403 nm. Thus, a qualitative method has only been developed for the determination of platinum using 310nm absorption peak (Ayres et al., 1951; Berman et al., 1959). Since aqua regia was used in our studies to remove platinum from membranes (section 3.2.2.1), we had to focus on the 403 nm absorption peak as the peak at 310 nm was not clearly visible due to the effect of the aqua regia on the platinum (IV)-tin (II) complex.

Since the quantitative determination of platinum loading on a cation-exchange membrane by gravimetric method has many limitations, the quantitative determination of platinum loading on a cation-exchange membrane by UV spectrophotometric analysis is explored in this study. The limitations of the gravimetric method are the following:

- There is greater risk of error when using small membrane samples rather than large membrane samples, as the mass of platinum on small membrane samples is more affected by small spillage than the larger membrane samples.
- Membranes are able to absorb water from the surrounding atmosphere during the weighing process. This can result in a distortion of the actual mass of the membrane.

The aim of the present study was to determine a suitable UV spectrophotometric method for the quantitative determination of platinum deposited on cation-exchange membranes. Ayres et al. (1951) and Berman et al. (1959) used the absorption peak at 310 nm, in this study the focus is on the absorption peak at 403 nm. The absorption peak at 310 nm was not used due to the noise that was often exhibited in this region. The noise was ascribed to the presence of aqua regia. In some cases the quantitative amounts thereof were difficult to determine and resulted in shifts in the absorbance maxima of solutions containing platinum ions. Furthermore, the dynamic behaviour of the aqua regia affects the absorbance at 310 nm more than it does at 403 nm. The results obtained for the quantitative determination of the platinum loading on a membrane by UV spectrophotometric analysis of tin-platinum complexes are similar to the results obtained by Berman et al. (1959) (see Fig 3.1).

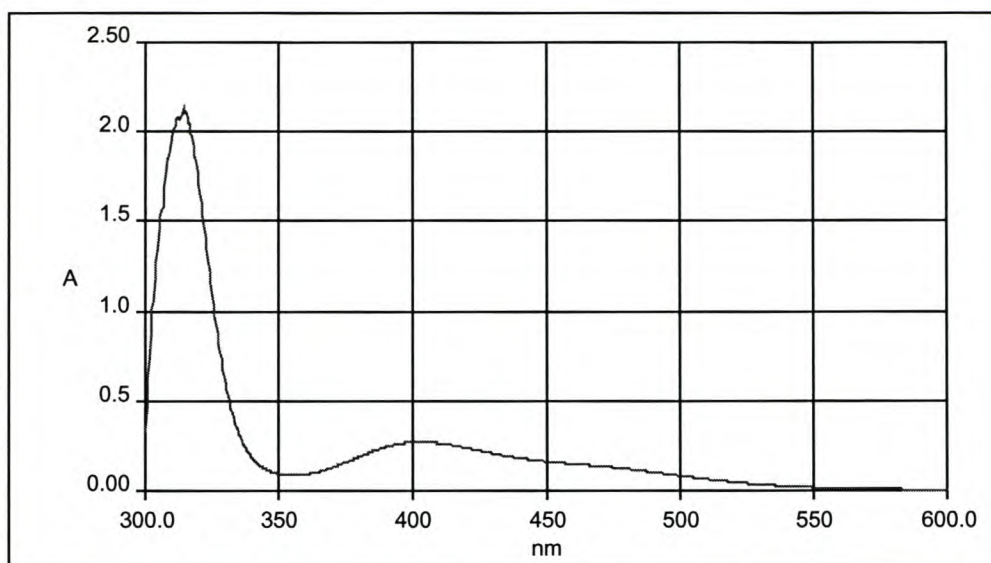
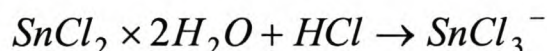


Figure 3.1. Typical UV absorption spectrum with peaks at 403 nm and 310 nm of a solution containing 0.5 ml 0.5M platinic acid solution, 2 ml aqua regia and 2 ml tin chloride solution.

3.1.1. Preparation of a tin chloride solution for quantitative analysis

0.5M of a tin chloride solution was prepared from 56.42g $\text{SnCl}_2 \times 2\text{H}_2\text{O}$, 250 ml 5M HCl and 250 ml distilled water. The reaction can be represented as follows (Cotton et al., 1988):



3.1.2. Determination of platinum ions within solutions by UV spectrophotometric analysis: Time-drive spectra

3.1.2.1. UV spectrophotometric analysis of solutions containing platinum ions without aqua regia

2 ml 0.08M platinic acid solution was diluted with distilled water to a final volume of 100 ml. A mixture of 2 ml of this solution and 5 ml 0.5M SnCl_3^- was diluted with distilled water to a final volume of 25 ml. The reference solution consisted of 5 ml 0.5M SnCl_3^- solution and 20 ml distilled water. The UV absorbance of the solution containing platinum ions was measured, after 180 min, between the wavelengths 350 nm and 600 nm, to determine the absorbance maximum (Fig. 3.2). The solutions containing platinum ions (without aqua regia) were further analysed by measuring its absorbance at a wavelength of 402.27 nm for 1800 min (Fig. 3.3).

3.1.2.2. UV spectrophotometric analysis of solutions containing platinum ions with low concentration of aqua regia

2 ml 0.08M platonic acid solution was diluted with distilled water to a final volume of 100 ml. A mixture of 2 ml of this solution, 5 ml 0.5M SnCl_3^- and 0.25 ml aqua regia was diluted with distilled water to a final volume of 25 ml. The reference solution consisted of 5 ml 0.5M SnCl_3^- and 20 ml distilled water. The UV absorbance of the solutions containing platinum ions was measured, after 180 min, between the wavelengths 350 nm and 600 nm (Fig. 3.4). The solutions containing platinum ions were further analysed by measuring its absorbance at a wavelength of 402.27 nm for 1800 min (Fig. 3.6).

3.1.2.3. UV spectrophotometric analysis of solutions containing platinum ions with high concentration of aqua regia

2 ml 0.08M platonic acid solution was diluted with distilled water to a final volume of 100 ml. A mixture of 2 ml of this solution, 5 ml 0.5M SnCl_3^- and 2 ml aqua regia was diluted with distilled water to a final volume of 25 ml. The reference solution consisted of 5 ml 0.5M SnCl_3^- and 20 ml distilled water. The solutions containing platinum ions were analysed by measuring their absorbance at a wavelength of 402.27 nm for 1800 min (Fig. 3.7). The UV absorbance of the solutions containing platinum ions was measured after 1800 min between the wavelength of 290 nm and 600 nm (Fig. 3.8).

3.1.3. UV spectrophotometric results of solutions containing platinum ions

The absorbance maximum of a solution containing platinum ions without aqua regia was 0.67 at a wavelength of 402.27 nm (Fig. 3.2). The UV absorbance of the solutions containing platinum ions without aqua regia gradually increased with time (Fig 3.3). It can be seen from Figure 3.3 that the time-drive spectrum is inconsistent between 0 min and 150 min. It becomes less inconsistent after 150 min.

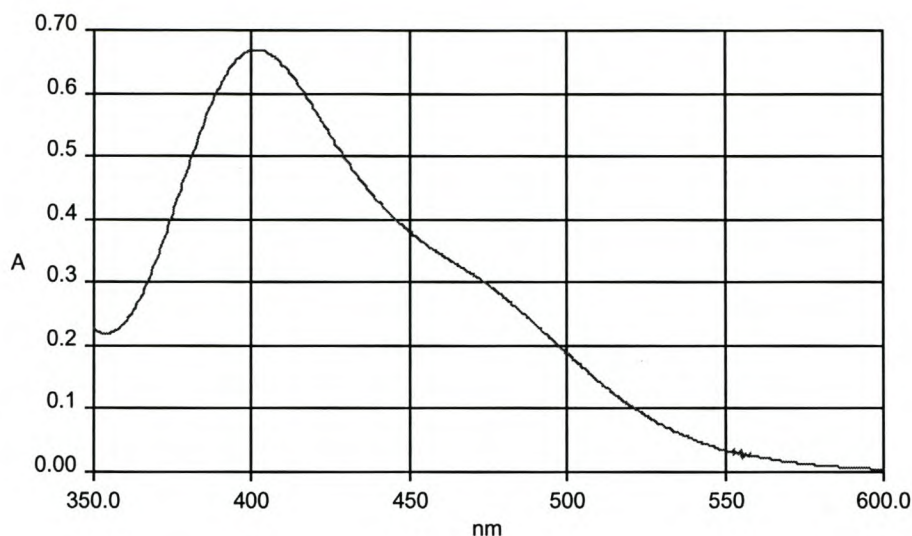


Figure 3.2. *UV absorption spectrum of a solution containing platinum ions without aqua regia after 180 min.*

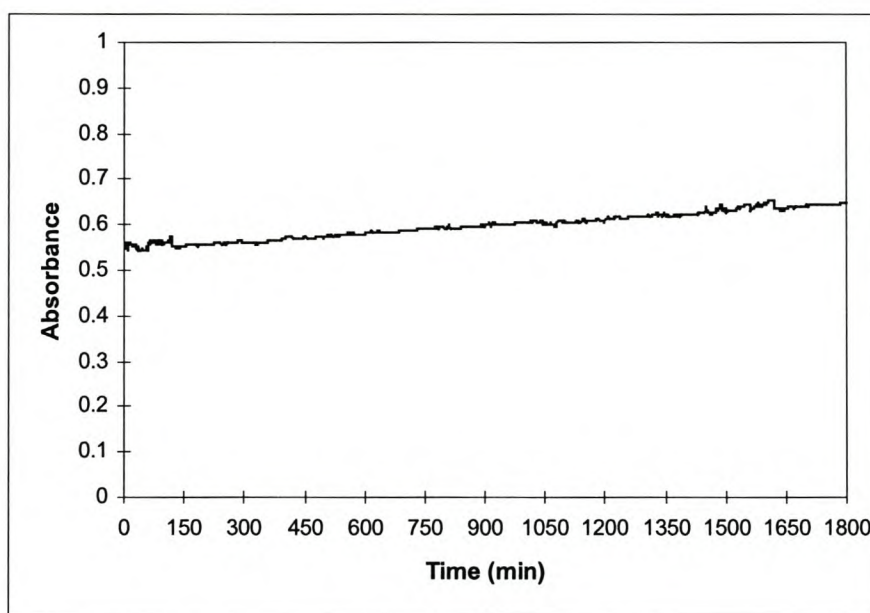


Figure 3.3. *Time-drive spectrum of the absorbance of a solution containing platinum ions without aqua regia, over a time period of 1800 min at a wavelength of 402.23 nm. It is seen that the first 150 min of the time-drive spectrum is considerably inconsistent.*

A solution containing platinum ions with a low concentration of aqua regia exhibited an absorbance maximum of 0.58 at a wavelength of 402.27 nm (Fig. 3.4). The noise that occurred at wavelengths lower than 320 nm can be seen in Figure 3.5 for the UV absorption spectrum of a solution containing platinum ions with a low concentration of aqua regia.

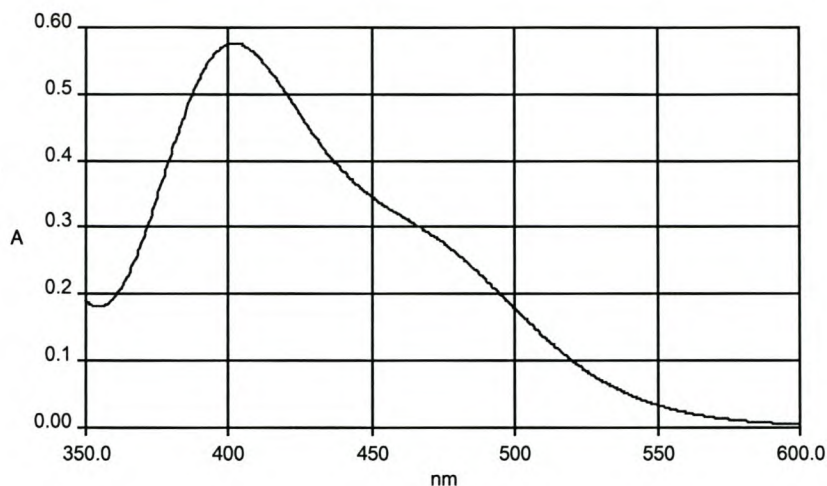


Figure 3.4. *UV absorption spectrum of a solution containing platinum ions with a low concentration of aqua regia after 180 min.*

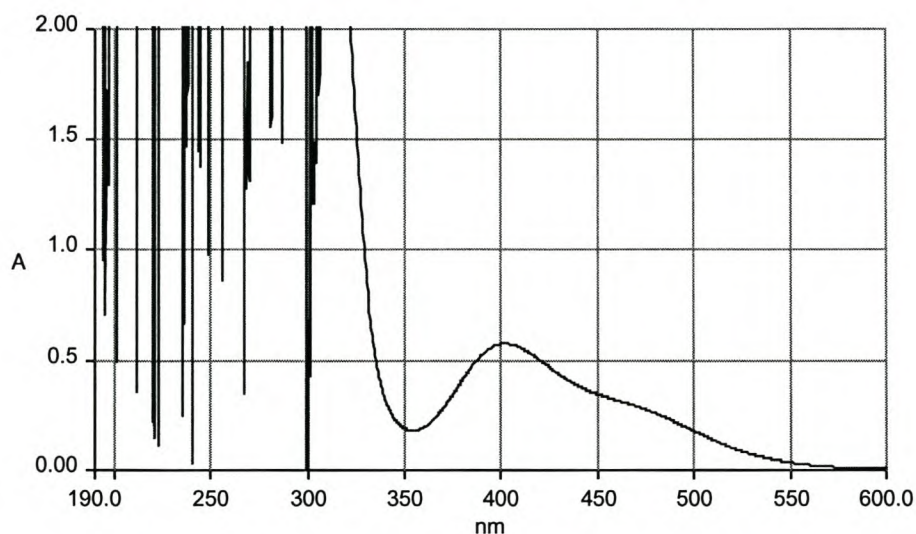


Figure 3.5. *UV absorption spectrum of a solution containing platinum ions with a low concentration of aqua regia after 180 min, between the wavelengths of 600 nm and 190 nm.*

The absorbance of solutions containing platinum ions with a low concentration of aqua regia gradually increased with increasing time of interaction of the aqua regia with the Pt (IV)-tin (II) complex. The absorbance of a solution containing platinum ions with a low concentration of aqua regia was inconsistent for the first 480 min (Fig. 3.6).

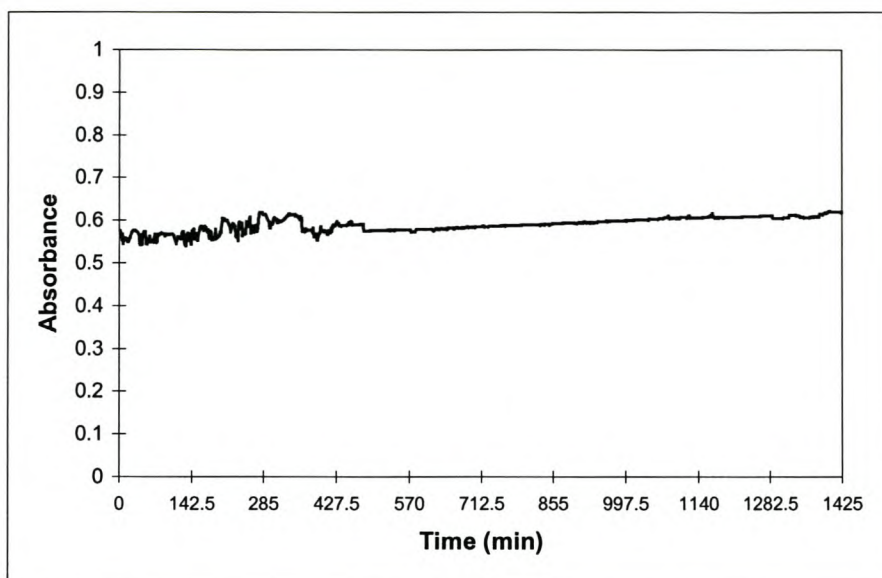


Figure 3.6. Time-drive spectrum for the absorbance of a solution containing platinum ions with a low concentration of aqua regia over a time period of 1425 min, at a wavelength of 402.27 nm.

The absorbance of a solution containing platinum ions with a high concentration of aqua regia was consistent between 180 min and 260 min, as well as between 320 min and 420 min. A decrease in absorbance from 0.517 to zero was observed after 450 min (Fig. 3.7).

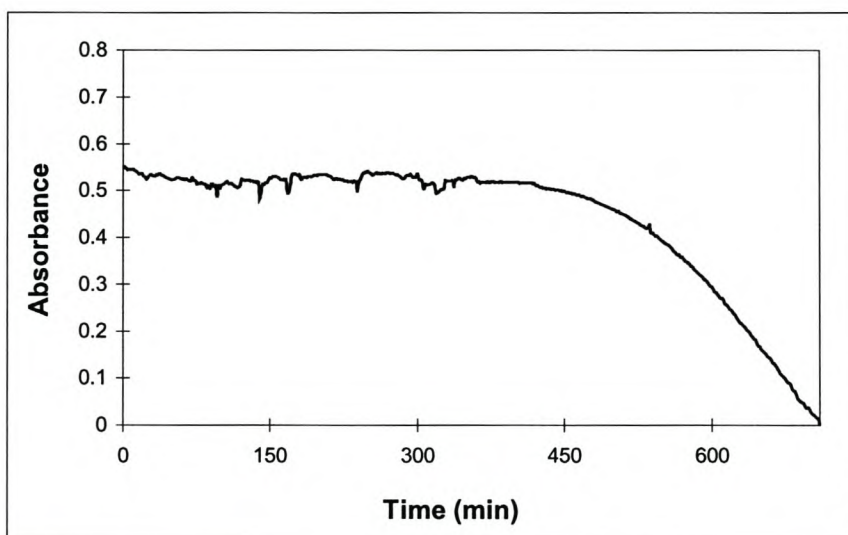


Figure 3.7. Time-drive spectrum for the absorbance of a solution containing platinum ions with a high concentration of aqua regia over a time period of 1800 min, at a wavelength of 402.27 nm.

A solution containing platinum ions with a high concentration of aqua regia exhibited an absorbance maximum of 1.60 at a wavelength of 310 nm after 1800 min (Fig. 3.8). The results showed that the absorbance maximum occurred at a lower wavelength after 1800 min (Fig. 3.8).

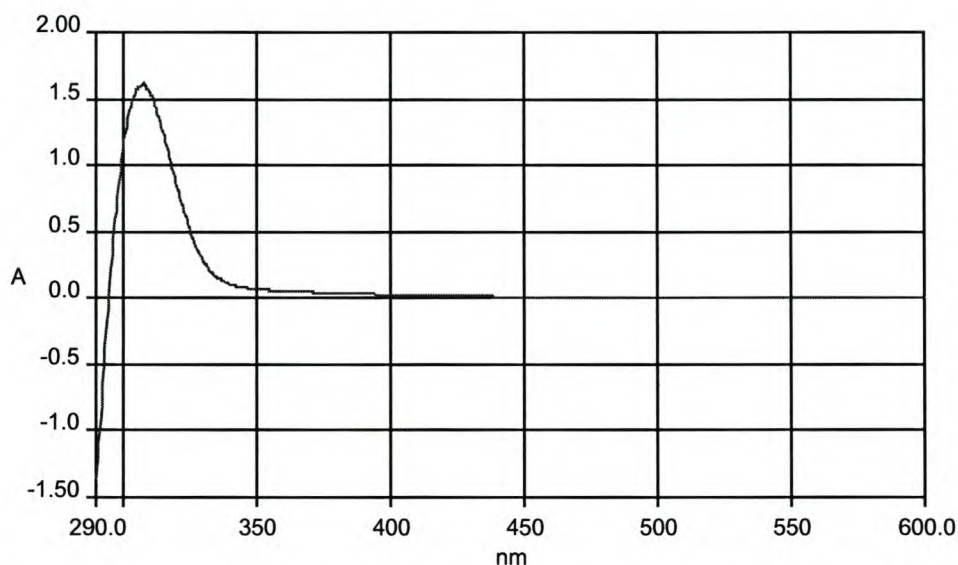


Figure 3.8. *UV absorption spectrum of a solution containing platinum ions with a high concentration of aqua regia after 1800 min.*

3.1.4. Discussion

It was important to establish the effect of aqua regia on the Pt(IV)-tin (II) complex, as aqua regia was used to remove the platinum catalyst from platinum-containing membranes. This was done to determine the most suitable conditions for the quantitative determination of the platinum loading on a membrane by UV spectrophotometric analysis.

There was little difference between the absorbance of platinum solutions without aqua regia and those with a low concentration of aqua regia (Fig. 3.9). This suggests that a low concentration of aqua regia has little effect on the Pt(IV)-Sn(II) complex, as it has little effect on the absorbance of the platinum solution (Fig. 3.9).

Platinum solutions with a high concentration of aqua regia have a lower absorbance than those without aqua regia (Fig. 3.9). These results suggest that the high concentration of aqua regia has a greater effect on the Pt(IV)-Sn(II) complex, as the absorbance of the platinum solutions decreased considerably.

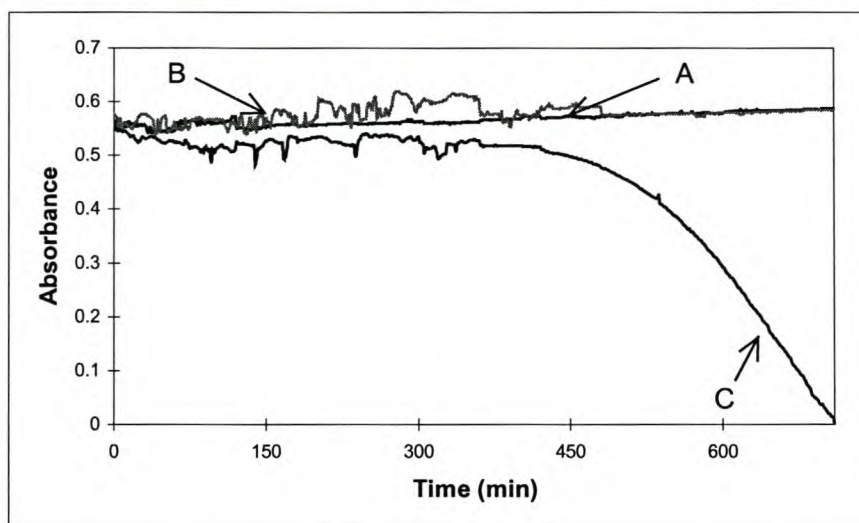


Figure 3.9. Time-drive spectrum at a wavelength of 402.27 of platinum solutions without aqua regia (A), with a low concentration of aqua regia (B) and with a high concentration of aqua regia (C).

The absorbance of a platinum solution with a high concentration of aqua regia decreases to zero after 450 min (Fig. 3.9). This decline can be attributed to the presence of aqua regia, as no decline in absorbance is observed for platinum solutions without aqua regia (Fig. 3.9(A)).

The platinum solution with a high concentration of aqua regia exhibits an absorbance maximum at a wavelength of 310 nm, while a platinum solution without aqua regia exhibits an absorbance maximum at 402.27 nm (Figs. 3.8 and 3.2). The results showed that the absorbance maximum of a platinum solution with a high concentration of aqua regia shifts to a lower wavelength as the time of interaction between the aqua regia and the Pt(IV)-Sn(II) complex increases (Fig. 3.8). The lower absorbance of platinum solutions with a high concentration of aqua regia obtained at a wavelength of 402.27 nm can be explained by the shift of the absorbance maximum to a lower wavelength (Fig. 3.8).

The results showed that platinum solutions with a high concentration of aqua regia are stable before 450 min, with the greatest stability occurring between 180 min and 260 min, as well as between 320 min and 420 min. Thus, in our studies, platinum solutions with a high concentration of aqua regia were used in the quantitative determination of platinum loading on cation-exchange membranes. UV spectrophotometric measurements were carried out after 180 minutes.

3.1.5. Final remarks and recommendations

The results of this work have led to the development of a experimental protocol for the quantitative determination of the platinum loading on a cation-exchange membrane by UV spectrophotometric analysis, which is as follows:

1. Preparation of tin chloride solution for quantitative analysis

0.5M SnCl_3^- solution was prepared with 56.42g $\text{SnCl}_2 \times 2\text{H}_2\text{O}$, 250 ml 5M HCl and 250 ml distilled water.

2. Determination of a calibration curve

Preparation of standard solutions for UV spectrophotometric analysis

2 ml 0.05M platonic acid solution was measured into a 100 ml volumetric flask. The remaining volume of the volumetric flask was filled with distilled water. 0.25, 0.5, 1 and 2 ml samples of this solution were measured into separate 25 ml volumetric flasks. 5 ml 0.5M SnCl_3^- and 2ml aqua regia (3HCl:1HNO₃) were added to each 25 ml volumetric flask. The remaining volume of the volumetric flask was filled with distilled water. The reference solution contained 5 ml 0.5M SnCl_3^- solution and 20 ml distilled water. The absorbance of the platinum solutions by UV spectrophotometric analysis was measured after 180 min at a wavelength of 402.27nm. The results were used to plot a calibration curve.

3. Determination of the total platinum loading on cation-exchange membranes

Removal of platinum catalyst from platinum-containing membranes

Platinum-containing membranes were placed in 5 ml aqua regia and heated to 80°C to remove platinum from the membranes. The solution of aqua regia and platinum was poured into 25 ml volumetric flasks. Air was bubbled through these platinum solutions to remove NO_x and the remaining volume of the volumetric flask was filled with distilled water.

Quantitative determination of the platinum loading on a cation-exchange membrane by UV spectrophotometric analysis

1 ml of each platinum solution (as prepared above) was measured into separate 25 ml volumetric flasks. 5 ml 0.5M SnCl_3^- was added to each volumetric flask and the

remaining volume of the volumetric flask was filled with distilled water. The reference solution contained 5 ml 0.5M SnCl_3^- and 20 ml distilled water. The UV absorbance of the platinum solutions was measured after 180 minutes at the wavelength 402.27nm.

This study succeeded in establishing an experimental protocol for the quantitative determination of the platinum loading on a cation-exchange membrane through colorimetric analysis using UV spectrophotometric analysis.

3.2. Quantitative determination of the platinum loading on cation-exchange membranes by UV spectrophotometric and gravimetric analyses

The determination of the platinum loading on platinum-containing membranes was explored in this section by following the protocol that was developed in section 3.1.

3.2.1. Preparation of standard solutions for UV spectrophotometric analysis

2 ml 0.05M platonic acid solution was measured into a 100 ml volumetric flask. The remaining volume of the volumetric flask was filled with distilled water. 0.25, 0.5, 1 and 2 ml samples of this solution were measured into separate 25 ml volumetric flasks. 5 ml 0.5M SnCl_3^- and 2 ml aqua regia ($3\text{HCl}:1\text{HNO}_3$) were added to each 25 ml volumetric flask. The remaining volumes of the volumetric flasks were filled with distilled water. The reference solution contained 5 ml 0.5M SnCl_3^- solution and 20 ml distilled water. The absorbance of the solutions containing platinum ions was measured after 180 min (Fig. 3.10).

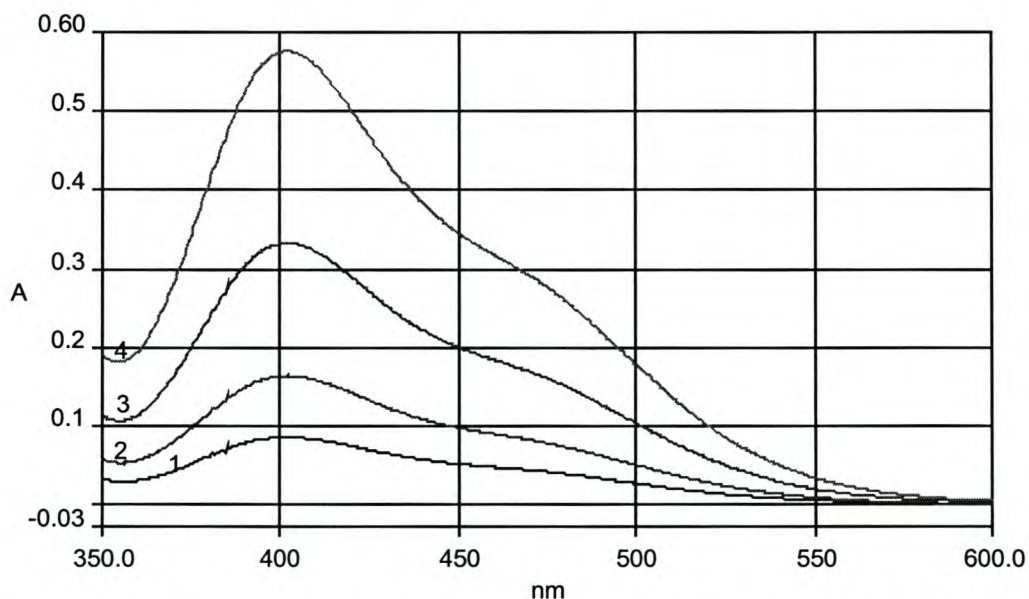


Figure 3.10. UV absorption spectrum of standard solutions, containing platonic acid solution, SnCl_3^- and aqua regia, of concentrations 1×10^{-5} (1), 2×10^{-5} (2), 4×10^{-5} (3) and 8×10^{-5} (4) mol/L.

The absorbance of each standard solution is tabulated in Table 3.1.

Table 3.1. Absorbance of standard solutions containing platonic acid solution, SnCl_3^- and aqua regia, which were measured at a wavelength of 402.27nm.

Concentration of standard solutions containing Pt ions (mol/L)	Absorbance at wavelength of 402.27 nm
1×10^{-5}	0.09
2×10^{-5}	0.16
4×10^{-5}	0.33
8×10^{-5}	0.58

The results obtained from UV spectrophotometric analysis were used to plot a calibration curve (Fig. 3.11).

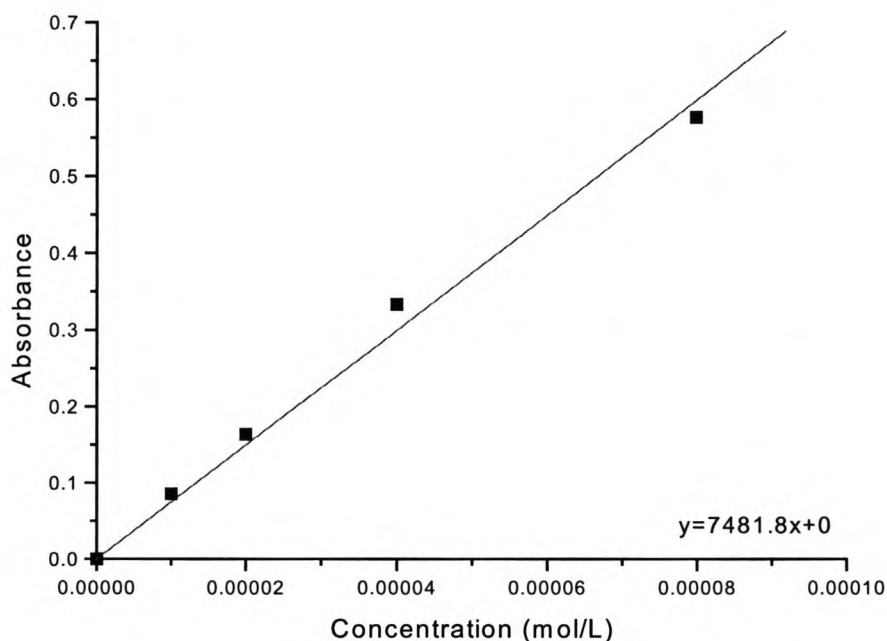


Figure 3.11. Calibration curve of standard solutions, containing platonic acid solution, SnCl_3^- and aqua regia, of concentrations 1×10^{-5} , 2×10^{-5} , 4×10^{-5} and 8×10^{-5} mol/L.

3.2.2. Determination of platinum loading on membranes by UV spectrophotometric analysis

3.2.2.1. Removal of platinum catalyst from platinum-containing membranes

Platinum-containing membranes were placed in 5 ml aqua regia ($3\text{HCl}:1\text{HNO}_3$) and heated to 80°C to remove platinum from the membranes. The solutions containing platinum ions were poured into 25 ml volumetric flasks. Air was bubbled through

these solutions to remove NO_x and the remaining volume of the volumetric flask was filled with distilled water.

3.2.2.2. Preparation of solutions containing platinum ions for UV spectrophotometric analysis

1 ml of each solution containing platinum ions (as described in section 3.2.2.1) was measured into separate 25 ml volumetric flasks. 5 ml 0.5M SnCl_3^- was added to each volumetric flask and the remaining volume of the volumetric flask was filled with distilled water. The reference solution contained 5 ml 0.5M SnCl_3^- and 20 ml distilled water. The absorbance of the solutions containing platinum ions was measured after 180 minutes.

3.2.3. Determination of platinum loading on membranes by gravimetric method

Platinum-containing membranes were dried in a vacuum oven for 5 hours at 80 °C. The membranes were cooled in a dessicator and weighed. The platinum catalyst was removed from the platinum-containing membranes (as described in section 3.2.2.1) and then dried again in a vacuum oven for 5 hours at 80 °C. The membranes were cooled in a dessicator and weighed again.

3.2.4. Quantitative determination of platinum embedded on cation-exchange membranes by the reduction of 0.05M platonic acid solution with sodium borohydride at 40 °C (see Section 2.5.5.1.b)

3.2.4.1. Quantitative determination of the platinum loading on cation-exchange membranes by UV spectrophotometric analysis

The platinum loading on the membranes was determined by UV spectrophotometric analysis (as described in section 3.2.2). The results are shown in Figure 3.12.

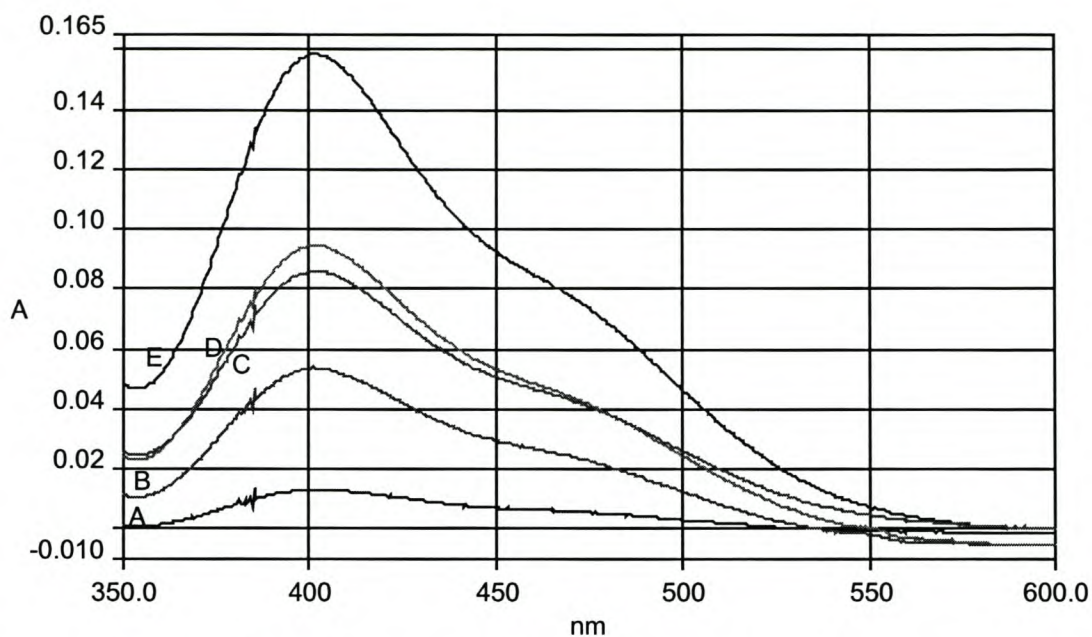


Figure 3.12. UV absorption spectrum of solutions containing platinum ions of unknown concentrations. The platinum catalyst was deposited by the reduction of 0.05M platinic acid solution with NaBH_4 . The total time of platinisation was 4.5(A), 6.5(B), 10.5(C), 12.5(D) and 16.5(E) minutes.

The absorbance of each solution containing platinum ions is tabulated in Table 3.2.

Table 3.2. Concentration of the solutions containing platinum ions, as determined from the calibration curve.

Total time of platinisation ^a for the reduction of 0.05M platinic acid solution by NaBH_4 (min)	Absorbance of solutions containing Pt ions at the wavelength of 402.27 nm	Concentration of solutions containing Pt ions (mol/L)
4.5	0.013	1.74×10^{-6}
6.5	0.054	7.22×10^{-6}
10.5	0.086	1.15×10^{-5}
12.5	0.095	1.27×10^{-5}
16.5	0.158	2.11×10^{-5}

^a Total time of platinisation = time of contact of platinic acid solution with membrane (1 minute) + time of reduction of platinic acid by reducing agent.

The results of UV spectrophotometric analysis were used to determine the total platinum loading on the membranes, achieved by the reduction of 0.05M platonic acid solution with sodium borohydride at different time intervals (Table 3.3).

Table 3.3. *UV spectrophotometric results of platinum loading on cation-exchange membranes by the reduction of 0.05M platonic acid solution with NaBH₄ for total time of platinisation of 4.5, 6.5, 10.5, 12.5 and 16.5 minutes for a membrane area of 2.26 cm².*

Total time of platinisation for the reduction of 0.05M platonic acid solution by NaBH ₄ (min)	Absorbance of solutions containing Pt ions at the wavelength of 402.27nm	Concentration of solutions containing Pt ions (mol/L)	Mass of Pt deposited on membrane (g) ^b	Mass of Pt deposited on membrane for 39% Pt in H ₂ PtCl ₆ ·XH ₂ O (g) ^c	Total Pt loading on membrane (mg/cm ²) ^d
4.5	0.013	1.74×10^{-6}	5.44×10^{-4}	2.12×10^{-4}	0.09
6.5	0.054	7.22×10^{-6}	2.26×10^{-3}	8.80×10^{-4}	0.39
10.5	0.086	1.15×10^{-5}	3.59×10^{-3}	1.40×10^{-3}	0.62
12.5	0.095	1.27×10^{-5}	3.97×10^{-3}	1.55×10^{-3}	0.69
16.5	0.158	2.11×10^{-5}	6.59×10^{-3}	2.57×10^{-3}	1.14

3.2.4.2. Quantitative determination of the platinum loading on cation-exchange membranes by gravimetric analysis

The total platinum loading on membranes was determined by gravimetric analysis (as described in section 3.2.3). The results are tabulated in Table 3.4.

^b $m = C \times V \times DC \times MM_{H_2PtCl_6 \cdot 5H_2O}$, where C is the concentration of the platonic acid (determined from calibration curve); V is the initial volume of the platinum solution (0.025L); DC is the "dilution" coefficient (25) and $MM_{H_2PtCl_6 \cdot 5H_2O}$ is the molecular mass of the platonic acid solution (500)

^c H₂PtCl₆·XH₂O, containing 38-40 % of Pt, was purchased from Aldrich (catalogue #26023-84-7). We chose to use an average value of 39 % Pt.

^d Calculated for dry membrane, diameter = 34mm

Table 3.4. Results of gravimetric and spectrophotometric analysis of the total platinum loading on membranes by the reduction of 0.05M platonic acid solution with NaBH_4 for the total time of platinisation of 4.5, 6.5, 10.5, 12.5 and 16.5 minutes.

Total time of platinisation for the reduction of 0.05M platonic acid solution by NaBH_4 (min)	Pt loading on membranes as determined by gravimetric analysis (g)	Total Pt loading on membranes as determined by gravimetric analysis (mg/cm^2)	Total Pt loading on membranes as determined by spectrophotometric analysis (mg/cm^2)
4.5	1×10^{-4}	0.04	0.09
6.5	1.1×10^{-3}	0.49	0.39
10.5	1.3×10^{-3}	0.58	0.62
12.5	1.5×10^{-3}	0.66	0.69
16.5	2.8×10^{-3}	1.24	1.14

Figure 3.13 shows a comparison of the results of the total platinum loading on membranes as determined by gravimetric and spectrophotometric analyses.

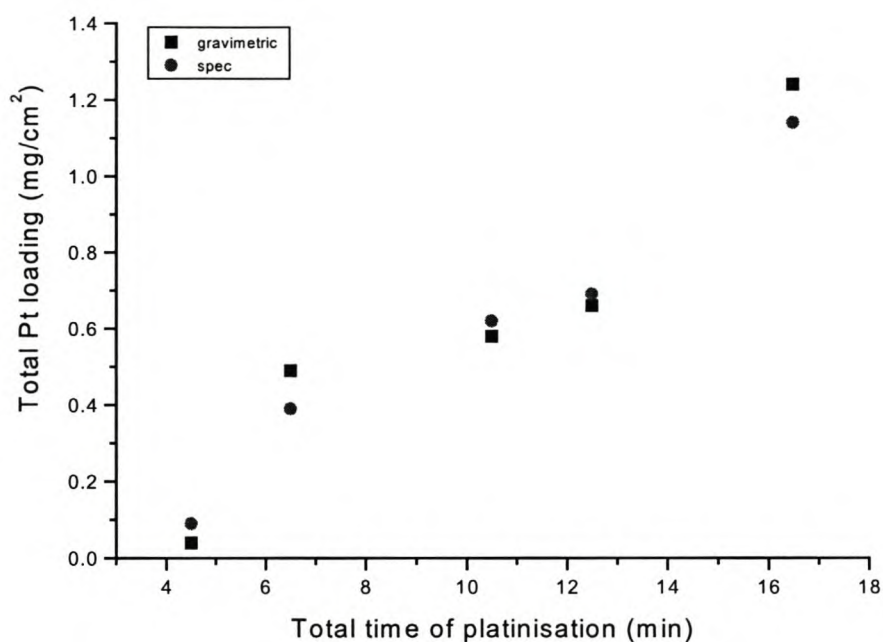


Figure 3.13. Plot of total platinum loading on membranes achieved by the reduction of 0.05M platonic acid solution with NaBH_4 for total time of platinisation of 4.5, 6.5, 10.5, 12.5 and 16.5 minutes, as determined by gravimetric and spectrophotometric (spec) analysis.

3.2.5. Quantitative determination of the platinum embedded on cation-exchange membranes by the reduction of 0.03M platinic acid solution with sodium borohydride at 40 °C (see Section 2.5.5.2.a)

3.2.5.1. Quantitative determination of the platinum loading on cation-exchange membranes by UV spectrophotometric analysis

The platinum loading on the membranes was determined by UV spectrophotometric analysis (as described in section 3.2.2). The results are represented in Figure 3.14.

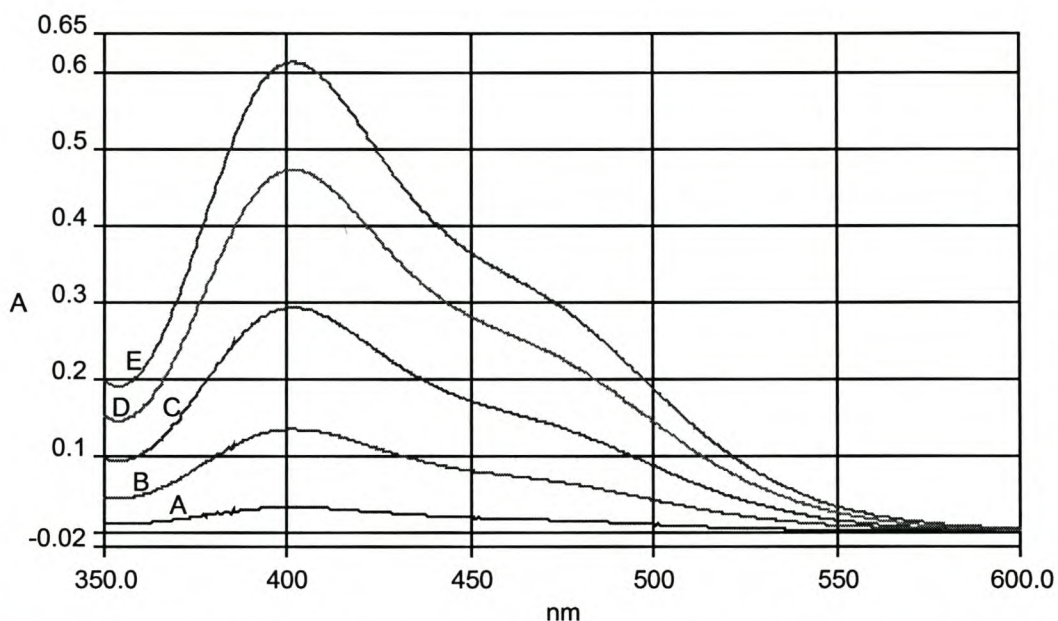


Figure 3.14. UV absorption spectrum of solutions containing platinum ions of unknown concentrations. The platinum catalyst was deposited by the reduction of 0.03M platinic acid solution with NaBH_4 for the total time of platinisation of 4.5(A), 12.5(B), 16.5(C), 26.5(D) and 36.5(E) minutes.

The absorbance of each solution containing platinum ions is tabulated in Table 3.5.

Table 3.5. Concentration of the solutions containing platinum ions as determined from the calibration curve

Total time of platinisation for the reduction of 0.03M platonic acid solution by NaBH ₄ (min)	Absorbance of solutions containing Pt ions at a wavelength of 402.27 nm	Concentration of solutions containing Pt ions (mol/L)
4.5	0.03	4.01×10^{-6}
12.5	0.14	1.87×10^{-5}
16.5	0.30	4.01×10^{-5}
26.5	0.47	6.28×10^{-5}
36.5	0.61	8.15×10^{-5}

The results of UV spectrophotometric analysis were used to determine the total platinum loading on the membranes, achieved by the reduction of 0.03M platonic acid solution with sodium borohydride at different time intervals (Table 3.6).

Table 3.6. UV spectrophotometric results of platinum loading on cation-exchange membranes by the reduction of 0.03M platonic acid solution with NaBH₄ for total time of platinisation of 4.5, 12.5, 16.5, 26.5 and 36.5 minutes for a membrane area of 2.26 cm².

Total time of platinisation for the reduction of 0.03M platonic acid by NaBH ₄ (min)	Absorbance of solutions containing Pt ions at the wavelength of 402.27nm	Concentration of solutions containing Pt ions (mol/L)	Mass of Pt deposited on membrane (g)	Mass of Pt deposited on membrane for 39% Pt in H ₂ PtCl ₆ xXH ₂ O (g)	Total Pt loading on membrane (mg/cm ²)
4.5	0.033	4.01×10^{-6}	1.25×10^{-3}	4.89×10^{-4}	0.22
12.5	0.135	1.87×10^{-5}	5.84×10^{-3}	2.28×10^{-3}	1.01
16.5	0.293	4.01×10^{-5}	1.25×10^{-2}	4.89×10^{-3}	2.16
26.5	0.472	6.28×10^{-5}	1.96×10^{-2}	7.65×10^{-3}	3.38
36.5	0.612	8.15×10^{-5}	2.55×10^{-2}	9.93×10^{-3}	4.39

3.2.5.2. Quantitative determination of the platinum loading on cation-exchange membranes by gravimetric analysis

The total platinum loading on membranes was determined by gravimetric analysis (see section 3.2.3). The results are tabulated in Table 3.7.

Table 3.7. Results of gravimetric and spectrophotometric analysis of the total platinum loading on membranes by the reduction of 0.03M platonic acid solution with NaBH_4 for total times of platinisation of 4.5, 12.5, 16.5, 26.5 and 36.5 minutes.

Total time of platinisation for the reduction of 0.03M platonic acid solution by NaBH_4 (min)	Pt loading on membranes as determined by gravimetric analysis (g)	Total Pt loading on membranes as determined by gravimetric method (mg/cm^2)	Total Pt loading on membranes as determined by spectrophotometric analysis (mg/cm^2)
4.5	7.0×10^{-4}	0.31	0.22
12.5	2.2×10^{-3}	0.97	1.01
16.5	4.7×10^{-3}	2.08	2.16
26.5	6.7×10^{-3}	2.96	3.38
36.5	1.0×10^{-2}	4.42	4.39

Figure 3.15 shows a comparison of the results of the total platinum loading on membranes, as determined by gravimetric and spectrophotometric analyses.

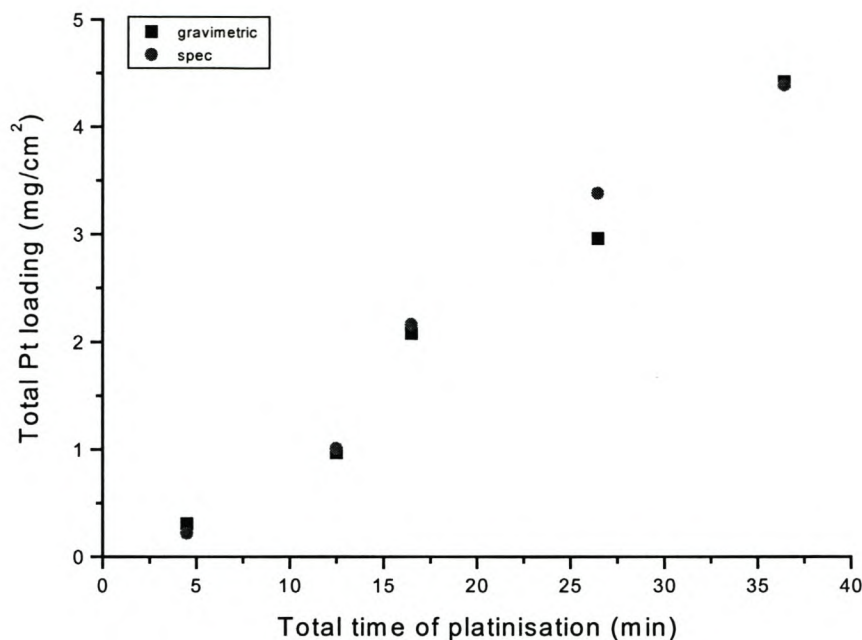


Figure 3.15. Plot of total platinum loading on membranes achieved by the reduction of 0.03M platonic acid solution with NaBH_4 for total time of platinisation of 4.5, 12.5, 16.5, 26.5 and 36.5 minutes, as determined by gravimetric and spectrophotometric (*spec*) analysis.

3.2.6. Quantitative determination of the platinum embedded on cation-exchange membranes by the reduction of 0.05M platonic acid solution with hydrazine at 40 °C (see Section 2.5.5.1.a)

3.2.6.1. Quantitative determination of the platinum loading on cation-exchange membranes by UV spectrophotometric analysis

The platinum loading on membranes was determined by UV spectrophotometric analysis (as described in section 3.2.2). The results are represented in Figure 3.16.

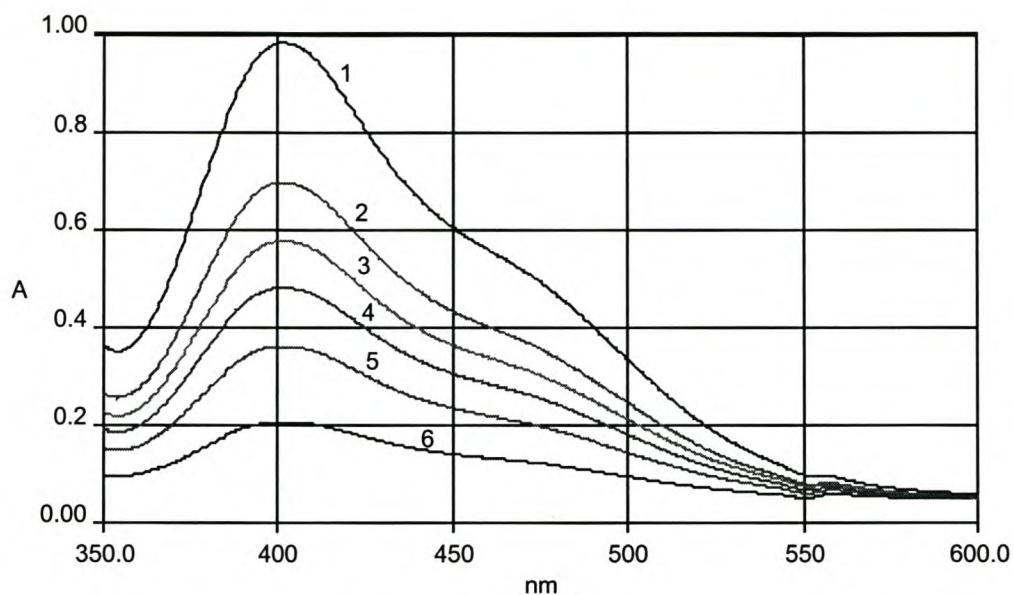


Figure 3.16. UV absorption spectrum of solutions containing platinum ions of unknown concentrations. The platinum catalyst was deposited by the reduction of 0.05M platinic acid solution with hydrazine. The total time of platinisation was 16.5(1), 12.5(2), 10.5(3), 8.5(4), 6.5(5) and 4.5(6) minutes.

The absorbance of each solution containing platinum ions is tabulated in Table 3.8.

Table 3.8. Concentration of the solutions containing platinum ions, as determined from the calibration curve

Total time of platinisation for the reduction of 0.05M platinic acid solution by hydrazine (min)	Absorbance of solutions containing Pt ions at the wavelength of 402.27 nm	Concentration of solutions containing Pt ions (mol/L)
4.5	0.205	2.74×10^{-5}
6.5	0.361	4.83×10^{-5}
8.5	0.451	6.43×10^{-5}
10.5	0.577	7.71×10^{-5}
12.5	0.697	9.32×10^{-5}
16.5	0.985	1.32×10^{-4}

The results of UV spectrophotometric analysis were used to determine the total platinum loading on the membranes, achieved by the reduction of 0.05M platonic acid solution with hydrazine at different time intervals (Table 3.9).

Table 3.9. *UV spectrophotometric results of the platinum loading on cation-exchange membranes by the reduction of 0.05M platonic acid solution with hydrazine for the total times of platinisation of 4.5, 6.5, 8.5, 10.5, 12.5 and 16.5 minutes for a membrane area of 9 cm².*

Total time of platinisation for the reduction of 0.05M platonic acid solution by hydrazine (min)	Absorbance of solutions containing Pt ions at the wavelength of 402.27nm	Concentration of solutions containing Pt ions (mol/L)	Mass of Pt deposited on membrane (g)	Mass of Pt deposited on membrane for 39% Pt in H ₂ PtCl ₆ ·XH ₂ O (g)	Total Pt loading on membrane (mg/cm ²)
4.5	0.205	2.74×10^{-5}	8.56×10^{-3}	3.34×10^{-3}	0.37
6.5	0.361	4.83×10^{-5}	1.51×10^{-2}	5.89×10^{-3}	0.70
8.5	0.481	6.43×10^{-5}	2.01×10^{-2}	7.84×10^{-3}	0.87
10.5	0.577	7.71×10^{-5}	2.41×10^{-2}	9.40×10^{-3}	1.04
12.5	0.697	9.32×10^{-5}	2.91×10^{-2}	1.14×10^{-2}	1.27
16.5	0.985	1.32×10^{-4}	4.13×10^{-2}	1.61×10^{-2}	1.79

3.2.6.2. Quantitative determination of the platinum loading on cation-exchange membranes by gravimetric analysis

The total platinum loading on membranes was determined by gravimetric analysis (as described in section 3.2.3). The results are tabulated in Table 3.10. Figure 3.17 shows a comparison of the results of the total platinum loading on a membrane as determined by gravimetric and spectrophotometric analyses.

Table 3.10. Results of gravimetric and spectrophotometric analysis of the total platinum loading on membranes by the reduction of 0.05M platonic acid solution with hydrazine for the total times of platinisation of 4.5, 6.5, 8.5, 10.5, 12.5 and 16.5 minutes.

Total time of platinisation for the reduction of 0.05M platonic acid solution by N ₂ H ₄ (min)	Pt loading on membrane as determined by gravimetric analysis (g)	Total Pt loading on membrane as determined by gravimetric analysis (mg/cm ²)	Total Pt loading on membrane as determined by spectrophotometric analysis (mg/cm ²)
4.5	1.4×10^{-3}	0.16	0.37
6.5	2.4×10^{-3}	0.27	0.70
8.5	5.2×10^{-3}	0.58	0.87
10.5	6.8×10^{-3}	0.76	1.04
12.5	8.7×10^{-3}	1.00	1.27
16.5	1.25×10^{-2}	1.40	1.79

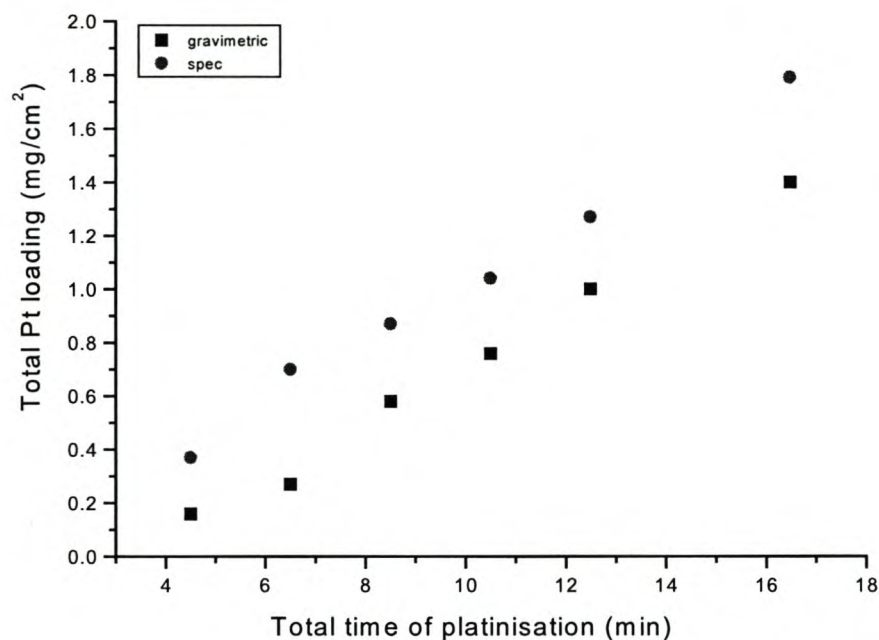


Figure 3.17. Plot of total platinum loading on membranes achieved by the reduction of 0.05M platonic acid solution with N₂H₄ for the total time of platinisation of 4.5, 6.5, 8.5, 10.5, 12.5 and 16.5 minutes, as determined by gravimetric and spectrophotometric (spec) analysis.

3.2.7. Quantitative determination of the platinum embedded on pre-treated cation-exchange membranes by the reduction of 0.05M platinic acid solution with hydrazine at room temperature (see Section 2.5.4)

3.2.7.1. Quantitative determination of the platinum loading on cation-exchange membranes by UV spectrophotometric analysis

Platinum was removed from platinum containing membranes with aqua regia (as described in section 3.2.2.1). 0.5 ml of each solution containing platinum ions (as prepared in section 3.2.2.1) was measured into separate 25 ml volumetric flasks. 5 ml 0.5M SnCl_3^- was added to each volumetric flask and the remaining volume of the volumetric flask was filled with distilled water. The reference solution contained 5 ml 0.5M SnCl_3^- and 20 ml distilled water. The UV absorbance of the solutions containing platinum ions was measured after 180 min (Fig. 3.18).

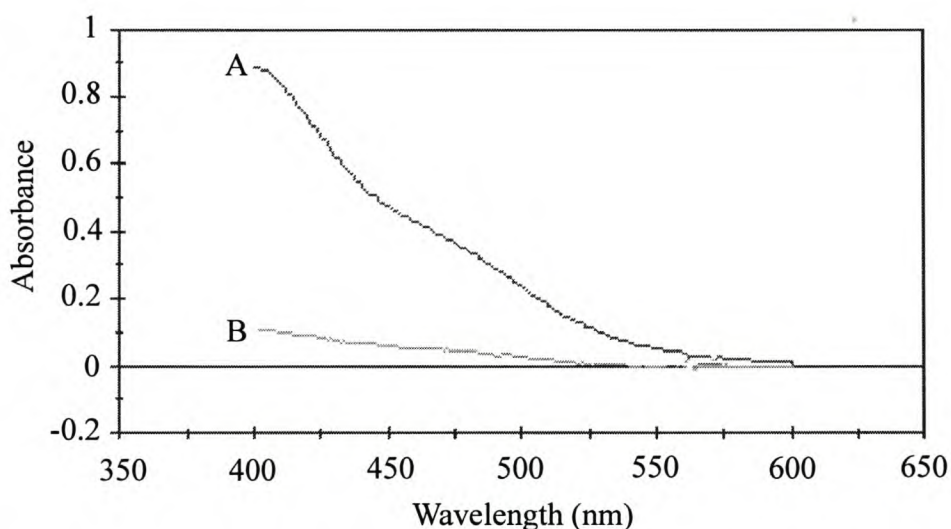


Figure 3.18. UV absorption spectrum of solutions containing platinum ions of unknown concentrations. The platinum catalyst was deposited on membranes (A) pre-treated with $\text{H}_2\text{O}/\text{MeOH}$ and (B) pre-treated with boiling water.

The results of the UV spectrophotometric analysis were used to determine the total platinum loading on the membranes achieved by the reduction of 0.05M platinic acid solution with hydrazine at different time intervals (Table 3.11).

Table 3.11. *UV spectrophotometric results of platinum loading on cation-exchange membranes by the reduction of 0.05M platinic acid solution with hydrazine for a total time of platinisation of 11 minutes.*

Conditions of pre-treatment	Absorbance of solutions containing Pt ions at a wavelength of 402.27 nm	Concentration of solutions containing Pt ions (mole/L)	Mass of Pt deposited on membrane (g) ^a	Mass of Pt deposited on membrane for 39% Pt in H ₂ PtCl ₆ ·XH ₂ O (g)	Total Pt loading on membrane (mg/cm ²) ^b
H ₂ O/MeOH	0.8346	10.30x10 ⁻⁵	0.258	0.101	2.42
Water	0.1007	1.31x10 ⁻⁵	0.033	0.013	0.31

3.2.7.2. Quantitative determination of the platinum loading on cation-exchange membranes by gravimetric analysis

The total platinum loading on the membranes was determined by gravimetric analysis (see section 3.2.3). The results are tabulated in Table 3.12.

Table 3.12. *Results of gravimetric and spectrophotometric analysis of the total platinum loading on membranes by the reduction of 0.05M platinic acid solution with hydrazine for the total time of platinisation of 11 minutes at room temperature.*

Pre-treatment conditions	Total Pt loading on membranes as determined by gravimetric analysis (mg/cm ²)	Total Pt loading on membranes as determined by spectrophotometric analysis (mg/cm ²)
H ₂ O/MeOH	2.08	2.42
Water	0.43	0.31

^a $m = C \times V \times DC \times MM_{H_2PtCl_6 \cdot 5H_2O}$, where C is the concentration of the platinic acid (determined from calibration curve); V is the initial volume of the platinum solution (0.1L); DC is the "dilution" coefficient (50) and $MM_{H_2PtCl_6 \cdot 5H_2O}$ is the molecular mass of the platinic acid solution (500)

^b Calculated for the dry membrane of diameter = 73mm

3.2.8. Discussion

The effect of the time of the deposition process

The platinum loading on membranes increased as the total time of platinisation increased, irrespective of the conditions of the deposition process (Fig. 3.19). This is attributed to greater reduction of the platinumic acid solution by the reducing agent, as the time of contact of the reducing agent with the platinumic acid solution (through a membrane) is increased.

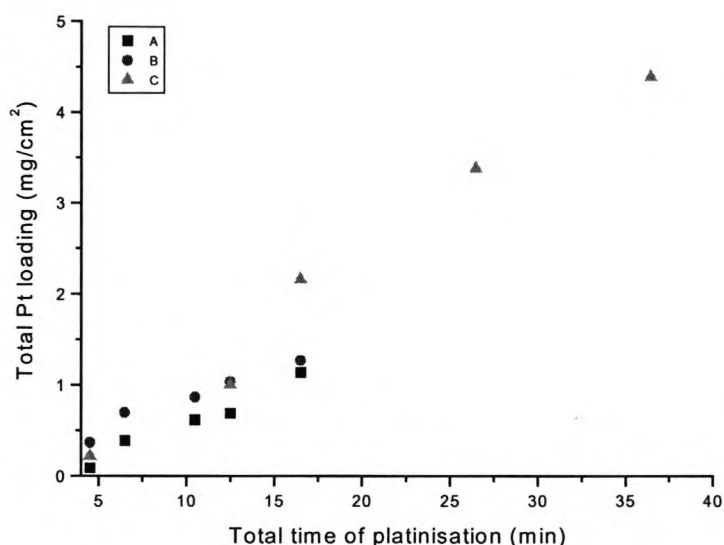


Figure 3.19. Results of UV spectrophotometric analysis of the total platinum loading on a membrane when (A) 0.05M platinumic acid solution is reduced by NaBH_4 , (B) 0.05M platinumic acid solution is reduced by N_2H_4 and (C) 0.03M platinumic acid solution is reduced by NaBH_4 .

The effect of temperature of the reducing agent

The platinum loading on membranes was 0.31 mg/cm^2 with the reduction of 0.05M platinumic acid solution by hydrazine for 11 minutes at room temperature. The platinum loading on a membrane was 1.04 mg/cm^2 with the reduction of 0.05M platinumic acid by hydrazine for 10.5 minutes at a temperature of $40 \text{ }^\circ\text{C}$. Thus, the increase in temperature of the reducing agent, results in the platinum loading on a membrane increasing. This can be attributed to the increase in the rate of the reaction, for the electroless deposition of platinum, with the increase in temperature.

The effect of pre-treating membranes

Greater platinum loading on cation-exchange membranes was achieved when membranes were pre-treated with a solution of H₂O (70% vol.) and MeOH (30% vol.) prior to the deposition process (as described in section 2.5.1). Pre-treatment of membranes with boiling water exhibited no significant increase in platinum loading (Table 3.11). Increased platinum loading, due to pre-treatment with a solution of H₂O (70% vol.) and MeOH (30% vol.) can be attributed to the methanol increasing the pore size of the membrane. Greater permeation of the reducing agent through the membrane will result as the membrane pore size increases. This will allow for greater reduction of the platonic acid solution by the reducing agent.

The effect of the platonic acid concentration

When using sodium borohydride as the reducing agent in the process of electroless deposition, greater platinum loading on membranes was achieved for 0.03M platonic acid solution compared to 0.05M platonic acid solution (Fig. 3.19). Although these experiments were repeated several times, these results were confirmed (SEM analysis in section 4.2.4 also verified these results). This can be attributed to the process of the electroless deposition of platinum being a complex process, which involves various stages such as: the diffusion of a reducing agent via a membrane, delivering of [PtCl₆]²⁻ ions to the surface of a membrane, changing of pH during the reduction of platonic acid solution by the reducing agent, blocking of diffusion channels of the membrane by the formation of platinum particles, etc. Therefore, the deposition process is of a very dynamic nature with variations in the kinetic, diffusional and other modes of the deposition process.

It can be seen from Figure 3.19 (from the first 15 minutes) that the slope and shape of the dependence of platinum loading on the time of platinisation differs for the various reducing agents and concentrations of platonic acid solution. Understanding these complexities of the deposition process, it can be assumed that the reduction of 0.03M platonic acid by sodium borohydride, is more favorable for platinum particle formation based on the consideration of the above variables. The dynamic nature of this electroless deposition process can further be seen in the variations of the Hurst exponent results for the surface roughness profile of a platinum catalyst (see section 8.7).

This same phenomenon was not observed when 0.03M platonic acid solution was reduced by hydrazine, as seen with sodium borohydride (Table 3.13). It can be concluded that it is not the rate of permeation of the sodium borohydride that results in low platinum loading as suggested by Fedkiw et al. (1990). The results indicate that sodium borohydride is slow in reducing $[\text{PtCl}_6]^{2-}$ ions to platinum metal. Since this is not the case with hydrazine (Table 3.13), it can be concluded that hydrazine is more efficient at reducing platonic acid solution as compared with sodium borohydride.

Table 3.13. Results of the reduction of platonic acid solution by hydrazine for 15.5 minutes at a temperature of 40 °C

Concentration of platonic acid solution (M)	Mass of platinum-containing membrane (g)	Mass of membrane without platinum (g)	Pt loading on membrane as determined by gravimetric analysis (g)	Total Pt loading on membrane (mg/cm^2)
0.05	0.93	0.92	0.01	2.75
0.03	0.96	0.96	0.0041	1.18

Effect of the nature of the reducing agent

Autocatalytic electroless deposition of a metal catalyst onto ion-exchange membranes is thermodynamically possible if the following condition is valid:

$$\Delta E = E_{\text{ME}} - E_{\text{RED}} > 0$$

Where E_{ME} and E_{RED} are the potentials of a metal in a solution containing its ions and a reducing agent, respectively.

Many chemicals are suitable to act as reducing agents, such as, for example formaldehyde, hypophosphite, borohydride, hydrazine, and some others. The statistical probability (ω) of the formation of a metal catalytic nucleus during the autocatalytic process is proportional to the following equation:

$$\omega \approx \exp \left[\left(\frac{\Delta E}{RT/F} \right)^{-2} \right]$$

An equation for the critical size of stable nucleus (ρ) also includes ΔE variable:

$$\rho = 2\sigma V / zF\Delta E$$

Where, σ is surface tension between catalytic particle and a solution, V is a metal molar volume, z is a number of electrons, and F is Faradic number.

It is seen from these equations that the nature of a reducing agent allows control of the morphology (e.g., size, distribution profile, etc.) of platinum particles by means of a large number of variables, such as concentration of solutions, their pH, temperature, etc. All these variables effect the rate of the formation of the nucleus and the rate of the autocatalytic process itself (Bessarabov et al., 2001).

The results show that greater platinum loading on a membrane was achieved when platinic acid solution was reduced by hydrazine, as compared to sodium borohydride (Figure 3.20). This can be attributed to hydrazine being a stronger reducing agent than sodium borohydride (see Table 1.5, section 1.4.3.1).

Ohno et al. (1985) showed that the catalytic activity of a metal, such as platinum, varies according to the nature of the reducing agent. The deposition rate of an electroless-deposition system is determined by the catalytic activity of the metal to be deposited. Since the catalytic activity of platinum is greater in the presence of hydrazine than sodium borohydride, greater platinum loading on a membrane will be achieved with hydrazine than sodium borohydride.

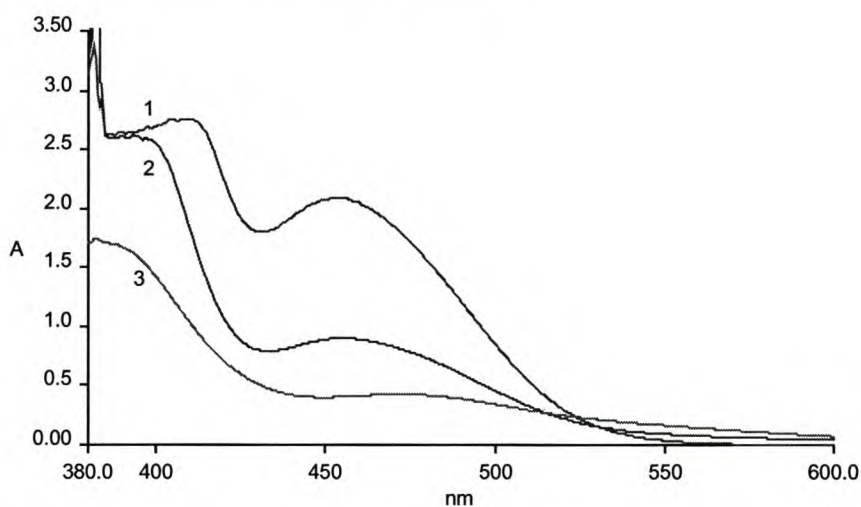


Figure 3.20. UV spectrophotometric results of (1) 0.05M platinic acid solution, (2) platinic acid solution after reduction with NaBH_4 and (3) platinic acid solution after reduction with N_2H_4 . Platinic acid solution was reduced by NaBH_4 and N_2H_4 for a time of 40 minutes.

Also, since the diffusion rate of the anionic borohydride (BH_4^-) through the membrane is slower than that of hydrazine, the rate of platinum formation on the membrane will be slower when using sodium borohydride (Fedkiw et al., 1990). This explains the

greater platinum loading achieved when using hydrazine than with sodium borohydride (Fig. 3.20). However, the slower diffusion of sodium borohydride through a membrane might allow for better control of the deposition process.

Analysis of platinum loading

There are disadvantages in using both UV spectrophotometric and gravimetric analyses for the quantitative determination of platinum loading on membranes. In gravimetric analysis the disadvantages are the following:

- greater risk of error when using small membrane samples as the mass of platinum mass is greatly affected by any small spillage, and
- the membrane samples absorbing water from the surrounding atmosphere during the weighing process results in the distortion of the actual mass of the membrane.

In UV spectrophotometric analysis, shifts of absorption peaks under various conditions and rapid fading of solutions with increasing exposure to the surrounding atmosphere indicate that this is not an entirely satisfactory method for the quantitative determination of platinum loading on membranes (Yates, 1983). In this study, ideal conditions for UV spectrophotometric analysis were established through the development of a protocol for the quantitative determination of platinum loading on membranes by UV spectrophotometric analysis.

The difference in the results obtained for UV spectrophotometric analysis and gravimetric analysis seem to be due to inaccurate membrane sample masses, which occurred with the sorption of water by membranes during gravimetric analysis.

3.3. Conclusions

Experimental work was carried out to determine a suitable protocol for the analysis of platinum (IV) by UV spectrophotometry. The results showed that:

- The platinum solution without aqua regia was fairly stable compared to the platinum solution containing aqua regia, thereby indicating that aqua regia had an effect on Pt (IV)-tin (II) chloride solution.
- Pt (IV)-tin (II) chloride solution with high concentration of aqua regia was stable between 180 and 260 minutes, as well as between 320 min and 420 min.

- The absorbance for a Pt (IV)-tin (II) chloride solution with a low concentration of aqua regia and a Pt (IV)-tin (II) chloride solution without aqua regia, are similar.
- Pt (IV)-tin (II) chloride solution with a high concentration of aqua regia exhibits a rapid decrease in absorbance after 450 min. Therefore, Pt (IV)-tin (II) chloride solution with a high concentration of aqua regia becomes unstable after 450 min.

The quantitative determination of the platinum loading on a membrane by UV spectrophotometric and gravimetric analyses was explored. It was established that the results for UV spectrophotometric analysis was of greater accuracy than gravimetric analysis. Although, UV spectrophotometric analysis has many disadvantages in the quantitative determination of the platinum loading on a membrane, suitable conditions for its use can be determined through the development of a protocol.

Our study did not aim to investigate the chemical effect of aqua regia on the Pt (IV)-tin complex. Thus, the nature of the interaction of aqua regia and the Pt (IV)-tin complex is not presented in this work.

Different variables such as, nature of the reducing agent, temperature of the reducing agent, time of platinisation, pre-treatment of membranes and concentration of the platinic acid, were investigated to determine their effect on the platinum loading on membranes. The determination of the platinum loading on membranes is important for the selection of appropriate conditions to achieve optimal platinum loading.

The characterisation of the platinum catalyst on a cation-exchange membrane is explored in the following chapter. The morphology (size, shape, distribution profile, etc.) of the platinum catalyst layer on the cation-exchange membrane was investigated by different characterisation techniques.

References

1. Ayres GH and Meyer AS, 1951, Spectrophotometric study of the platinum (IV)-tin (II) chloride system, *Analytical Chemistry*, 23, 2, 299-304
2. Ayres GH, Tuffly BL and Forrester JS, 1955, Determination of Rh with Sn (II) chloride- Determination of Rh and Pt, *Analytical Chemistry*, 27, 1742

3. Berman SS and Goodhue EC, 1959, A new spectrophotometric procedure for platinum with tin (II) chloride, *Canadian Journal of Chemistry*, 37, 370-374
4. Bessarabov D and Michaels W, 2001, Morphological diversity of Pt clusters deposited onto proton-exchange perfluorinated membranes for catalytic applications, *Membrane Technology/Intern. Newsletter*, 2001, in press
5. Cotton, Wilkinson and Gaus, 1988, *Basic Inorganic Chemistry*, second edition, Canada: John Wiley & Sons
6. Cramer RD, Lindsey Jr. RV, Prewitt CT and Stolberg UG, 1965, *J.A.C.S.*, 87, 658
7. Fedkiw PS, Potente JM and Her WH, 1990, Electroreduction of gaseous ethylene on a platinized Nafion membrane, *J. Electrochem. Soc.*, Vol. 137, No. 5, 1451-1460
8. Koch K and Ahmed N, 1984, The liquid-liquid extraction of the platinum in the presence of tin (II) chloride for diluted hydrochloric acid into 4-methyl-2-pentanone, *Analytica Chimica Acta*, 162, 347-356
9. Koch K, Brackenbury KFG, Jones L, Nel I and Wyrley-Birch JM, 1987, Tin (II) chloride in the analytical chemistry of the platinum metals: from the "purple of cassius" to polyurethane foams, *Polyhedron*, 6, 1, 71-78
10. Koch KR and Yates J, 1983, The effect of tin (II) chloride on the liquid-liquid extraction of tetrachloroplatinate (II) ions by triphenylphosphine in dichloromethane, *Analytica Chimica Acta*, 147, 235-245
11. Payne TS, 1960, The separation and determination of platinum metals, *Analyst*, 85, 698
12. Sexton A, 1892, *Outlines of qualitative analysis*, third edition, p45, C. Griffin, London
13. Sheppard S.-A, Campbell SA, Smith JR, Lloyd GW, Ralph TR and Walsh FC, 1998, Electrochemical and microscopic characterisation of platinum-coated perfluorosulfonic acid (Nafion 117) materials, *Analyst*, 123, 1923
14. Wöhler L and Spengel A, 1910, Red Pt as analogous to cassius' purple, *Z. Chem. Ind. Kolloide*, 7, 243
15. Yates JE, 1981, The effect of stannous chloride on the solvent extraction of tetrachloroplatinate(2)ion by triphenylphosphine, M.Sc thesis, University of Cape Town
16. Young JF, Gillard JL and Wilkinson G, 1964, Complexes of Ru, Rh, Ir and Pt with Sn (II) chloride, *J. Chem. Soc.*, 5176

Characterisation of electrocatalytic solid polymer electrolyte membranes

Abstract

In this chapter the morphology of electrocatalytic SPE membranes was investigated by means of various characterisation techniques. Information on the surface profile of the membranes and the platinum catalyst on the membranes were obtained. The effect of temperature, concentration of the platinic acid solution, use of different reducing agents, applied external activation in the deposition process and membrane pre-treatment on the morphology of the electrocatalytic SPE membranes was investigated. The porosity of the pre-treated membranes was also investigated.

4.1. Characterisation of the morphology of the platinum catalyst embedded on the cation-exchange membrane by Atomic Force Microscopy (AFM)

It is possible to obtain a layer of platinum with varying surface roughness on a membrane by changing the variables of the chemical deposition process. In our study, the effect of variables such as, temperature, concentration of the platinic acid solution, use of different reducing agents, pre-treatment of the membranes and external activation during the process of chemical deposition on the surface roughness of the layer of platinum on the membrane was investigated.

In Atomic Force Microscopy (AFM) a sharp tip on the end of a flexible cantilever is scanned across a sample surface while maintaining a small, constant force. The scanning motion is conducted by a piezoelectric tube scanner, which scans the tip of the sample. The tip-sample interaction is monitored by reflecting a laser from the back of the cantilever into a split photodiode detector. Changes in the cantilever deflection or oscillation amplitude are determined by detecting the difference in the photodetector output voltages (Russell et al., 2001).

The most commonly used modes of operation are contact-mode AFM and tapping (non-contact) mode, which are conducted in air or liquid environments. Contact-mode AFM entails scanning the probe across the surface of a sample while

monitoring the change in cantilever deflection by vertically moving the scanner to maintain a constant photodetector difference signal. Tapping mode AFM entails oscillating the cantilever at its resonance frequency and lightly tapping on the surface of the sample during scanning. A feedback loop maintains a constant oscillation amplitude by moving the scanner vertically at every x,y data point. The advantage of the tapping mode compared with contact mode is that it eliminates the lateral shear forces present in the contact mode. This enables tapping mode to image soft, fragile and adhesive surfaces without damaging them, which can be a drawback of contact-mode AFM (Russell et al., 2001).

AFM can provide compositional information by differentiating materials based on physical properties, such as stiffness, elasticity, compliance, friction, adhesion, magnetic and electrostatic fields, carrier concentration, temperature distribution, spreading resistance and conductivity (Russell et al., 2001).

SPE electrocatalytic membranes were imaged with the Topometrix explorer TM×2000 AFM. The images were recorded with an AFM-J piezoelectric scanner, which has a lateral scan area of $130\mu\text{m}\times 130\mu\text{m}$. The spring constant of the cantilever tips was between $30\text{-}80\text{ Nm}^{-1}$. Images were recorded in the non-contact mode, during which the tip of the probe vertically oscillates onto the sample.

The artifacts that appear in the AFM images are due to the samples being contaminated. Contamination of a sample results in the appearance of a deep pit on the AFM image, which causes the tunneling current to decrease rapidly. The probe will move closer to the sample. Contact of the probe with the sample results in additional artifacts. This is a disadvantage of using AFM for determining surface roughness. Other methods of quantifying surface roughness have been explored such as, standard deviation, power spectrum, mean range and R/S analysis (Parkhutik et al., 2000). Standard deviation is a measure of the average deviation from the mean of the roughness data. A power spectrum displays the distribution of the variance with frequency. The mean range yields the average height of roughness profile (Parkhutik et al., 2000).

AFM, nonetheless, remains a useful tool for determining surface roughness as it (Kiely et al., 1997):

- covers many orders of magnitude of length scale,
- provides three-dimensional (3D) data in digital format at nanometre level,

- allows extensive mathematical treatment of data,
- quantification of surface structure can be based on several fundamental methods of characterising surface features such as, the distribution of heights above or below some reference height, using a spectrum of wavelengths to approximate the surface, or using the correlation of heights over some lateral separation, and
- can be a powerful tool for determining surface roughness when combined with statistical parameters such as, root-mean-square roughness (measure of the variation in height), autocovariance (measure of spatial correlation of heights) and power density (measure of wavelengths of periodic features).

The main objective of the work described in this chapter was to investigate the surface roughness of the platinum catalyst on a membrane by atomic force microscopy (AFM), which provides information on the surface morphology, surface roughness, nanoscale structures and molecular- and atomic-scale lattices.

4.1.1. Surface roughness analysis of platinum catalyst embedded on cation-exchange membranes by the reduction of platinumic acid solution at 40 °C

4.1.1.1. AFM imaging of membranes embedded with platinum catalyst by the reduction of 0.05M platinumic acid solution with hydrazine at 40 °C.

Figures 4.1 and 4.2 are two-dimensional and three-dimensional surface images ($20\mu\text{m}\times 20\mu\text{m}$) of cation-exchange membranes embedded with platinum catalyst by the reduction of 0.05M platinumic acid solution with hydrazine for 3.5 minutes at 40 °C. The average roughness of the platinum catalyst on the membrane is 101.43 nm and the average height of the platinum catalyst on the membrane is 478.9 nm. The surface area of the electrocatalytic membrane is $478.1\ \mu\text{m}^2$. The fractal dimension of the surface of the SPE electrocatalytic membrane is 2.59. The platinum layer is characteristic of small platinum particles that are densely packed (Figs. 4.1 and 4.2). The surface roughness profile of the electrocatalytic membrane can be seen in the line analysis plot (Fig. 4.3). The surface roughness of the platinum on the membrane can be described (qualitatively) as rutted (Fig. 4.3).

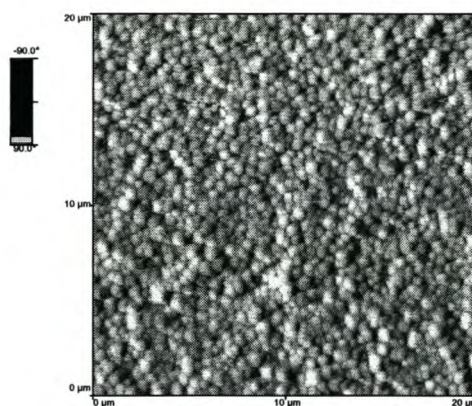


Figure 4.1. AFM surface image ($20\mu\text{m}\times 20\mu\text{m}$) of a cation-exchange membrane embedded with platinum catalyst by the reduction of 0.05M platinumic acid solution with hydrazine for 3.5 minutes at 40 °C.

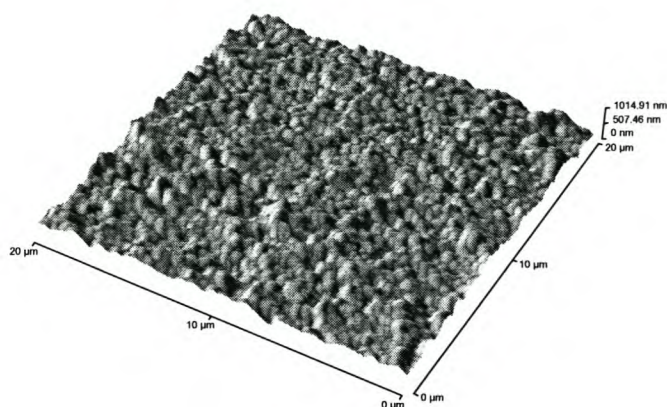


Figure 4.2. Three-dimensional AFM surface image ($20\mu\text{m}\times 20\mu\text{m}$) of a cation-exchange membrane embedded with platinum catalyst by the reduction of 0.05M platinic acid solution with hydrazine for 3.5 minutes at $40\text{ }^\circ\text{C}$.

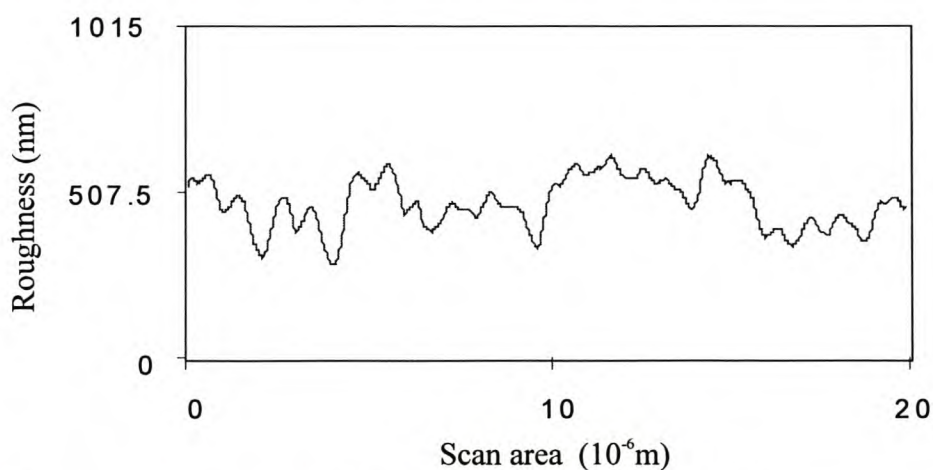


Figure 4.3. Line analysis plot of the surface roughness of a cation-exchange membrane embedded with platinum catalyst by the reduction of 0.05M platinic acid solution with hydrazine for 3.5 minutes at $40\text{ }^\circ\text{C}$.

Figures 4.4 and 4.5 are two-dimensional and three-dimensional surface images ($130\mu\text{m}\times 130\mu\text{m}$) of cation-exchange membranes embedded with platinum catalyst by the reduction of 0.05M platinic acid solution with hydrazine for 3.5 minutes at $40\text{ }^\circ\text{C}$. The average roughness of the layer of platinum catalyst is 411.9 nm and the average height of the platinum catalyst is 1840.4 nm . The surface area of the platinum catalyst is $17766\text{ }\mu\text{m}^2$. The fractal dimension of the platinum catalyst embedded on the surface of the membrane is 2.39. The profile of the platinum catalyst embedded on the membrane is uneven (Figs. 4.4 and 4.5). The surface roughness profile of the

platinum catalyst embedded on the membrane can be seen in the line analysis plot (Fig. 4.6). The surface roughness of the platinum on the membrane can be described (qualitatively) as uneven (Fig. 4.6).

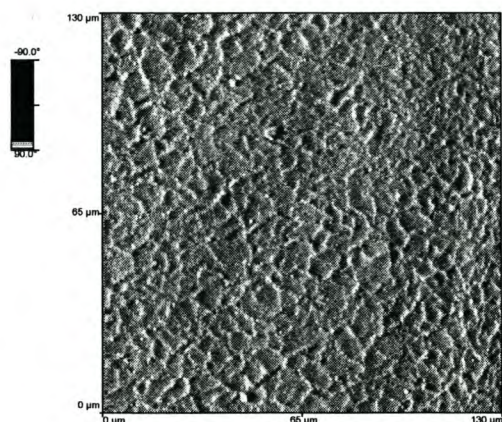


Figure 4.4. *AFM surface image (130 μ m \times 130 μ m) of a cation-exchange membrane embedded with platinum catalyst by the reduction of 0.05M platinic acid solution with hydrazine for 3.5 minutes at 40 °C.*

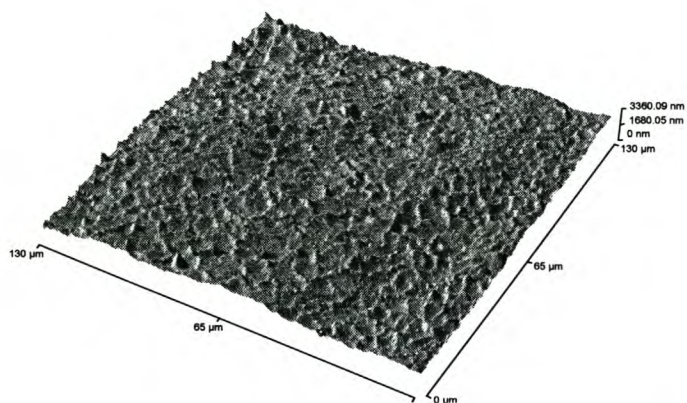


Figure 4.5. *Three-dimensional AFM surface image (130 μ m \times 130 μ m) of a cation-exchange membrane embedded with platinum catalyst by the reduction of 0.05M platinic acid solution with hydrazine for 3.5 minutes at 40 °C.*

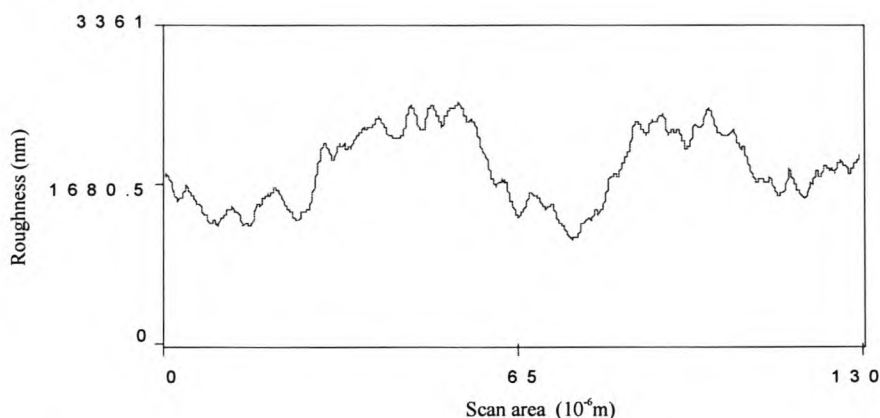


Figure 4.6. Line analysis plot of the surface roughness of a cation-exchange membrane embedded with platinum catalyst by the reduction of 0.05M platinic acid solution with hydrazine for 3.5 minutes at 40 °C.

Figures 4.7 and 4.8 are two-dimensional and three-dimensional surface images (20 $\mu\text{m}\times 20\mu\text{m}$) of cation-exchange membranes embedded with platinum catalyst by the reduction of 0.05M platinic acid solution with hydrazine for 5.5 minutes at 40 °C. The average roughness of the layer of platinum catalyst is 393.4 nm and the average height of the layer of the platinum catalyst is 945.5 nm. The surface area of the platinum catalyst is 490.6 μm^2 . The fractal dimension of the platinum catalyst embedded on the membrane surface is 2.25.

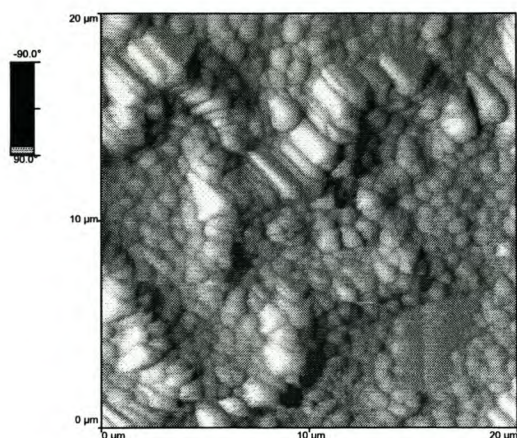


Figure 4.7. AFM surface image (20 $\mu\text{m}\times 20\mu\text{m}$) of a cation-exchange membrane embedded with platinum catalyst by the reduction of 0.05M platinic acid solution with hydrazine for 5.5 minutes at 40 °C.

The platinum catalyst embedded on the membrane consists of large particles dispersed with small platinum particles (Figs. 4.7 and 4.8). The surface roughness profile of the platinum catalyst embedded on the membrane can be seen in the line analysis plot (Fig. 4.9). The surface roughness of the platinum catalyst embedded on the membrane can be described (qualitatively) as wavy (Fig. 4.9).

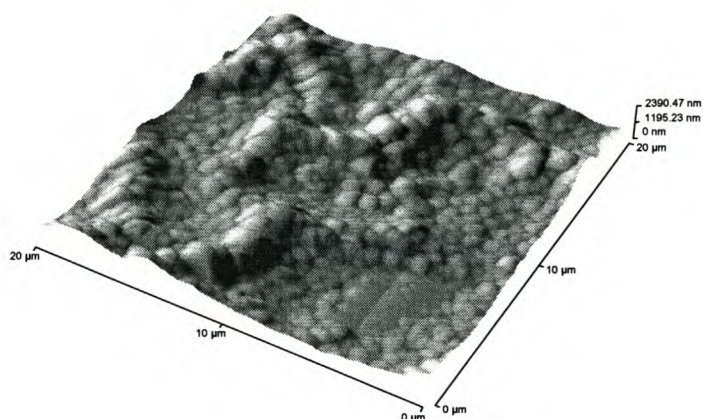


Figure 4.8. Three-dimensional AFM surface image ($20\mu\text{m}\times 20\mu\text{m}$) of a cation-exchange membrane embedded with platinum catalyst by the reduction of 0.05M platinic acid solution with hydrazine for 5.5 minutes at 40 °C.

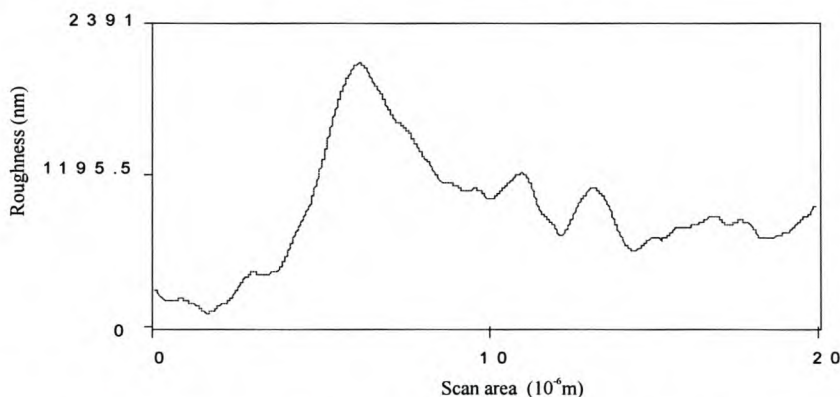


Figure 4.9. Line analysis plot of the surface roughness of a cation-exchange membrane embedded with platinum catalyst by the reduction of 0.05M platinic acid solution with hydrazine for 5.5 minutes at 40 °C.

Figures 4.10 and 4.11 are two-dimensional and three-dimensional surface images ($130\mu\text{m}\times 130\mu\text{m}$) of cation-exchange membranes embedded with platinum catalyst by the reduction of 0.05M platinic acid solution with hydrazine for 5.5 minutes at 40 °C. The average roughness of the layer of platinum catalyst on the membrane is 415.7 nm

and the average height of the layer of the platinum on the membrane is 1711.3 nm. The surface area of the platinum catalyst is $18230 \mu\text{m}^2$. The fractal dimension of the platinum catalyst embedded on the surface of the membrane is 2.44. The profile of the platinum catalyst is uneven (Figs. 4.10 and 4.11). The surface roughness profile of the platinum embedded on the membrane can be seen in the line analysis plot (Fig. 4.12). The surface roughness of the platinum embedded on the membrane can be described (qualitatively) as rutted (Fig. 4.12).

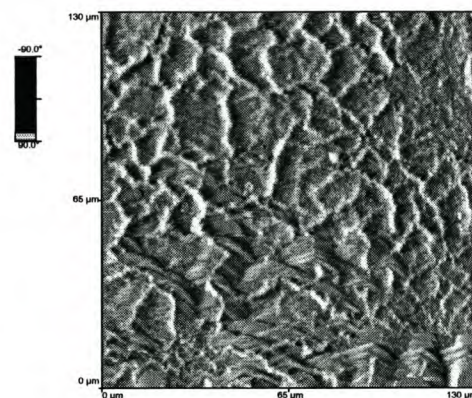


Figure 4.10. *AFM surface image ($130\mu\text{m}\times 130\mu\text{m}$) of a cation-exchange membrane embedded with platinum catalyst by the reduction of 0.05M platinic acid solution with hydrazine for 5.5 minutes at 40 °C.*

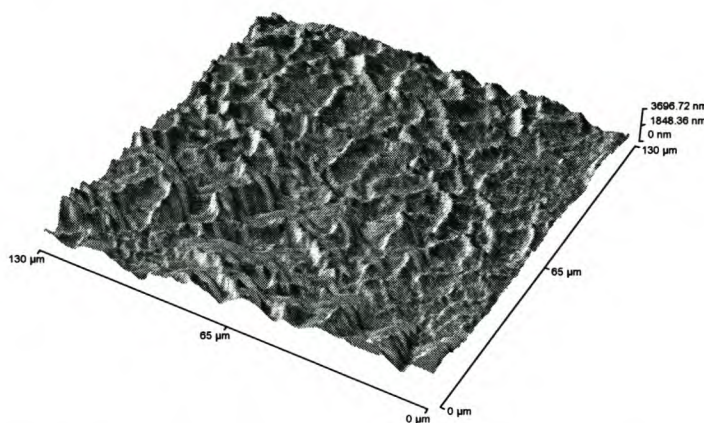


Figure 4.11. *Three-dimensional AFM surface image ($130\mu\text{m}\times 130\mu\text{m}$) of a cation-exchange membrane embedded with platinum catalyst by the reduction of 0.05M platinic acid solution with hydrazine for 5.5 minutes at 40 °C.*

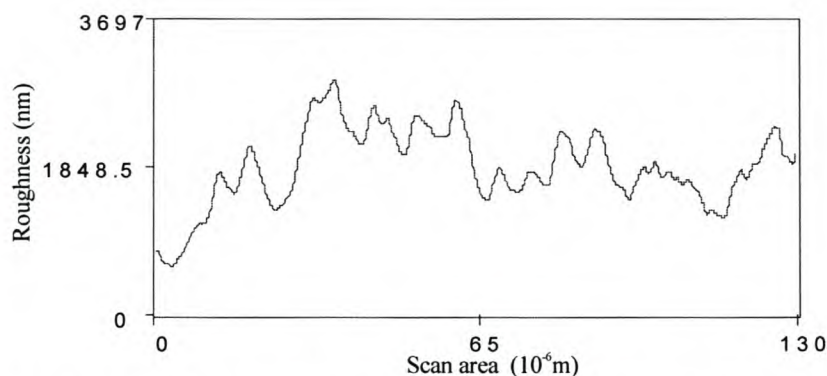


Figure 4.12. Line analysis plot of the surface roughness of a cation-exchange membrane embedded with platinum catalyst by the reduction of 0.05M platonic acid solution with hydrazine for 5.5 minutes at 40 °C.

Figures 4.13 and 4.14 are two-dimensional and three-dimensional surface images ($20\mu\text{m}\times 20\mu\text{m}$) of cation-exchange membranes embedded with platinum catalyst by the reduction of 0.05M platonic acid solution with hydrazine for 7.5 minutes at 40 °C. The average roughness of the platinum catalyst embedded on the membrane is 610.4 nm and the average height of the layer of the platinum catalyst is 2001.8 nm. The surface area of the platinum catalyst is $497.1\ \mu\text{m}^2$. The fractal dimension of the platinum catalyst embedded on the membrane surface is 2.14.

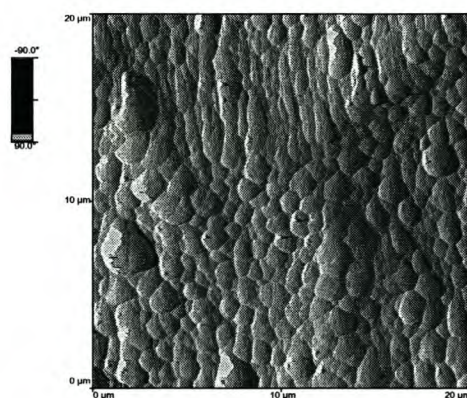


Figure 4.13. AFM surface image ($20\mu\text{m}\times 20\mu\text{m}$) of a cation-exchange membrane embedded with platinum catalyst by the reduction of 0.05M platonic acid solution with hydrazine for 7.5 minutes at 40 °C.

The platinum catalyst embedded on the membrane is characteristic of large platinum particles (Figs. 4.13 and 4.14). The surface roughness profile of the platinum catalyst embedded on the membrane can be seen in the line analysis plot (Fig. 4.15). The

surface roughness of the platinum catalyst embedded on the membrane can be described (qualitatively) as wavy (Fig. 4.15).

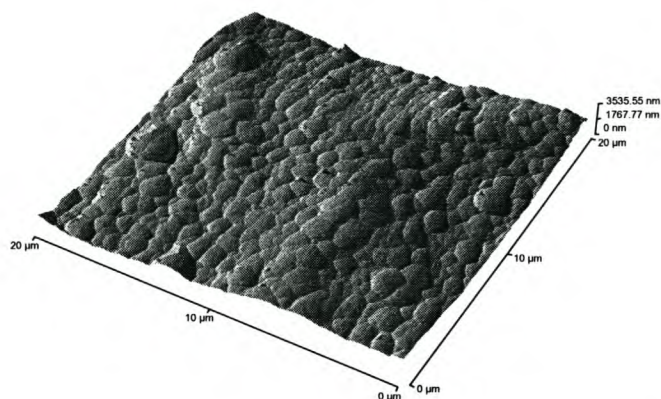


Figure 4.14. Three-dimensional AFM surface image ($20\mu\text{m}\times 20\mu\text{m}$) of a cation-exchange membrane embedded with platinum catalyst by the reduction of 0.05M platinum acid solution with hydrazine for 7.5 minutes at $40\text{ }^\circ\text{C}$.

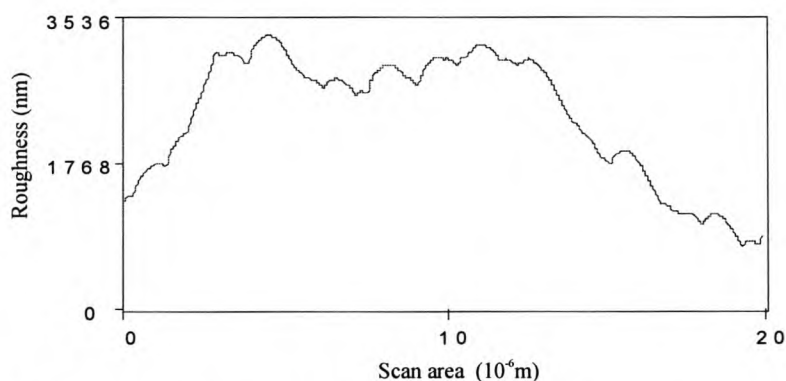


Figure 4.15. Line analysis plot of the surface roughness of a cation-exchange membrane embedded with platinum by the reduction of 0.05M platinum acid solution with hydrazine for 7.5 minutes at $40\text{ }^\circ\text{C}$.

Figures 4.16 and 4.17 are two-dimensional and three-dimensional surface images ($130\mu\text{m}\times 130\mu\text{m}$) of cation-exchange membranes embedded with platinum catalyst by the reduction of 0.05M platinum acid solution with hydrazine for 7.5 minutes at $40\text{ }^\circ\text{C}$. The average roughness of the layer of the platinum catalyst is 678.7 nm and the average height of the platinum catalyst embedded on the membrane is 2761.4 nm . The surface area of the platinum catalyst is $21272\text{ }\mu\text{m}^2$. The fractal dimension of the platinum catalyst embedded on the surface of the membrane is 2.40. The profile of the

platinum catalyst embedded on the membrane is uneven (Figs. 4.16 and 4.17). The surface roughness profile of the platinum catalyst embedded on the membrane can be seen in the line analysis plot (Fig. 4.18). The surface roughness of the platinum catalyst embedded on the membrane can be described (qualitatively) as irregular (Fig. 4.18).

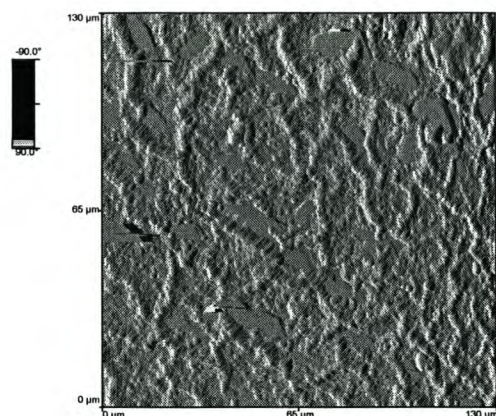


Figure 4.16. *AFM surface image (130 μ m \times 130 μ m) of a cation-exchange membrane embedded with platinum catalyst by the reduction of 0.05M platinic acid solution with hydrazine for 7.5 minutes at 40 °C.*

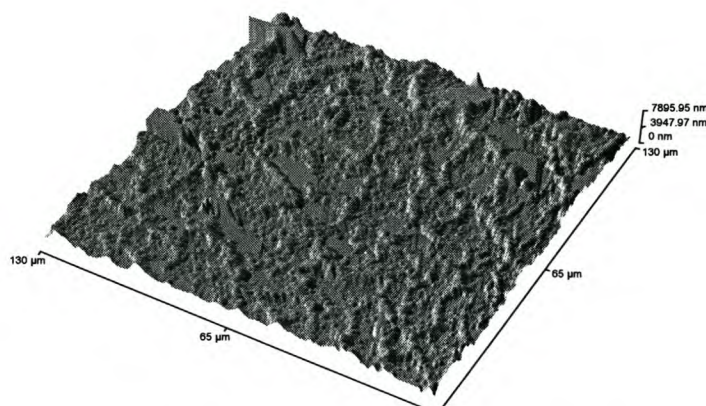


Figure 4.17. *Three-dimensional AFM surface image (130 μ m \times 130 μ m) of a cation-exchange membrane embedded with platinum catalyst by the reduction of 0.05M platinic acid solution with hydrazine for 7.5 minutes at 40 °C.*

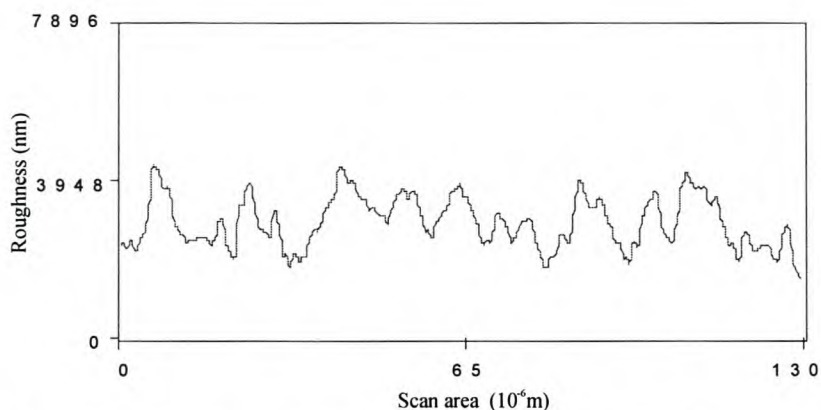


Figure 4.18. Line analysis plot of the surface roughness of a cation-exchange membrane embedded with platinum catalyst by the reduction of 0.05M platinic acid solution with hydrazine for 7.5 minutes at 40 °C.

Figures 4.19 and 4.20 are two-dimensional and three-dimensional surface images (20 $\mu\text{m}\times 20\mu\text{m}$) of cation-exchange membranes embedded with platinum catalyst by the reduction of 0.05M platinic acid solution with hydrazine for 9.5 minutes at 40 °C. The average roughness of the platinum catalyst embedded on the membrane surface is 179.8 nm and the average height of the layer of platinum catalyst is 913.6 nm. The surface area of the platinum catalyst is 437.5 μm^2 . The fractal dimension of the platinum embedded on the surface of the membrane is 2.30.

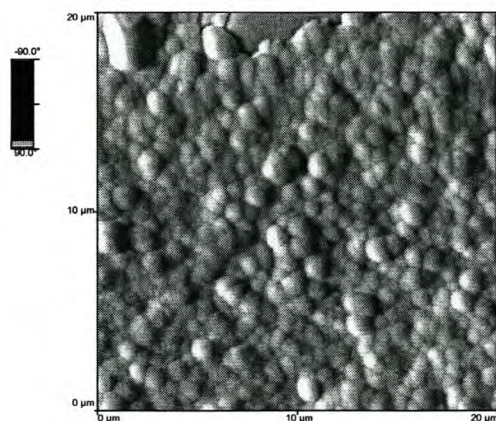


Figure 4.19. AFM surface image (20 $\mu\text{m}\times 20\mu\text{m}$) of a cation-exchange membrane embedded with platinum catalyst by the reduction of 0.05M platinic acid solution with hydrazine for 9.5 minutes at 40 °C.

The platinum catalyst embedded on the membrane is characteristic of large platinum particles (Figs. 4.19 and 4.20). The surface roughness profile of the layer of platinum embedded on the membrane can be seen in the line analysis plot (Fig. 4.21). The

surface roughness of the platinum catalyst embedded on the membrane can be described (qualitatively) as wavy (Fig. 4.21).

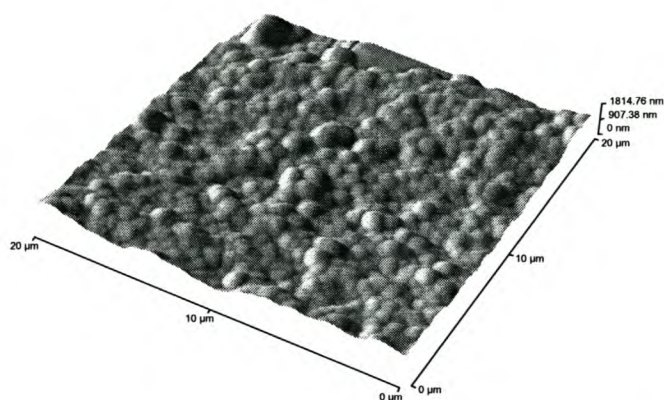


Figure 4.20. Three-dimensional AFM surface image ($20\mu\text{m}\times 20\mu\text{m}$) of a cation-exchange membrane embedded with platinum catalyst by the reduction of 0.05M platinic acid solution with hydrazine for 9.5 minutes at $40\text{ }^{\circ}\text{C}$.

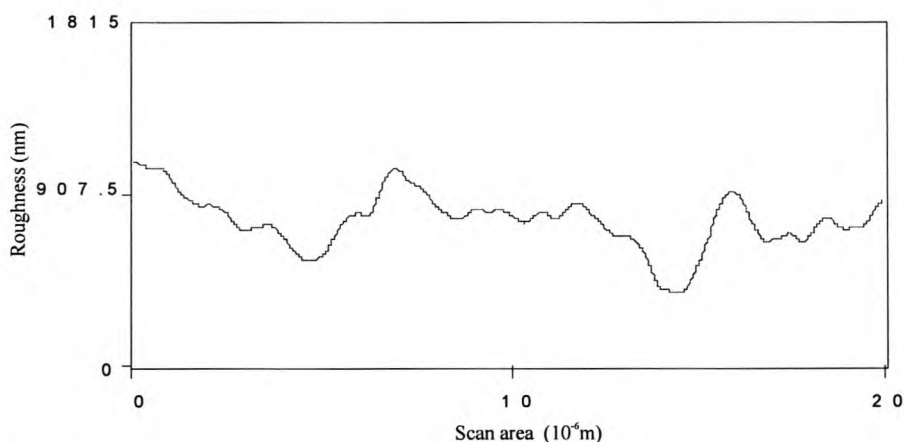


Figure 4.21. Line analysis plot of the surface roughness of a cation-exchange membrane embedded with platinum catalyst by the reduction of 0.05M platinic acid solution with hydrazine for 9.5 minutes at $40\text{ }^{\circ}\text{C}$.

Figures 4.22 and 4.23 are two-dimensional and three-dimensional surface images ($20\mu\text{m}\times 20\mu\text{m}$) of cation-exchange membranes embedded with platinum catalyst by the reduction of 0.05M platinic acid solution with hydrazine for 11.5 minutes at $40\text{ }^{\circ}\text{C}$. The average roughness of the platinum catalyst embedded on the membrane is 118.3 nm and the average height of the layer of platinum catalyst embedded on the membrane is 437.9 nm . The surface area of the platinum catalyst is $417.4\text{ }\mu\text{m}^2$. The fractal dimension of the platinum catalyst embedded on the surface of the membrane

is 2.33. The platinum embedded on the membrane is characteristic of large platinum particles (Figs. 4.22 and 4.23). The surface roughness profile of the platinum catalyst embedded on the membrane can be seen in the line analysis plot (Fig. 4.24). The surface roughness of the platinum catalyst embedded on the membrane can be described (qualitatively) as wavy (Fig. 4.24).

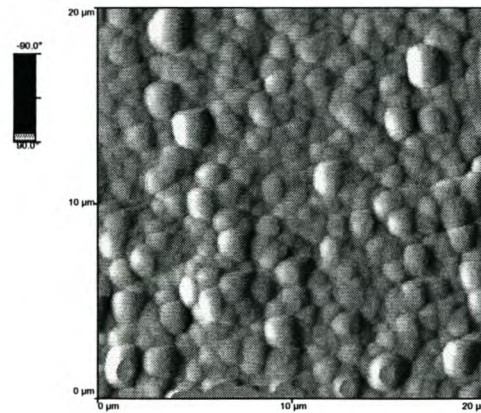


Figure 4.22. *AFM surface image (20μm×20μm) of a cation-exchange membrane embedded with a platinum catalyst by the reduction of 0.05M platinic acid solution with hydrazine for 11.5 minutes at 40 °C.*

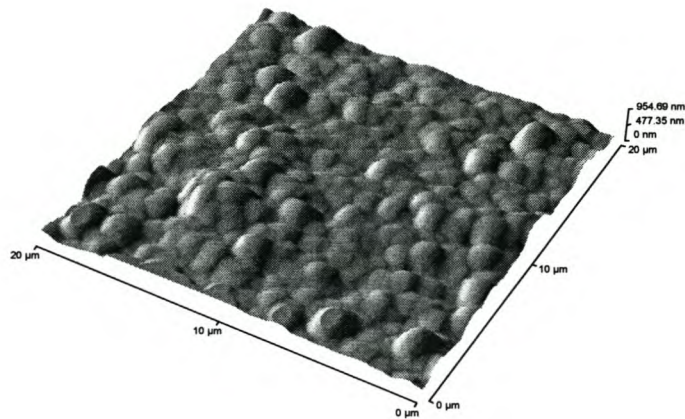


Figure 4.23. *Three-dimensional AFM surface image (20μm×20μm) of a cation-exchange membrane embedded with platinum catalyst by the reduction of 0.05M platinic acid solution with hydrazine for 11.5 minutes at 40 °C.*

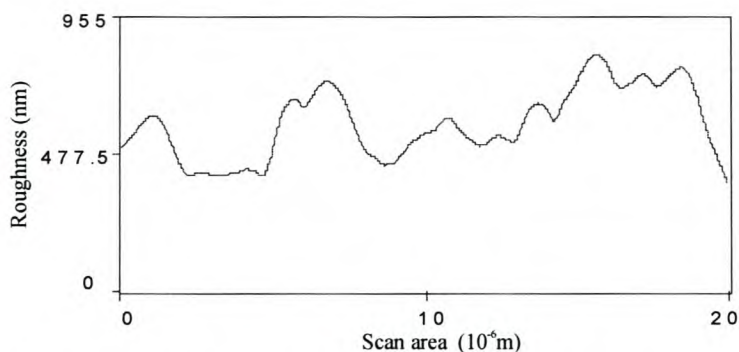


Figure 4.24. Line analysis plot of the surface roughness of a cation-exchange membrane embedded with platinum catalyst by the reduction of 0.05M platinic acid solution with hydrazine for 11.5 minutes at 40 °C.

Figures 4.25 and 4.26 are two-dimensional and three-dimensional surface images ($20\mu\text{m}\times 20\mu\text{m}$) of cation-exchange membranes embedded with platinum catalyst by the reduction of 0.05M platinic acid solution with hydrazine for 15.5 minutes at 40 °C. The average roughness of the platinum catalyst embedded on the membrane is 109.1 nm and the average height of the layer of the platinum catalyst is 335.7 nm. The surface area of the platinum catalyst is $419.7\ \mu\text{m}^2$. The fractal dimension of the platinum embedded on the surface of the membrane is 1.94.

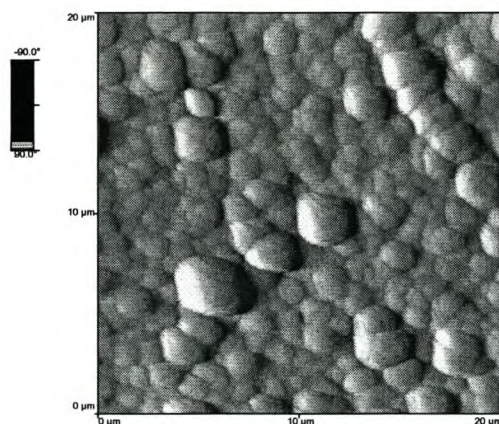


Figure 4.25. AFM surface image ($20\mu\text{m}\times 20\mu\text{m}$) of a cation-exchange membrane embedded with platinum by the reduction of 0.05M platinic acid solution with hydrazine for 15.5 minutes at 40 °C.

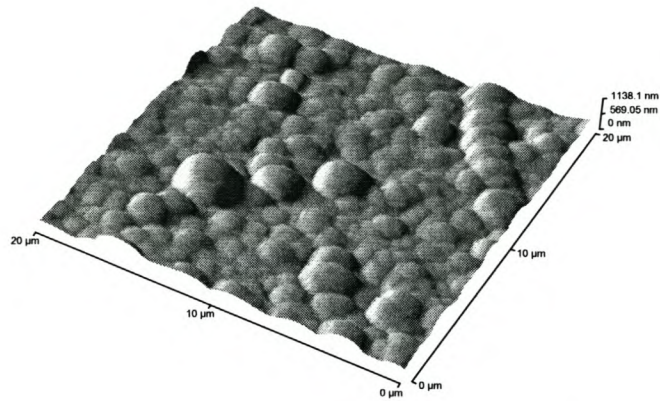


Figure 4.26. Three-dimensional AFM surface image ($20\mu\text{m}\times 20\mu\text{m}$) of a cation-exchange membrane embedded with platinum catalyst by the reduction of 0.05M platinic acid solution with hydrazine for 15.5 minutes at 40 °C.

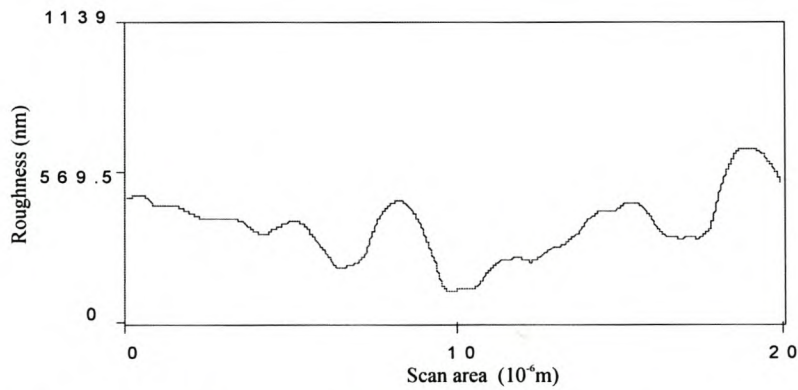


Figure 4.27. Line analysis plot of the surface roughness of a cation-exchange membrane embedded with platinum catalyst by the reduction of 0.05M platinic acid solution with hydrazine for 15.5 minutes at 40 °C.

Table 4.1. Results of AFM images for the scan area $20\mu\text{m}\times 20\mu\text{m}$ of membranes embedded with platinum catalyst by the reduction of 0.05M platinic acid solution with hydrazine at 40 °C for varying lengths of time.

Time of platinisation for the reduction of 0.05M platinic acid by N_2H_4 (min)	Average roughness of the Pt catalyst on the membrane (nm)	Average height of Pt catalyst embedded on membrane (nm)	Surface area of Pt catalyst on membrane (μm^2)	Fractal dimension of Pt catalyst (FD)
3.5	101.4	478.9	478.1	2.59
5.5	393.4	945.5	490.6	2.25
7.5	610.4	2001.8	497.1	2.14
9.5	179.8	913.6	437.5	2.30
11.5	118.3	437.9	417.4	2.33
15.5	109.1	335.7	419.7	1.94

Table 4.2. Results of AFM images for the scan area $130\mu\text{m}\times 130\mu\text{m}$ of membranes embedded with platinum catalyst by the reduction of 0.05M platinic acid solution with hydrazine at 40 °C for varying lengths of time.

Time of platinisation for the reduction of 0.05M platinic acid by N_2H_4 (min)	Average roughness of the Pt catalyst on the membrane (nm)	Average height of Pt catalyst embedded on membrane (nm)	Surface area of Pt catalyst on membrane (μm^2)	Fractal dimension of Pt catalyst (FD)
3.5	411.9	1840.4	17766	2.39
5.5	415.7	1711.3	18230	2.44
7.5	678.8	2761.5	21272	2.40
9.5	<i>Unable to analyse platinum-containing membrane samples of $130\mu\text{m}\times 130\mu\text{m}$ scan area due to the presence of artifacts in these images.</i>			
11.5				
15.5				

4.1.1.2. Atomic force microscopy imaging of membranes embedded with platinum catalyst by the reduction of 0.03M platinum acid solution with hydrazine at 40 °C.

Figures 4.28 and 4.29 are two-dimensional and three-dimensional surface images ($20\mu\text{m}\times 20\mu\text{m}$) of cation-exchange membranes embedded with platinum catalyst by the reduction of 0.03M platinum acid solution with hydrazine for 7 minutes at 40 °C. The average roughness of the platinum catalyst embedded on the membrane is 167.9 nm and the average height of the platinum catalyst embedded on the membrane is 693 nm. The surface area of the platinum catalyst is $500.1\ \mu\text{m}^2$. The fractal dimension of the platinum catalyst embedded on the surface of the membrane is 2.35. The platinum catalyst embedded on the membrane is characteristic of platinum particles that are densely packed (Figs. 4.28 and 4.29). The surface roughness profile of the platinum catalyst on the membrane can be seen in the line analysis plot (Fig. 4.30). The surface roughness of the platinum catalyst on the membrane can be described (qualitatively) as irregular (Fig. 4.30).

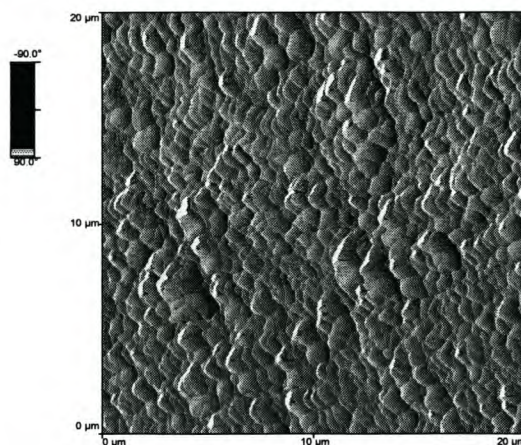


Figure 4.28. *AFM surface image ($20\mu\text{m}\times 20\mu\text{m}$) of a cation-exchange membrane embedded with platinum catalyst by the reduction of 0.03M platinum acid solution with hydrazine for 7 minutes at 40 °C.*

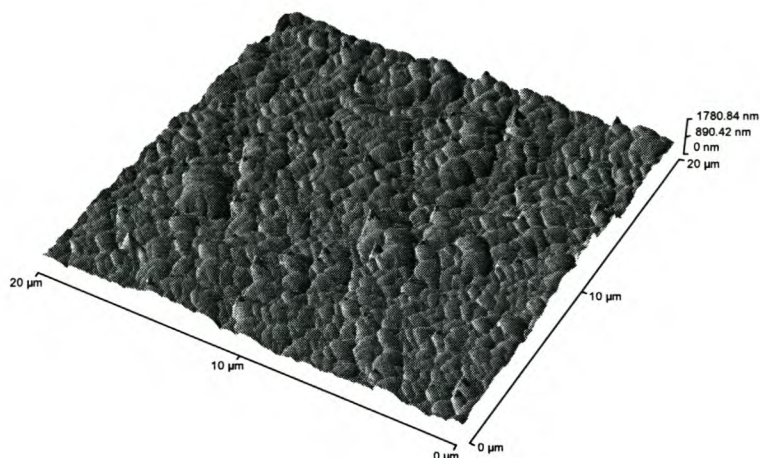


Figure 4.29. Three-dimensional AFM surface image ($20\mu\text{m}\times 20\mu\text{m}$) of a cation-exchange membrane embedded with platinum catalyst by the reduction of 0.03M platinumic acid solution with hydrazine for 7 minutes at $40\text{ }^\circ\text{C}$.

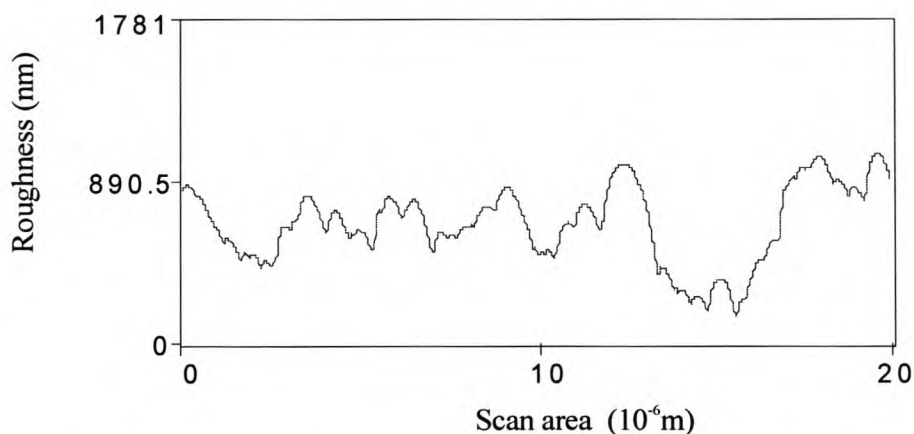


Figure 4.30. Line analysis plot of the surface roughness of a cation-exchange membrane embedded with platinum catalyst by the reduction of 0.03M platinumic acid solution with hydrazine for 7 minutes at $40\text{ }^\circ\text{C}$.

Figures 4.31 and 4.32 are two-dimensional and three-dimensional surface images ($20\mu\text{m}\times 20\mu\text{m}$) of cation-exchange membranes embedded with platinum. The platinum catalyst was embedded on the membrane by the reduction of 0.03M platinumic acid solution with hydrazine for 7 minutes at $40\text{ }^\circ\text{C}$, while pulses between 20 and 40 kHz were rippled through the platinumic acid solution. The average roughness of the platinum catalyst on the membrane is 106.4 nm and the average height of the platinum catalyst is 512.3 nm . The surface area of the platinum catalyst is $479.2\text{ }\mu\text{m}^2$. The fractal dimension of the platinum embedded on the membrane surface is 2.51.

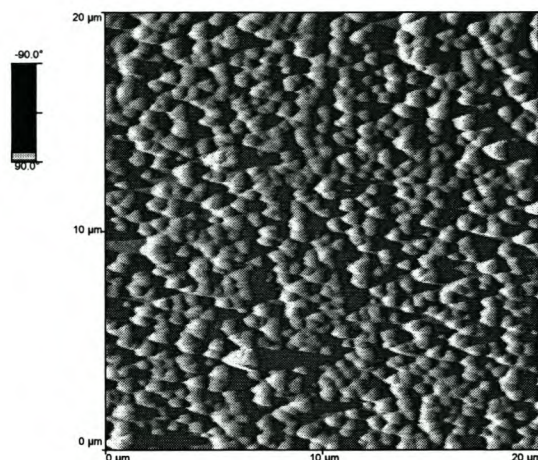


Figure 4.31. *AFM surface image (20 μ m \times 20 μ m) of a cation-exchange membrane embedded with platinum by the reduction of 0.03M platinic acid with hydrazine for 7 minutes at 40 °C, while pulses between 20 and 40 kHz were rippled through the platinic acid solution.*

The platinum catalyst on the membrane is characteristic of oval-shaped particles that are densely packed. The surface roughness profile of the platinum catalyst on the membrane can be seen in the line analysis plot (Fig. 4.33). The surface roughness of the platinum catalyst can be described (qualitatively) as serrated (Fig. 4.33).

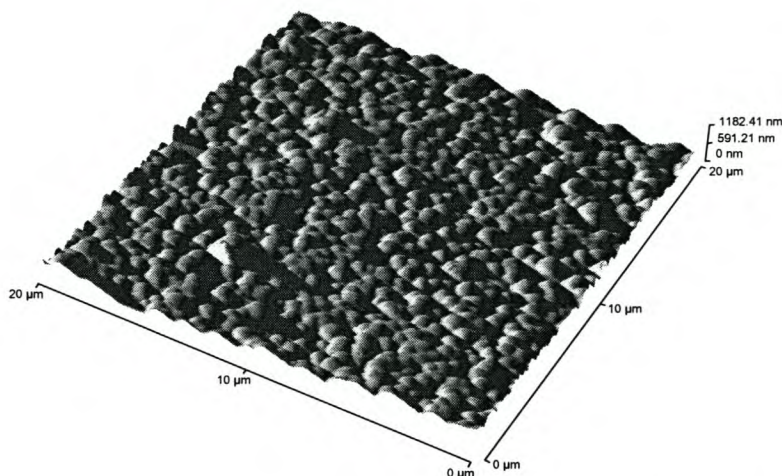


Figure 4.32. Three-dimensional AFM surface image ($20\mu\text{m}\times 20\mu\text{m}$) of a cation-exchange membrane embedded with platinum catalyst by the reduction of 0.03M platinic acid solution with hydrazine for 7 minutes at 40 °C, while pulses between 20 and 40 kHz were rippled through the platinic acid solution.

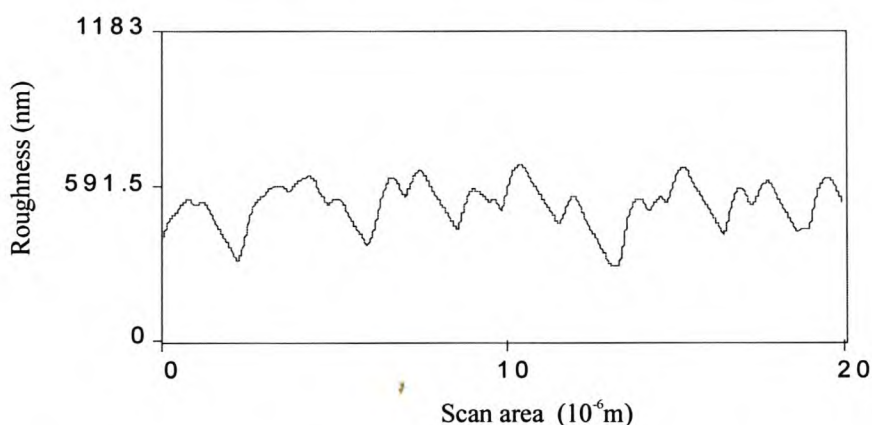


Figure 4.33. Line analysis plot of the surface roughness of a cation-exchange membrane embedded with platinum catalyst by the reduction of 0.03M platinic acid solution with hydrazine for 7 minutes at 40 °C, while pulses between 20 and 40 kHz were rippled through the platinic acid solution.

Figures 4.34 and 4.35 are two-dimensional and three-dimensional surface images ($130\mu\text{m}\times 130\mu\text{m}$) of cation-exchange membranes embedded with platinum. The platinum catalyst was embedded on the membrane by the reduction of 0.03M platinic acid solution with hydrazine for 7 minutes at 40 °C, while pulses between 20 and 40 kHz were rippled through the platinic acid solution. The average roughness of the

platinum catalyst is 338.3 nm and the average height of the platinum catalyst is 1483 nm. The surface area of the platinum catalyst is 18698 μm^2 . The fractal dimension of the platinum catalyst embedded on the surface of the membrane is 2.37. The surface roughness profile of the platinum catalyst on the membrane can be seen in the line analysis plot (Fig. 4.36). The surface roughness of the platinum catalyst embedded on the membrane can be described (qualitatively) as irregular (Fig. 4.36).

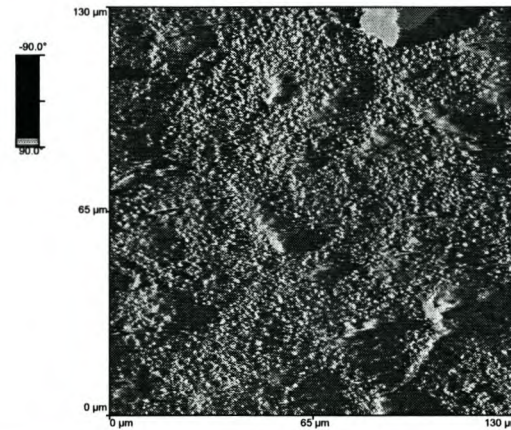


Figure 4.34. *AFM surface image (130 μm \times 130 μm) of a cation-exchange membrane embedded with platinum catalyst by the reduction of 0.03M platonic acid solution with hydrazine for 7 minutes at 40 °C, while pulses between 20 and 40 kHz were ripped through the platonic acid solution.*

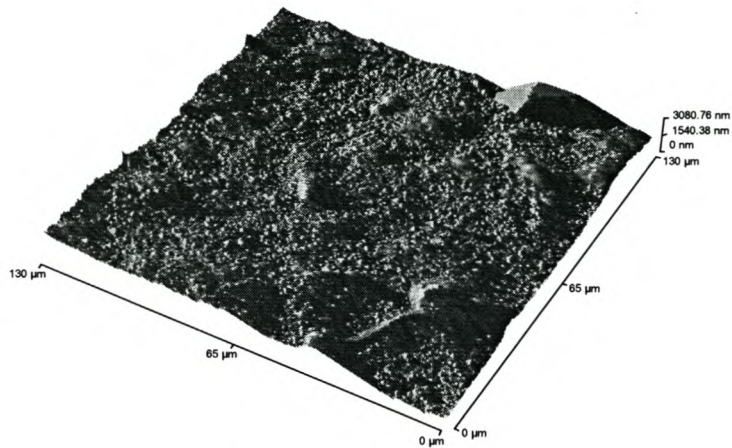


Figure 4.35. Three-dimensional AFM surface image ($130\mu\text{m}\times 130\mu\text{m}$) of a cation-exchange membrane embedded with platinum catalyst by the reduction of 0.03M platinic acid solution with hydrazine for 7 minutes at $40\text{ }^{\circ}\text{C}$, while pulses between 20 and 40 kHz were rippled through the platinic acid solution.

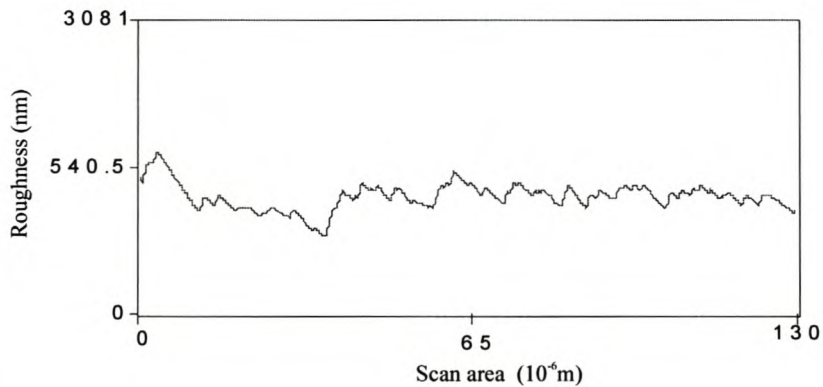


Figure 4.36. Line analysis plot of the surface roughness of a cation-exchange membrane embedded with platinum catalyst by the reduction of 0.03M platinic acid solution with hydrazine for 7 minutes at $40\text{ }^{\circ}\text{C}$, while pulses between 20 and 40 kHz were rippled through the platinic acid solution.

Table 4.3. Results of AFM images for the scan area $20\mu\text{m}\times 20\mu\text{m}$ of membranes embedded with platinum catalyst by the reduction of 0.03M platinic acid solution with hydrazine at 40 °C, while pulses between 20 and 40 kHz were rippled through platinic acid solution.

Time of platinisation for the reduction of 0.03M platinic acid by N₂H₄ (min)	Average roughness of Pt catalyst on membrane (nm)	Average height of Pt catalyst on membrane (nm)	Surface area of Pt catalyst on membrane (μm^2)	Fractal dimension of Pt catalyst (FD)
7	167.9	693	500.1	2.35
7*	106.4	512.3	479.2	2.51

* Sonication of platinic acid solution during the deposition of platinum catalyst on membranes

4.1.1.3. AFM imaging of membranes embedded with platinum catalyst by the reduction of 0.05M platinic acid solution with sodium borohydride at 40 °C.

Figures 4.37 and 4.38 are two-dimensional and three-dimensional surface images ($130\mu\text{m}\times 130\mu\text{m}$) of cation-exchange membranes embedded with platinum by the reduction of 0.05M platinic acid solution with sodium borohydride for 3.5 minutes at 40 °C. The average roughness of the layer of platinum catalyst is 381.9 nm and the average height of the platinum catalyst is 1742.2 nm. The surface area of the platinum catalyst is $28808\mu\text{m}^2$. The fractal dimension of the platinum catalyst embedded on the surface of the membrane is 2.70. The profile of the layer of the platinum catalyst is coarse (Figs. 4.37 and 4.38). The surface roughness profile of the platinum catalyst embedded on the membrane can be seen in the line analysis plot (Fig. 4.39). The surface roughness of the platinum catalyst can be described (qualitatively) as jagged (Fig. 4.39).

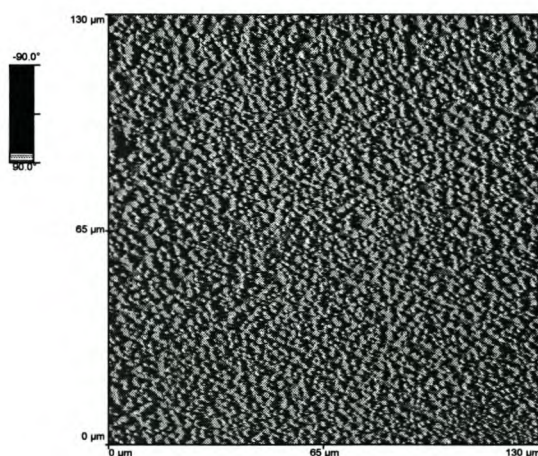


Figure 4.37. AFM surface image ($130\mu\text{m}\times 130\mu\text{m}$) of a cation-exchange membrane embedded with platinum by the reduction of 0.05M platinic acid solution with sodium borohydride for 3.5 minutes at 40 °C.

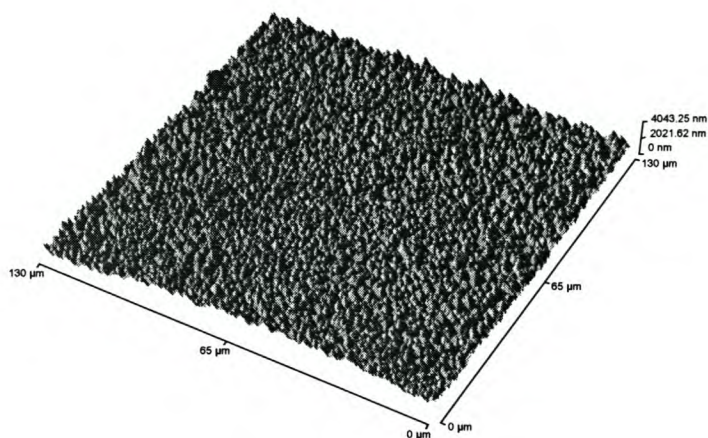


Figure 4.38. Three-dimensional AFM surface image ($130\mu\text{m}\times 130\mu\text{m}$) of a cation-exchange membrane embedded with platinum by the reduction of 0.05M platinumic acid solution with sodium borohydride for 3.5 minutes at 40 °C.

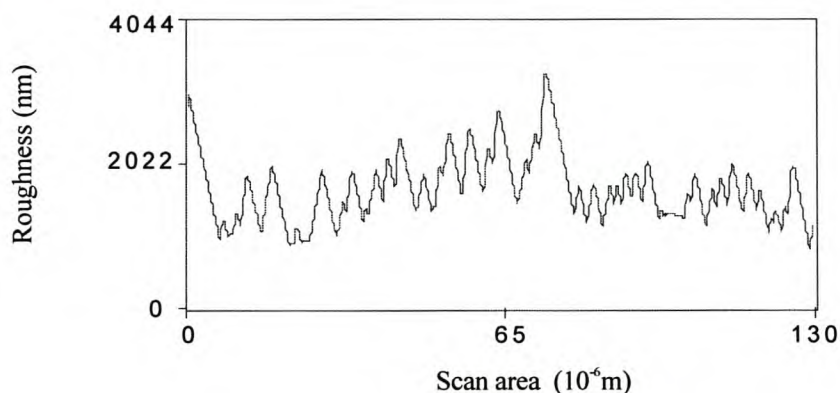


Figure 4.39. Line analysis plot of the surface roughness of a cation-exchange membrane embedded with platinum by the reduction of 0.05M platinumic acid solution with sodium borohydride for 3.5 minutes at 40 °C.

Figures 4.40 and 4.41 are two-dimensional and three-dimensional surface images ($130\mu\text{m}\times 130\mu\text{m}$) of cation-exchange membranes embedded with platinum catalyst by the reduction of 0.05M platinumic acid solution with sodium borohydride for 5.5 minutes at 40 °C. The average roughness of the platinum catalyst is 411.2 nm and the average height of the platinum catalyst is 1388.9 nm. The surface area of the platinum catalyst is $20359\mu\text{m}^2$. The fractal dimension of the platinum catalyst embedded on the surface of the membrane is 2.17. The profile of the platinum catalyst is coarse (Figs. 4.40 and 4.41). The surface roughness profile of the platinum catalyst embedded on the

membrane can be seen in the line analysis plot (Fig. 4.42). The surface roughness of the platinum deposition can be described (qualitatively) as irregular (Fig. 4.42).

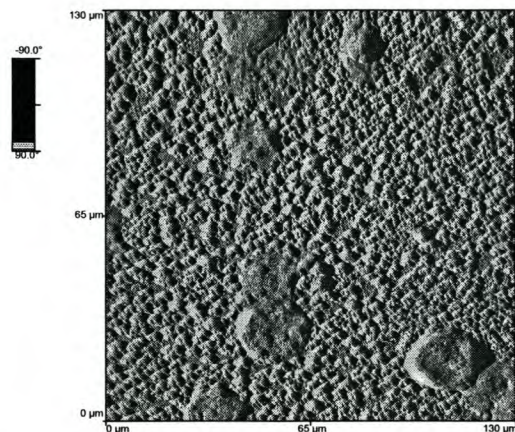


Figure 4.40. *AFM surface image ($130\mu\text{m}\times 130\mu\text{m}$) of a cation-exchange membrane embedded with platinum catalyst by the reduction of 0.05M platinic acid with sodium borohydride for 5.5 minutes at 40 °C.*

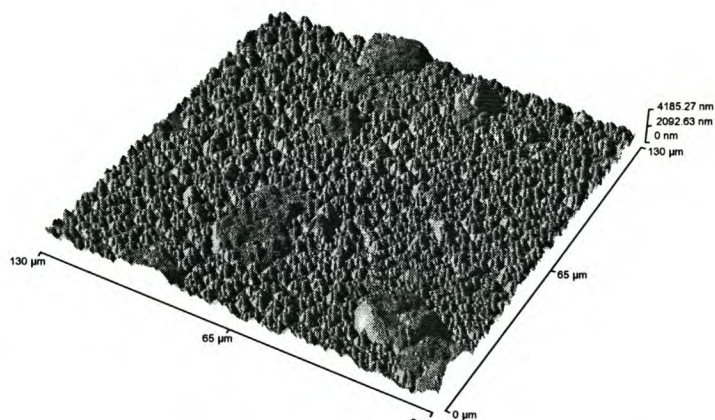


Figure 4.41. *Three-dimensional AFM surface image ($130\mu\text{m}\times 130\mu\text{m}$) of a cation-exchange membrane embedded with platinum catalyst by the reduction of 0.05M platinic acid solution with sodium borohydride for 5.5 minutes at 40 °C.*

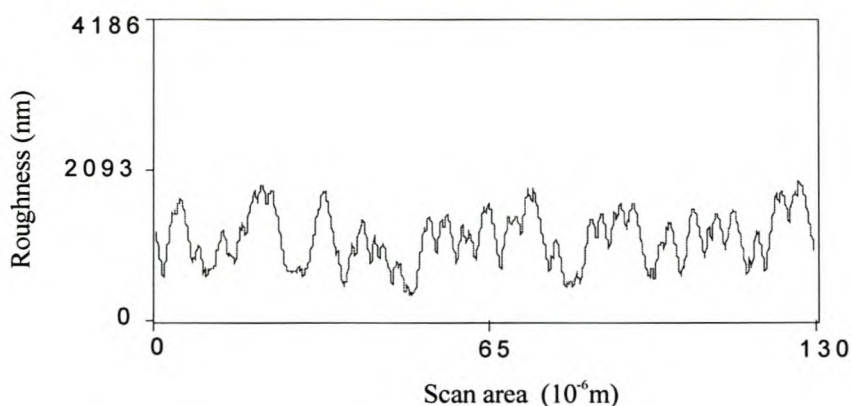


Figure 4.42. Line analysis plot of the surface roughness of a cation-exchange membrane embedded with platinum catalyst by the reduction of 0.05M platinic acid solution with sodium borohydride for 5.5 minutes at 40 °C.

Figures 4.43 and 4.44 are two-dimensional and three-dimensional surface images (130 $\mu\text{m}\times 130\mu\text{m}$) of cation-exchange membranes embedded with platinum catalyst by the reduction of 0.05M platinic acid solution with sodium borohydride for 7.5 minutes at 40 °C. The average roughness of the platinum catalyst is 132.9 nm and the average height of the platinum catalyst is 869.4 nm. The surface area of the platinum catalyst is 17625 μm^2 . The fractal dimension of the platinum catalyst embedded on the surface of the membrane is 3.00.

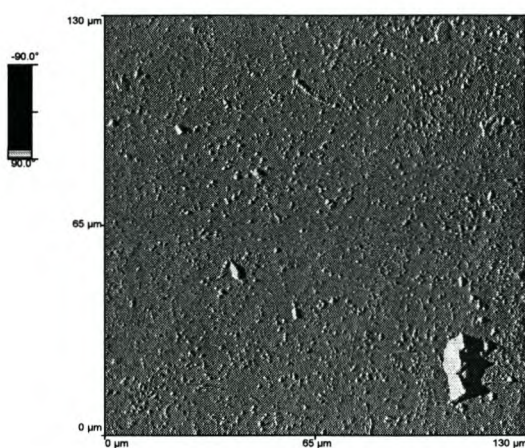


Figure 4.43. AFM surface image (130 $\mu\text{m}\times 130\mu\text{m}$) of a cation-exchange membrane embedded with platinum catalyst by the reduction of 0.05M platinic acid solution with sodium borohydride for 7.5 minutes at 40 °C.

The profile of the platinum catalyst is smooth with fine irregularities on the surface (Figs. 4.43 and 4.44). The surface roughness profile of the platinum catalyst embedded on the membrane can be seen in the line analysis plot (Fig. 4.45). The surface roughness of the platinum catalyst can be described (qualitatively) as serrated (Fig. 4.45).

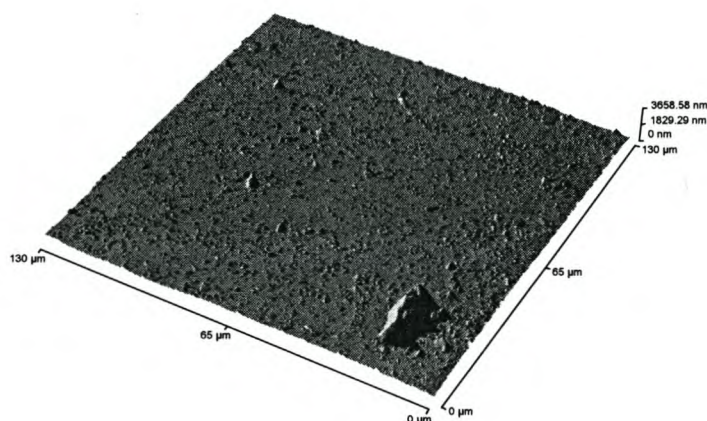


Figure 4.44. Three-dimensional AFM surface image ($130\mu\text{m}\times 130\mu\text{m}$) of a cation-exchange membrane embedded with platinum catalyst by the reduction of 0.05M platinumic acid solution with sodium borohydride for 7.5 minutes at $40\text{ }^{\circ}\text{C}$.

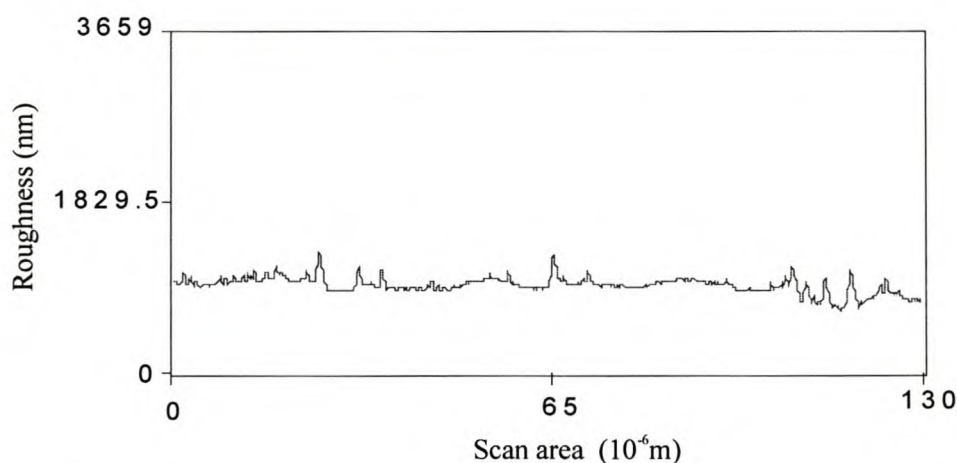


Figure 4.45. Line analysis plot of the surface roughness of a cation-exchange membrane embedded with platinum catalyst by the reduction of 0.05M platinumic acid solution with sodium borohydride for 7.5 minutes at $40\text{ }^{\circ}\text{C}$.

Figures 4.46 and 4.47 are two-dimensional and three-dimensional surface images ($130\mu\text{m}\times 130\mu\text{m}$) of cation-exchange membranes embedded with platinum catalyst by

the reduction of 0.05M platinumic acid solution with sodium borohydride for 9.5 minutes at 40 °C. The average roughness of the platinum catalyst is 327.7 nm and the average height of the platinum catalyst on the membrane is 1607.5 nm. The surface area of the platinum catalyst is 22683 μm^2 . The fractal dimension of the platinum catalyst embedded on the surface of the membrane is 2.78. The profile of the platinum catalyst is coarse (Figs. 4.46 and 4.47). The surface roughness profile of the platinum catalyst on the membrane can be seen in the line analysis plot (Fig. 4.48). The surface roughness of the platinum catalyst can be described (qualitatively) as jagged (Fig. 4.48).

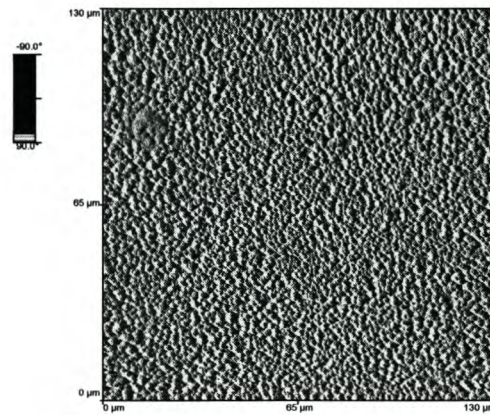


Figure 4.46. *AFM surface image (130 μm ×130 μm) of a cation-exchange membrane embedded with platinum catalyst by the reduction of 0.05M platinumic acid solution with sodium borohydride for 9.5 minutes at 40 °C.*

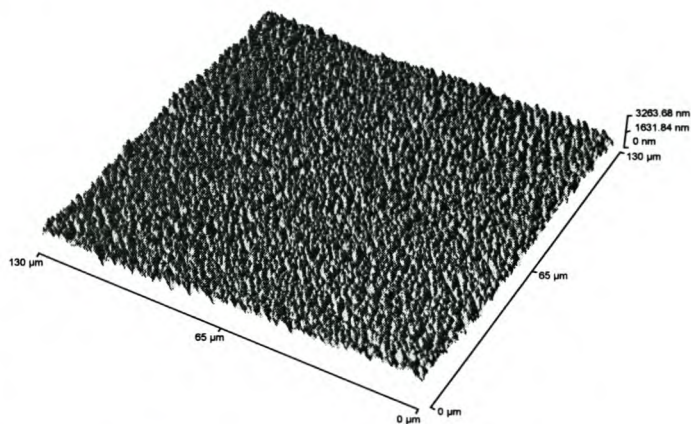


Figure 4.47. *Three-dimensional AFM surface image (130 μm ×130 μm) of a cation-exchange membrane embedded with platinum catalyst by the reduction of 0.05M platinumic acid solution with sodium borohydride for 9.5 minutes at 40 °C.*

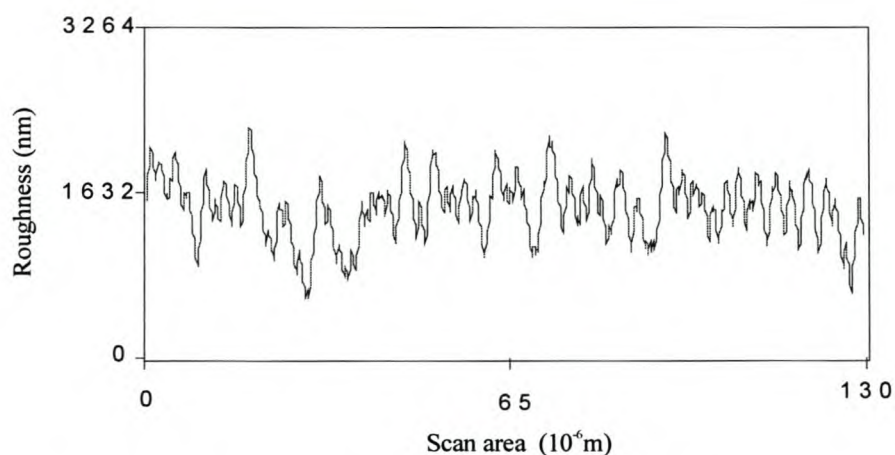


Figure 4.48. Line analysis plot of the surface roughness of a cation-exchange membrane embedded with platinum by the reduction of 0.05M platinic acid solution with sodium borohydride for 9.5 minutes at 40 °C.

Figures 4.49 and 4.50 are two-dimensional and three-dimensional surface images (130 $\mu\text{m}\times 130\mu\text{m}$) of cation-exchange membranes embedded with platinum catalyst by the reduction of 0.05M platinic acid solution with sodium borohydride for 11.5 minutes at 40 °C. The average roughness of the platinum catalyst is 518.9 nm and the average height of the platinum catalyst is 1573.7 nm. The surface area of the platinum catalyst is 22441 μm^2 . The fractal dimension of the platinum catalyst embedded on the surface of the membrane is 1.64.

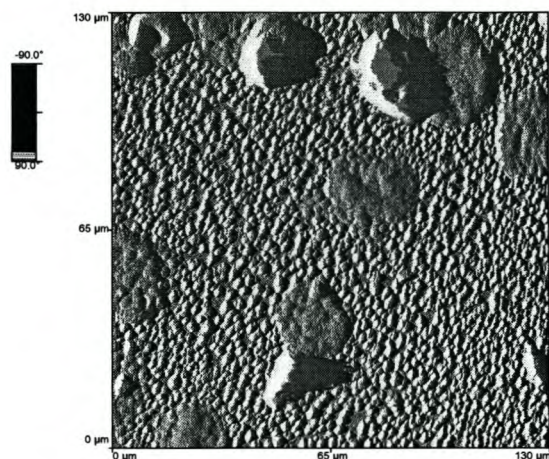


Figure 4.49. AFM surface image (130 $\mu\text{m}\times 130\mu\text{m}$) of a cation-exchange membrane embedded with platinum by the reduction of 0.05M platinic acid solution with sodium borohydride for 11.5 minutes at 40 °C.

The profile of the platinum catalyst is coarse with large lumps projecting outward of the surface (Figs. 4.49 and 4.50). The surface roughness profile of the platinum catalyst embedded on the membrane can be seen in the line analysis plot (Fig. 4.51). The surface roughness of the platinum catalyst on the membrane can be described (qualitatively) as serrated (Fig. 4.51).

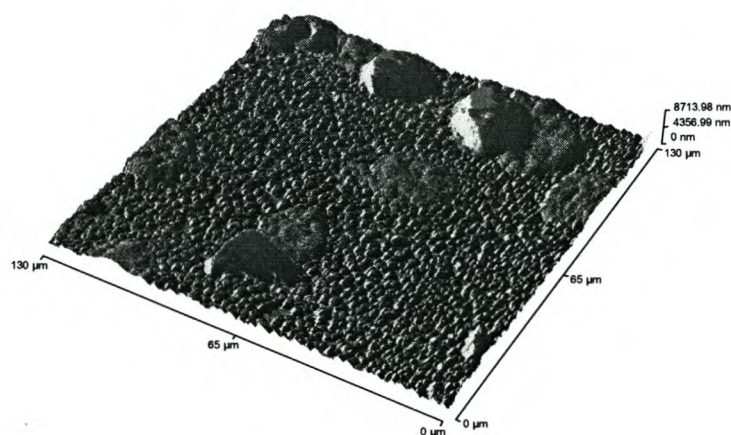


Figure 4.50. Three-dimensional AFM surface image ($130\mu\text{m}\times 130\mu\text{m}$) of a cation-exchange membrane embedded with platinum catalyst by the reduction of 0.05M platinic acid solution with sodium borohydride for 11.5 minutes at 40 °C.

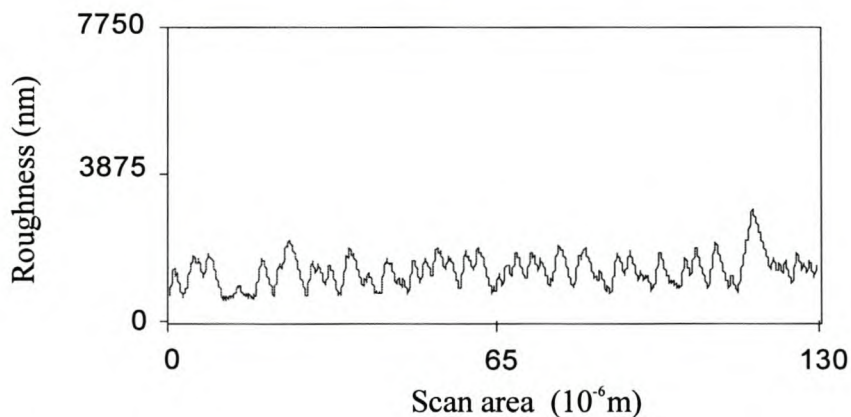


Figure 4.51. Line analysis plot of the surface roughness of a cation-exchange membrane embedded with platinum catalyst by the reduction of 0.05M platinic acid solution with sodium borohydride for 11.5 minutes at 40 °C.

Figures 4.52 and 4.53 are two-dimensional and three-dimensional surface images ($130\mu\text{m}\times 130\mu\text{m}$) of cation-exchange membranes embedded with platinum catalyst by the reduction of 0.05M platinic acid solution with sodium borohydride for 15.5

minutes at 40 °C. The average roughness of the platinum catalyst is 533.4 nm and the average height of the platinum catalyst is 2046.3 nm. The surface area of the platinum catalyst is 21214 μm^2 . The fractal dimension of the platinum catalyst embedded on the surface of the membrane is 2.13. The profile of the platinum catalyst is coarse with large lumps projecting outward of the surface (Figs. 4.52 and 4.53). The surface roughness profile of the platinum catalyst embedded on the membrane can be seen in the line analysis plot (Fig. 4.54). The surface roughness of the platinum catalyst can be described (qualitatively) as serrated (Fig. 4.54).

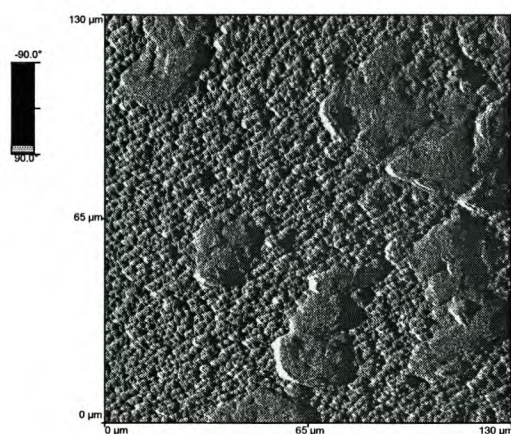


Figure 4.52. AFM surface image (130 $\mu\text{m}\times 130\mu\text{m}$) of a cation-exchange membrane embedded with platinum catalyst by the reduction of 0.05M platinumic acid solution with sodium borohydride for 15.5 minutes at 40 °C.

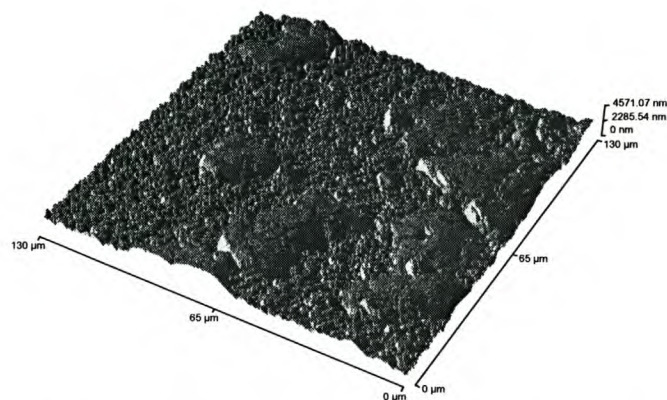


Figure 4.53. Three-dimensional AFM surface image (130 $\mu\text{m}\times 130\mu\text{m}$) of a cation-exchange membrane embedded with platinum catalyst by the reduction of 0.05M platinumic acid solution with sodium borohydride for 15.5 minutes at 40 °C.

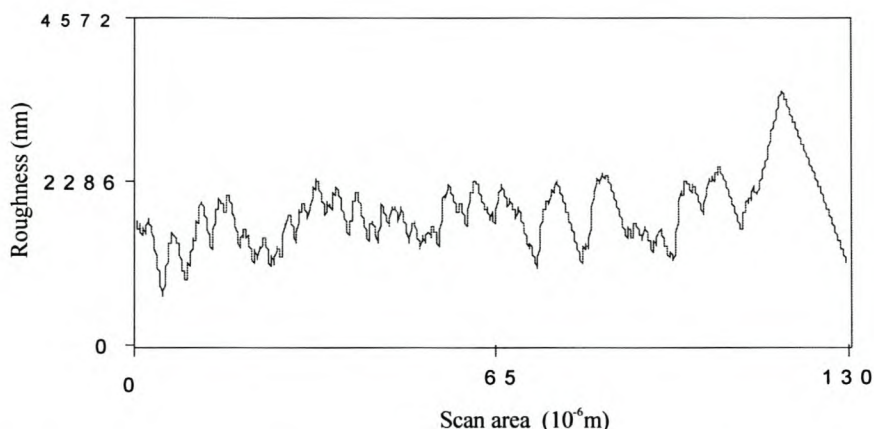


Figure 4.54. Line analysis plot of the surface roughness of a cation-exchange membrane embedded with platinum catalyst by the reduction of 0.05M platinic acid solution with sodium borohydride for 15.5 minutes at 40 °C.

Table 4.4. Results of AFM images for the scan area 130µm×130µm of membranes embedded with platinum catalyst by the reduction of 0.05M platinic acid solution with sodium borohydride at 40 °C for varying lengths of time.

Time of platinisation for the reduction of 0.05M platinic acid solution by NaBH ₄ (min)	Average roughness of Pt catalyst on membrane (nm)	Average height of Pt catalyst embedded on membrane (nm)	Surface area of Pt catalyst on membrane (µm ²)	Fractal dimension of Pt catalyst (FD)
3.5	381.9	1742.2	28808	2.70
5.5	411.2	1388.9	20359	2.17
7.5	132.9	869.4	17625	3.0
9.5	327.7	1607.5	22683	2.78
11.5	518.9	1573.7	22441	1.64
15.5	533.4	2046.3	21214	2.13

4.1.1.4. AFM imaging of membranes embedded with platinum catalyst by the reduction of 0.03M platinum acid solution with sodium borohydride at 40 °C.

Figures 4.55 and 4.56 are two-dimensional and three-dimensional surface images ($20\mu\text{m}\times 20\mu\text{m}$) of cation-exchange membranes embedded with platinum catalyst by the reduction of 0.03M platinum acid solution with sodium borohydride for 3.5 minutes at 40 °C. The average roughness of the platinum catalyst is 260.7 nm and the average height of the platinum catalyst is 638.8 nm. The surface area of the platinum catalyst is $474.6\mu\text{m}^2$. The fractal dimension of the platinum catalyst embedded on the surface of the membrane is 2.08. The platinum catalyst is characteristic of large spherical particles (Figs. 4.55 and 4.56). The surface roughness profile of the platinum catalyst embedded on the membrane can be seen in the line analysis plot (Fig. 4.57). The surface roughness of the platinum catalyst can be described (qualitatively) as wavy (Fig. 4.57).

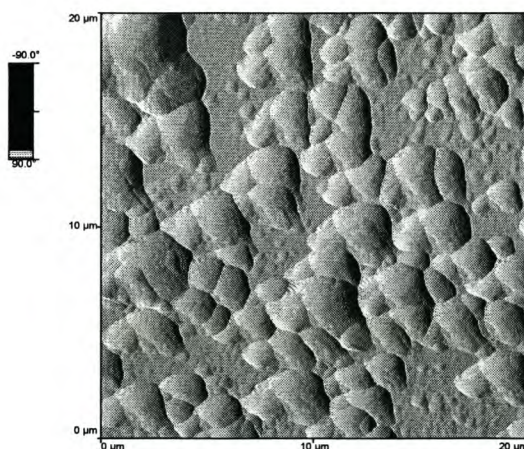


Figure 4.55. *AFM surface image ($20\mu\text{m}\times 20\mu\text{m}$) of a cation-exchange membrane embedded with platinum catalyst by the reduction of 0.03M platinum acid solution with sodium borohydride for 3.5 minutes at 40 °C.*

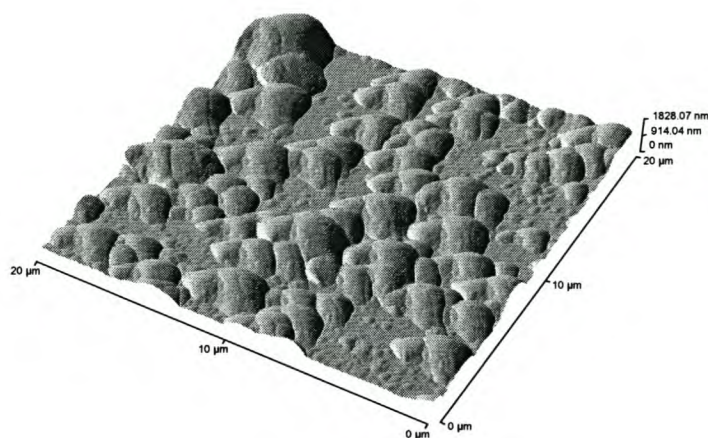


Figure 4.56. Three-dimensional AFM surface image ($20\mu\text{m}\times 20\mu\text{m}$) of a cation-exchange membrane embedded with platinum catalyst by the reduction of 0.03M platinumic acid solution with sodium borohydride for 3.5 minutes at $40\text{ }^\circ\text{C}$.

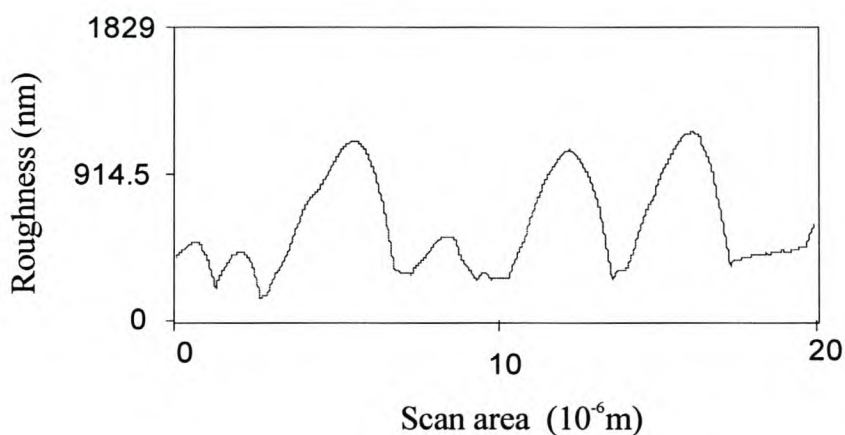


Figure 4.57. Line analysis plot of the surface roughness of a cation-exchange membrane embedded with platinum catalyst by the reduction of 0.03M platinumic acid solution with sodium borohydride for 3.5 minutes at $40\text{ }^\circ\text{C}$.

Figures 4.58 and 4.59 are two-dimensional and three-dimensional surface images ($130\mu\text{m}\times 130\mu\text{m}$) of cation-exchange membranes embedded with platinum catalyst by the reduction of 0.03M platinumic acid solution with sodium borohydride for 3.5 minutes at $40\text{ }^\circ\text{C}$. The average roughness of the platinum catalyst is 402.5 nm and the average height of the platinum catalyst is 1301.5 nm . The surface area of the platinum catalyst is $21762\text{ }\mu\text{m}^2$. The fractal dimension of the platinum catalyst embedded on the surface of the membrane is 2.28. The profile of the platinum catalyst is coarse (Figs. 4.58 and 4.59). The surface roughness profile of the platinum catalyst embedded on the

membrane can be seen in the line analysis plot (Fig. 4.60). The surface roughness of the platinum catalyst can be described (qualitatively) as serrated (Fig. 4.60).

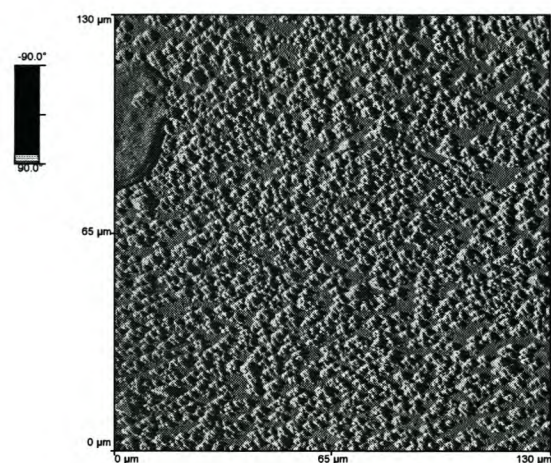


Figure 4.58. *AFM surface image (130 μ m \times 130 μ m) of a cation-exchange membrane embedded with platinum catalyst by the reduction of 0.03M platinic acid solution with sodium borohydride for 3.5 minutes at 40 °C.*

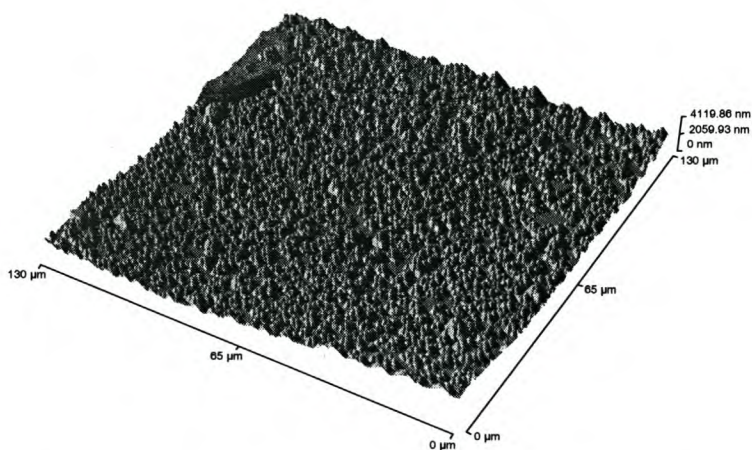


Figure 4.59. *Three-dimensional AFM surface image (130 μ m \times 130 μ m) of a cation-exchange membrane embedded with platinum catalyst by the reduction of 0.03M platinic acid solution with sodium borohydride for 3.5 minutes at 40 °C.*

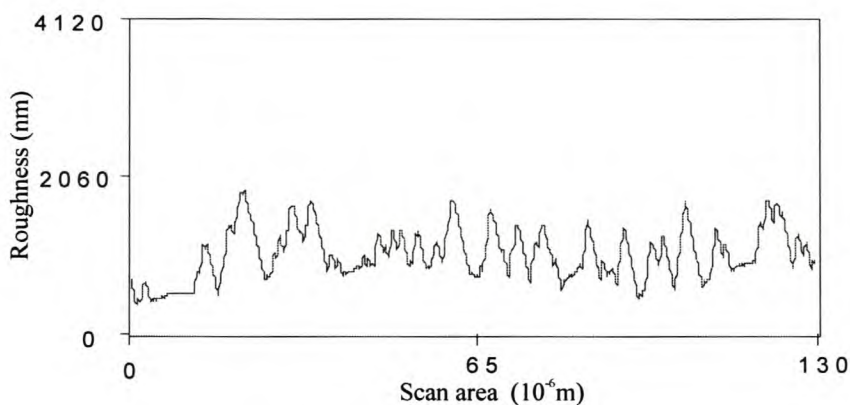


Figure 4.60. Line analysis plot of the surface roughness of a cation-exchange membrane embedded with platinum catalyst by the reduction of 0.03M platonic acid solution with sodium borohydride for 3.5 minutes at 40 °C.

Figures 4.61 and 4.62 are two-dimensional and three-dimensional surface images ($20\mu\text{m}\times 20\mu\text{m}$) of cation-exchange membranes embedded with platinum catalyst by the reduction of 0.03M platonic acid solution with sodium borohydride for 11.5 minutes at 40 °C. The average roughness of the platinum catalyst is 461.3 nm and the average height is 1500.4 nm. The surface area is $528\mu\text{m}^2$. The fractal dimension of the platinum catalyst embedded on the surface of the membrane is 2.11. The platinum catalyst is characteristic by large globular particles (Figs. 4.61 and 4.62). The surface roughness profile of the platinum catalyst embedded on the membrane can be seen in the line analysis plot (Fig. 4.63). The surface roughness of the platinum catalyst can be described (qualitatively) as wavy (Fig. 4.63).

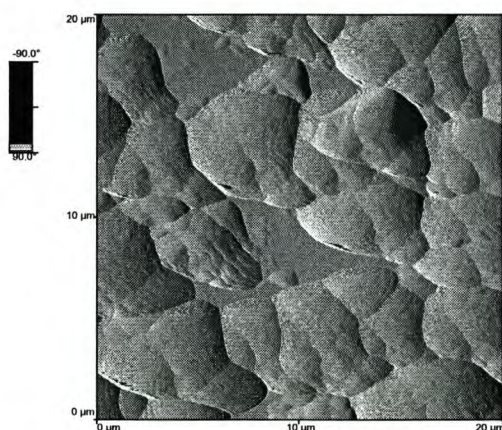


Figure 4.61. AFM surface image ($20\mu\text{m}\times 20\mu\text{m}$) of a cation-exchange membrane embedded with platinum catalyst by the reduction of 0.03M platonic acid solution with sodium borohydride for 11.5 minutes at 40 °C.

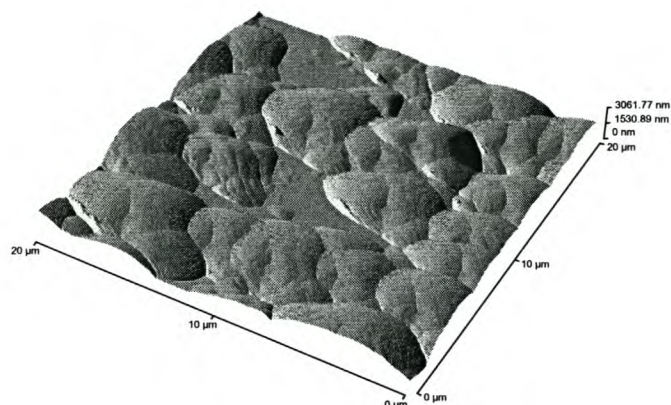


Figure 4.62. Three-dimensional AFM surface image ($20\mu\text{m}\times 20\mu\text{m}$) of a cation-exchange membrane embedded with platinum catalyst by the reduction of 0.03M platinic acid solution with sodium borohydride for 11.5 minutes at $40\text{ }^{\circ}\text{C}$.

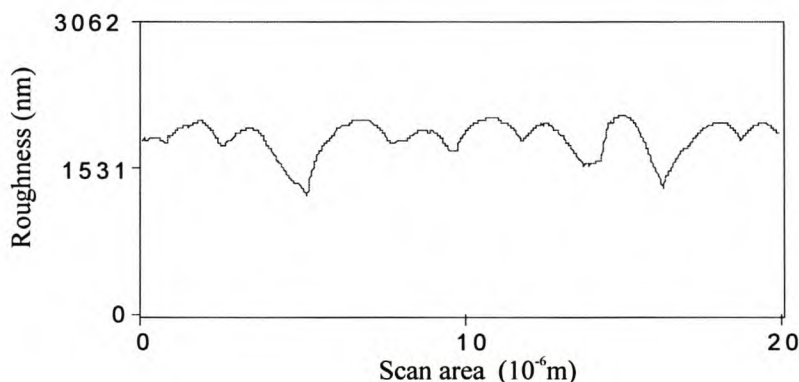


Figure 4.63. Line analysis plot of the surface roughness of a cation-exchange membrane embedded with platinum catalyst by the reduction of 0.03M platinic acid solution with sodium borohydride for 11.5 minutes at $40\text{ }^{\circ}\text{C}$.

Figures 4.64 and 4.65 are two-dimensional and three-dimensional surface images ($130\mu\text{m}\times 130\mu\text{m}$) of cation-exchange membranes embedded with platinum catalyst by the reduction of 0.03M platinic acid solution with sodium borohydride for 11.5 minutes at $40\text{ }^{\circ}\text{C}$. The average roughness of the platinum catalyst is 400.6 nm and the average height is 1474.7 nm . The surface area of the platinum catalyst is $20643\text{ }\mu\text{m}^2$. The fractal dimension of the platinum catalyst embedded on the surface of the membrane is 2.13. The profile of the platinum catalyst is coarse (Figs. 4.64 and 4.65). The surface roughness profile of the platinum catalyst embedded on the membrane

can be seen in the line analysis plot (Fig. 4.66). The surface roughness of the platinum catalyst can be described (qualitatively) as jagged (Fig. 4.66).

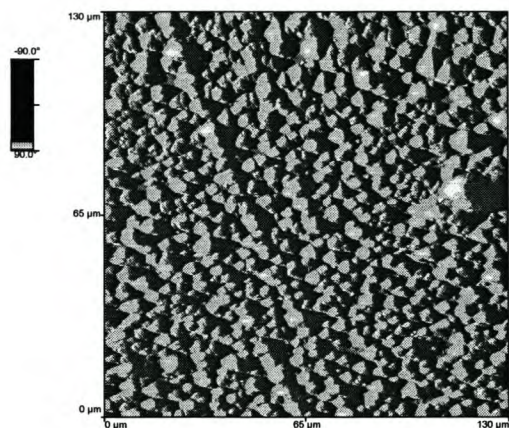


Figure 4.64. *AFM surface image (130 μ m \times 130 μ m) of a cation-exchange membrane embedded with platinum catalyst by the reduction of 0.03M platonic acid solution with sodium borohydride for 11.5 minutes at 40 °C.*

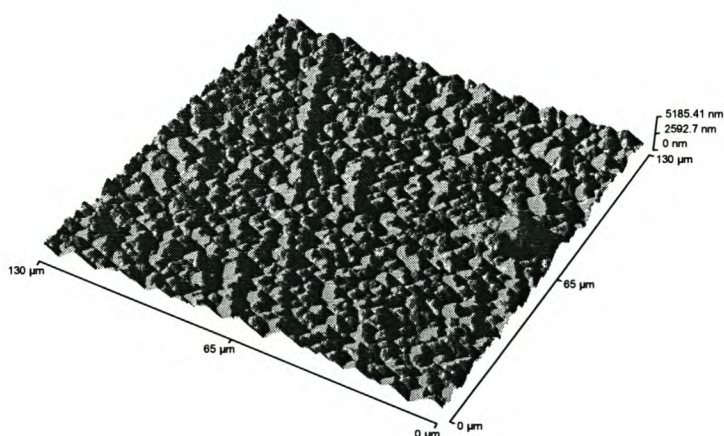


Figure 4.65. *Three-dimensional AFM surface image (130 μ m \times 130 μ m) of a cation-exchange membrane embedded with platinum catalyst by the reduction of 0.03M platonic acid solution with sodium borohydride for 11.5 minutes at 40 °C.*

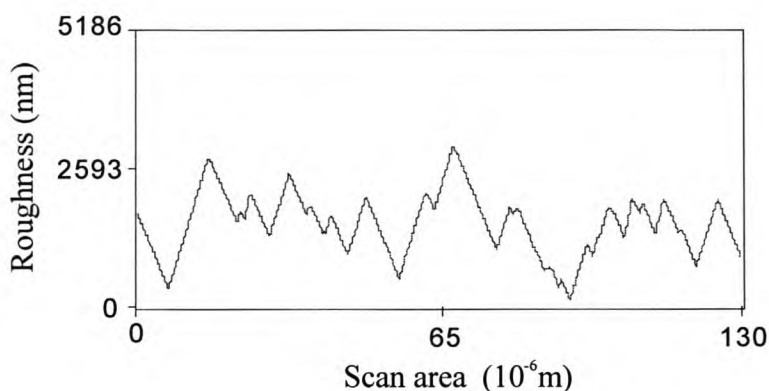


Figure 4.66. Line analysis plot of the surface roughness of a cation-exchange membrane embedded with platinum by the reduction of 0.03M platinic acid solution with sodium borohydride for 11.5 minutes at 40 °C.

Figures 4.67 and 4.68 are two-dimensional and three-dimensional surface images (130µm×130µm) of cation-exchange membranes embedded with platinum catalyst by the reduction of 0.03M platinic acid solution with sodium borohydride for 15.5 minutes at 40 °C. The average roughness of the platinum catalyst is 488.7 nm and the average height is 2343.7 nm. The surface area of the platinum catalyst is 23460 µm². The fractal dimension of the platinum catalyst embedded on the surface of the surface is 2.43. The profile of the platinum catalyst is coarse (Figs. 4.67 and 4.68).

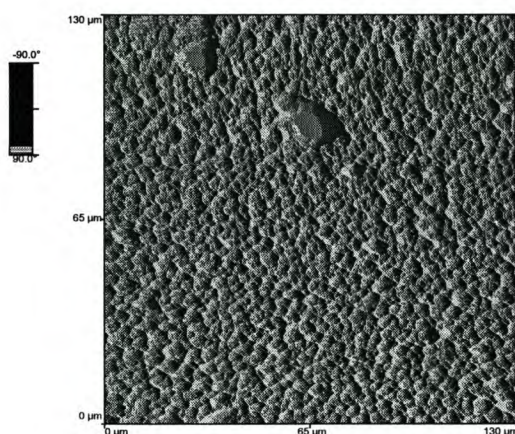


Figure 4.67. AFM surface image (130µm×130µm) of a cation-exchange membrane embedded with platinum catalyst by the reduction of 0.03M platinic acid solution with sodium borohydride for 15.5 minutes at 40 °C.

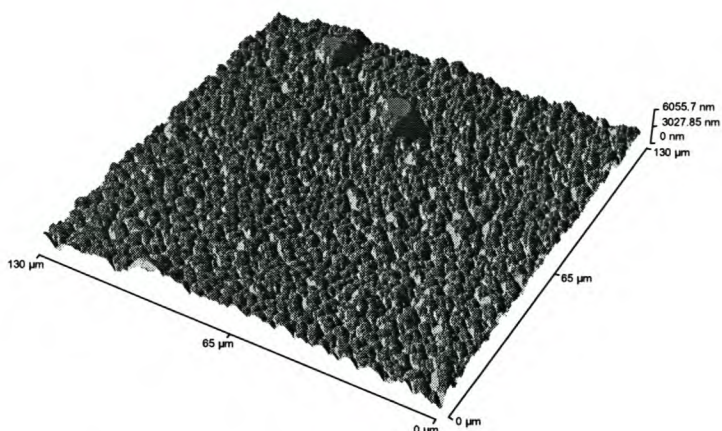


Figure 4.68. *Three-dimensional AFM surface image (130 μm \times 130 μm) of a cation-exchange membrane embedded with platinum catalyst by the reduction of 0.03M platinic acid with sodium borohydride for 15.5 minutes at 40 °C.*

The surface roughness profile of the platinum catalyst on the membrane can be seen in the line analysis plot (Fig. 4.69). The surface roughness of the platinum catalyst can be described (qualitatively) as jagged (Fig. 4.69).

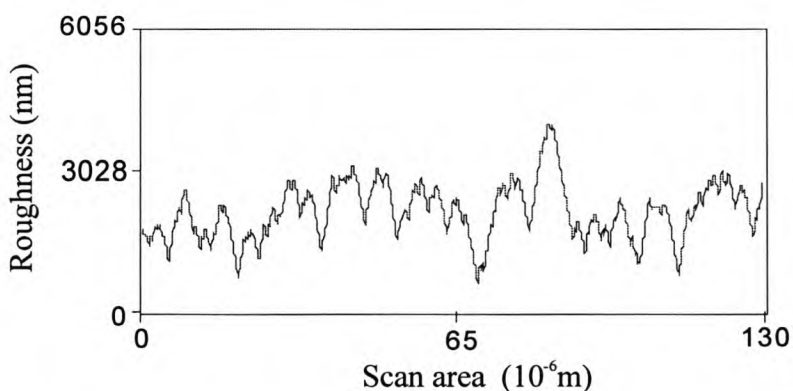


Figure 4.69. *Line analysis plot of the surface roughness of a cation-exchange membrane embedded with platinum catalyst by the reduction of 0.03M platinic acid solution with sodium borohydride for 15.5 minutes at 40 °C.*

Figures 4.70 and 4.71 are two-dimensional and three-dimensional surface images (130 μm \times 130 μm) of cation-exchange membranes embedded with platinum catalyst by the reduction of 0.03M platinic acid solution with sodium borohydride for 25.5 minutes at 40 °C. The average roughness of the platinum catalyst is 1012.2 nm and

the average height is 3944.2 nm. The surface area of the platinum catalyst is 20289 μm^2 . The fractal dimension of the platinum catalyst embedded on the surface of the membrane is 2.35. The profile of the platinum catalyst on the membrane is irregular (Figs. 4.70 and 4.71). The surface roughness profile of the platinum catalyst embedded on the membrane can be seen in the line analysis plot (Fig. 4.72). The surface roughness of the platinum catalyst can be described (qualitatively) as rutted (Fig. 4.72).

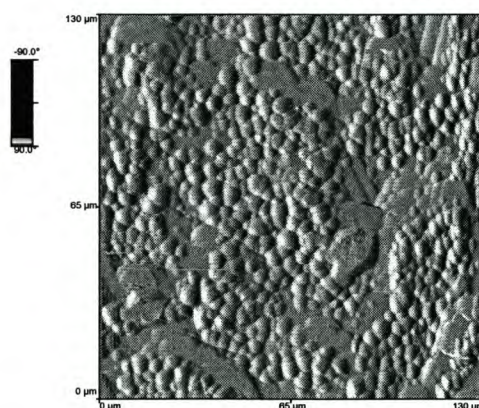


Figure 4.70. *AFM surface image (130µm×130µm) of a cation-exchange membrane embedded with platinum catalyst by the reduction of 0.03M platinic acid solution with sodium borohydride for 25.5 minutes at 40 °C.*

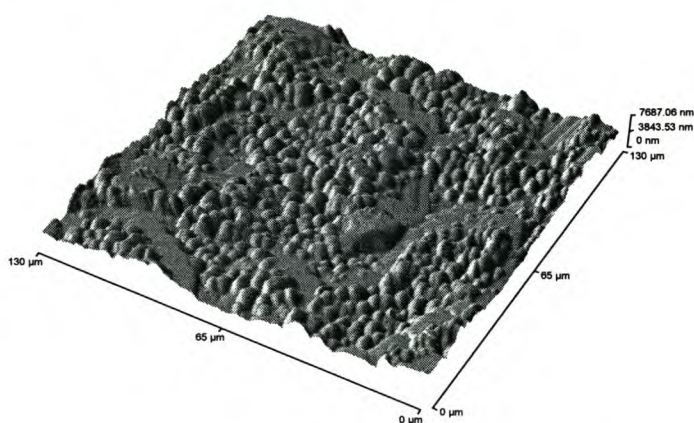


Figure 4.71. *Three-dimensional AFM surface image (130µm×130µm) of a cation-exchange membrane embedded with platinum catalyst by the reduction of 0.03M platinic acid solution with sodium borohydride for 25.5 minutes at 40 °C.*

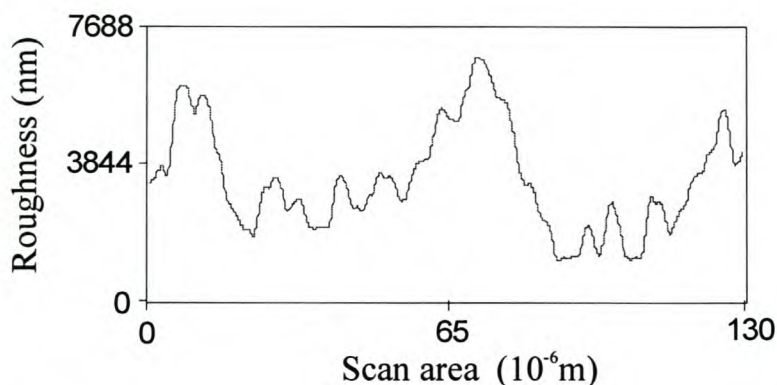


Figure 4.72. Line analysis plot of the surface roughness of a cation-exchange membrane embedded with platinum catalyst by the reduction of 0.03M platinic acid solution with sodium borohydride for 25.5 minutes at 40 °C.

Figures 4.73 and 4.74 are two-dimensional and three-dimensional surface images (130 $\mu\text{m}\times 130\mu\text{m}$) of cation-exchange membranes embedded with platinum by the reduction of 0.03M platinic acid solution with sodium borohydride for 35.5 minutes at 40 °C. The average roughness of the platinum catalyst is 770.16 nm and the average height is 2726.5 nm. The surface area of the platinum catalyst is 18781 μm^2 . The fractal dimension of the platinum catalyst embedded on the surface of the membrane is 2.30. The profile of the platinum catalyst is irregular (Figs. 4.73 and 4.74).

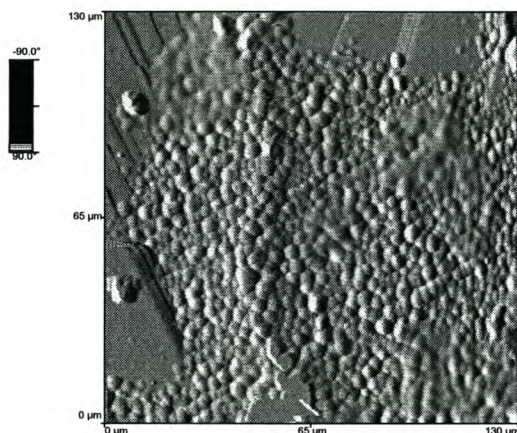


Figure 4.73. AFM surface image (130 $\mu\text{m}\times 130\mu\text{m}$) of a cation-exchange membrane embedded with platinum catalyst by the reduction of 0.03M platinic acid solution with sodium borohydride for 35.5 minutes at 40 °C.

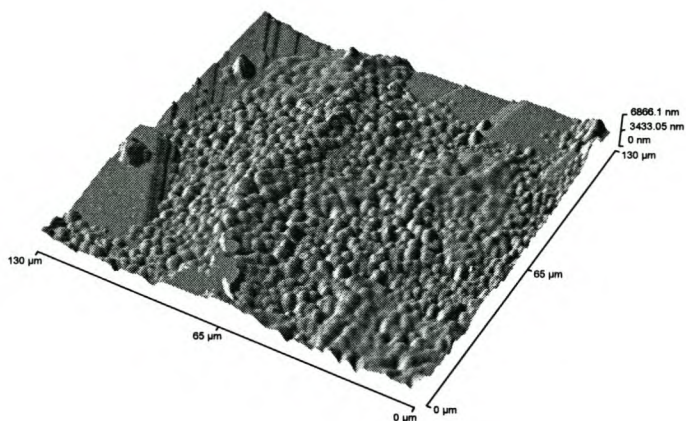


Figure 4.74. Three-dimensional AFM surface image ($130\mu\text{m}\times 130\mu\text{m}$) of a cation-exchange membrane embedded with platinum catalyst by the reduction of 0.03M platinic acid solution with sodium borohydride for 35.5 minutes at 40 °C.

The surface roughness profile of the platinum catalyst embedded on the membrane can be seen in the line analysis plot (Fig. 4.75). The surface roughness of the platinum catalyst can be described (qualitatively) as rutted (Fig. 4.75).

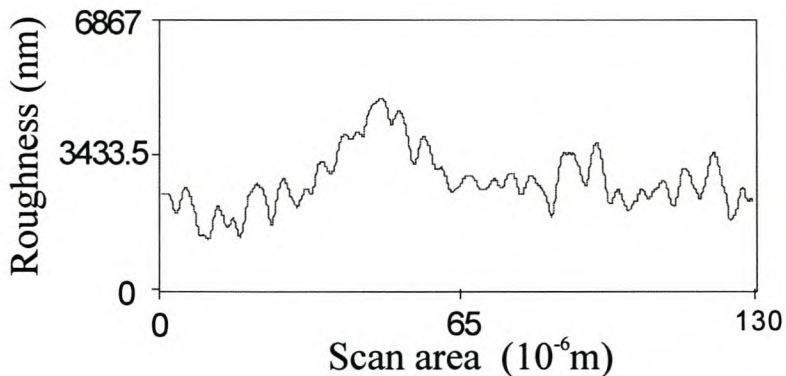


Figure 4.75. Line analysis plot of the surface roughness of a cation-exchange membrane embedded with platinum by the reduction of 0.03M platinic acid with sodium borohydride for 35.5 minutes at 40 °C.

Table 4.5. Results of AFM for the scan area $20\mu\text{m}\times 20\mu\text{m}$ of membranes embedded with platinum catalyst by the reduction of 0.03M platonic acid solution with sodium borohydride at 40 °C for varying lengths of time.

Time of platinisation for the reduction of 0.03M platonic acid with NaBH_4 (min)	Average roughness of Pt catalyst embedded on the membrane (nm)	Average height of Pt catalyst embedded on the membrane (nm)	Surface area of Pt catalyst embedded on the membrane (μm^2)	Fractal dimension of Pt catalyst (FD)
3.5	260.7	638.8	474.6	2.08
11.5	461.3	1500.4	528	2.11
15.5	<i>Unable to analyse platinum-containing membrane samples of $20\mu\text{m}\times 20\mu\text{m}$ scan area due to the presence of artifacts in these images.</i>			
25.5				
35.5				

Table 4.6. Results of AFM for the scan area $130\mu\text{m}\times 130\mu\text{m}$ of membranes embedded with platinum catalyst by the reduction of 0.03M platonic acid solution with sodium borohydride at 40 °C for varying lengths of time.

Time of platinisation for the reduction of 0.03M platonic acid with NaBH_4 (min)	Average roughness of Pt catalyst embedded on the membrane (nm)	Average height of Pt catalyst embedded on the membrane (nm)	Surface area of Pt catalyst embedded on the membrane (μm^2)	Fractal dimension of Pt catalyst (FD)
3.5	402.5	1301.5	21762	2.28
11.5	400.7	1474.7	20643	2.13
15.5	488.7	2343.7	23460	2.43
25.5	1012.2	3944.2	20289	2.35
35.5	770.2	2726.5	18781	2.30

4.1.2. Surface roughness analysis of platinum catalyst embedded on cation-exchange membranes by the reduction of platinumic acid solution with hydrazine at room temperature

Figures 4.76 and 4.77 are typical two-dimensional and three-dimensional surface images of platinum-containing membranes that were pre-treated with water and hydrolysed with sodium hydroxide. The average roughness of the platinum catalyst on membrane is 77.59 nm and the average height of the platinum catalyst on membrane is 441.34 nm. The surface area of the electrocatalytic membrane is $440.9 \mu\text{m}^2$. The fractal dimension of the surface of SPE electrocatalytic membrane is 2.68. The platinum catalyst layer is characteristic of small platinum particles that are densely packed (Figs. 4.76. and 4.77). The surface roughness profile of electrocatalytic membrane can be seen in the line analysis plot (Fig. 4.78). The surface roughness of the platinum catalyst on the membrane can be described (qualitatively) as rutted (Fig. 4.78).

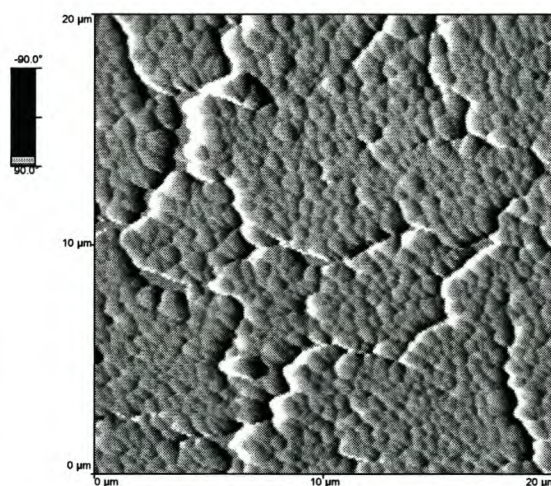


Figure 4.76. AFM surface image ($20\mu\text{m}\times 20\mu\text{m}$) of a cation-exchange membrane embedded with platinum by the reduction of 0.05M platinumic acid solution with hydrazine for 10 minutes at room temperature.

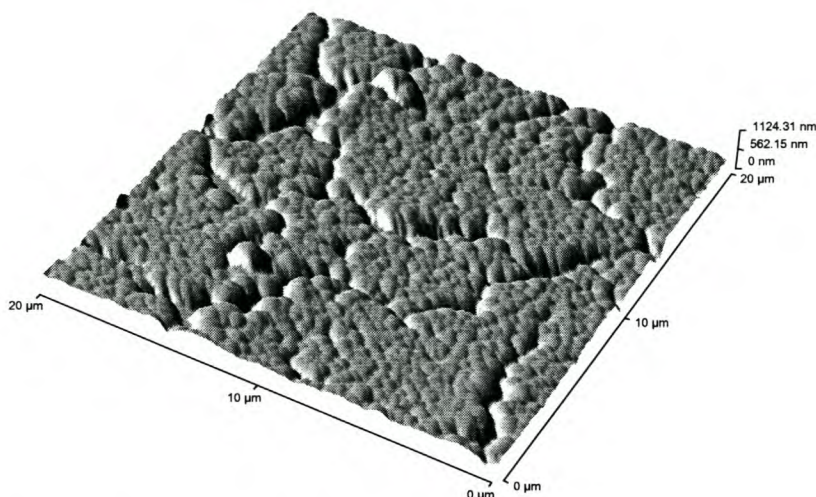


Figure 4.77. Three-dimensional AFM image ($20\mu\text{m}\times 20\mu\text{m}$) of a cation-exchange membrane embedded with platinum by the reduction of 0.05M platonic acid solution with hydrazine for 10 minutes at room temperature.

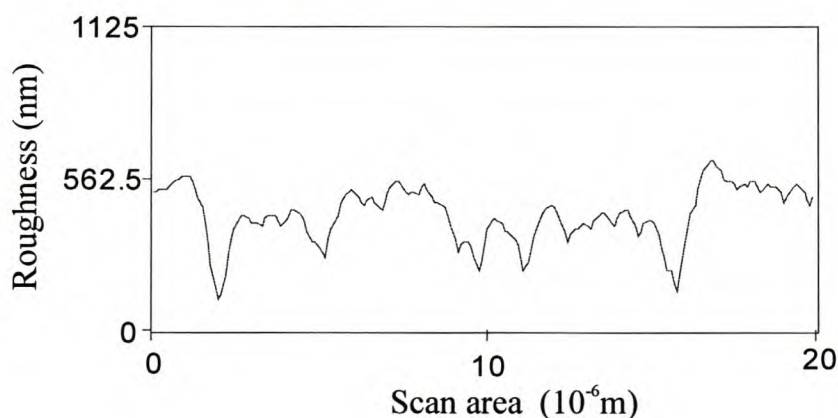


Figure 4.78. Line analysis plot of the surface roughness of a cation-exchange membrane embedded with platinum by the reduction of 0.05M platonic acid solution with hydrazine for 10 minutes at room temperature.

4.1.3. Surface roughness analysis of platinum catalyst embedded on pre-treated cation-exchange membranes by the reduction of platonic acid solution with hydrazine at room temperature

Figures 4.79 and 4.80 are typical two-dimensional and three-dimensional surface images platinum-containing membranes that were pre-treated with a solution of H_2O (70 vol. %) and MeOH (30 vol. %) and hydrolysed with sodium hydroxide. The average roughness of the platinum catalyst on membrane is 584.4 nm and the average

height of the platinum catalyst on membrane is 1562.3 nm. The surface area of electrocatalytic membrane is $484.6 \mu\text{m}^2$. The fractal dimension of the surface of the SPE electrocatalytic membrane is 2.48. The platinum layer is characteristic of small platinum particles that are densely packed (Figs. 4.79 and 4.80). The surface roughness profile of the electrocatalytic membrane can be seen in the line analysis plot (Fig. 4.81). The surface roughness of the platinum on the membrane can be described (qualitatively) as rutted (Fig. 4.81).

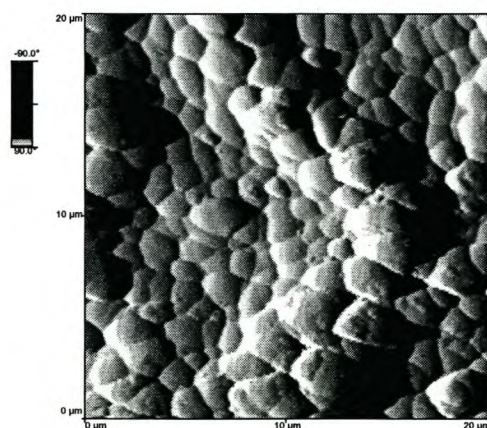


Figure 4.79. *AFM surface image ($20\mu\text{m}\times 20\mu\text{m}$) of a cation-exchange membrane embedded with platinum catalyst after membrane was pre-treated with a solution of H_2O (70 vol. %) and MeOH (30 vol. %) and hydrolysed with NaOH.*

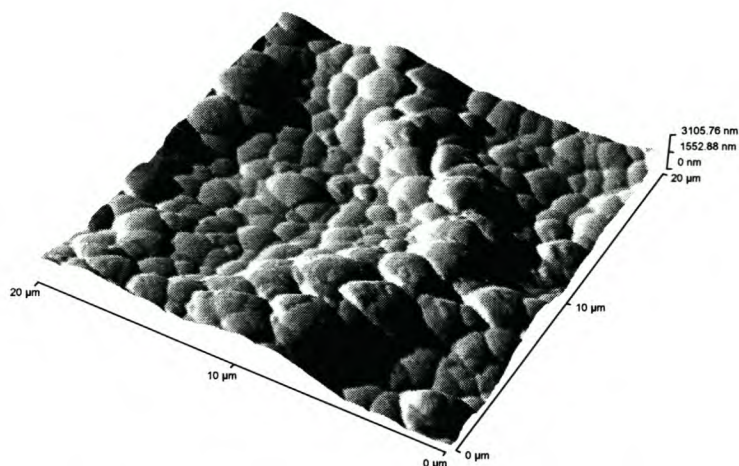


Figure 4.80. Three-dimensional AFM image ($20\mu\text{m}\times 20\mu\text{m}$) of a cation-exchange membrane embedded with platinum catalyst after membrane was pre-treated with a solution of H_2O (70 vol. %) and MeOH (30 vol. %) and hydrolysed with NaOH .

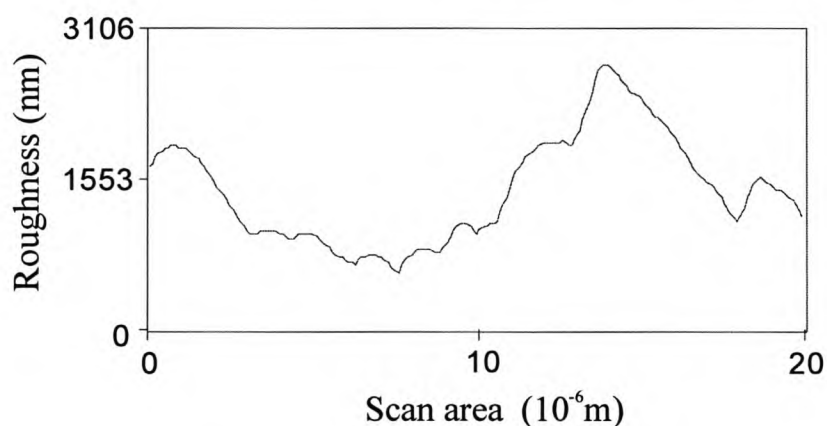


Figure 4.81. Line analysis plot of the surface roughness of a cation-exchange membrane embedded with platinum catalyst after membrane was pre-treated with a solution of H_2O (70 vol. %) and MeOH (30 vol. %) and hydrolysed with NaOH .

Figures 4.82 and 4.83 are typical two-dimensional and three-dimensional surface images of platinum-containing membranes that were pre-treated with a solution of H_2O (70 vol. %) and MeOH (30 vol. %) and hydrolysed with a solution of NaOH (70 vol. %) and MeOH (30 vol. %). The average roughness of the platinum catalyst on the membrane is 614.6 nm and the average height of the platinum catalyst on membrane is 1524.3 nm. The surface area of electrocatalytic membrane is $501.2\ \mu\text{m}^2$. The fractal dimension of the surface of the SPE electrocatalytic membrane is 2.56. The platinum layer is characteristic of small platinum particles that are densely packed (Figs. 4.82

and 4.83). The surface roughness profile of the electrocatalytic membrane can be seen in the line analysis plot (Fig. 4.84). The surface roughness of the platinum catalyst on the membrane can be described (qualitatively) as rutted (Fig. 4.84).

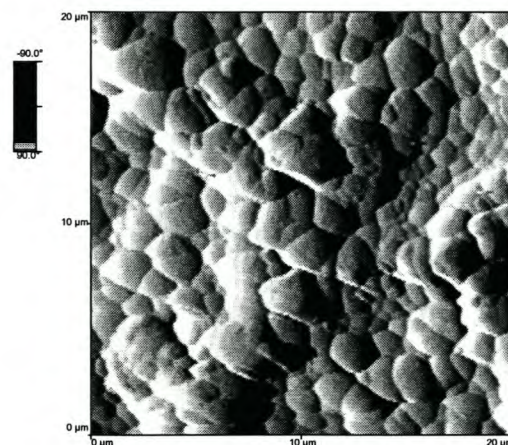


Figure 4.82. *AFM surface image (20µm×20µm) of a cation-exchange membrane embedded with platinum catalyst after membrane was pre-treated with a solution of H₂O (70 vol. %) and MeOH (30 vol. %) and hydrolysed with a solution of NaOH (70 vol. %) and MeOH (30 vol. %).*

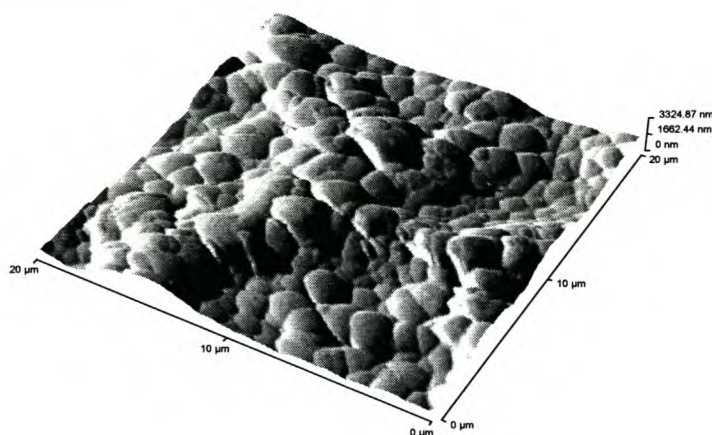


Figure 4.83. *Three-dimensional AFM image (20µm×20µm) of a cation-exchange membrane embedded with platinum catalyst after membrane was pre-treated with a solution of H₂O (70 vol. %) and MeOH (30 vol. %) and hydrolysed with a solution of NaOH (70 vol. %) and MeOH (30 vol. %).*

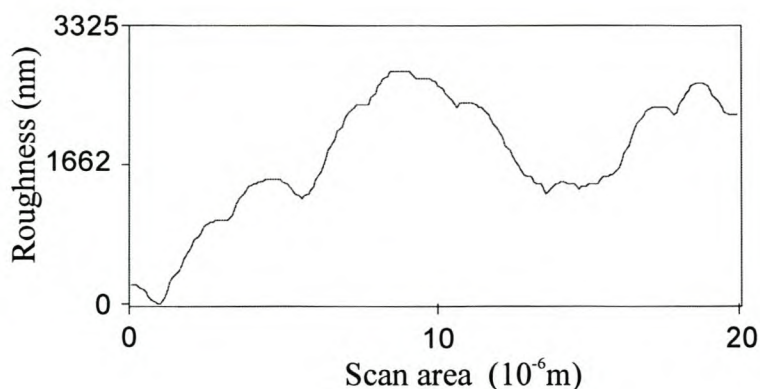


Figure 4.84. Line analysis plot of the surface roughness of a cation-exchange membrane embedded with platinum catalyst after membrane was pre-treated with a solution of H_2O (70 vol. %) and $MeOH$ (30 vol. %) and hydrolysed with a solution of $NaOH$ (70 vol. %) and $MeOH$ (30 vol. %).

Figures 4.85 and 4.86 are typical two-dimensional and three-dimensional surface images platinum-containing membranes that were pre-treated with water and hydrolysed with a solution of $NaOH$ (70 vol. %) and $MeOH$ (30 vol. %). The average roughness of the platinum catalyst on the membrane is 335.9 nm and the average height of the platinum catalyst on the membrane is 1216.1 nm. The surface area of the electrocatalytic membrane is $488.9 \mu m^2$. The fractal dimension of the surface of the SPE electrocatalytic membrane is 2.50. The platinum layer is characteristic of small platinum particles that are densely packed (Figs. 4.85 and 4.86). The surface roughness profile of the electrocatalytic membrane can be seen in the line analysis plot (Fig. 4.87). The surface roughness of the platinum catalyst on the membrane can be described (qualitatively) as rutted (Fig. 4.87).

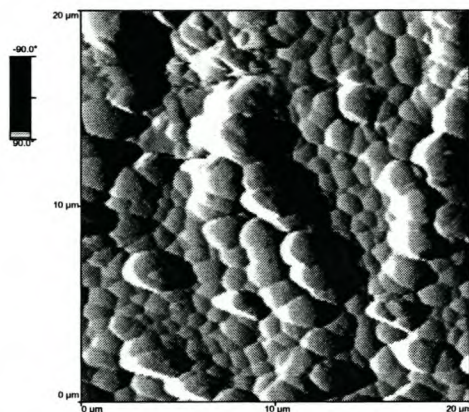


Figure 4.85. AFM surface image ($20\mu\text{m}\times 20\mu\text{m}$) of a cation-exchange membrane embedded with platinum catalyst after membrane was pre-treated with H_2O and hydrolysed with a solution of NaOH (70 vol. %) and MeOH (30 vol. %).

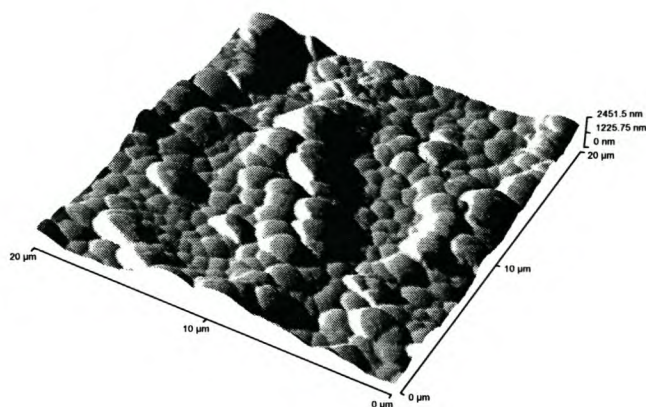


Figure 4.86. Three-dimensional AFM image ($20\mu\text{m}\times 20\mu\text{m}$) of a cation-exchange membrane embedded with platinum catalyst after membrane was pre-treated with H_2O and hydrolysed with a solution of NaOH (70 vol. %) and MeOH (30 vol. %).

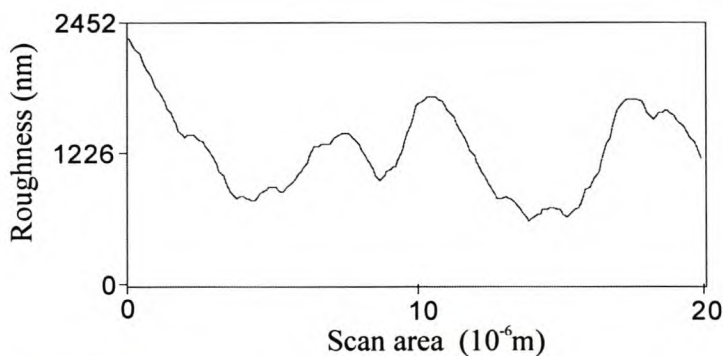


Figure 4.87. Line analysis plot of the surface roughness of a cation-exchange membrane embedded with platinum catalyst after membrane was pre-treated with H_2O and hydrolysed with a solution of NaOH (70 vol. %) and MeOH (30 vol. %).

4.1.4. Final remarks

The measurement of small areas of the platinum catalyst on a membrane by AFM provides information on the shape, size and arrangement of platinum particles on a membrane. The measurement of larger areas of the platinum-containing membranes by AFM provides more accurate information on the roughness profile, fractal dimension and average height of the platinum catalyst embedded on a membrane. The AFM results show that platinum catalyst on a membrane comprises of spherical-shaped platinum particles, as well as irregular 3D geometries scattered throughout the platinum catalyst layer.

The platinum catalyst that was deposited on membranes by the reduction of platinumic acid solution with hydrazine exhibits a decrease in fractal dimension and surface roughness with the increase in the time of platinisation. This can be attributed to the platinum catalyst smoothing (flattening) as the thickness of the platinum catalyst layer on the membrane increases. An optimum time in the preparation of platinum-containing membranes by counter-diffusion was observed. A maximum in the surface roughness and surface area was obtained for a time of platinisation of 7.5 minutes (Table 4.1).

The sonication of platinumic acid solution during the deposition process had no significant effect on the surface area and roughness of the platinum catalyst as compared when platinumic acid solution was not sonicated (Table 4.3).

The results show that the reduction of platinumic acid solution with sodium borohydride produces a platinum catalyst surface that has greater roughness as compared when platinumic acid solution is reduced by hydrazine. An optimum time in the preparation of platinum-containing membranes by counter-diffusion was observed for the reduction of 0.03M platinumic acid solution by sodium borohydride. A maximum in the surface roughness and surface area was obtained for a time of platinisation of 25.5 minutes when 0.03M platinumic acid was reduced by sodium borohydride (Table 4.6).

The surface roughness analysis of platinum-containing membranes for the reduction of 0.05M platinumic acid solution with sodium borohydride was more difficult to analyse as the platinum catalyst layer on membrane was very thin. However, the surface roughness of the platinum tends to increase as the time of platinisation increases (Table 4.4).

Greater roughness of the platinum catalyst on a membrane is obtained when membranes were pre-treated with a solution of H₂O (70 vol. %) and MeOH (30 vol. %) than with water. Membranes that were pre-treated exhibited a greater platinum catalyst roughness than membranes that were not pre-treated (Fig. 4.79).

The metal deposition behaviour depends strongly on the activation procedure of the substrate (Shu et al., 1993). The membranes that exhibited greater platinum loading, irrespective of the conditions of hydrolysis, was pre-treated with a solution of H₂O (70 vol. %) and MeOH (30 vol. %).

The inconsistency of some of the results obtained for fractal dimension and roughness values of platinum-containing membranes can be attributed to the heterogeneity in the membrane structure. The macro-nodule formation, due to the heterogeneity in the membrane structure, may alter the packing of the fine microstructure of the membrane in a way that increases the specific surface area and allows for the preferential deposition of platinum at specific membrane sites (Sheppard et al., 1998).

4.2. Characterisation of the surface profile of platinum catalyst embedded on a cation-exchange membrane by Scanning Electron Microscopy (SEM)

The surface profile of the platinum catalyst on the membrane was investigated by scanning electron microscopy (SEM). The SEM images provide information on the morphology of the platinum catalyst on the membrane and the distribution of the platinum particles within the bulk of the membrane.

In SEM, a beam of electrons is directed from a filament to the sample in a vacuum environment ranging from 10^{-4} to 10^{-10} Torr. The electrons are guided to the sample by a series of electromagnetic lenses. The electrons interact with the sample within a few nanometres to several microns of the surface, depending on beam parameters and sample type. Electrons are emitted from the sample as either backscattered electrons or secondary electrons. When these electrons escape from the sample surface, a scintillator-photomultiplier detector detects them (Russell et al., 2001).

Secondary electrons are low energy electrons, so only those formed within the first few nanometers of the sample surface have enough energy to escape and be detected. Backscattered electrons are beam electrons scattered back out the sample. These electrons go much deeper into the sample than secondary electrons, but are still able to emerge from the sample to be detected (Russell et al., 2001).

The SEM image formed is the result of the intensity of the secondary electron emission from the sample at each x,y data point during the scanning of the electron beam across the surface of the sample (Russell et al., 2001).

In this study a Leica S440 Scanning Electron Microscope with a backscattering detector was used to image SPE electrocatalytic membranes. The beam current (EHT) was 15.00kV. The amperage probe was 319pA. The working distance (WD) between the detector and the sample was 17 mm.

4.2.1. Surface profile analysis of the platinum catalyst embedded on cation-exchange membranes by the reduction of platonic acid solution at 40 °C

4.2.1.1. SEM imaging of membranes embedded with platinum catalyst by the reduction of 0.05M platonic acid solution with hydrazine at 40 °C

The reduction of 0.05M platonic acid solution by hydrazine for 3.5 minutes at 40 °C results in a layer of platinum catalyst on the membrane that is thin, continuous and uniform (Figs. 4.88 and 4.89). The platinum catalyst consists of platinum particles that are irregular shaped and of varying sizes. The thickness of the platinum layer on the surface of the membrane is 0.8 μ m.

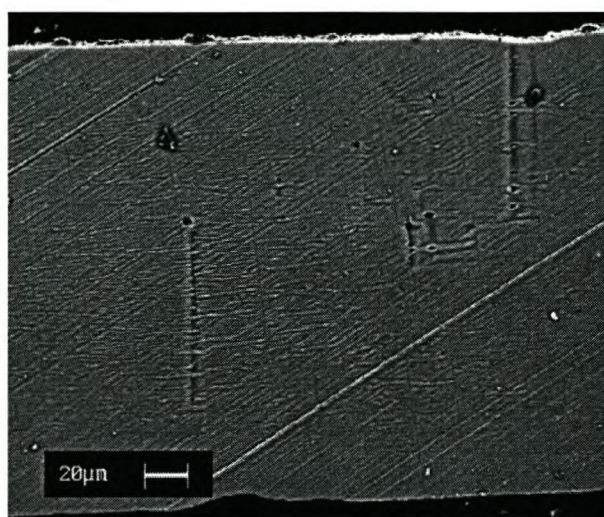


Figure 4.88. SEM image (using a backscattering detector) of a cation-exchange membrane embedded with platinum catalyst by the reduction of 0.05M platonic acid solution with hydrazine for 3.5 minutes at 40 °C.



Figure 4.89. High-magnification SEM image (using a backscattering detector) of a cation-exchange membrane embedded with platinum catalyst by the reduction of 0.05M platonic acid solution with hydrazine for 3.5 minutes at 40 °C.

The reduction of 0.05M platonic acid solution by hydrazine for 5.5 minutes at 40 °C results in a layer of platinum catalyst on the membrane that is continuous and uniform (Fig. 4.90). The thickness of the layer of platinum catalyst on the surface of the membrane is 2 μ m.

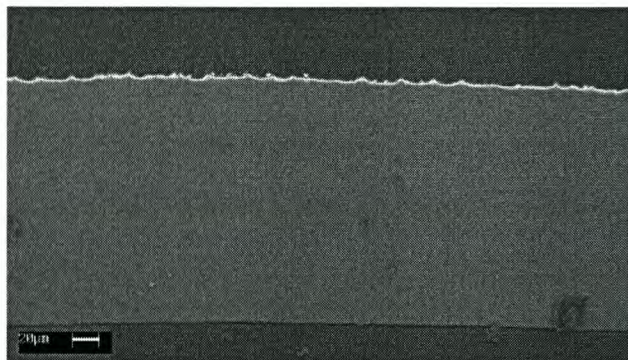


Figure 4.90. SEM image (using a backscattering detector) of a cation-exchange membrane embedded with platinum catalyst by the reduction of 0.05M platonic acid solution with hydrazine for 5.5 minutes at 40 °C.

The reduction of 0.05M platonic acid solution by hydrazine for 7.5 minutes at 40 °C results in a layer of platinum catalyst on the membrane that is continuous and uniform (Fig. 4.91). The thickness of the layer of platinum catalyst on the surface of the membrane is 2.5 μ m.

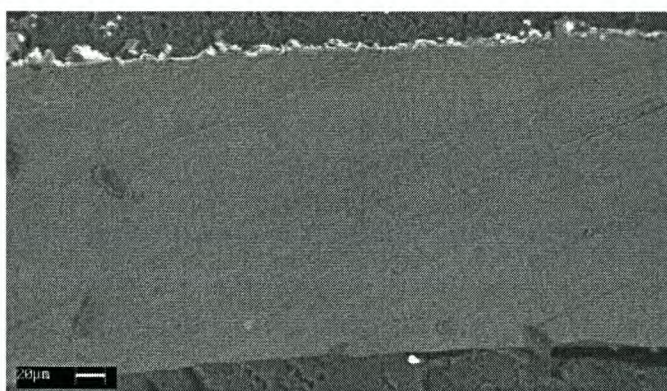


Figure 4.91. SEM image (using a backscattering detector) of a cation-exchange membrane embedded with platinum catalyst by the reduction of 0.05M platonic acid solution with hydrazine for 7.5 minutes at 40 °C.

The reduction of 0.05M platonic acid solution by hydrazine for 9.5 minutes at 40 °C results in a layer of platinum catalyst on the membrane that is continuous and uniform (Figs. 4.92 and 4.93). The layer of platinum catalyst on the membrane consists of

platinum particles of a regular shape. The thickness of the platinum catalyst embedded on the surface of the membrane is $2.8\mu\text{m}$.

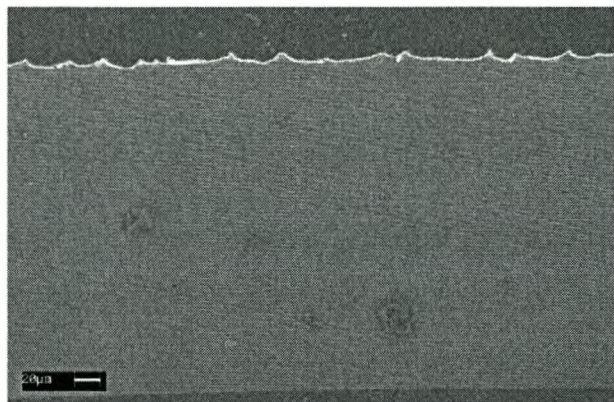


Figure 4.92. SEM image (using a backscattering detector) of a cation-exchange membrane embedded with platinum catalyst by the reduction of 0.05M platonic acid solution with hydrazine for 9.5 minutes at 40 °C.



Figure 4.93. High-magnification SEM image (using a backscattering detector) of a cation-exchange membrane embedded with platinum catalyst by the reduction of 0.05M platonic acid solution with hydrazine for 9.5 minutes at 40 °C.

The reduction of 0.05M platonic acid solution by hydrazine for 11.5 minutes at 40 °C results in a layer of platinum catalyst on the membrane that is continuous and uniform (Fig. 4.94). The thickness of the layer of platinum catalyst on the membrane on the surface of the membrane is $3\mu\text{m}$.

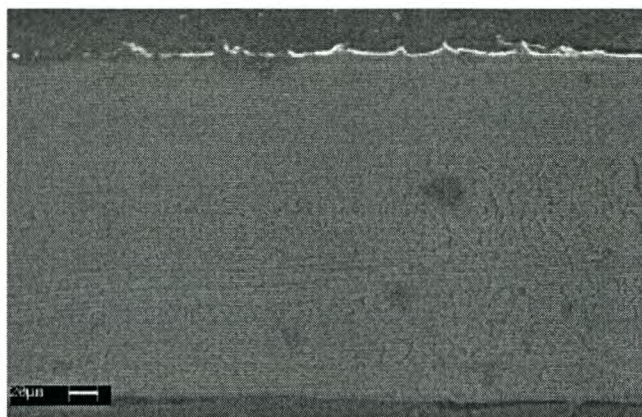


Figure 4.94. SEM image (using a backscattering detector) of a cation-exchange membrane embedded with platinum by the reduction of 0.05M platonic acid solution with hydrazine for 11.5 minutes at 40 °C.

The reduction of 0.05M platonic acid solution by hydrazine for 15.5 minutes at 40 °C is characteristic of regular shaped platinum particles embedded on the membrane (Figs. 4.95 and 4.96). The layer of platinum catalyst on the membrane consists of platinum clusters of a size larger than 1μm. The thickness of the layer of platinum catalyst on the surface of the membrane is 4.3μm.

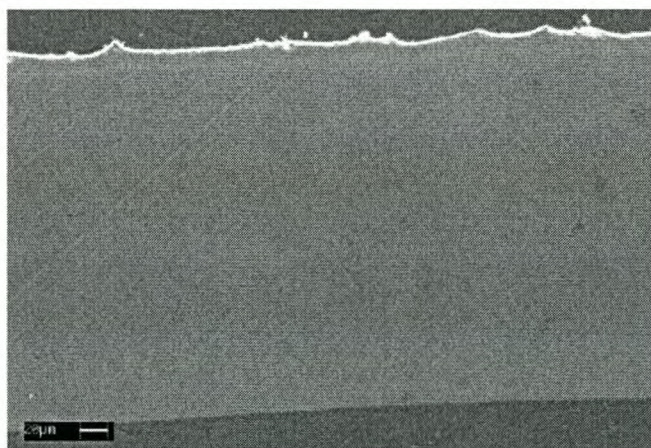


Figure 4.95. SEM image (using a backscattering detector) of a cation-exchange membrane embedded with platinum catalyst by the reduction of 0.05M platonic acid solution with hydrazine for 15.5 minutes at 40 °C.

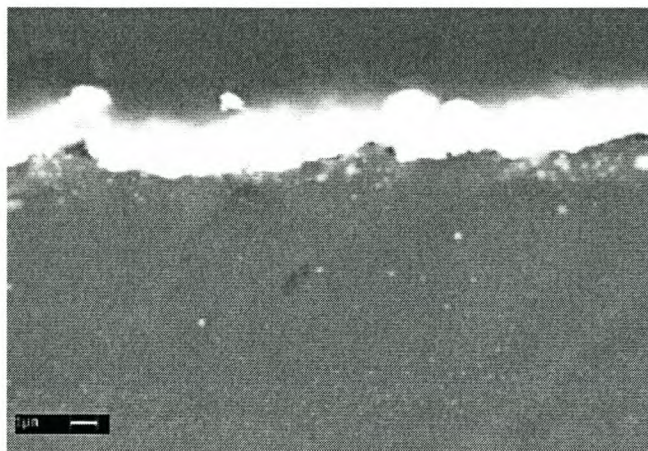


Figure 4.96. High-magnification SEM image (using a backscattering detector) of a cation-exchange membrane embedded with platinum catalyst by the reduction of 0.05M platinic acid solution with hydrazine for 15.5 minutes at 40 °C.

Table 4.7. Surface analysis of platinum catalyst deposited on membranes by the reduction of 0.05M platinic acid solution with hydrazine

Time of reduction of platinic acid solution with N₂H₄ (min)	Thickness of the layer of Pt on a membrane (μm)
3.5	0.8
5.5	2.0
7.5	2.5
9.5	2.8
11.5	3.0
15.5	4.3

4.2.1.2. SEM imaging of membranes embedded with platinum catalyst by the reduction of the sonicated 0.03M platinic acid solution with hydrazine at 40 °C

A platinum catalyst layer that is uniform and non-continuous was deposited on a membrane when 0.03M platinic acid solution was reduced by hydrazine for 7 minutes at 40 °C, while the platinic acid solution underwent sonication (Figs. 4.97 and 4.98). The platinum layer on the membrane comprises platinum particles that are of irregular shape and varying size. The thickness of the layer of platinum catalyst on the surface of the membrane is 1.1 μm .

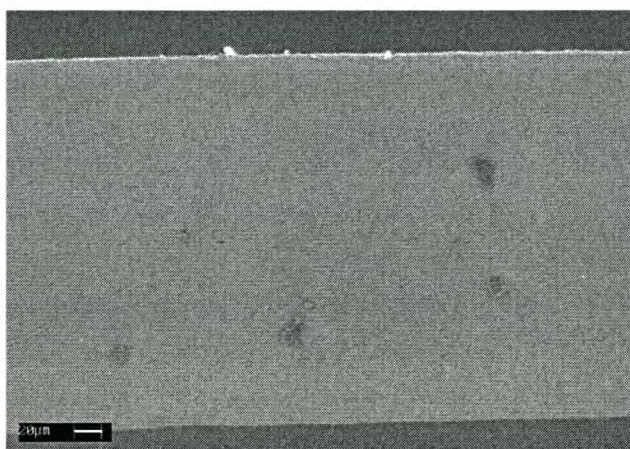


Figure 4.97. SEM image of a cation-exchange membrane embedded with platinum catalyst by the reduction of 0.03M platinic acid solution with hydrazine for 7 minutes at 40 °C, while the platinic acid solution underwent sonication

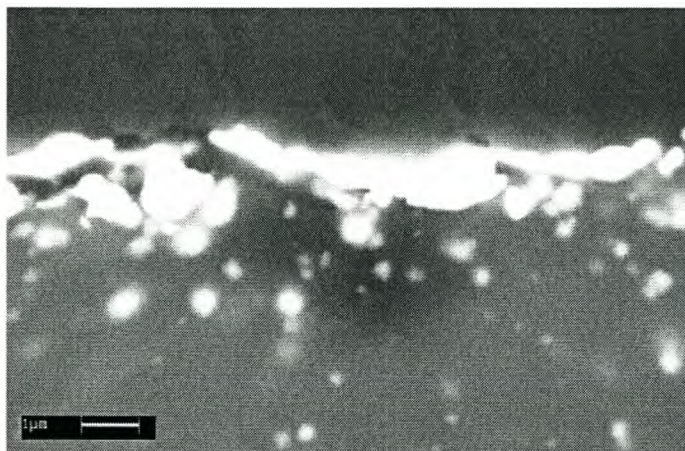


Figure 4.98. *High-magnification SEM image of a cation-exchange membrane embedded with platinum catalyst by the reduction of 0.03M platinic acid solution with hydrazine for 7 minutes at 40 °C, while the platinic acid solution underwent sonication*

The reduction of 0.03M platinic acid solution by hydrazine (without sonication) for 7 minutes at 40 °C results in a layer of platinum catalyst on a membrane that is thin, inconsistent and non-continuous (Figs. 4.99 and 4.100). The layer of platinum catalyst on the membrane consists of platinum particles that are of irregular shape and varying sizes. The thickness of the layer of platinum catalyst on the membrane surface is 0.8 μm.

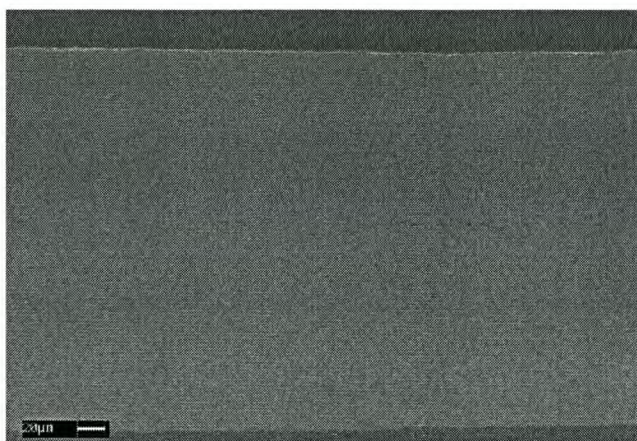


Figure 4.99. *SEM image (using a backscattering detector) of a cation-exchange membrane embedded with platinum catalyst by the reduction of 0.03M platinic acid solution with hydrazine for 7 minutes at 40 °C.*

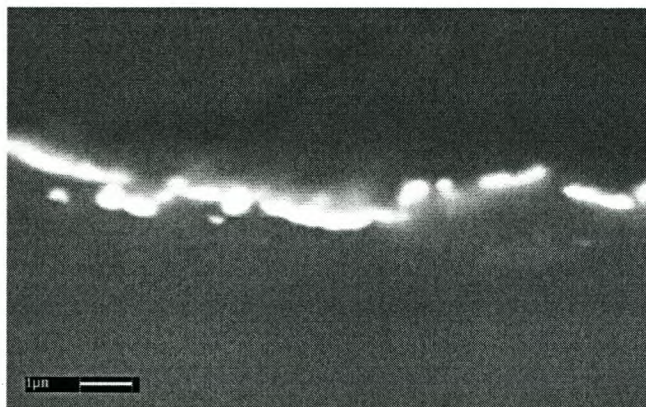


Figure 4.100. High-magnification SEM image (using a backscattering detector) of a cation-exchange membrane embedded with platinum catalyst by the reduction of 0.03M platinic acid solution with hydrazine for 7 minutes at 40 °C.

Table 4.8. Surface analysis of platinum catalyst that was deposited on membranes by the reduction of 0.03M platinic acid solution with hydrazine

Time of reduction of platinic acid solution with N ₂ H ₄ (min)	Thickness of the platinum layer on the membrane (μm)
7	0.8
7*	1.1

* Sonication of platinic acid solution during the deposition of platinum catalyst on membranes.

4.2.1.3. SEM imaging of membranes embedded with platinum catalyst by the reduction of 0.05M platinic acid solution with sodium borohydride at 40 °C

The reduction of 0.05M platinic acid solution by sodium borohydride for 3.5 minutes at 40 °C results in the layer of platinum catalyst on a membrane that is thin, inconsistent and non-continuous (Figs. 4.101 and 4.102). The layer of platinum catalyst on the membrane comprises platinum particles that are spherical in shape. The thickness of the layer of platinum catalyst on the membrane surface is 0.5 μm .

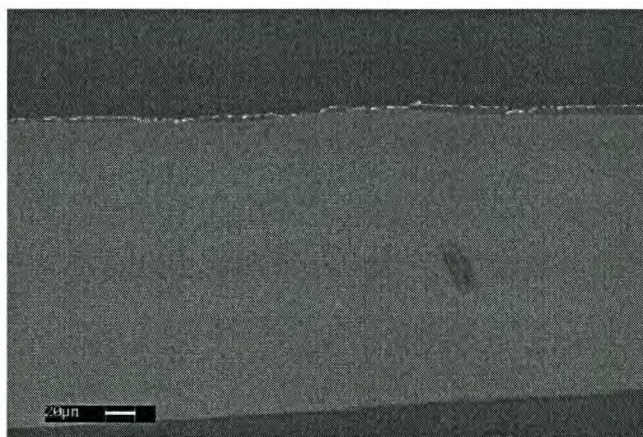


Figure 4.101. SEM image (using a backscattering detector) of a cation-exchange membrane embedded with platinum catalyst by the reduction of 0.05M platinic acid solution with sodium borohydride for 3.5 minutes at 40 °C.



Figure 4.102. High-magnification SEM image (using a backscattering detector) of a cation-exchange membrane embedded with platinum catalyst by the reduction of 0.05M platinic acid solution with sodium borohydride for 3.5 minutes at 40 °C.

The reduction of 0.05M platinic acid solution by sodium borohydride for 5.5 minutes at 40 °C results in a layer of platinum catalyst on membrane that is thin, inconsistent

and non-continuous (Fig. 4.103). The thickness of the layer of platinum catalyst on the membrane surface is 0.8 μm .

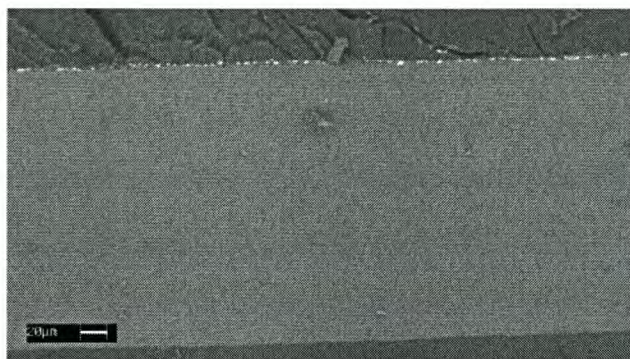


Figure 4.103. SEM image of a cation-exchange membrane (using a backscattering detector) embedded with platinum catalyst by the reduction of 0.05M platinic acid solution with sodium borohydride for 5.5 minutes at 40 °C.

The reduction of 0.05M platinic acid solution by sodium borohydride for 7.5 minutes at 40 °C results in a layer of platinum catalyst on membrane that is inconsistent and non-continuous (Fig. 4.104). The thickness of the layer of platinum catalyst on the membrane surface is 1.0 μm .

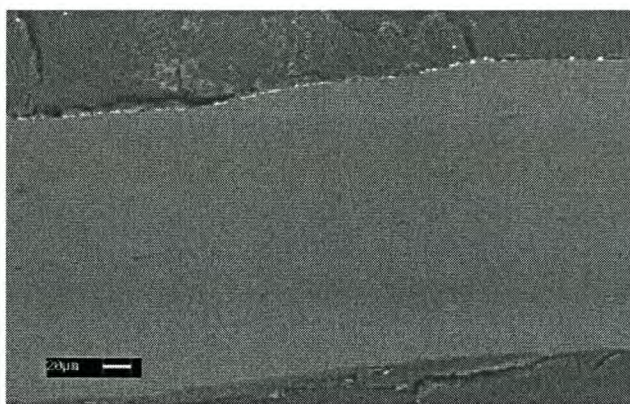


Figure 4.104. SEM image (using a backscattering detector) of a cation-exchange membrane embedded with platinum catalyst by reduction of 0.05M platinic acid solution with sodium borohydride for 7.5 minutes at 40 °C.

The reduction of 0.05M platinic acid solution by sodium borohydride for 9.5 minutes at 40 °C results in a layer of platinum catalyst on the membrane that is thin and inconsistent (Figs. 4.105 and 4.106). The layer of platinum catalyst on the membrane

consists of platinum particles that are spherical in shape. The thickness of the layer of platinum catalyst on the membrane surface is 1.1 μm .

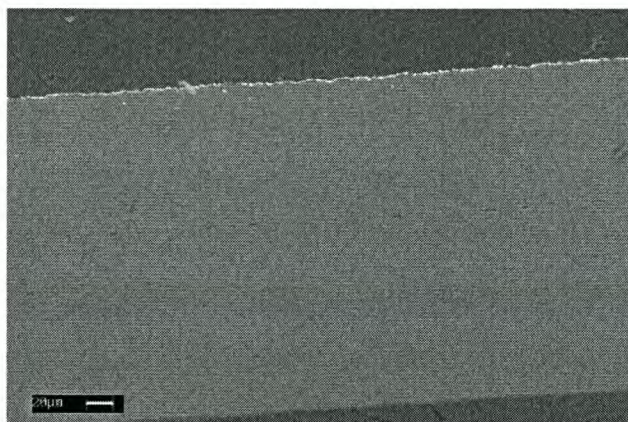


Figure 4.105. SEM image (using a backscattering detector) of a cation-exchange membrane embedded with platinum by the reduction of 0.05M platinic acid solution with sodium borohydride for 9.5 minutes at 40 °C.

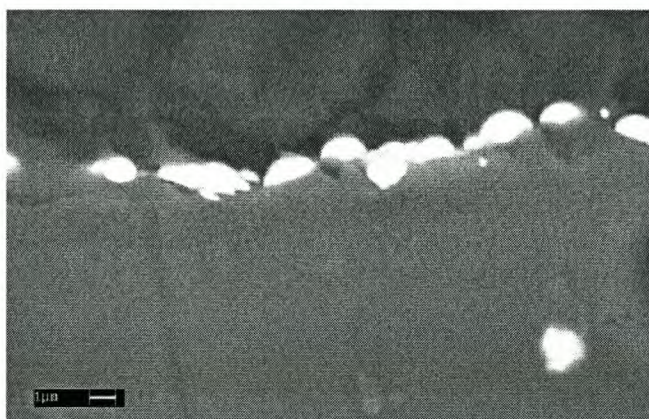


Figure 4.106. High-magnification SEM image (using a backscattering detector) of a cation-exchange membrane embedded with platinum catalyst by the reduction of 0.05M platinic acid solution with sodium borohydride for 9.5 minutes at 40 °C.

The reduction of 0.05M platinic acid solution by sodium borohydride for 11.5 minutes at 40 °C results in a layer of platinum catalyst on membrane that is inconsistent and non-continuous (Fig. 4.107). The thickness of the layer of platinum catalyst on the membrane surface is 1.5 μm .

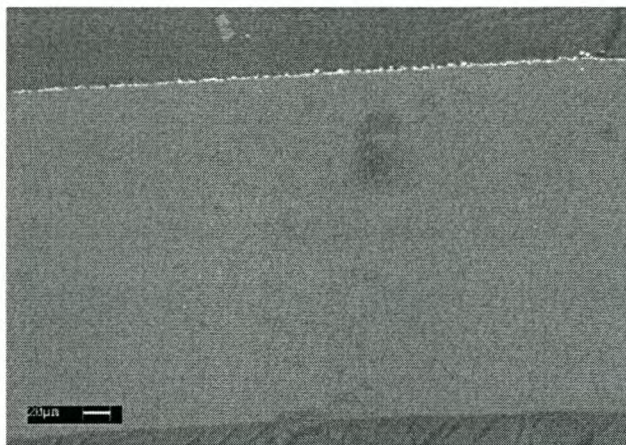


Figure 4.107. SEM image (using a backscattering detector) of a cation-exchange membrane embedded with platinum catalyst by the reduction of 0.05M platinic acid solution with sodium borohydride for 11.5 minutes at 40 °C.

The reduction of 0.05M platinic acid solution by sodium borohydride for 15.5 minutes at 40 °C results in a layer of platinum catalyst on the membrane that is thin and non-continuous (Figs. 4.108 and 4.109). The layer of platinum catalyst on the membrane comprises platinum particles that are spherical in shape. The thickness of the layer of platinum catalyst on the surface of the membrane is 1.25 μm .

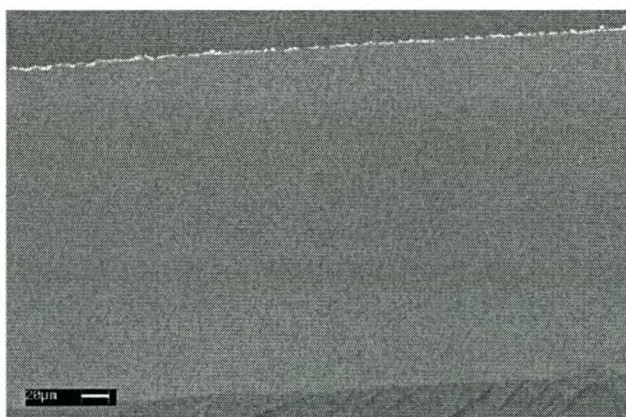


Figure 4.108. SEM image (using a backscattering detector) of a cation-exchange membrane embedded with platinum by the reduction of 0.05M platinic acid solution with sodium borohydride for 15.5 minutes at 40 °C.



Figure 4.109. High-magnification SEM image (using a backscattering detector) of a cation-exchange membrane embedded with platinum catalyst by the reduction of 0.05M platinic acid solution with sodium borohydride for 15.5 minutes at 40 °C.

Table 4.9. Surface analysis of platinum catalyst that was deposited on membranes by the reduction of 0.05M platinic acid solution with sodium borohydride

Time of reduction of platinic acid solution with NaBH₄ (min)	Thickness of the layer of Pt on a membrane (μm)
3.5	0.5
5.5	0.8
7.5	1.0
9.5	1.1
11.5	1.15
15.5	1.25

4.2.1.4. SEM imaging of membranes embedded with platinum catalyst by the reduction of 0.03M platinic acid solution with sodium borohydride at 40 °C

The reduction of 0.03M platinic acid solution by sodium borohydride for 3.5 minutes at 40 °C results in almost no platinum catalyst embedded on the membrane (Fig. 4.110). The layer of platinum catalyst on the membrane comprises platinum particles of spherical shape. The thickness of the layer of platinum catalyst on the surface of the membrane is 0.2 µm.

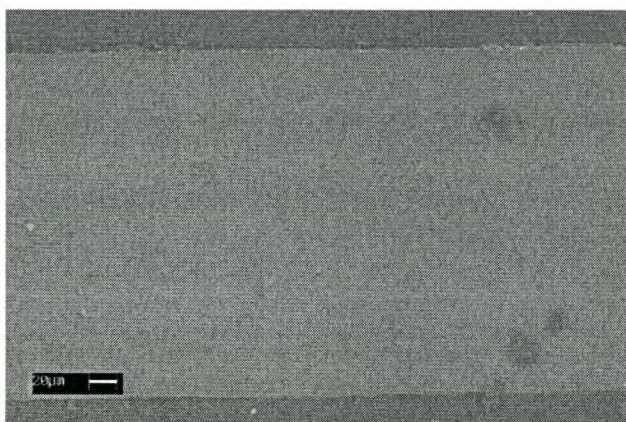


Figure 4.110. SEM image (using a backscattering detector) of a cation-exchange membrane embedded with platinum catalyst by the reduction of 0.03M platinic acid solution with sodium borohydride for 3.5 minutes at 40 °C.

The reduction of 0.03M platinic acid solution by sodium borohydride for 11.5 minutes at 40 °C results in a layer of platinum catalyst on the membrane that is thin, inconsistent and non-continuous (Fig. 4.111). The thickness of the layer of platinum catalyst on the surface of the membrane is 0.6 µm.

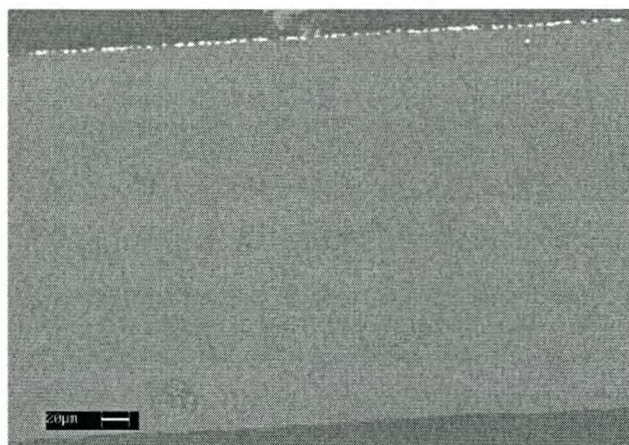


Figure 4.111. SEM image (using a backscattering detector) of a cation-exchange membrane embedded with platinum catalyst by the reduction of 0.03M platinic acid solution with sodium borohydride for 11.5 minutes at 40 °C.

The reduction of 0.03M platinic acid solution by sodium borohydride for 15.5 minutes at 40 °C results in a layer of platinum catalyst on the membrane that is thin and non-continuous (Figs. 4.112 and 4.113). The layer of platinum catalyst on the membrane comprises platinum particles that are spherical in shape, which are arranged irregularly. The thickness of the layer of platinum catalyst on the surface of the membrane is 1.8 μm.

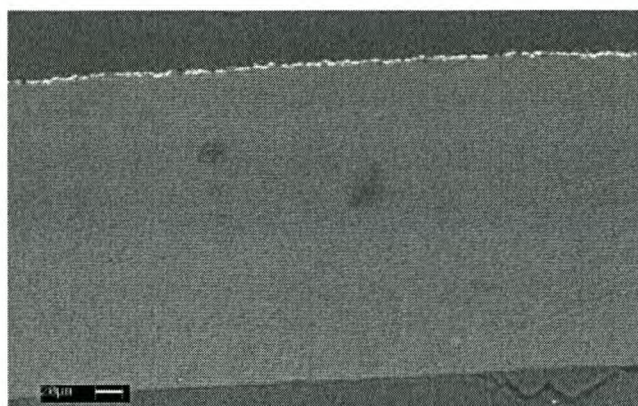


Figure 4.112. SEM image (using a backscattering detector) of a cation-exchange membrane embedded with platinum catalyst by the reduction of 0.03M platinic acid solution with sodium borohydride for 15.5 minutes at 40 °C.



Figure 4.113. *High-magnification SEM image (using a backscattering detector) of a cation-exchange membrane embedded with platinum catalyst by the reduction of 0.03M platinic acid solution with sodium borohydride for 15.5 minutes at 40 °C.*

The reduction of 0.03M platinic acid solution by sodium borohydride for 25.5 minutes at 40 °C results in a layer of platinum catalyst on a membrane that is thin and fairly continuous (Figs. 4.114 and 4.115). The layer of platinum catalyst on the membrane is characteristic of platinum particles that are spherical in shape, which are arranged irregularly. The thickness of the layer of platinum catalyst on the surface of the membrane is 2.9 μm.

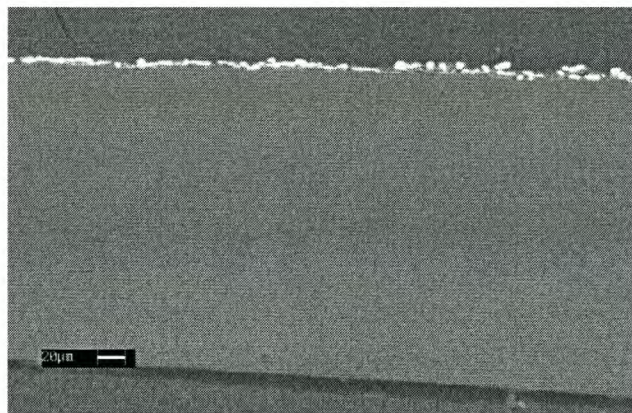


Figure 4.114. *SEM image (using a backscattering detector) of a cation-exchange membrane embedded with platinum catalyst by the reduction of 0.03M platinic acid solution with sodium borohydride for 25.5 minutes at 40 °C.*



Figure 4.115. *High-magnification SEM image (using a backscattering detector) of a cation-exchange membrane embedded with platinum catalyst by the reduction of 0.03M platinic acid solution with sodium borohydride for 25.5 minutes at 40 °C.*

The reduction of 0.03M platinic acid solution by sodium borohydride for 35.5 minutes at 40 °C results in a layer of platinum catalyst on the membrane that is thin and fairly continuous (Figs. 4.116 and 4.117). The thickness of the layer of platinum catalyst on the surface of the membrane is 3.1 μm.

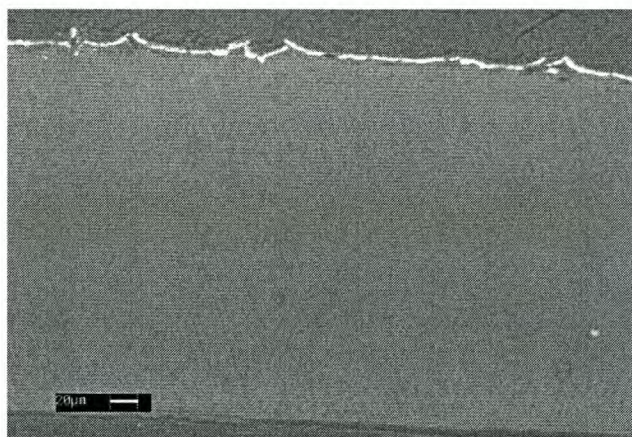


Figure 4.116. *SEM image (using a backscattering detector) of a cation-exchange membrane embedded with platinum catalyst by the reduction of 0.03M platinic acid solution with sodium borohydride for 35.5 minutes at 40 °C.*

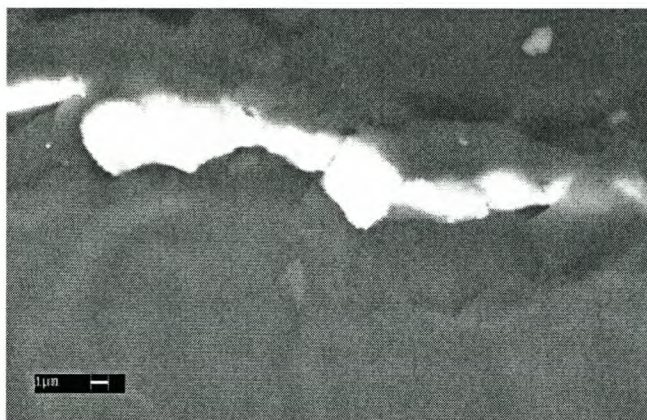


Figure 4.117. High-magnification SEM image (using a backscattering detector) of a cation-exchange membrane embedded with platinum catalyst by the reduction of 0.03M platinic acid solution with sodium borohydride for 35.5 minutes at 40 °C.

Table 4.10. Surface analysis of platinum catalyst that was deposited on membranes by the reduction of 0.03M platinic acid solution with sodium borohydride

Time of reduction of platinic acid solution with NaBH₄ (min)	Thickness of the layer of Pt on membrane (μm)
3.5	0.2
11.5	0.6
15.5	1.8
25.5	2.9
35.5	3.1

4.2.2. Surface roughness analysis of platinum catalyst embedded on cation-exchange membranes by the reduction of 0.05M platinic acid solution with hydrazine at room temperature

The reduction of 0.05M platinic acid solution with hydrazine at room temperature results in a platinum catalyst layer that is a non-continuous and thin (Fig. 4.118). No penetration of the platinum particles into the bulk of the membrane was observed. The total thickness of the layer of platinum is $\sim 0.5\mu\text{m}$. This layer consists of large platinum particle deposits on the surface of the membrane and smaller platinum particles within the membrane bulk (Fig. 4.119).

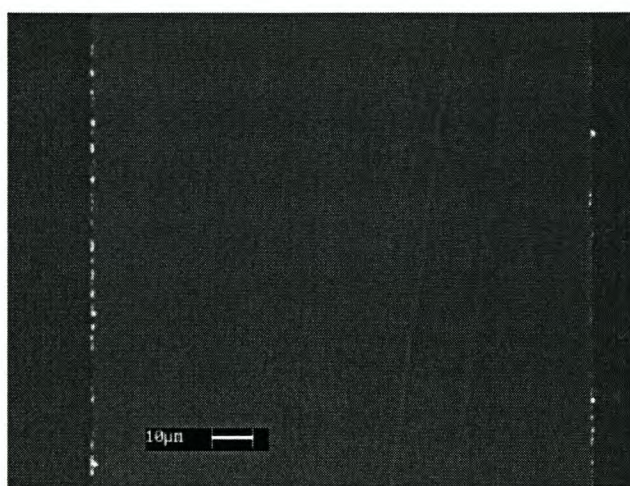


Figure 4.118. SEM image (using a backscattering detector) of the profile of the layer of platinum catalyst on a cation-exchange membrane



Figure 4.119. High-magnification SEM image (using a backscattering detector) of the profile of the layer of platinum on a cation-exchange membrane

4.2.3. Surface profile analysis of the platinum catalyst embedded on pre-treated cation-exchange membranes by the reduction of 0.05M platinic acid solution with hydrazine at room temperature

In Figs. 4.120 and 4.121 it can be seen that the layer of platinum catalyst on the surface of the membrane is uniform, with small breaks in continuity (Fig. 4.120). The platinum catalyst penetration into the bulk of the membrane can be seen in Figure 4.120. The total thickness of the platinum catalyst layer is $\sim 4.8\mu\text{m}$, which consists of large platinum particle deposits on the surface of the membrane and smaller platinum particles within the membrane bulk (Fig. 4.121). The thickness of the platinum catalyst layer on the surface of the membrane is $\sim 2\mu\text{m}$. The thickness of the platinum layer within the membrane bulk is $\sim 2.8\mu\text{m}$.

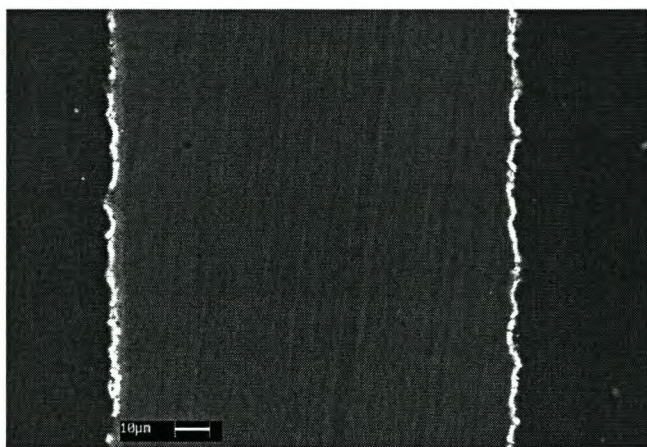


Figure 4.120. SEM image (using a backscattering detector) of the profile of the layer of platinum catalyst on a membrane hydrolysed with NaOH and pre-treated with a solution of H_2O (70 vol. %) and MeOH (30 vol. %).

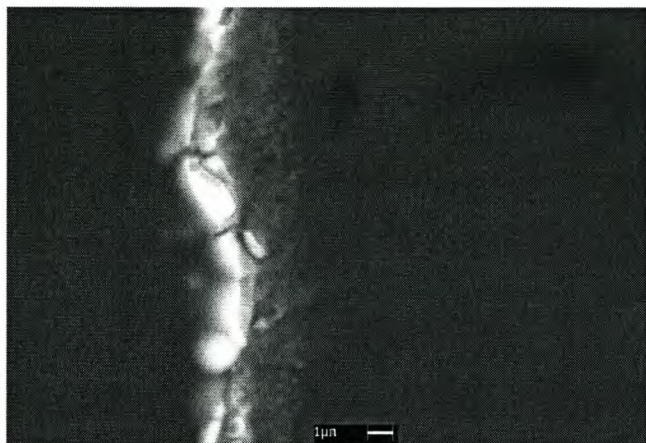


Figure 4.121. High-magnification SEM image (using a backscattering detector) of the profile of the layer of platinum catalyst on a membrane hydrolysed with NaOH and pre-treated with a solution of H₂O (70 vol. %) and MeOH (30 vol. %)

In Figs. 4.122 and 4.123 it can be seen that the layer of platinum catalyst on the membrane is non-continuous. The penetration of platinum particles into the bulk of the membrane is observed (Fig. 4.123). The total thickness of the layer of platinum is ~3.5 μm, which consists of large platinum particle deposits on the surface of the membrane and smaller platinum particles within the membrane bulk (Fig. 4.123). The thickness of the platinum layer on the surface of the membrane is ~1.7 μm. The thickness of the platinum layer within the membrane bulk is ~1.8 μm.

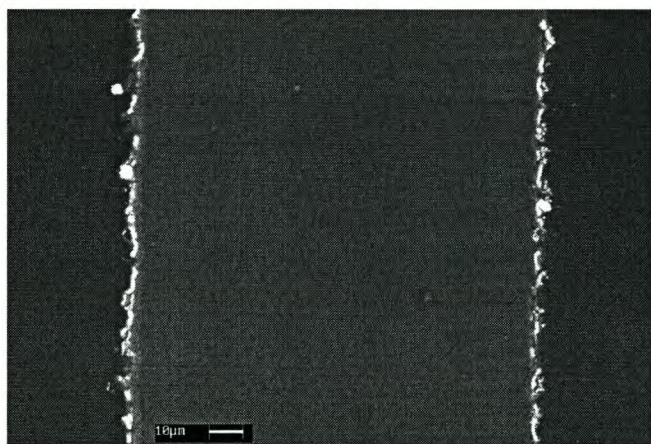


Figure 4.122. SEM image (using a backscattering detector) of the profile of the layer of platinum catalyst on a membrane hydrolysed with a solution of NaOH (70 vol. %) and MeOH (30 vol. %) and pre-treated with a solution of H₂O (70 vol. %) and MeOH (30 vol. %).

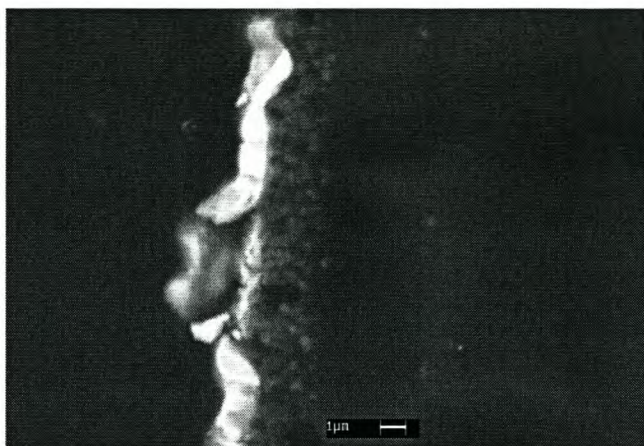


Figure 4.123. High-magnification SEM image (using a backscattering detector) of the profile of the layer of platinum catalyst on a membrane hydrolysed with a solution of NaOH (70 vol. %) and MeOH (30 vol. %) and pre-treated with a solution of H₂O (70 vol. %) and MeOH (30 vol. %).

In Figure 4.124 it can be seen that the layer of platinum catalyst on the membrane is uniform and fairly continuous. The total thickness of the layer of platinum catalyst is $\sim 0.7\mu\text{m}$, which consists of large platinum particle deposits on the surface of the membrane and smaller platinum particles within the membrane bulk (Fig. 4.125). The thickness of the platinum layer on the surface of the membrane is $\sim 0.7\mu\text{m}$. No penetration of the platinum particles within the membrane bulk was observed.

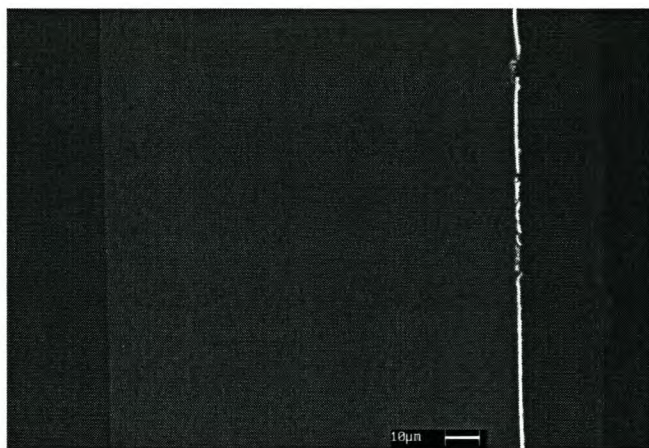


Figure 4.124. SEM image (using a backscattering detector) of the profile of the platinum catalyst on a cation-exchange membrane, which was hydrolysed with NaOH (70 vol. %) and MeOH (30 vol. %) and pre-treated with H₂O.

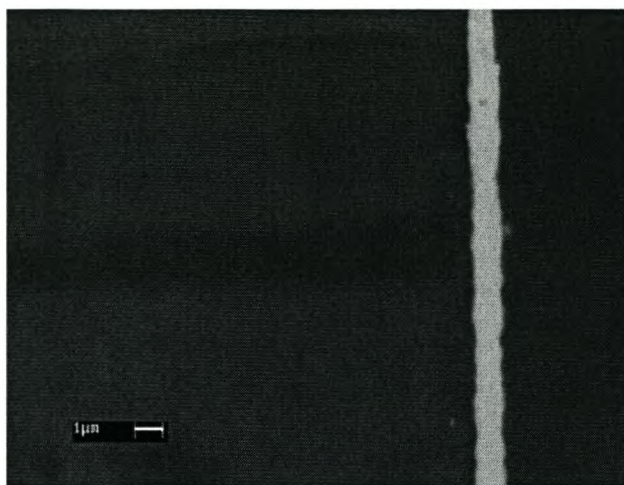


Figure 4.125. *High-magnification SEM image (using a backscattering detector) of the profile of the platinum catalyst on a cation-exchange membrane, which was hydrolysed with NaOH (70 vol. %) and MeOH (30 vol. %) and pre-treated with H₂O.*

4.2.4. Final remarks

The results of SEM analysis show that the loading of platinum catalyst on a membrane increases as the time of platinisation increases. The platinum catalyst occurs predominantly on the surface of the membrane. SEM results show that the type of reducing agent and concentration of the platonic acid solution influences the thickness of the platinum catalyst embedded on the membrane (Fig. 4.126). A thicker layer of platinum catalyst is embedded on a membrane when 0.05M platonic acid solution is reduced with hydrazine than when using sodium borohydride (Fig. 4.126). Greater platinum loading on a membrane is achieved with hydrazine than with sodium borohydride.

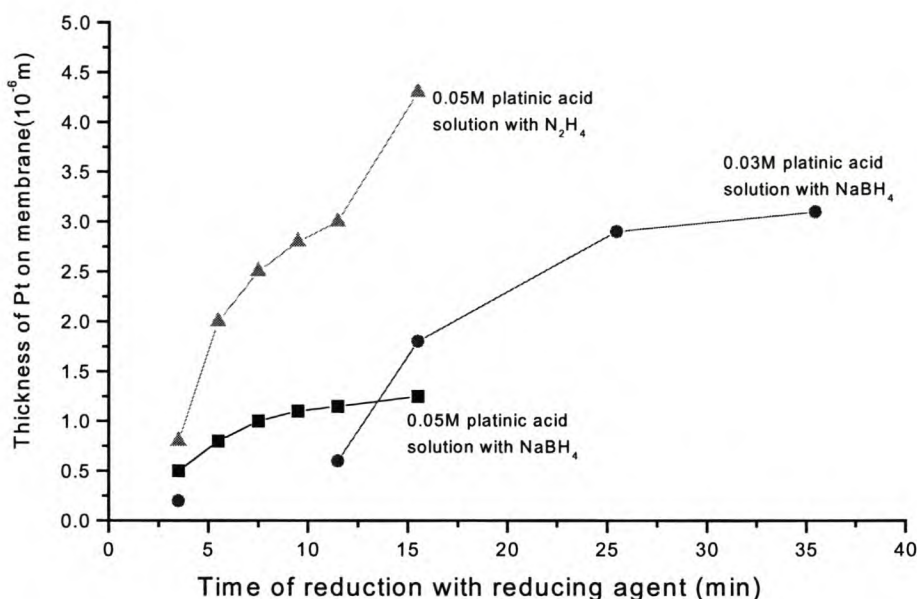


Figure 4.126. Plot of the thickness of the layer of platinum catalyst on a membrane under various conditions of the deposition process

SEM results show that platinum particles are embedded deep within the bulk of the membrane when the platonic acid solution is sonicated during the deposition process. This can be attributed to the increase in ionic transport of $[PtCl_6]^{2-}$ ions with the sonication of platonic acid solution, which usually would be restricted by electrostatic repulsion of sulphonic acid groups. This reduces the concentration polarisation effects within the membrane and extends the depth of penetration of the platinum particles within the membrane (Sheppard et al., 1998).

The SEM results show that the platinum catalyst on membranes when 0.03M platonic acid solution was used, are less compact and dense than when 0.05M platonic acid solution was used (Fedkiw et al., 1990). Fedkiw et al. (1990) showed that the morphology of the platinum embedded on the membrane was dependent on the concentration of the platonic acid solution. The results of Fedkiw et al. (1990) are consistent with the results that were obtained in the present study.

An increase in the deposition of platinum catalyst on a membrane is observed when the temperature of the reducing agent was 40 °C, as compared to room temperature. The increase in temperature in the deposition process causes the rate of the reaction to be increased. Thus, with the increase in the rate of reaction an increase

in the autocatalytic reduction of the platinumic acid solution will occur. This inevitably leads to greater deposition of platinum on a membrane (Figs. 4.119 and 4.93).

The SEM results for the pre-treatment of membranes show that membranes pre-treated with a solution of H₂O (70 vol. %) and MeOH (30 vol. %) exhibit greater platinum loading compared to membranes pre-treated with water (Figs. 4.120-4.123). SEM results of membranes pre-treated with a solution of H₂O (70 vol. %) and MeOH (30 vol. %) show greater penetration of platinum catalyst particles deep into the bulk of the membrane. Greater deposition of platinum catalyst on the surface of a membrane is achieved when membranes are pre-treated with water (Fig. 4.124). This phenomenon can be attributed to the methanol increasing the size of the pores of the membrane, which allows for the deeper penetration of [PtCl₆]²⁻ anions into the bulk of the membrane before it is autocatalytically reduced by the reducing agent.

Membranes that are pre-treated with a solution of H₂O (70 vol. %) and MeOH (30 vol. %) and hydrolysed with NaOH exhibit a thicker platinum catalyst layer than that of membranes pre-treated with a solution of H₂O (70 vol. %) and MeOH (30 vol. %) and hydrolysed with a solution of NaOH (70 vol. %) and MeOH (30 vol. %). This can be attributed to NaOH introducing a smaller counter-ion to the sulphonate ionic group than with the solution of NaOH (70 vol. %) and MeOH (30 vol. %). The smaller counter-ion offers less steric hindrance to ion transport during the deposition process. Therefore, a greater layer of platinum catalyst on the membrane is achieved when a membrane is hydrolysed with NaOH, rather than a solution of NaOH (70 vol. %) and MeOH (30 vol. %).

Interconnected platinum particles are important for catalytic processes to occur electronically. Isolated platinum particles do not allow for electron transfer during catalytic processes. Thus, chemical deposition conditions need to be of a nature that allow for interconnected platinum particles while achieving optimal platinum loading for a cost effective and viable technology. Characterisation of the surface profile of platinum containing membranes by scanning electron microscopy allows the investigation of these important aspects under various chemical deposition conditions.

4.3. Porosity determination of cation-exchange membranes by Brunauer Emmett Teller adsorption (BET)

The relationship between the amount of gas adsorbed by a given amount of adsorbent and the pressure of the gas can be used to determine the adsorption of an adsorbent. The adsorption measurement is of either the volume of gas adsorbed by a given amount of adsorbent or the change of weight of the adsorbent when it is exposed to a gas at a given pressure. The surface area of an adsorbent can be determined by estimating the area covered by a known amount of gas (Adamson, 1990).

There are different adsorption isotherms, such as chemisorption and physical adsorption. Chemisorption is accompanied by an adsorption isotherm, which rises steeply initially and then gradually flattens. The initial rise is due to the strong tendency of the surface to bind the gas molecules and the leveling off can be attributed to the saturation of these forces. Physical adsorption is accompanied by an adsorption isotherm that tends to have an increasingly positive slope with increasing gas pressure. Each incremental increase in gas pressure produces a larger increase in the amount of gas adsorbed, until the gas pressure equals the vapour pressure of the material being adsorbed. The adsorption isotherm ascends vertically at this pressure (Barrow, 1979).

In 1916, Langmuir presented a model for the adsorption process, particularly, for the chemisorption process. Other theories have been developed to explain the more complete adsorption process that leads to multilayer formation. In 1938, Brunauer, Emmett and Teller modified Langmuir's adsorption model. The result was the BET isotherm for multilayer physical adsorption that can be expressed as follows (Emmett, 1954; Adamson, 1990):

$$\frac{P}{a(P^* - P)} = \frac{1}{a_{mon}c} + \frac{c-1}{c} \left[\frac{P}{P^*} \right] \frac{1}{a_{mon}}$$

where a is the volume adsorbed at P , a_{mon} is the volume adsorbed in the high pressure limit when a monolayer covers the entire surface, c is a constant at a fixed temperature, and P^* is the vapour pressure of the adsorbate at the temperature of the experiment. The constant a_{mon} can be obtained from the slope of a plot $P/a(P^*-P)$ versus P/P^* . When a_{mon} has been determined from the BET isotherm, the number of molecules needed to form a monolayer is known and the surface area of the solid

adsorbent can be estimated by using an estimated value for the surface area occupied by one adsorbed molecule.

4.3.1. Preparation of membranes for characterisation by BET analysis

4.3.1.1. Hydrolysis of cation-exchange membranes

Membranes were boiled in 6N NaOH solution for 7 hours. The membranes were washed with distilled water and placed in distilled water at 60 °C for 10 minutes.

4.3.1.2. Pretreatment of hydrolysed membranes

Hydrolysed membranes in Na⁺-ionic form were pre-treated by boiling in distilled water, as well as in a solution of H₂O (70 vol. %) and MeOH (30 vol. %) for 2 hours, prior to the chemical deposition process.

4.3.1.3. Chemical deposition of platinum catalyst onto a membranes at room temperature

15ml 0.05M platinic acid solution was poured onto each membrane in the membrane holder. The time of contact of the platinic acid solution with the membrane was 1 minute. Thereafter, the membrane holder with the membrane and platinic acid solution was placed for 10 minutes into a bath containing the reducing agent, hydrazine. The total time of the platinisation was 11 minutes. After the deposition process was complete, the remaining platinic acid solution on the membrane was decanted into a beaker. The membrane was then washed with distilled water and boiled in distilled water for 2 hours.

4.3.2. Results of the BET analysis of cation-exchange membranes

Hydrolysed membranes (without platinum catalyst) and pre-treated membranes embedded with platinum catalyst was analysed by BET. The results are tabulated in Table 4.9. The adsorption isotherms for the hydrolysed membranes without platinum catalyst and the pre-treated membranes embedded with platinum catalyst are shown in Figures 4.127 and 4.128 respectively.

Table 4.11. BET results of pre-treated membranes embedded with platinum catalyst and hydrolysed membranes without platinum catalyst.

	Hydrolysed membranes without Pt catalyst	Pre-treated membranes embedded with Pt catalyst
Mass of membrane (g)	0.47	0.49
BET surface area (sq. m/g)	0.86	1.12
Average pore diameter (Å)	34.86	35.25
Pore volume (cc/g)	5.6×10^{-4}	5.3×10^{-4}

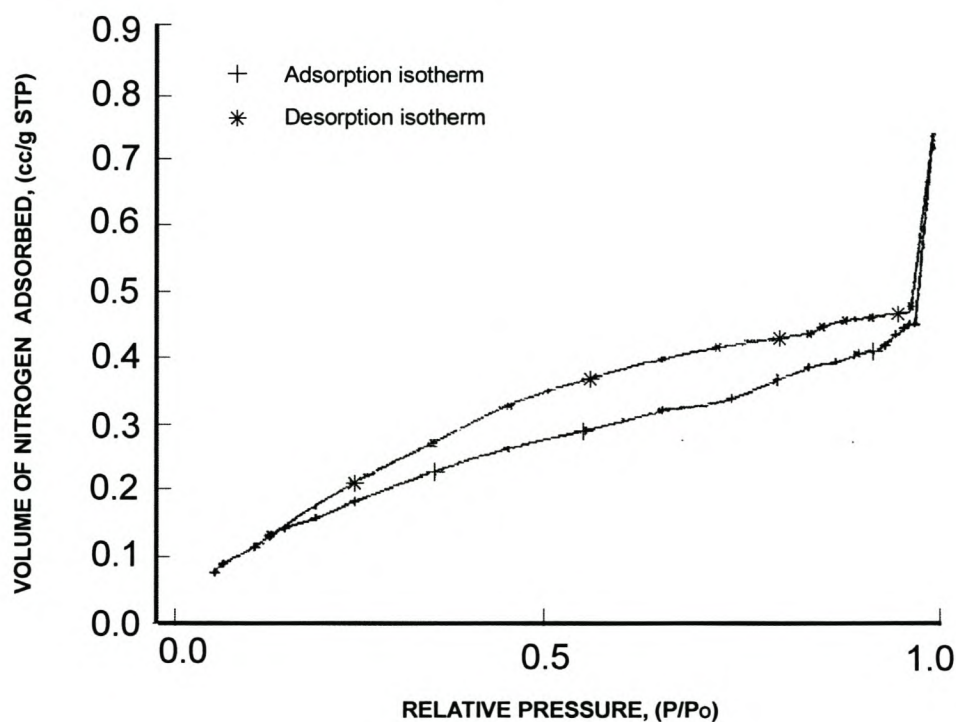


Figure 4.127. Adsorption isotherm of the adsorption (+) and desorption (*) of nitrogen gas on a hydrolysed membrane without platinum catalyst.

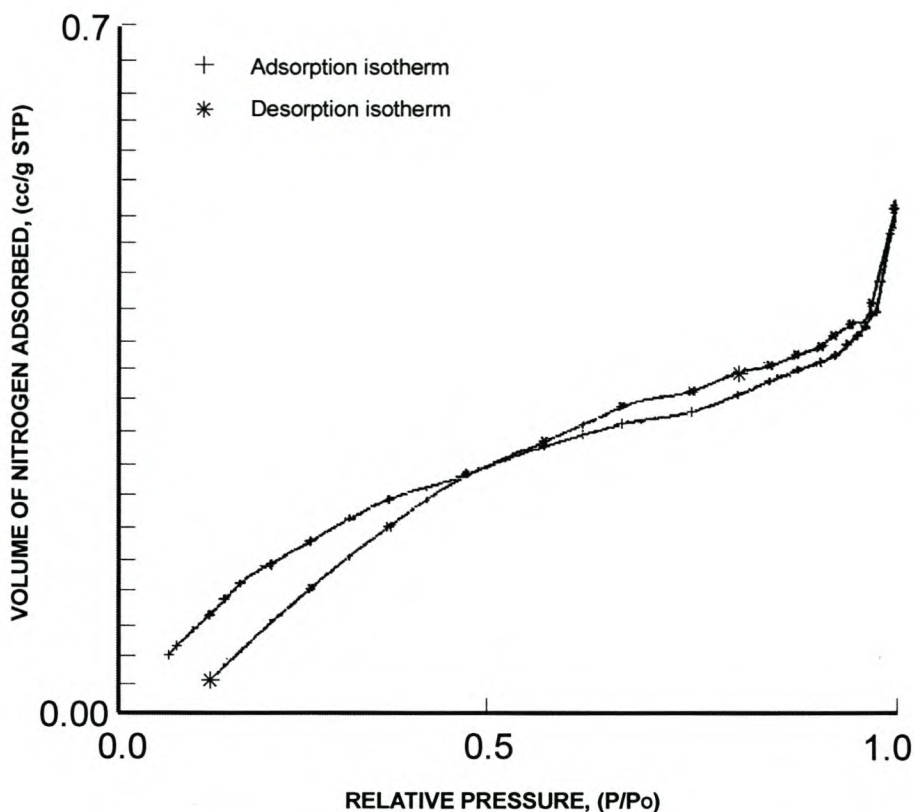


Figure 4.128. Adsorption isotherm of the adsorption (+) and desorption (*) of nitrogen gas on a pre-treated membrane embedded with platinum catalyst.

4.3.3. Final remarks

The BET results showed that membranes without platinum catalyst exhibited a surface area of 0.86 sq.m/g compared with the surface area of 1.12 sq.m/g of pre-treated membranes embedded with platinum catalyst. The BET results showed that the membrane surface area of membranes embedded with platinum catalyst was greater than for membranes without platinum catalyst (Table 4.11). The increase in surface area can be attributed to the increased surface roughness of the platinum catalyst on the membranes.

The pore volume of the membranes without platinum catalyst, determined by the amount of N_2 adsorbed by the pore of the adsorbent, was 5.6×10^{-4} cc/g. The pore volume of a pre-treated membrane embedded with platinum catalyst was 5.3×10^{-4} cc/g. The pore diameter of membranes without platinum catalyst was 34.86 Å, compared to 35.25 Å for pre-treated membranes embedded with platinum catalyst. There was no significant difference between the pore volume and pore diameter of

membranes without platinum catalyst and membranes embedded with platinum catalyst. However, characterisation techniques, such as SEM, showed that morphological differences between membranes with and without platinum catalyst do exist, although, this was not observed in the pore volume and pore diameter results of the BET analysis.

The determination of properties of catalytic systems, such as pore volume and pore diameter, are important for understanding the catalytic ability of a catalyst system. This is because in some cases the pore dimensions are important for determining the inward diffusion of reactants and the outward diffusion of products (Emmett, 1954). This study was therefore aimed at investigating the porosity of membrane catalytic systems.

Characterisation techniques, such as SEM and AFM, showed that membranes without platinum catalyst differed morphologically to membranes embedded with platinum catalyst. However, BET analysis was unable to detect any significant differences between these membranes. The results showed that BET analysis was not an effective technique for characterising membranes of this nature.

4.4. Conclusions

Since the profile of the platinum catalyst can be attributed to the parameters of the deposition process such as, concentration of platinumic acid solution, type of reducing agent and temperature of reducing agent, characterisation of platinum-containing membranes is useful in providing this information. Characterisation of platinum-containing membranes by BET provides information on the porosity, while SEM and AFM provide information on the morphology and roughness of the platinum catalyst.

AFM results verified the spherical shape of platinum particles previously reported by Fedkiw et al. (1989; 1990). AFM was used to analyse platinum-containing membranes in three-dimension for calculation of roughness and surface area variations with different deposition parameters. Inconsistencies in the results of roughness calculations for platinum-containing membranes were found. These can be attributed to the heterogeneity of membranes.

SEM results showed that the platinum loading increased with increasing time of platinisation, temperature of reducing agent and pre-treatment of membranes with a solution of water (70 vol. %) and methanol (30 vol. %). SEM results also showed that

the platinum catalyst occurred predominantly on the surface of the membrane, except with the sonication of the platinic acid solution.

BET was not effective for characterising membranes of this nature since it was unable to provide useful information on the porosity of platinum-containing membranes.

The information provided by different characterisation techniques such as, SEM, AFM and BET is important for obtaining a platinum catalyst loading on a membrane that is optimum for a cost effective and viable technology.

References

1. Adamson AW, 1990, *Physical Chemistry of Surfaces*, fifth edition, John Wiley and Sons, USA, 777 pages
2. Barrow GM, 1979, *Physical Chemistry*, fourth edition, McGraw-Hill Inc., USA, 832 pages
3. Brunauer S, 1943, *The Adsorption of Gases and Vapours*, Princeton University Press, Princeton, 511 pages
4. Emmett PH, 1954, *Catalysis*, Vol. 1 (Fundamental principles), Waverly Press inc., USA, 394 pages
5. Fedkiw PS and Her W.-H, 1989, An impregnation-reduction method to prepare electrodes on nafion SPE, *J. Electrochem. Soc.*, 136, 899
6. Fedkiw PS, Potente JM and Her W, 1990, Electroreduction of gaseous ethylene on a platinized Nafion membrane, *J. Electrochem. Soc.*, 137, 5, 1451-1460
7. Kiely JD and Bonnell DA, 1997, Quantification of topographic structure by scanning probe microscopy, *J. Vac. Sci. Technol. B*, 1483-1493
8. Russell P and Batchelor D, 2001, SEM and AFM: Complementary techniques for surface investigations, *Microscopy and Analysis*, Asia/Pacific edition, Iss 22 (July), 13-16
9. Sheppard S, Campbell SA, Smith JR, Lloyd GW, Ralph TR and Walsh FC, 1998, Electrochemical and microscopic characterisation of platinum-coated perfluorosulfonic acid (Nafion 117) materials, *Analyst*, 123, 1923-1929
10. Shu J, Grandjean BPA, Ghali E and Kaliaguine S, 1993, Simultaneous deposition of Pb and Ag on porous stainless steel by electroless plating, *Journal of Membrane Science*, 77, 181-195

Surface modification of flat sheet cation-exchange membranes

Abstract

Perfluorinated cation-exchange membranes were modified to investigate the influence of the surface modification of membranes on the process of platinum deposition. Modification of the membrane surface, profile of the platinum distribution on a modified membrane and the chemical structure of the modified membranes were investigated by means of electrical resistance measurements, Scanning Electron Microscopy (SEM), Atomic Force Microscopy (AFM) and IR spectrometry. Dielectric analysis (DEA) was used to investigate the dipole and ion mobility of membranes modified with ethylene diamine.

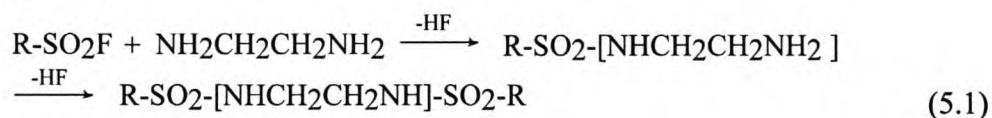
5.1. Chemical modification of the surface of a cation-exchange membrane with ethylene diamine (EDA)

The chemical modification of ion-exchange membrane surfaces is a powerful method by which to change membrane surface properties, as well as conditions and results of the electroless deposition of catalysts. These include the size, shape and distribution of catalyst particles in a membrane, membrane electrical properties, etc. Nidola et al. (1982) describes an example of the chemical surface modification of SPE membranes to improve the morphology of the catalytic layer. The modification involves coating SPE membranes with an appropriate reagent, capable of reacting both as an acid and as a base. According to Nidola et al. (1982), these amphoteric materials generally contain an amine radical as well as carboxylic or carboxamide radicals. Chemical modification of a membrane causes a change in the charge distribution of the surface of the membrane, which results in an improved metal coating structure and a stronger adhesion of the metal layer to the membrane surface (Nidola et al., 1982).

The present study investigates the effect of membrane modification on the morphology of the platinum catalyst embedded on the membrane. Chemical modification of cation-exchange membranes was one method that was used.

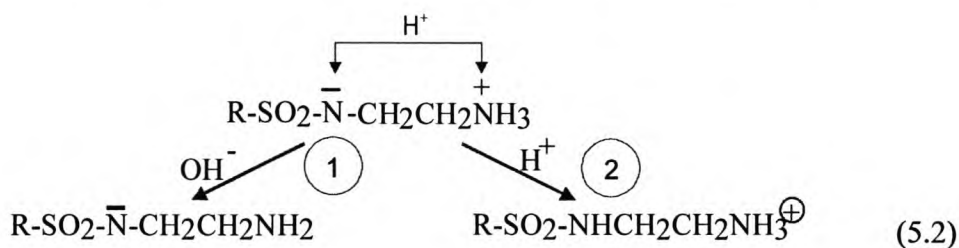
5.1.1. Modification of cation-exchange membranes with EDA

It has been reported that the low cation selectivity of standard perfluorosulfonic acid membranes can be improved by the amine modification of the sulfonyl halide form with ethylenediamine (EDA) (Hora et al., 1977). Further work describes this reaction and its effect on membrane selectivity (Grot, 1976 and 1977) The following chemical reaction describes the surface modification of perfluorinated membranes by EDA (Timashev, 1991):



where R is a general description of a perfluorinated polymeric matrix.

According to Covitch et al. (1982), the terminal amino group of the EDA sulfonamide is a good leaving group, and the zwitterionic nature of this structure promotes displacement even at the neutral pH. The zwitter ion in equation 5.2 may form various ionogenic groups, depending on whether the medium is acidic or alkaline (Timashev, 1991):



The chemical modification of perfluorinated cation-exchange membranes with EDA was studied using infrared spectrometry (IR), electrical conductivity measurements and dielectric analysis (DEA). The morphology of the platinum catalyst on the modified membranes was studied using Scanning Electron Microscopy (SEM) with a back-scattering detector and Atomic Force Microscopy (AFM).

5.1.1.1. Modification of both sides of a non-hydrolysed membrane with ethylene diamine (EDA)

Non-hydrolysed membranes were washed with ethanol to remove impurities. The membranes were treated on both sides with ethylene diamine for 0.5, 2.5, 5, 15 and 30 minutes at room temperature. The membranes were washed with 0.4N HCl to stop

modification. The membranes were washed with distilled water to remove excess HCl and EDA.

5.1.1.2. Modification of one-side of a non-hydrolysed membrane with ethylene diamine (EDA)

Non-hydrolysed membranes were washed with ethanol to remove impurities. The membranes were washed with distilled water to remove excess ethanol and then dried in a dessicator for 8 hours. The membranes were placed in a membrane holder and ethylene diamine was poured onto one-side of the membrane. The membranes were modified with 20 ml of EDA for 20 sec, 45 sec, 1 min, 1 min 25 sec, 2 min, 5 min, 10 min, 30 min, 60 min and 5 days. Membranes were then washed with HCl to stop modification. The modified membranes were washed with distilled water to remove excess HCl.

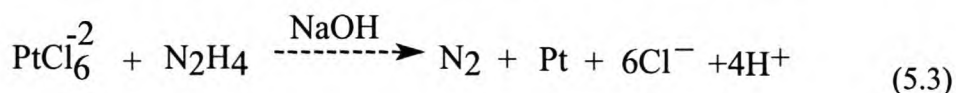
5.1.2. Deposition of platinum catalyst on membranes modified with EDA

5.1.2.1. Hydrolysis of membranes modified with EDA

The membranes that were modified on one-side and on both sides were boiled separately in a solution of 6N NaOH (70 vol. %) and methanol (30 vol. %) for 20 hours under reflux. The membranes were washed in distilled water and boiled in 0.4N HCl for 20 minutes. The membranes were washed with distilled water and boiled in distilled water for 30 minutes to remove excess HCl from the membranes.

5.1.2.2. Chemical deposition of platinum on membranes modified with EDA

The deposition of a thin layer of platinum on membranes modified with EDA was achieved by autocatalytic reduction of $[\text{PtCl}_6]^{2-}$ complex anions with hydrazine, the reducing agent. The chemical deposition of platinum was achieved by the Takenaka-Torikai method, based on the following chemical reaction (Liu et al., 1992):



5.1.2.3. Deposition of platinum on a membrane modified with EDA for 20 seconds

5ml of 0.04M platinic acid solution was poured onto a cation-exchange membrane in a membrane cell. The time of contact of the 0.04M platinic acid solution with the

membrane was 9 minutes. The platinum solution was autocatalytically reduced in a bath of hydrazine for 16 minutes at room temperature.

5.1.2.4. Deposition of platinum on a membrane modified with EDA for 45 seconds

5ml of 0.04M platonic acid solution was poured onto a cation-exchange membrane in a membrane cell. The time of contact of the 0.04M platonic acid solution with the membrane was 7.5 minutes. The platinum solution was autocatalytically reduced in a bath of hydrazine for 46.5 minutes. The concentration of the hydrazine was increased by the addition of 5g NaOH and 5g hydrazine after a total time of 34 minutes at 40 °C.

5.1.2.5. Deposition of platinum on a membrane modified with EDA for 1 minute

The concentration of the hydrazine was again increased with the addition of 5g hydrazine and 5g NaOH. 5 ml of 0.04M platonic acid solution was poured onto a cation-exchange membrane in a membrane cell. The time of contact of the 0.04M platonic acid solution with the membrane was 7 minutes. The platinum solution was autocatalytically reduced in a bath of hydrazine for 23 minutes at 40 °C.

5.1.2.6. Deposition of platinum on a membrane modified with EDA for 1 minute 25 seconds

5ml of 0.04M platonic acid solution was poured onto a cation-exchange membrane in a membrane cell. The time of contact of the 0.04M platonic acid solution with the membrane was 8.5 minutes. The concentration of the hydrazine was again increased with the addition of 5g hydrazine and 5g NaOH. The platinum solution was autocatalytically reduced in a bath of hydrazine for 31.5 minutes at a temperature of 40 °C.

5.1.2.7. Deposition of platinum on a membrane modified with EDA for 2 minutes

5ml of 0.04M platonic acid solution was poured onto a cation-exchange membrane in a membrane cell. The time of contact of the 0.04M platonic acid solution with the membrane was 14.5 minutes. The platinum solution was autocatalytically reduced in a bath of hydrazine for 41.5 minutes at a temperature of 40 °C.

5.1.3. SEM characterisation of membranes modified on one-side with EDA with an embedded platinum catalyst

Figure 5.1 shows that platinum particles penetrate deeper into the bulk of a membrane that is modified with EDA. The layer of platinum on the surface of the membrane is very thin and non-continuous. The total thickness of the layer of platinum, on the surface and within the membrane, is $\sim 8\mu\text{m}$ (Fig. 5.1). The thickness of the platinum layer on the surface of the membrane is between $0.2\text{-}0.6\mu\text{m}$. The thickness of the platinum layer within the bulk of the membrane is between $6\text{-}9\mu\text{m}$.

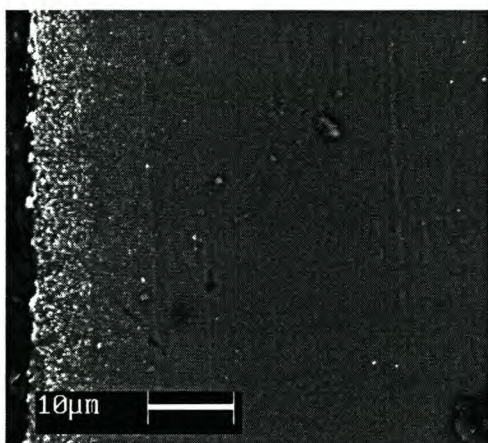


Figure 5.1. Magnified SEM image (using a backscattering detector) of a profile of a layer of platinum on a membrane modified on one-side with EDA for one minute¹.

The SEM results showed that a deeper penetration of platinum particles into the bulk of the membrane was obtained for membranes modified with EDA compared with unmodified membranes (see Section 4.2). This can be attributed to the anion-exchange properties exhibited by the membrane when modified with EDA. The anion-exchange properties of the membrane allow for easier penetration of the $[\text{PtCl}_6]^{2-}$ ions into the bulk of the membrane. Thus, the reduction of the platinumic acid by hydrazine occurs after the $[\text{PtCl}_6]^{2-}$ ions have penetrated the bulk of the membrane.

The platinum in the bulk of the modified membrane consists of small isolated particles of platinum. The presence of these isolated particles of platinum in the membrane is not ideal for catalytic processes, as electron transfer can only occur when platinum particles are interconnected (Poirier et al., 1994).

¹ 0.05M platinumic acid solution was reduced for 65 minutes by hydrazine.

5.1.4. Infra-red spectrometry characterisation of membranes modified with ethylene diamine

5.1.4.1. IR characterisation of unmodified membranes

The IR spectra of hydrolysed membranes (unmodified) exhibit an absorption band in the region of 1059 cm^{-1} . This band was not observed for non-hydrolysed membranes. The 1059 cm^{-1} absorption band is characteristic of the SO_3^- anion oscillations (Fig. 5.2) (Timashev, et al., 1991).

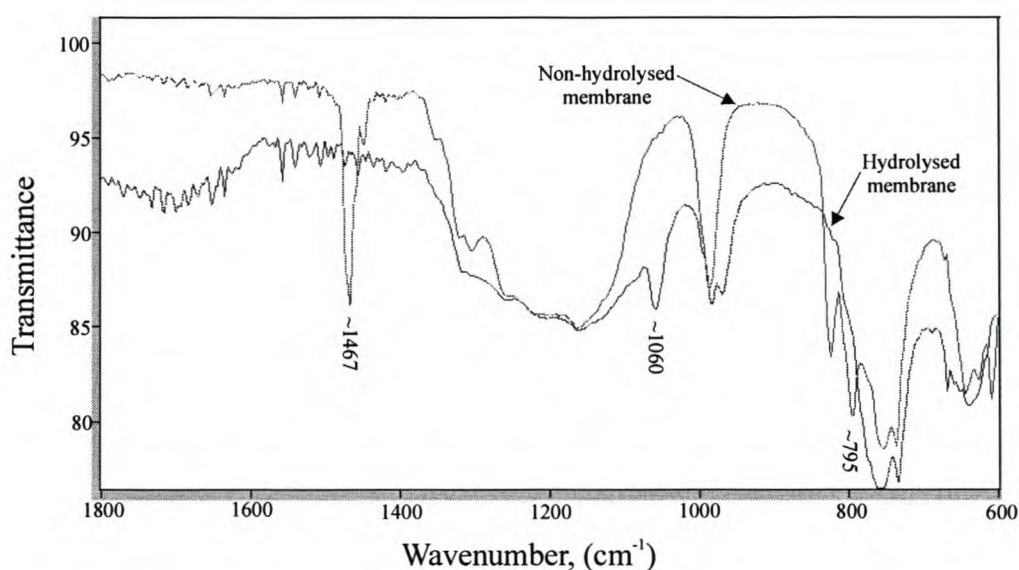


Figure 5.2. IR spectra of hydrolysed and non-hydrolysed cation-exchange membranes not modified with EDA

5.1.4.2. IR characterisation of membranes modified with EDA

Infrared spectrometry was used to investigate the chemical modification of membranes that were modified with EDA for 30 and 5 minutes. Membranes modified for 30 minutes have absorption bands in the 3164 cm^{-1} and 1376 cm^{-1} regions (Fig. 5.3). These absorption bands do not appear in the respective IR spectra of unmodified membranes (Fig. 5.2). The absorption band in the 3164 cm^{-1} region is small and broad, while the absorption band in the 1376 cm^{-1} region is small and sharp (Fig 5.3).

Membranes modified for 5 minutes have absorption bands in the 1376 cm^{-1} region, which do not appear in the respective IR spectra of unmodified membranes (Fig. 5.3). The absorption band in the 1376 cm^{-1} region of membranes modified for 30 minutes is larger and broader than the corresponding absorption band of membranes modified for 5 minutes. Also, membranes modified for 5 minutes do not exhibit an

absorption band in the 3164 cm^{-1} region as membranes modified for 30 minutes. This can be attributed to the greater modification that occurs when membranes are modified for 30 minutes as compared to 5 minutes.

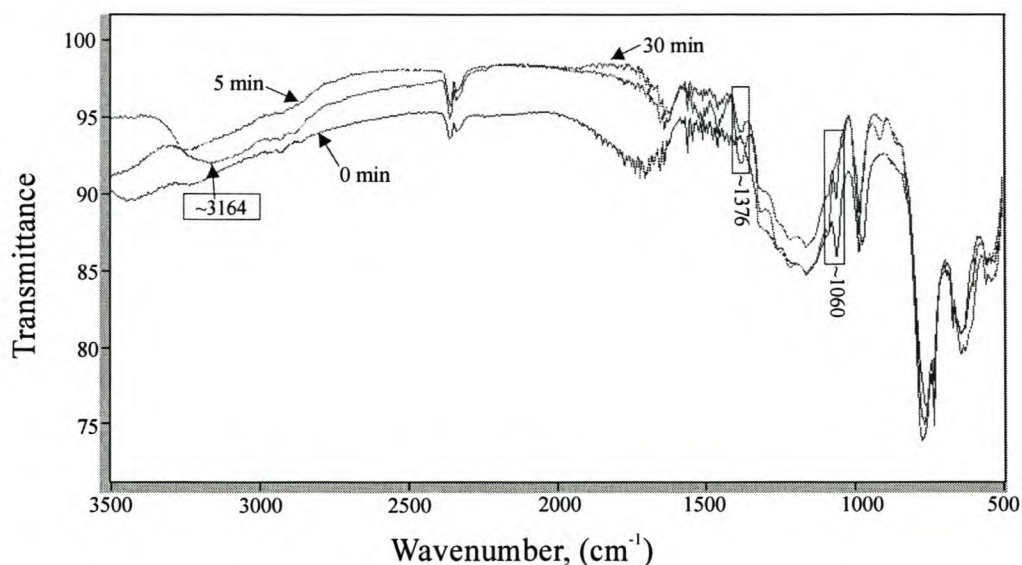


Figure 5.3. IR spectra of EDA-modified (5 min and 30 min) and unmodified (0 min) hydrolysed membranes

5.1.4.3. IR characterisation of membranes modified with EDA for 5 days

Membranes that were modified with EDA for 5 days (in Na^+ -ionic and H^+ -ionic form) exhibits broad bands in $\approx 3176\text{ cm}^{-1}$ and $\approx 3025\text{ cm}^{-1}$ regions. The stretching frequencies of these broad bands correspond to the stretching frequencies of aminium ions (NH_3^+), which occur in the region of $3135 \pm 105\text{ cm}^{-1}$ (Roeges, 1994). EDA-modified membranes also exhibit absorption bands in the 1376 cm^{-1} , 1610 cm^{-1} , 1504 cm^{-1} and 1051 cm^{-1} regions (Fig. 5.4). The absorption band in the 1376 cm^{-1} region corresponds to the antisymmetric deformations that occur in the $1300 \pm 70\text{ cm}^{-1}$ region (Roeges, 1994). The absorption band in the region of 1610 cm^{-1} corresponds to the antisymmetrical in-plane deformation of NH_3^+ that occurs in the $1610 \pm 25\text{ cm}^{-1}$ region (Roeges, 1994). The absorption band in the 1504 cm^{-1} region corresponds to the symmetrical in-plane deformation of NH_3^+ that occurs in the $1505 \pm 25\text{ cm}^{-1}$ region (Roeges, 1994). The absorption band in the 1051 cm^{-1} region corresponds to the SO_3^- oscillations that occur in $\approx 1060\text{ cm}^{-1}$ region for hydrolysed membranes (Roeges, 1994).

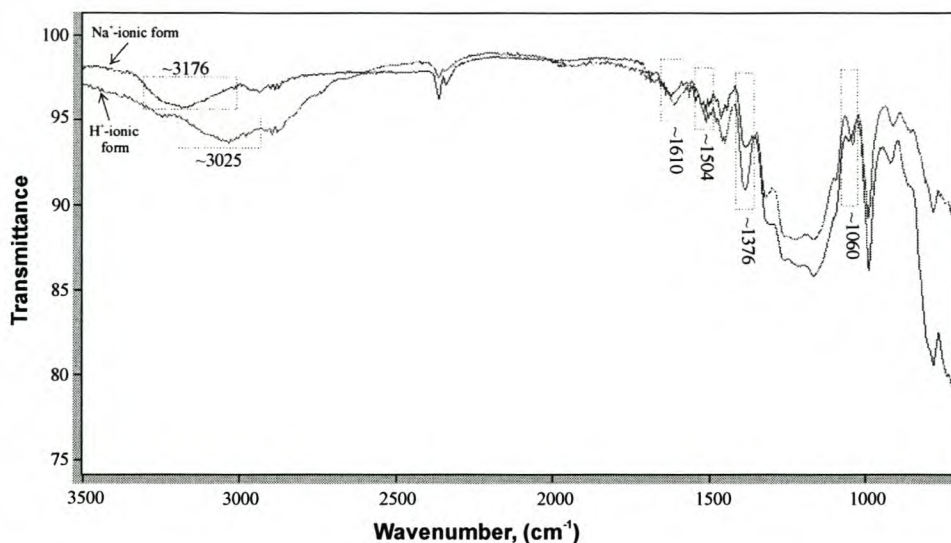
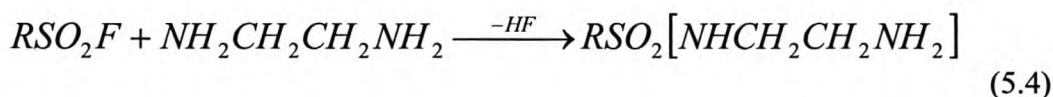


Figure 5.4. IR spectra of membranes modified for 5 days with EDA in the Na^+ -ionic form and the H^+ -ionic form

5.1.4.4. Discussion

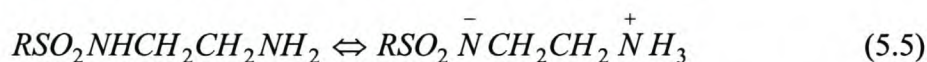
The IR spectra of membranes modified with EDA were investigated with the assumption that the perfluorinated membranes modified with ethylene diamine resulted in the following reaction (Timashev, 1991):



In aliphatic and alicyclic primary amines, the NH_2 anti-symmetric stretching vibrations occur in the region of $3365 \pm 25 \text{ cm}^{-1}$ (Roeges, 1994). The scissoring vibration gives rise to a broad strong band in the region of $1600 \pm 50 \text{ cm}^{-1}$ (Roeges, 1994). Associated α -saturated primary amines show a characteristic broad band between 1000 cm^{-1} and 700 cm^{-1} (Roeges, 1994). The NH stretching vibration in secondary sulfonamides is observed in the region of $3270 \pm 65 \text{ cm}^{-1}$ (Roeges, 1994).

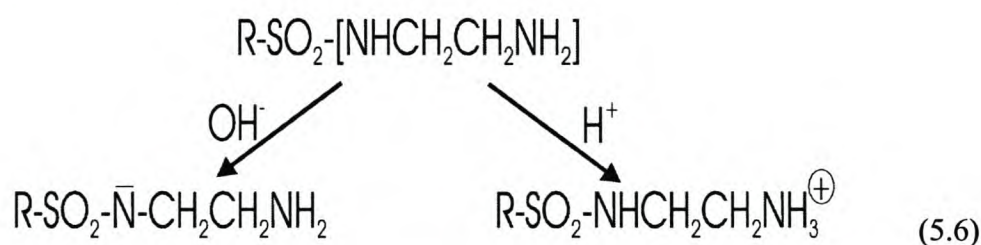
The formation of amino groups was expected in membranes modified with ethylene diamine. However, none of the above vibrations characteristic of amino groups were present in the IR spectra of membranes modified with EDA. The absence of amino groups can be explained by the formation of aminium ion groups (NH_3^+) (Covitch et al., 1982). The formation of aminium ions (NH_3^+) occurs because the

terminal amino group of the EDA sulfanamide is a good leaving group. The zwitterionic nature of the EDA sulfanamide promotes displacement at neutral pH, which leads to the protonation of amino groups (Covitch et al., 1982).



The stretching frequencies of NH_3^+ occur in the region $3350\text{-}3150\text{ cm}^{-1}$ (Roeges, 1994). The NH_3^+ antisymmetric deformations occur in the region $1700\text{-}1200\text{ cm}^{-1}$ (Roeges, 1994). These stretching frequencies for NH_3^+ correspond to our results obtained for EDA-modified membranes. In Figure 5.3 the stretching frequencies of NH_3^+ occur in the region of $\sim 3164\text{ cm}^{-1}$ and the antisymmetric deformations occur in the region of $\sim 1376\text{ cm}^{-1}$.

Membranes modified with EDA for 5 days, which were in the H^+ -ionic form and Na^+ -ionic form, exhibit absorption bands in $\sim 1376\text{ cm}^{-1}$, $\sim 1610\text{ cm}^{-1}$, $\sim 1504\text{ cm}^{-1}$ and $\sim 3025\text{ cm}^{-1}$ regions. These correspond to the stretching frequencies for NH_3^+ . These results show that the protonation of amino groups occurs in the presence and absence of protons (Reaction 5.5). However, the presence of excess protons results in the increased formation of aminium ions (NH_3^+) through the protonation of amino groups (Reaction 5.6) (Timashev, 1991).



This can be concluded because the absorption bands in the $\sim 1376\text{ cm}^{-1}$, $\sim 1610\text{ cm}^{-1}$ and $\sim 1504\text{ cm}^{-1}$ regions of the IR spectra of the membranes modified with EDA in the H^+ -ionic form are larger than the absorption bands of the membranes modified with EDA in the Na^+ -ionic form.

Thus, characterisation of the membranes by IR analysis verified the chemical surface modification of membranes with EDA.

5.1.5. Characterisation of membranes modified with EDA by dielectric analysis

Dielectric analysis (DEA) is a widely used technique for the characterisation of polymers. Dielectric analysis is the study of the mobility of ions and dipoles in a material. The physical and chemical structure of polymers and other organic materials can be investigated by the measurement of their dielectric properties. Analysis of dielectric properties was determined with the Micromet Instruments Eumetric system III Microdielectrometer (DEA).

5.1.5.1. $\tan \delta$ of a membrane modified with EDA

$\tan \delta$ is used to characterise molecular relaxations and identify rheological transformations. $\tan \delta$ is dependent on the inverse of the storage modulus. The storage modulus is high when molecular mobility is restricted. A high storage modulus results in the lowering of $\tan \delta$. In Fig. 5.5 it can be seen that the $\tan \delta$ decreases as the time of treatment of the membrane with EDA is increased. The membrane modified with EDA for 60 minutes has the lowest $\tan \delta$ (Fig. 5.5).

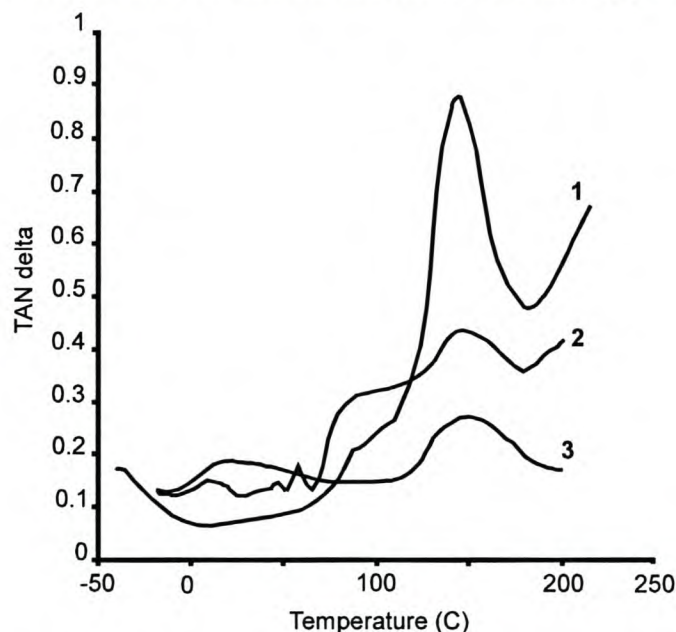


Figure 5.5. Dependence of the $\tan \delta$ upon temperature at frequency of 100 kHz for membranes modified with EDA on one side for 1, 5 and 60 minutes (curves 1, 2 and 3 respectively).

5.1.5.2. Loss factor at frequency of 60 Hz for membranes modified on one-side with EDA

A formulation of the loss factor at low frequencies can be represented as follows:

$$\epsilon = \epsilon_{\text{dipole}} + \sigma/\omega\epsilon_0 \quad (5.7)$$

ϵ = loss factor

ϵ_{dipole} = energy loss in aligning dipoles

σ = bulk ionic conductivity (Ω/cm)

ω = angular frequency (rad/sec)

ϵ_0 = permittivity of free space

At low frequencies, the conductivity term is dominant. When the conductivity is low in relation to the dipole term, the loss factor can be used to identify molecular relaxations. The mobility of molecules within an EDA-treated membrane increases with the increase in temperature. The mobility of the molecules within a membrane at increasing temperature is dependent on the degree of EDA treatment of the membrane (Fig. 5.6, curves 2-4).

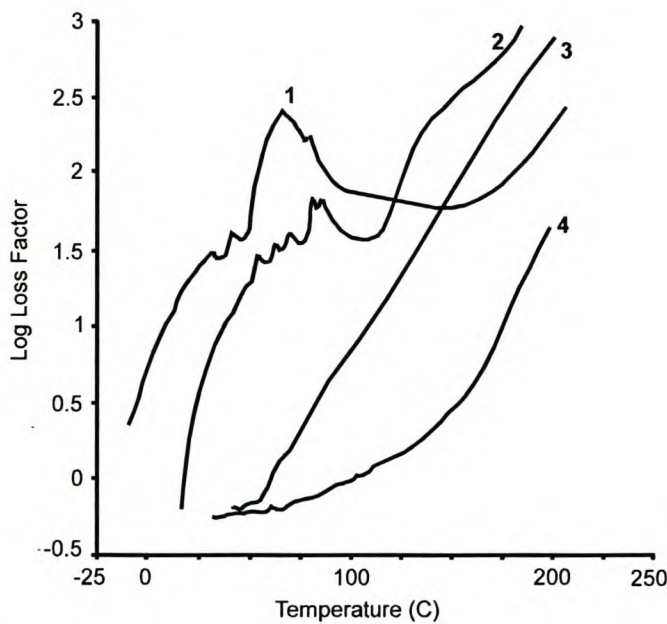


Figure 5.6. Dependence of the loss factor upon temperature at frequency of 60 Hz for membranes exposed to EDA treatment for various times: no treatment (curve 1), 1 minute (curve 2), 5 minutes (curve 3) and 60 minutes (curve 4) of treatment.

5.1.5.3. DEA of the loss factor at high frequency of 100 kHz for membranes modified on one-side with EDA

At high frequencies the dipole term becomes dominant in the loss factor (equation 5.7). The energy loss for aligning dipoles is high when there are no restrictions to

molecular mobility for aligning dipoles to the applied electric field. Thus, a high loss factor is due to a high dipole term (equation 5.7). Figure 5.7 shows that the loss factor decreases with an increase in the time of treatment of the membrane with EDA at high frequencies.

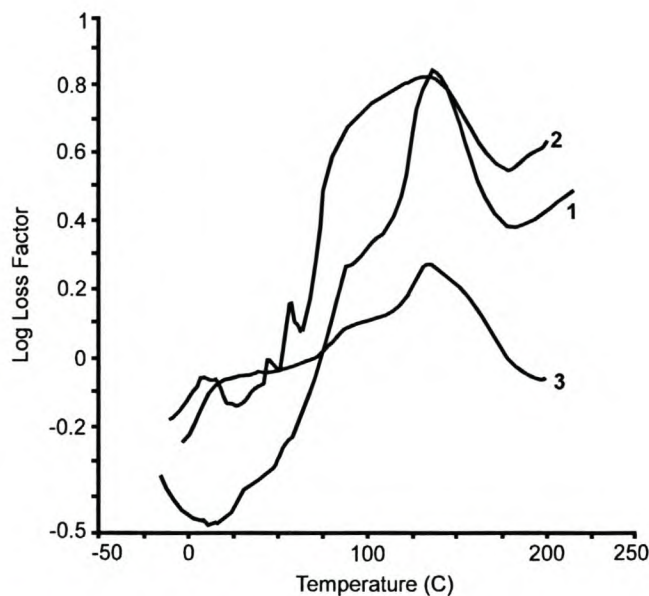


Figure 5.7. Dependence of the loss factor upon temperature at frequency of 100 kHz for membranes modified on one side for 1 minute with EDA (curve 1), for 5 minutes (curve 2) and for 60 minutes (curve 3).

5.1.5.4. Discussion

The DEA results show that an increase in the modification of the membrane with EDA results in a decrease in $\tan \delta$. This can be attributed to the large molecular groups of the modified membrane, which hinder mobility. The decrease in mobility results in the decrease of $\tan \delta$ (Fig. 5.5)

An increase in the treatment time with EDA results in greater restrictions for aligning dipoles due to the steric hindrance of large molecular groups. The dipole factor in these cases will be low, which will result in a low loss factor at a high frequency of 100 kHz (Fig. 5.7).

Dielectric analysis provides further information on the mobility of ions and dipoles of modified membranes. The DEA results show that the mobility of ions and dipoles decrease with the increase in modification of membranes with EDA.

5.1.6. Resistance measurements of cation-exchange membranes modified with EDA

5.1.6.1. Electromembrane cell for resistance measurements of membranes modified with EDA

The degree of modification of membranes with EDA was determined by measuring the conductivities of the modified membranes in a 0.01N aqueous NaCl solution within a two-compartment cell, consisting of platinum electrodes (Fig. 5.8). The resistance of the membranes was determined by measuring the conductivity of the membranes modified with EDA using a Radiometer conductivity meter CDM 83 for the membrane area of 0.28 cm².

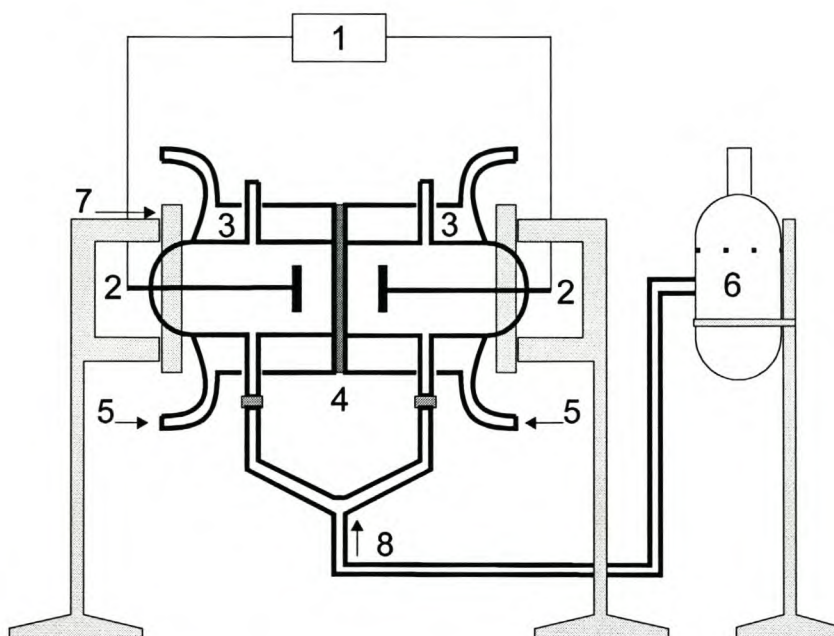


Figure 5.8. Schematic representation of a two-compartment cell used to measure resistance of cation-exchange membranes modified with EDA. 1-conductivity meter, 2-Pt electrodes, 3-water jacket for thermal stability, 4-membrane, 5-inlet for water from thermostat, 6-vessel with NaCl solution, 7-O-rings, 8-inlet for NaCl solution.

5.1.6.2. Characterisation of membranes modified with EDA by resistance measurements

The resistance (R) of the modified membranes were calculated using the following equations:

$$R_{\text{membrane}} = R_{\text{solution and membrane}} - R_{\text{solution}}$$

$$R_{\text{solution}} = k / \lambda_{\text{solution}}$$

$$R_{\text{solution and membrane}} = k / \lambda_{\text{solution and membrane}}$$

where,

$$k \text{ (cell constant) (cm}^{-1}\text{)} = 1.099\text{cm}^{-1}$$

$\lambda_{\text{solution and membrane}}$ = specific conductivity of the NaCl solution and membrane (mScm^{-1})

$\lambda_{\text{solution}}$ = specific conductivity of the NaCl solution (mScm^{-1})

The total specific resistance of a membrane can be represented as follows:

$$\rho = R_{\text{membrane}} \times S \times h^{-1}$$

where,

ρ = total specific resistance ($\Omega\cdot\text{cm}$)

S = membrane area (cm^2)

h = thickness of membrane (cm)

The resistance of membranes treated for 0, 20, 45, 60, 85, 125, 300 and 600 seconds with EDA were measured after the modified membranes were equilibrated at pH=9 with 0.1N NaCl. The resistance of the membranes treated with EDA was determined with the above equations and the results are tabulated in Table 5.1. The conductivity of the 0.1N NaCl solution at pH=9 was 10.40mScm^{-1} and the resistance was determined as 105.67Ω .

Table 5.1. Results of the resistance measurements of membranes modified with EDA for 0, 20, 45, 60, 85, 125, 300 and 600 seconds, which were equilibrated at pH=9

Time of treatment with EDA (sec)	$\lambda_{\text{solution and membrane}}$ (mScm ⁻¹)	$R_{\text{solution and membrane}}$ (Ω)	R_{membrane} (Ω)	log R_m
0	10.21	107.63	1.96	0.29
20	9.97	110.23	4.56	0.66
45	9.02	121.84	16.17	1.21
60	8.19	134.19	28.52	1.46
85	5.94	185.02	79.35	1.90
125	4.22	260.42	154.75	2.19
300	1.59	691.19	585.52	2.77
600	0.64	1717.19	1611.52	3.21

The resistance of membranes treated for 0, 20, 45, 60, 85, 125, 300 and 600 seconds with EDA were measured after membranes were equilibrated at pH=6 with 0.1N NaCl. The resistance of the modified membranes equilibrated at pH=6 was determined as in Table 5.1 and the results are tabulated in Table 5.2. The conductivity of the 0.1N NaCl solution at pH=6 was 10.29mScm⁻¹.

Table 5.2. Results of resistance measurements of membranes modified with EDA for 0, 20, 45, 60, 85, 125, 300 and 600 seconds, which were equilibrated at pH=6

Time of treatment with EDA (sec)	R_{membrane} (Ω)	log R_m
0	2.27	0.36
20	8.36	0.92
45	24.47	1.38
60	50.41	1.70
85	127.20	2.10
125	157.90	2.20
300	608.0	2.78
600	4149.0	3.61

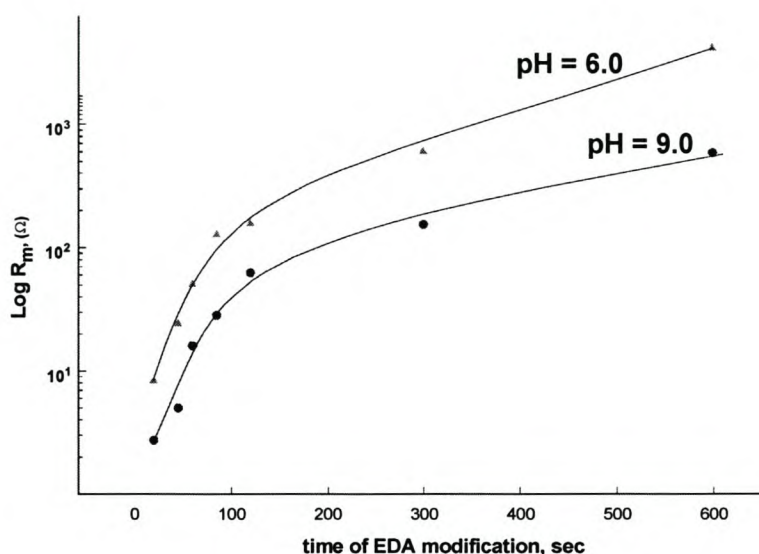


Figure 5.9. Dependence of membrane resistance (R_m) on the time of treatment of one-side of the membrane with EDA. Membranes were equilibrated with 0.1N NaCl solution at pH=6.0 and pH=9.0.

Membranes modified with EDA and equilibrated in an alkaline medium of pH=9 have less protons available for the protonation of NH_2 groups. The resistance of membranes equilibrated at pH=9 will therefore be lower than membranes equilibrated at pH=6.

Similar results were obtained for resistance measurements of membranes treated with EDA for longer time periods (Fig. 5.10). There was a gradual increase in the resistance of membranes with increasing time of EDA treatment. The resistance of membranes modified with EDA reached a plateau after 60 minutes. No significant changes in membrane resistance were observed after 60 minutes. It can therefore be deduced that complete modification of membranes is achieved after 60 minutes of treatment with EDA.

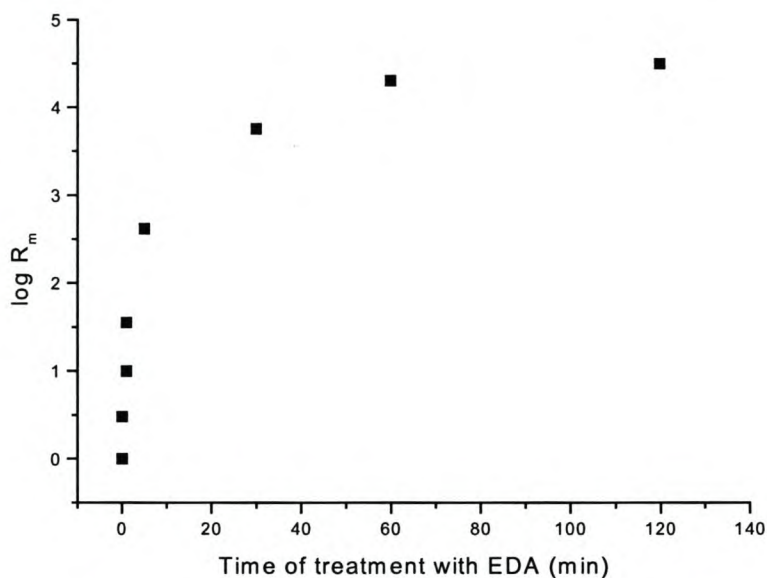


Figure 5.10. *Dependence of membrane resistance on the time of treatment of the membrane with EDA*

5.1.7. The sorption of water by cation-exchange membranes modified with ethylene diamine

5.1.7.1. Preparation of membranes modified with ethylene diamine

A hydrolysed membrane was boiled in 1N HCl to convert the membrane to the H⁺-ionic form. Another hydrolysed membrane was modified by ethylene diamine for 5 days. The membrane modified with EDA was then washed with distilled water. The membranes were placed in a desiccator to dry for 4 days. The membranes were then weighed and their masses recorded. The membranes were placed in distilled water for 3 days, dried with filter paper and weighed. The membrane modified with EDA was placed in a vacuum oven at 140°C for 5 hours and then cooled in a desiccator. The membrane was weighed and the mass recorded. The membrane was then placed in distilled water for 5 days, dried with filter paper and weighed.

5.1.7.2. Results of the sorption of water by modified membranes

The results of the water sorption for a membrane in H⁺-ionic form, EDA-modified membrane and EDA-modified membrane that underwent heat treatment, is tabulated in Table 5.3.

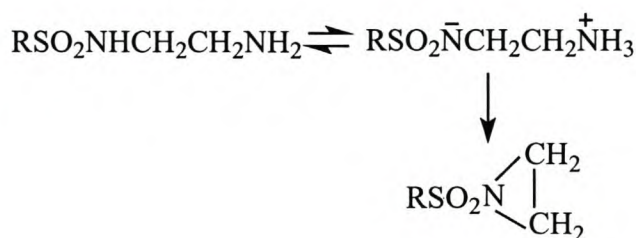
Table 5.3. Results of water sorption for a membrane in the H⁺-ionic form, EDA-modified membrane and EDA-modified membrane that underwent heat treatment

Membrane treatment	Mass of water sorption (g)	H ₂ O uptake per 1g of membrane (g)
H ⁺ -ionic form	0.0298	0.21
Modified with EDA	0.0343	0.05
Modified with EDA and then heat treatment	0.0149	0.025

The results show that membranes in the H⁺-ionic form absorb a greater amount of water per gram of membrane as compared to membranes modified with EDA. The water uptake per gram of membrane decreased by 50% for EDA-modified membranes that were heat-treated.

5.1.7.3. Discussion

The sorption of water per gram of membrane is directly related to the ion transport within the channels of the membrane. The sorption of water by membranes modified with EDA that underwent heat treatment was lower compared to modified membranes that were not heat-treated. This is attributed to the crosslinking of the difunctional amine with the heat treatment of EDA-modified membranes (Covitch et al., 1982).



The formation of these crosslinks within the channels of the membrane hinders ion transport and the sorption of water, which can explain the lower sorption of water per gram of membrane.

bipolar membrane technology. Although bipolar membrane technology is an emerging technology, these membranes are already being used on an industrial scale (Franken, 2000).

5.2. Development of unique textured platinum particles by modification of the surface of the membrane

The ability to synthesise materials with controlled textured platinum electrodes has led to new fields of study in Chemistry and Materials Science. This technology makes it possible to control the morphology (structure, size, etc.) of catalyst particles by the use of surfactant aggregates.

An example of the use of surfactant aggregates is the preparation of a structured platinum catalyst by allowing a ternary mixture of surfactant, water and hydrazine hydrate to make contact with a system containing ammonium tetrachloroplatinate (Attard, 1997).

This study involved the modification of perfluorinated cation-exchange membranes by cetyltrimethylammonium bromide ($\text{CH}_3(\text{CH}_2)_{15}\text{N}(\text{CH}_3)_3\text{Br}$) surfactant and deposition of a platinum catalyst onto the modified membranes by means of the Takenaka-Torikai method. The chemical interaction between the ionic surfactant and membrane was studied by infrared spectrometry (IR) and electrical resistance measurements. The morphology of the platinum embedded on membranes treated with surfactant was investigated by Atomic Force Microscopy (AFM).

5.2.1. Surface modification of flat-sheet cation-exchange membranes with surfactant

Non-hydrolysed membranes were hydrolysed with 6N aqueous NaOH for 20 hours under reflux conditions. One side of each hydrolysed membrane sample was in contact with an aqueous 1 wt. % solution of $\text{CH}_3(\text{CH}_2)_{15}\text{N}(\text{CH}_3)_3$ surfactant for 2 minutes at a temperature of 70 °C. The membranes were then washed with distilled water to remove excess surfactant.

5.2.2. Chemical deposition of platinum catalyst onto cation exchange membranes modified with surfactant

The deposition of platinum onto the surfactant-treated membranes was achieved by the autocatalytic reduction of $[\text{PtCl}_6]^{2-}$ complex anions with hydrazine as a reducing agent (Takenaka-Torikai method). 5ml 0.05M platinic acid solution was poured onto a cation-exchange membrane modified with surfactant. The time of contact of 0.05M platinic acid solution with the membrane was 1 minute. The platinic acid solution was autocatalytically reduced in a bath of hydrazine for 50 minutes at a temperature of 40 °C.

5.2.3. Characterisation of platinum catalyst deposited on surfactant-treated membranes by Atomic Force Microscopy (AFM)

5.2.3.1. AFM imaging of platinum particles on the surface of a membrane modified with 1% $\text{CH}_3(\text{CH}_2)_{15}\text{N}(\text{CH}_3)_3\text{Br}$ surfactant

Figures 5.11 and 5.12 are two-dimensional and three-dimensional surface images ($5\mu\text{m}\times 5\mu\text{m}$) of platinum catalyst embedded on membranes treated with 1% $\text{CH}_3(\text{CH}_2)_{15}\text{N}(\text{CH}_3)_3\text{Br}$ surfactant. The platinum catalyst was deposited onto surfactant-treated membranes by the Takenaka-Torikai method.

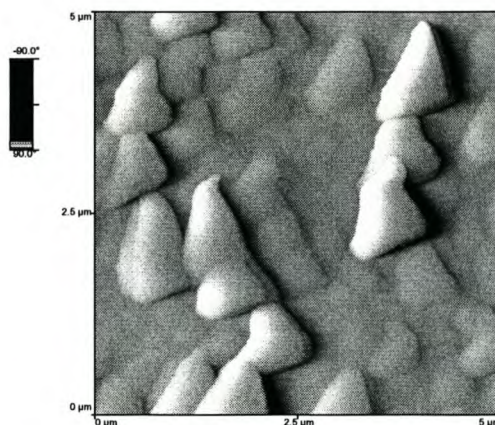


Figure 5.11. AFM surface image ($5\mu\text{m}\times 5\mu\text{m}$) of platinum catalyst embedded on a cation-exchange membrane that was treated with 1% $\text{CH}_3(\text{CH}_2)_{15}\text{N}(\text{CH}_3)_3\text{Br}$ surfactant

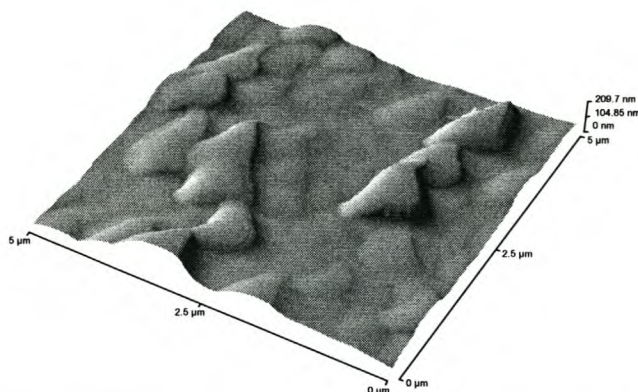


Figure 5.12. Three-dimensional AFM surface image ($5\mu\text{m}\times 5\mu\text{m}$) of platinum catalyst embedded on a cation-exchange membrane that was treated with 1% $\text{CH}_3(\text{CH}_2)_{15}\text{N}(\text{CH}_3)_3\text{Br}$ surfactant

The platinum catalyst embedded on the surfactant-treated membranes consisted of small pyramidal-like platinum particles protruding outwards from the membrane surface. The surface profile of the platinum catalyst deposited onto the surfactant-treated membranes can be seen from the line analysis plot (Fig.5.13).

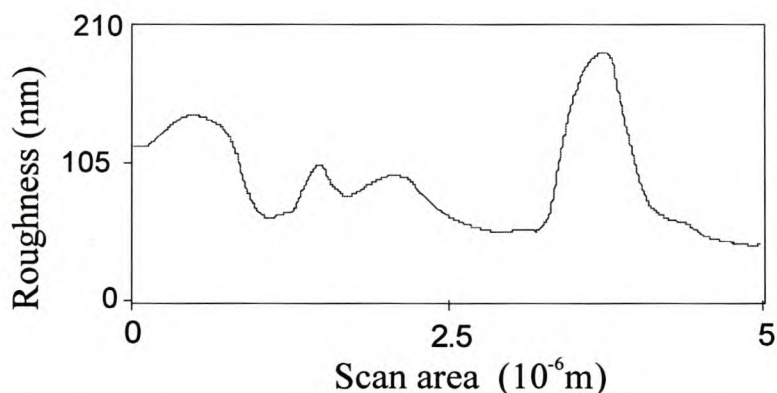


Figure 5.13. Line analysis of the surface profile of the platinum catalyst embedded on a cation-exchange membrane that was treated with 1% $\text{CH}_3(\text{CH}_2)_{15}\text{N}(\text{CH}_3)_3\text{Br}$ surfactant

Figures 5.14 and 5.15 are two-dimensional and three-dimensional surface images ($10\mu\text{m}\times 10\mu\text{m}$) of platinum catalyst particles embedded on membranes treated with 1% $\text{CH}_3(\text{CH}_2)_{15}\text{N}(\text{CH}_3)_3\text{Br}$ surfactant. The pyramidal-shaped platinum particles are unevenly distributed within the platinum deposition. The surface profile of the platinum catalyst deposited onto the surfactant-treated membranes can be seen from the line analysis plot (Fig. 5.16).

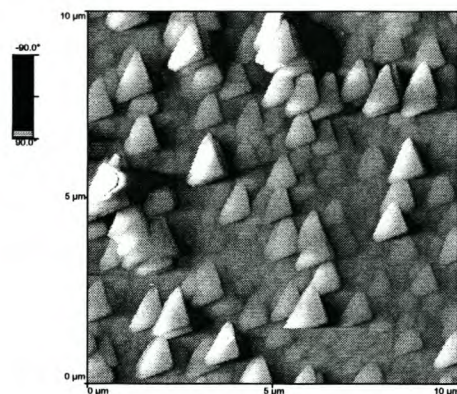


Figure 5.14. AFM surface image (10 μm x 10 μm) of platinum catalyst embedded on a cation-exchange membrane that was treated with 1% $\text{CH}_3(\text{CH}_2)_{15}\text{N}(\text{CH}_3)_3\text{Br}$ surfactant

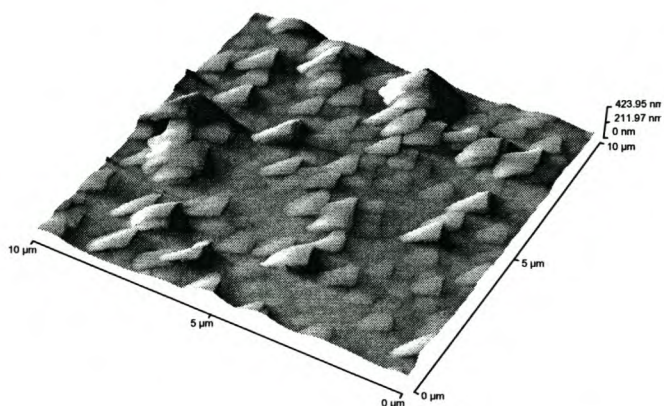


Figure 5.15. Three-dimensional AFM surface image (10 μm x 10 μm) of platinum catalyst embedded on a cation-exchange membrane that was treated with 1% $\text{CH}_3(\text{CH}_2)_{15}\text{N}(\text{CH}_3)_3\text{Br}$ surfactant

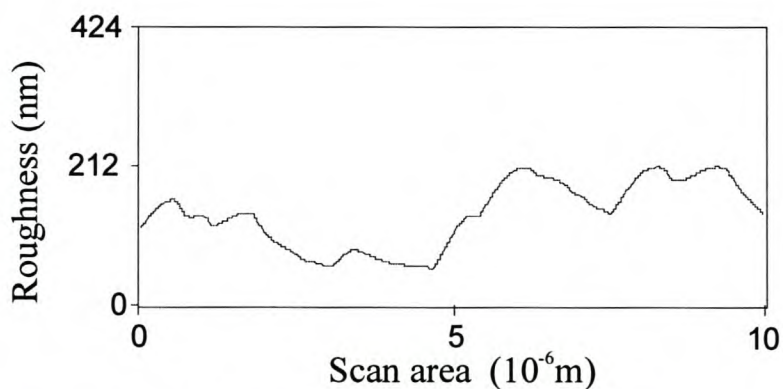


Figure 5.16. Line analysis of the surface profile of the platinum catalyst embedded on a cation-exchange membrane that was treated with 1% $\text{CH}_3(\text{CH}_2)_{15}\text{N}(\text{CH}_3)_3\text{Br}$ surfactant

Figures 5.17 and 5.18 are two-dimensional and three-dimensional surface images ($20\mu\text{m}\times 20\mu\text{m}$) of platinum catalyst embedded on a surfactant-treated membrane. The platinum catalyst appears rough, with pyramidal-like platinum particles protruding outwards from the membrane surface. The surface profile of the platinum catalyst on the surfactant-treated membrane can be seen from the line analysis (Fig. 5.19).

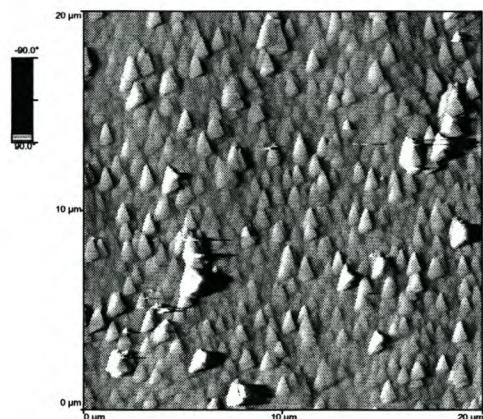


Figure 5.17. *AFM surface image ($20\mu\text{m}\times 20\mu\text{m}$) of platinum catalyst embedded on a cation-exchange membrane that was treated with 1% $\text{CH}_3(\text{CH}_2)_{15}\text{N}(\text{CH}_3)_3\text{Br}$ surfactant*

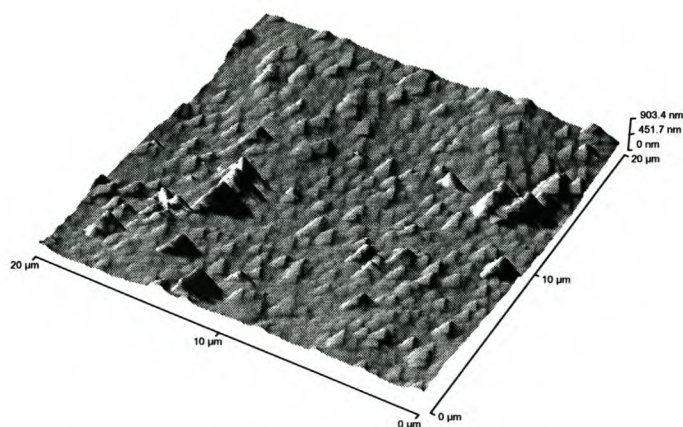


Figure 5.18. *Three-dimensional AFM surface image ($20\mu\text{m}\times 20\mu\text{m}$) of platinum catalyst embedded on a cation-exchange membrane that was treated with 1% $\text{CH}_3(\text{CH}_2)_{15}\text{N}(\text{CH}_3)_3\text{Br}$ surfactant*

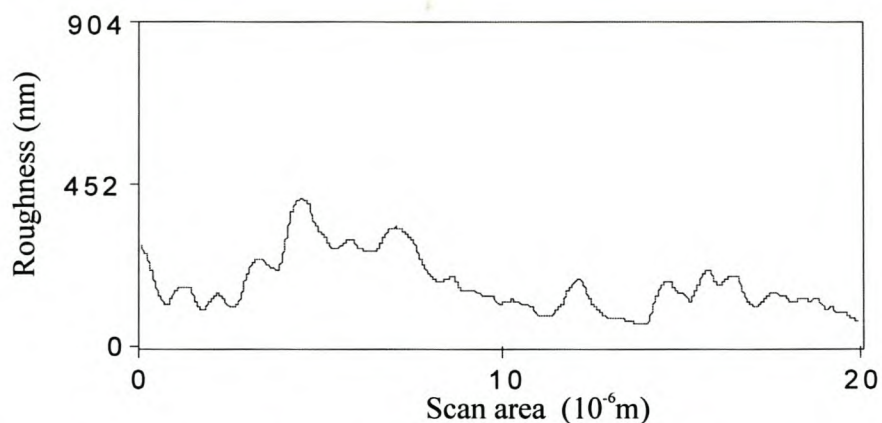


Figure 5.19. Line analysis of the surface profile of the platinum catalyst embedded on a cation-exchange membrane that was treated with 1% $\text{CH}_3(\text{CH}_2)_{15}\text{N}(\text{CH}_3)_3\text{Br}$ surfactant

5.2.3.2. Discussion

The platinum catalyst on surfactant-treated membranes consisted of pyramidal-like particles distributed throughout the surfactant-treated membrane surface. The layer of platinum on the membrane appears uniform with pyramidal-like platinum particles protruding outwards from the membrane surface (Bessarabov et al., 2001). This regular structure of the platinum particles could be attributed to the lyotropic phase of the surfactant-polyelectrolyte structure, which acts as a structure-forming medium during the deposition process (Attard et al., 1997). However, the change in the shape of the platinum catalyst particles could also be attributed to a low transfer rate of the hydrazine solution through a membrane as a result of the modification of membranes with surfactant.

5.2.4. Characterisation of the modification of membranes with surfactant by infrared spectrometry

5.2.4.1. Preparation of cation-exchange membranes for modification with surfactant

Hydrolysed cation-exchange membranes were boiled in 1N HCl to convert membranes to the H⁺-ionic form. The hydrolysed membranes were placed in a 20% CH₃(CH₂)₁₅N(CH₃)₃Br surfactant solution for 24 hours. The membranes that were modified with surfactant were washed with distilled water, dried and then characterised by IR spectrometry.

5.2.4.2. Removal of surfactant from modified membranes with base solution by ion-exchange

Modified membranes were placed in 6N NaOH for 48 hours. Some modified membranes were boiled in 6N NaOH for 5 hours. Modified membranes were also boiled in 3N NaCl for 5 hours. The membranes were washed with distilled water, dried and characterised by IR spectrometry.

5.2.4.3. Removal of surfactant from modified membranes with acid solution by ion-exchange

Modified membranes were boiled in separate solutions of 5% HNO₃, 30% HNO₃ and 50% HNO₃ for 5 hours. The membranes were washed with distilled water to remove excess HNO₃, dried and characterised by IR spectrometry.

5.2.4.4. Characterisation of membranes modified with surfactant by IR spectrometry

The absorption band that is characteristic of the SO₃⁻ anion oscillations appears in the region of 1051 cm⁻¹ in the IR spectra of hydrolysed modified and hydrolysed unmodified membranes (Fig. 5.20) (Timashev et al., 1991). The structural interaction of membranes with surfactant results in absorption bands occurring at ~2929 cm⁻¹ and ~2855 cm⁻¹, which correspond to antisymmetric stretching vibrations in the 2929 cm⁻¹ region and symmetric stretching vibrations in the 2855 cm⁻¹ region for nitrogen-methyl interaction (Roeges, 1994).

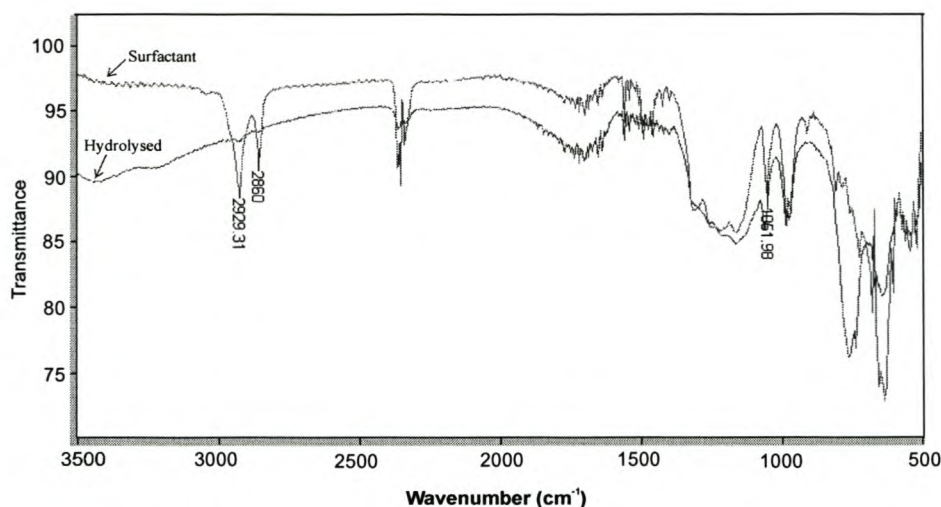


Figure 5.20. IR spectra of unmodified and surfactant-modified hydrolysed membranes

5.2.4.5. IR spectrometry of the removal of surfactant from modified membranes with sodium hydroxide by ion-exchange

The structural interaction of membranes with surfactant is verified by the occurrence of absorption bands at 2929 cm^{-1} and 2855 cm^{-1} (Roeges, 1994). The removal of the surfactant from the modified membranes by sodium hydroxide can be seen from the decrease in size of the absorption bands characteristic for surfactant-membrane interaction (Fig. 5.21). The absorption bands that are characteristic of surfactant-membrane interaction decrease in size with the treatment of modified membranes with NaOH. Absorption bands that are characteristic of surfactant-membrane interaction are smaller for modified membranes boiled in 6N NaOH for 5 hours compared to modified membranes placed in 6N NaOH for 48 hours (Fig. 5.21). This can be attributed to greater removal of the surfactant from the modified membranes when modified membranes were boiled for 5 hours in 6N NaOH as compared to when modified membranes were placed in 6N NaOH for 48 hours.

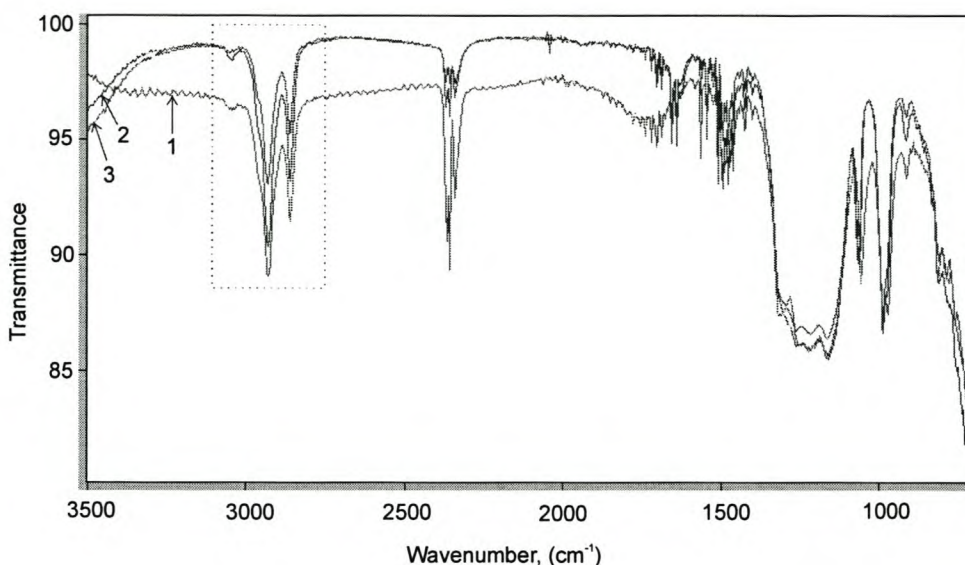


Figure 5.21. IR spectra of a modified membrane (1), modified membrane placed in 6N NaOH for 48 hours (2) and modified membrane boiled in 6N NaOH for 5 hours (3)

There is a slight difference in the size of the absorption bands at 2929 cm⁻¹ and 2855 cm⁻¹ for modified membranes treated with 6N NaOH and 3N NaCl (Roeges, 1994). The absorption bands that are characteristic for surfactant-membrane interaction are similar for modified membranes treated with either 3N NaCl or 6N NaOH (Figure 5.22).

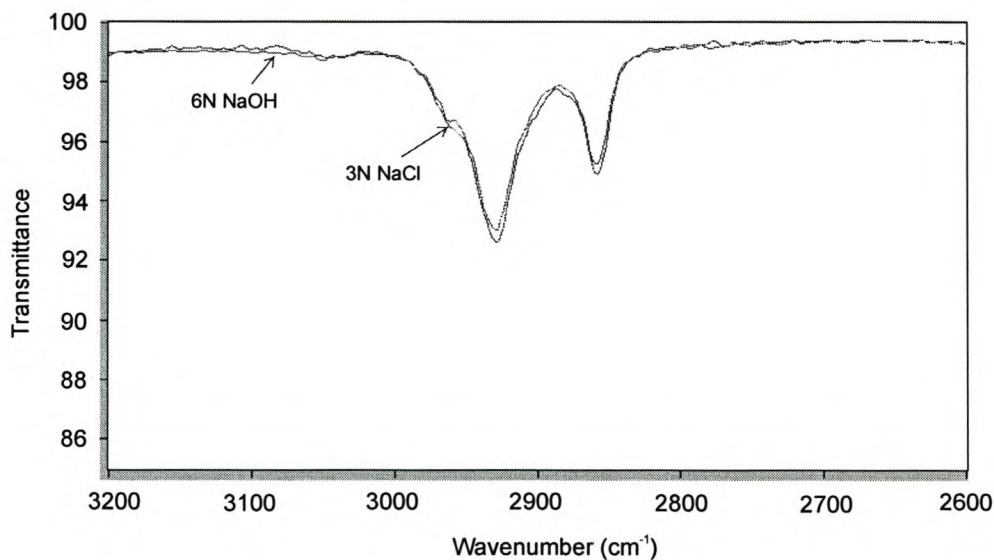


Figure 5.22. IR spectra of modified membranes after treatment with 3N NaCl and 6N NaOH

5.2.4.6. IR spectrometry of the removal of surfactant from modified membranes with nitric acid by ion-exchange

The removal of surfactant from the modified membranes by treatment with 5% HNO₃, 30% HNO₃ and 50% HNO₃ can be seen with the decrease in size of the absorption bands characteristic for surfactant-membrane interaction (Fig. 5.23). The absorption bands that are characteristic of surfactant-membrane interaction decrease in size with treatment with HNO₃. Greater removal of surfactant from modified membranes was achieved when modified membranes were boiled in 50% HNO₃ for 5 hours than when modified membranes were boiled in 5% HNO₃ for 5 hours. Absorption bands that are characteristic for surfactant-membrane interaction were smaller when modified membranes were boiled for 5 hours in 50% HNO₃, compared to when modified membranes were boiled in 5% HNO₃ (Fig. 5.23).

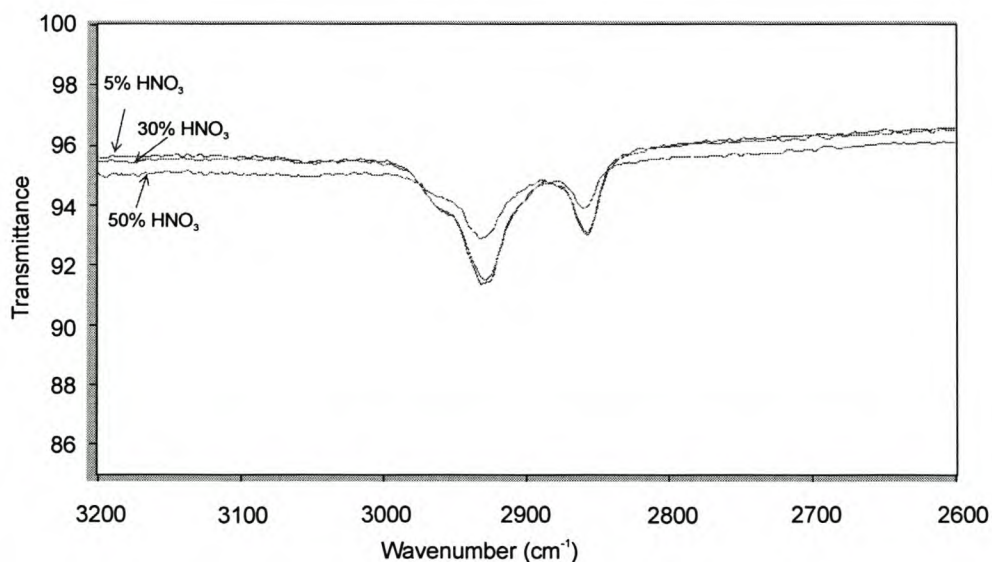


Figure 5.23. IR spectra of modified membranes after treatment with 5%, 30% and 50% HNO₃

5.2.4.7. Discussion

The IR characterisation of membranes modified with surfactant exhibited absorption bands at 2929 cm⁻¹ and 2855 cm⁻¹ (Fig. 5.20). The decrease in the size of these absorption bands is characteristic of the removal of surfactant from surfactant-modified membranes.

In Figure 5.22, the removal of surfactant from modified membranes is similar for the use of NaCl and NaOH solutions. However, a lower concentration of NaCl produces a similar result as with the use of a higher concentration of NaOH. Thus, NaCl is more effective than NaOH for removing surfactant from surfactant-modified membranes.

The degree of surfactant removal from modified membranes increased with the increase in nitric acid concentration. Greater surfactant removal from surfactant-modified membranes was achieved with high concentrations of nitric acid (Fig. 5.23).

The study showed that the increasing removal of surfactant from modified membranes resulted in a decrease in the size of absorption bands characteristic for membrane-surfactant interaction. Thus, membranes can be modified with surfactant to influence the morphology of the platinum catalyst during the deposition process. The surfactant can then be removed after the deposition of platinum.

5.2.5. The effect of electrical resistance on surfactant-treated cation-exchange membranes

5.2.5.1. Preparation of membranes for electrical resistance measurements in an electromembrane cell

The electromembrane cell was filled with 0.5% $\text{CH}_3(\text{CH}_2)_{15}\text{N}(\text{CH}_3)_3\text{Br}$ surfactant solution. The electrical resistance of 0.5% $\text{CH}_3(\text{CH}_2)_{15}\text{N}(\text{CH}_3)_3\text{Br}$ surfactant solution in a two-compartment electromembrane cell was measured with a Radiometer conductivity meter CDM 83. The electrical resistance of a hydrolysed cation-exchange membrane in the electromembrane cell filled with 0.5% $\text{CH}_3(\text{CH}_2)_{15}\text{N}(\text{CH}_3)_3\text{Br}$ surfactant solution was measured at 1 minute time intervals for 25 minutes. The membrane was then removed from the electromembrane cell and the electrical resistance of 0.5% $\text{CH}_3(\text{CH}_2)_{15}\text{N}(\text{CH}_3)_3\text{Br}$ surfactant solution was again measured. This procedure was then followed for 7.5% and 0.05% $\text{CH}_3(\text{CH}_2)_{15}\text{N}(\text{CH}_3)_3\text{Br}$ surfactant solutions.

5.2.5.2. Electrical resistance measurements of surfactant-treated membranes

The electrical resistance (R) of the surfactant-treated membranes were calculated with the following equations:

$$R_{\text{membrane}} = R_{\text{solution and membrane}} - R_{\text{solution}}$$

$$R_{\text{solution}} = k / \lambda_{\text{solution}}$$

$$R_{\text{solution and membrane}} = k / \lambda_{\text{solution and membrane}}$$

where,

$$k = \text{cell constant} = 1.099 \text{cm}^{-1}$$

$\lambda_{\text{solution and membrane}}$ = specific conductivity of surfactant/NaCl solution and membrane (mScm^{-1})

$\lambda_{\text{solution}}$ = specific conductivity of the surfactant/NaCl solution (mScm^{-1})

The resistance of surfactant-treated membranes was determined with the above equations. The specific conductivity of the surfactant/NaCl solutions ($\lambda_{\text{solution}}$) is tabulated in Table 5.4.

Table 5.4. *The electrical resistance of 0.05%, 0.5% and 7.5% surfactant solutions before and after electrical resistance measurements of cation-exchange membranes*

	$\lambda_{0.05\% \text{ surfactant solution}}$ (mS/cm)	$\lambda_{0.5\% \text{ surfactant solution}}$ (mS/cm)	$\lambda_{7.5\% \text{ surfactant solution}}$ (mS/cm)
Before electrical resistance measurements	10.26	8.00	12.88
After electrical resistance measurements	10.29	8.15	13.10

The resistance of cation-exchange membranes was determined using the specific conductivity of the surfactant/NaCl solutions. The resistance of 0.05%, 0.5% and 7.5% surfactant/NaCl solutions (R_{solution}) were determined to be 107.12Ω , 137.38Ω and 85.33Ω .

Table 5.5. Results of electrical resistance measurements of cation-exchange membranes treated with 0.05% $\text{CH}_3(\text{CH}_2)_{15}\text{N}(\text{CH}_3)_3\text{Br}$ surfactant solution at time intervals of 1 minute

Time interval (min)	$\lambda_{0.05\%}$ surfactant solution and membrane (mScm^{-1})	$R_{\text{solution and membrane}}$ (Ω)	R_{membrane} (Ω)	$\log R_m$
1	10.15	108.28	1.16	0.06
2	10.00	109.90	2.78	0.44
3	9.77	112.49	5.37	0.73
4	9.55	115.08	7.96	0.90
5	9.20	119.46	12.34	1.09
13	8.95	122.79	15.67	1.20
19	8.09	135.85	28.73	1.46

Table 5.6. Results of electrical resistance measurements of cation-exchange membranes treated with 0.5% $\text{CH}_3(\text{CH}_2)_{15}\text{N}(\text{CH}_3)_3\text{Br}$ surfactant solution at time intervals of 1 minute

Time (min)	$\lambda_{0.5\%}$ solution and membrane (mScm^{-1})	$R_{\text{solution and membrane}}$ (Ω)	R_{membrane} (Ω)	$\log R_m$
0	7.62	144.23	6.85	0.84
2	6.67	164.77	27.39	1.44
3	6.43	170.92	33.54	1.53
4	6.20	177.26	39.88	1.60
5	5.98	183.78	46.40	1.66
6	5.76	190.80	53.42	1.73
7	5.55	198.02	60.64	1.78
8	5.38	204.28	66.90	1.83
9	5.21	210.94	73.56	1.87
10	5.06	217.19	79.81	1.90
11	4.91	223.83	86.45	1.94
12	4.77	230.40	93.02	1.97
13	4.64	236.85	99.47	2.00
14	4.52	243.14	105.76	2.02
15	4.41	249.21	111.83	2.05
16	4.30	255.58	118.20	2.07
17	4.20	261.67	124.29	2.09
18	4.11	267.40	130.02	2.11
19	4.02	273.38	136.00	2.13
20	3.94	278.93	141.55	2.15
22	3.78	290.74	153.36	2.19
25	3.58	306.98	169.60	2.23

Table 5.7. Results of electrical resistance measurements of cation-exchange membranes treated with 7.5% $\text{CH}_3(\text{CH}_2)_{15}\text{N}(\text{CH}_3)_3\text{Br}$ surfactant solution at time intervals of 1 minute

Time (min)	$\lambda_{7.5\%}$ surfactant solution and membrane (mScm^{-1})	$R_{\text{solution and membrane}}$ (Ω)	R_{membrane} (Ω)	$\log R_m$
0	10.70	102.71	17.38	1.24
1	8.81	124.74	39.41	1.60
2	8.03	136.86	51.53	1.71
3	7.48	146.93	61.60	1.79
4	7.04	156.11	70.78	1.85
5	6.68	164.52	79.19	1.90
6	6.38	172.26	86.93	1.94
7	6.12	179.58	94.25	1.97
8	5.89	186.59	101.26	2.01
9	5.68	193.49	108.07	2.03
10	5.49	20.18	114.85	2.06
11	5.34	205.81	120.48	2.08
12	5.19	211.75	126.42	2.10
13	5.06	217.19	131.86	2.12
14	4.94	222.47	137.14	2.14
15	4.82	228.01	142.68	2.15
16	4.72	232.84	147.51	2.17
17	4.62	237.88	152.55	2.18
19	4.45	246.97	161.65	2.21
20	4.37	251.49	166.16	2.22
21	4.30	255.58	170.25	2.23
22	4.23	259.81	174.48	2.24
23	4.15	264.82	179.49	2.25
24	4.10	268.05	182.72	2.26
25	4.04	272.03	186.70	2.27

The electrical resistance measurements of membranes treated with 0.05% $\text{CH}_3(\text{CH}_2)_{15}\text{N}(\text{CH}_3)_3\text{Br}$ surfactant solutions show that low concentrations of surfactant solutions have a slight effect on the electrical resistance of the membranes (Fig. 5.24). The electrical resistance measurements of membranes treated with 0.5% and 7.5% $\text{CH}_3(\text{CH}_2)_{15}\text{N}(\text{CH}_3)_3\text{Br}$ surfactant solutions show a gradual increase in electrical resistance with increasing time of surfactant treatment (Fig. 5.24).

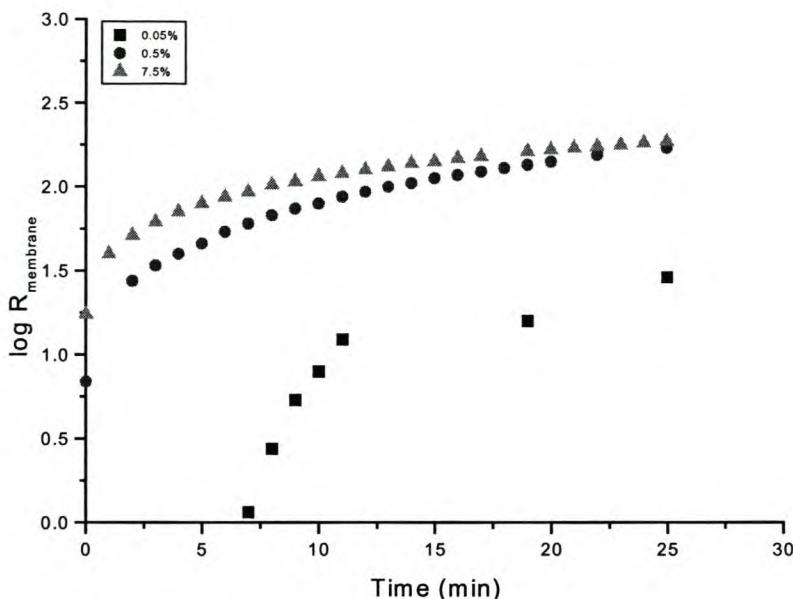


Figure 5.24. Plot of the resistance of membranes ($\log R_{\text{membrane}}$) treated with surfactant solutions of concentrations 0.05%, 0.5% and 7.5% at time intervals of 1 minute

5.2.5.3. Discussion

The low electrical resistance exhibited by membranes treated with 0.05% surfactant solution can be attributed to low concentrations of surfactant solutions having an insignificant effect on the electrical resistance of membranes (Fig. 5.24). Results show that the treatment of membranes with low concentrations of surfactant solutions has an insignificant effect on the transport of ions through the cation-exchange membranes. Thus, less membrane modification occurs with low concentrations of surfactant solutions.

A gradual increase in the electrical resistance of membranes treated with 7.5% and 0.5% surfactant solutions is observed with increasing time of surfactant treatment. The increase in the electrical resistance of these membranes can be attributed to the surfactant molecules replacing Na^+ ions and forming associations with SO_3^- ions in the channels of the cation-exchange membranes. These large surfactant molecules within the membrane channels hinder the transport of ions through the membrane channels, which results in the electrical resistance of the membranes increasing.

Electrical resistance measurements provide information on the ion-exchange properties of membranes. This information assists in determining the optimum ion-

exchange conditions for the deposition of platinum on a membrane modified with surfactant. The increased modification of membranes with surfactant results in an increase in electrical resistance. Thus, the greater the modification of membranes, the slower the autocatalytic reduction of $[\text{PtCl}_6]^{2-}$ ions in the chemical deposition process. This will contribute to the time for the deposition of platinum on modified membranes increasing.

5.2.6. The sorption of water by cation-exchange membranes modified with surfactant

5.2.6.1. Preparation of membranes modified with surfactant

Hydrolysed membranes were boiled in 1N HCl to convert membranes to the H^+ -ionic form. A hydrolysed membrane was placed in 20% $\text{CH}_3(\text{CH}_2)_{15}\text{N}(\text{CH}_3)_3\text{Br}$ surfactant solution for 24 hours. The membrane was then washed with distilled water and placed in a desiccator to dry for 4 days. The membranes were weighed and their masses recorded. The membranes were then placed in distilled water for 3 days and dried with filter paper. The masses of the membranes, after water sorption, were recorded.

5.2.6.2. Results of the sorption of water by modified membranes

The results of water sorption of membranes in the H^+ -ionic form and membranes modified with surfactant are tabulated in Table 5.9. The results show that membranes in the H^+ -ionic form sorb a greater amount of water per gram of membrane than the membranes modified with surfactant.

Table 5.8. Results of the water sorption of a membrane modified with surfactant and a membrane in H^+ -ionic form

	Mass after drying (g)	Mass after placed in water (g)	Mass of water absorption (g)	H_2O uptake per 1g of membrane (g)
Membrane in H^+ -ionic form	0.1422	0.1720	0.0298	0.21
Surfactant-treated membrane	0.1787	0.2037	0.0250	0.14

5.2.6.3. Discussion

A greater uptake of water per 1g of membrane was observed for membranes in the H^+ -ionic form than for membranes modified with surfactant. This can be attributed to the surfactant forming associations with SO_3^- ions in the channels of the cation-exchange membranes. Since the surfactant consists of large bulky groups, the movement of ions through the channels of the membrane is hindered. This results in a decrease in the water uptake of modified membranes, which explains the results obtained.

5.2.7. Final Remarks

Perfluorinated cation-exchange membranes were modified with $CH_3(CH_2)_{15}N(CH_3)_3Br$ ionic surfactant. The formation of a complex between a solid polyelectrolyte (SPE) membrane and surfactant was verified by IR spectrometry. The deposition of platinum on these modified membranes was achieved by the Takenaka-Torikai method.

The platinum catalyst on the modified membranes was investigated by AFM. The platinum catalyst on modified membranes consisted of pyramidal-like platinum particles protruding outwards from the membrane surface (Fig. 5.25).

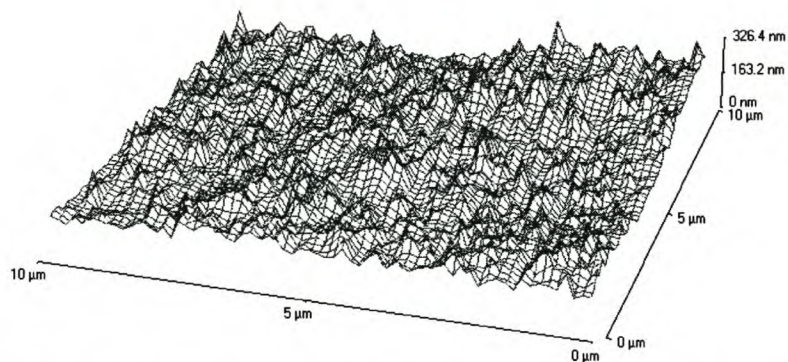


Figure 5.25. Typical three-dimensional AFM image of a textured platinum catalyst embedded on a membrane. The platinum particles are small in size and pyramidally textured.

The shape and size of these platinum particles differed from previously reported work (refs 5, 7-15). The shape of the platinum particles of previously reported work was flake-like (Fig. 5.26), spherical (Fig. 5.27) or mossy.

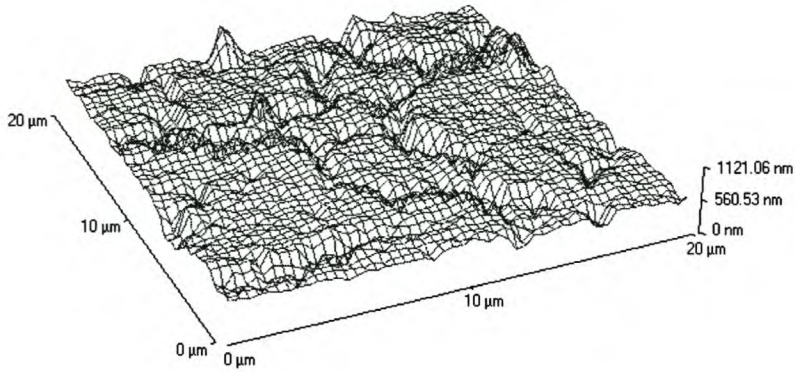


Figure 5.26. Typical AFM image (three-dimensional mesh view) of the surface of a unmodified membrane with platinum catalyst (seen as “flakes”).

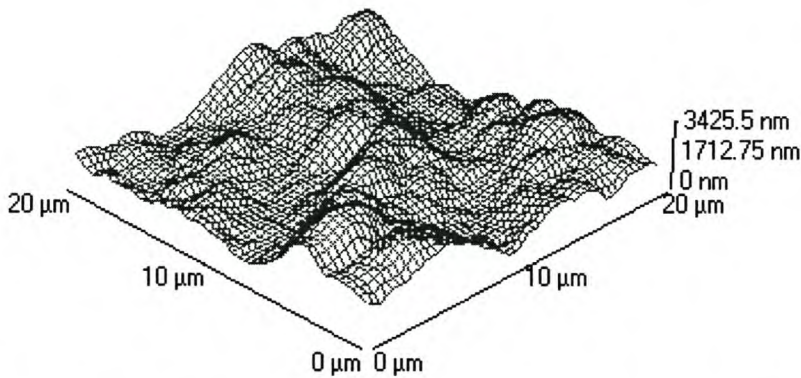


Figure 5.27. Typical AFM image (three-dimensional mesh view) of the surface of a unmodified membrane with platinum catalyst (seen as unevenly distributed, semi-spherical particles).

The regular structure of platinum particles of surfactant-modified membranes can be attributed to the lyotropic phase of the surfactant-polyelectrolyte structure, which acts as a structure-forming medium during the deposition process (Attard et al., 1997). However, the pyramidal platinum structures can also be due to the structural arrangement of micelles on a membrane. The arrangement of micelles on a membrane creates pyramid-like spaces for the formation of platinum structures within these spaces (Fig. 5.28).

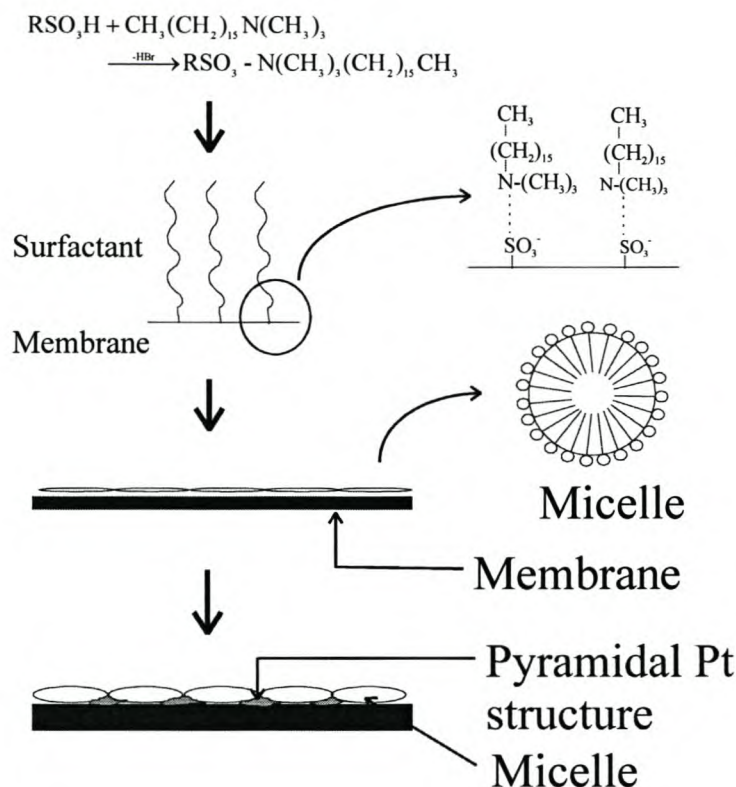


Figure 5.28. Structural arrangement of micelles on a membrane that contribute to the pyramidal shape of the platinum structures

Another reason for the pyramidal shape of the platinum particles can be attributed to a lower transfer rate of hydrazine solution through the membranes due to membrane modification.

Modification of membranes resulted in an increase in their electrical resistance. However, the conductivity of the membranes can be restored by the removal of the surfactant from the modified membranes by ion-exchange.

Further studies are required to determine the structural formation of a surfactant with a polyelectrolyte membrane. Previous work has investigated the interaction between polyelectrolyte networks and surfactants (Dembo et al., 1996). However, less research has investigated the structure of a surfactant-polyelectrolyte complex (Attard et al., 1997).

The use of surfactants in the synthesis of textured platinum catalyst electrodes with high surface area is advantageous for electrocatalytic applications. The combination of a high surface area with a continuous electron-conduction pathway can be advantageous in fuel cells, batteries and sensors, whose performance is determined by mass transport and interfacial processes (Attard et al., 1997).

Our study has demonstrated that the use of surfactants provides a new method for controlling the structure and size of platinum particles deposited on membranes (Bessarabov et al., 2001).

5.3. Conclusions

It was shown that the modification of membranes with EDA resulted in a considerable change in the distribution of platinum throughout a membrane, compared to the results obtained for unmodified membranes. A non-uniform platinum deposition with a weaker adhesion between the platinum particles and modified membrane, compared to Pt/membrane composites obtained using the Takenaka-Torikai method, was observed. A fine dispersion of small platinum particles within the bulk of the modified membrane was observed by means of SEM.

The conductivity of membranes modified with surfactant decreased, but the ability to recover their electrical conductivity was demonstrated. The modification of membranes resulted in a change in the shape of the platinum particles. The platinum particles were small in size and pyramidally textured. The shape and size of the platinum particles obtained in this study are unique and differ from previously reported work (refs 5, 7-15). The average size of the particles (measured as an average height) was approximately 10 nm, and the average length was approximately 0.3 μm .

The results show that modification of membranes influences the platinum particle shape, size and distribution within a membrane, which is important for determining the catalytic activity of an electrocatalytic solid polymer electrolyte.¹

¹ There are two papers published in Journal of Membrane Science on the modification of cation-exchange membranes with surfactant and EDA.
Bessarabov DG and Michaels WC, 2001, Solid polyelectrolyte (SPE) membranes containing a textured platinum catalyst, Journal of Membrane Science, 194, 1, 141-144
Bessarabov DG, Michaels W and Sanderson RD, 2000, Preparation and characterisation of chemically-modified perfluorinated cation-exchange platinum-containing membranes, Journal of Membrane Science, 179, 221-229

References

1. Attard GS, Göttner CG, Corker JM, Henke S and Templer R, 1997, Liquid-crystal templates for nanostructured metals, *Angewandte Chemie Intl. Edn. Engl.*, 36, No. 12, 1315-1317
2. Bartlett PN, 2000, Electrode materials with regular nanostructures made using soap and water, presented at the 14th International Forum on Applied Electrochemistry, "Electrochemical technology for the 21st Century", November 12-16, Florida
3. Bellamy LJ, 1975, *The Infra-red Spectra of Complex Molecules*, 433 pages, Halsted Press, USA
4. Bessarabov DG and Michaels WC, 2001, Solid polyelectrolyte (SPE) membranes containing a textured platinum catalyst, *Journal of Membrane Science*, 194, 1, 141-144
5. Bessarabov DG and Michaels WC, 2001, Morphological diversity of Pt clusters deposited onto proton-exchange perfluorinated membranes for catalytic applications, *Membrane Technology*, 139, 5-9
6. Bessarabov DG, Michaels W and Sanderson RD, 2000, Preparation and characterisation of chemically-modified perfluorinated cation-exchange platinum-containing membranes, *Journal of Membrane Science*, 179, 221-229
7. Brügel W, 1962, *An Introduction to Infrared Spectroscopy*, 419 pages, Methuen & Co Ltd, London
8. Chu B, Yeh E, Sokolov EL, Starodoubtsev SG and Khokhlov AR, 1995, *Macromolecules*, 28, 380
9. Covitch MJ, Lowry SR, Gray CL and Blackford B, 1982, Thermal Crosslinking of a Chemically-Modified Ionomer, *Polymer Science and Technology*, 16, 257-267
10. Degering ED, 1942, *An Outline of Organic Nitrogen Compounds*, 381 pages
11. Delime F, Léger JM and Lamy C, 1998, Optimization of platinum dispersion in Pt-PEM electrodes: Application to the electrooxidation of ethanol, *J. Appl. Electrochem.* 28, 27
12. Dembo AT, Yakunin AN, Zaitsev VS, Mironov AV, Starodoubtsev SG, Khokhlov AR and Chu B, 1996, Regular Microstructures in gel-surfactant complexes: Influence of water content and comparison with the surfactant structure in water, *Journal of Polymer Physics: Part B: Polymer Physics*, 34, 2893-2898

13. Dermer OC and Ham GE, 1969, Ethyleneimine and Other Aziridines, Chemistry and Applications, Academic Press, New York
14. DeWulf DW and Bard AJ, 1988, Application of Nafion/platinum electrodes (solid polymer electrolyte structures) to voltammetric investigations of highly resistive solutions, *J. Electrochem. Soc.: Electrochemical Science and Technology*, 135, 8, 1977
15. Fedkiw PS and Her W.-H, 1989, An impregnation-reduction method to prepare electrodes on nafion SPE, *J. Electrochem. Soc.*, 136, 899
16. Fedkiw PS, Potente JM and Her W.-H, 1990, Electroreduction of gaseous ethylene on a platinized nafion membrane, *J. Electrochem. Soc.*, 137, 5, 1451
17. Fournier J, Faubert G, Tilquin JY, Côte R, Guay D and Dodelet JP, 1997, High performance, low Pt content catalysis for electroreduction of oxygen in polymer-electrolyte fuel cells, *J. Electrochem. Soc.*, 144, 1, 145
18. Franken T, 2000, Bipolar membrane technology and its applications, *Membrane Technology*, 125, 8-10
19. Grot WG, 1976, Heat-treated fluorocarbon sulfonylamine cation permselectivity, US patent 3,969,285
20. Grot WG, 1977, Electrolysis cell using cation exchange membranes of improved permselectivity, US patent 4,026,783
21. Grot WG, 1977, Process for producing halogen and metal hydroxides with cation exchange membranes of improved permselectivity, US patent 4,030,988
22. Hirano S, Kim J and Srinivasan S, 1997, High performance proton exchange membrane fuel cells with sputter-deposited Pt layer electrodes, *Electrochim. Acta*, 42, 10, 1587
23. Holze R and Ahn J, 1992, Advances in the use of perfluorinated cation exchange membranes in integrated water electrolysis and hydrogen/oxygen fuel cells, *J. Membr. Sci.*, 73, 87
24. Hora CJ and Maloney DE, 1977, *Electrochemical Society extended abstract*, 77, 2, 1145
25. Liu R and Fedkiw, 1992, Partial oxidation of methanol on a metallized nafion polymer electrolyte membrane, *J. Electrochem. Soc.*, 139, 12, 3514
26. Liu R, Her W.-H and Fedkiw PS, 1992, In Situ electrode formation on a Nafion membrane by chemical platinization, *J. Electrochem. Soc.*, 139, 1, 15

27. Lowry and Richardson, 1981, Mechanism and Theory in Organic Chemistry, 2nd Edition, Harper and Row, New York, 991 pages
28. Nidola A and Martelli G, 1982, Deposition of Catalytic Electrodes on Ion-Exchange Membranes, U.S Patent 4,364,803
29. Poirier JA and Stoner GE, 1994, Microstructural effects on electrocatalytic oxygen reduction activity of nano-grained thin-film platinum in acid media, Journal of Electrochemical Society, 141, 2, 425-430
30. Roeges NPG, 1994, A Guide to the Complete Interpretation of Infrared Spectra of Organic Structures, 340 pages, John Wiley and Sons, England
31. Sheppard S.-A, Campbell SA., Smith JR, Lloyd GW, Ralph TR and Walsh FC, 1998, Electrochemical and microscopic characterisation of platinum-coated perfluorosulfonic acid (Nafion 117) materials, Analyst, 123, 1923
32. Sokolov EL, Yeh F, Khokhlov A and Chu B, 1996, Nanoscale Supramolecular Ordering in Gel-Surfactant Complexes: Sodium Alkyl Sulfates in Poly(diallyldimethylammonium Chloride), Langmuir, 12, 26, 6229-6234
33. Solomons, 1981, Organic Chemistry, 6th Edition, 1218 pages, John Wiley and Sons, United States
34. Timashev SF, 1991, Physical chemistry of membrane processes, Ellis Horwood series in Physical Chemistry, New York
35. Timashev SF, Vorobiev AV, Kirichenko VI, Popkov Yu, Volkov VI, Shifrina RR, Lyapunov AY, Bondarenko AG, Bobrova LP, 1991, Specifics of Highly Selective Ammonia Transport through Gas-Separating Membranes based on Perfluorinated Copolymer in the form of Hollow Fibres, Journal of Membrane Science, 59, 117

Galvanodynamic study of the electrochemical switching effect in perfluorinated cation-exchange membranes modified with ethylene diamine¹

Abstract

*Perfluorinated sulfonyl-fluoride cation-exchange membranes were treated with ethylene diamine to investigate the influence of EDA-treatment on the process of electrochemical “switching” in EDA-modified membranes. The galvanodynamic method was used to obtain *i-V* cyclic curves of modified membranes. Electroless chemical deposition of platinum particles on modified membranes was achieved using the Takenaka-Torikai method. Galvanodynamic *i-V* cyclic curves of platinum-containing aminated membranes, unmodified membranes and modified membranes were compared.*

6.1. Introduction

An interesting study of chemical surface modification of perfluorosulfonic polymeric membranes was aimed at the development of new membrane/catalyst composites for electrocatalytic applications (Nidola et al., 1982). The chemical modification of ion-exchange membrane surfaces is a powerful method by which to change membrane surface properties, which results in a change in the morphology of the catalyst on a membrane surface, distribution of catalyst particles in membranes, membrane electrical properties, etc. (Bessarabov et al., 2000).

6.2. Switching effect in modified perfluorinated membranes

The phenomenon of “switching” membrane conductivity during the flow of electrical current through a perfluorinated cation-exchange membrane modified with ethylene diamine (EDA) was studied by means of the galvanodynamic electrochemical method (Timashev, 1991). According to Timashev (1991), the “switching” conductivity

¹ This chapter is published in the form of an article in Journal of Membrane Science. Bessarabov DG, Michaels W and Sanderson RD, 2000, Preparation and characterisation of chemically-modified perfluorinated cation-exchange platinum-containing membranes, Journal of Membrane Science, 179, 1-2, 221

consists of a jumpwise reversible transition of the system from a high-ohmic to a low-ohmic state and is induced by an electric field whose intensity exceeds some threshold value. A term “negative differential resistance” (NDR) was introduced when describing S-shaped, cyclic i - V curves of membranes. According to Timashev (1991), the switching effect could be related to the formation of additional fixed charged groups in the aminated layers of membranes. This could be caused by the heterolytic dissociation of water that takes place at the membrane-solution interface, accompanied by the formation of H^+ and OH^- ions.

The present study investigates the phenomenon of switching conductivity in cation-exchange membranes that are chemically modified with ethylene diamine (EDA), as well as verification of the mechanism of the switching effect proposed by Timashev (1991). The effect of modified membranes that are platinised on the phenomenon of switching conductivity is also investigated.

6.3. Galvanodynamic characterisation of modified membranes

6.3.1. Galvanodynamic characterisation of membranes modified on one side with EDA

A four-compartment, thermostated electrochemical cell comprising two platinum electrodes and the potentiostat Solartron SI 1280B electrochemical measurement unit were used to determine the membrane potential by cyclic galvanodynamic measurements. The total volume of the electrochemical cell was 80 ml. The membranes that were under investigation were placed between the two central compartments (chambers II and III) of the electrochemical cell (Fig. 6.1). The membrane layer modified with EDA (e.g. the aminated layer) faced chamber III of the cell in all the experiments. The other chambers of the electrochemical cell were separated by two perfluorinated, unmodified, hydrolysed cation-exchange membranes. The potential difference across the membrane was measured with a $Ag/AgCl[KCl(sat.)]$ reference electrode linked to a potentiostat and coupled to Luggin capillaries. The membrane under investigation was placed between Luggin capillaries and the membrane potential measurements were carried out in the electrochemical cell filled with 0.1N NaCl at a temperature of 22 °C.

In galvanodynamic experiments, the electrical current was changed at a rate of 0.1 mA/sec. The active area of the central membrane in the electrochemical cell was 0.28 cm² and the active area of each side-positioned membranes was 3 cm².

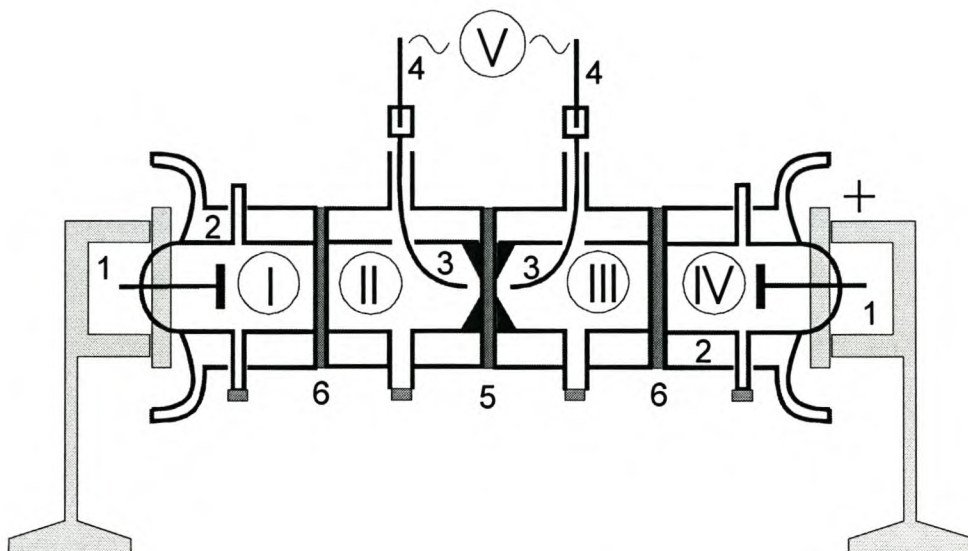


Figure 6.1. Schematic representation of a four-compartment cell used in galvanodynamic measurements of cation-exchange membranes modified with EDA. (1) Platinum electrodes; (2) water jacket for thermal stability; (3) Luggin capillaries; (4) Ag/AgCl/KCl reference electrodes; (5) Cation-exchange membrane modified with EDA from the right side; (6) cation-exchange membranes. I, II, III and IV are the chambers of the cell.

6.3.2. Results of galvanodynamic cycling of aminated membranes without platinum particles

6.3.2.1. Unmodified hydrolysed membranes without platinum catalyst

Figure 6.2 shows a typical *i*-*V* cyclic curve obtained for a hydrolysed, unmodified perfluorinated membrane in a neutral (pH≈6) solution of 0.1M NaCl. It can be seen that the *i*-*V* cyclic curve is symmetrical (Fig. 6.2).

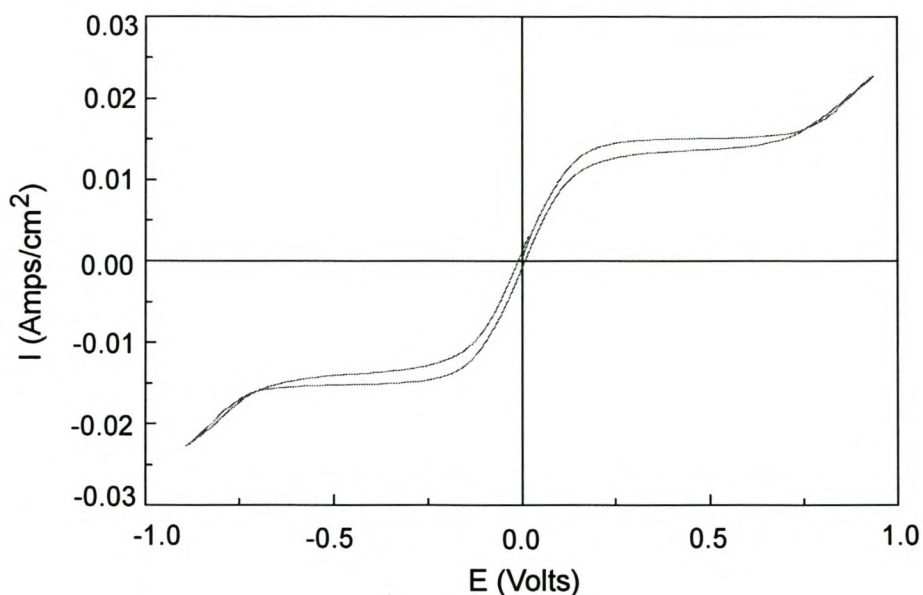


Figure 6.2. A typical cyclic i - V curve of a unmodified perfluorinated membrane in $0.1M$ $NaCl$, equilibrated at $pH=6$.

6.3.2.2. Membranes modified with EDA for 85 seconds without platinum catalyst

The i - V cyclic curve obtained for membranes modified for 85 seconds with EDA is asymmetrical (Fig. 6.3). It can be seen from Figure 6.3 that the potential at which the switching effect occurred decreased with an increase in the number of galvanodynamic cycles. It took a few hours before a steady potential value was reached. This was exhibited in all the modified membranes, not only membranes modified with EDA for 85 seconds.

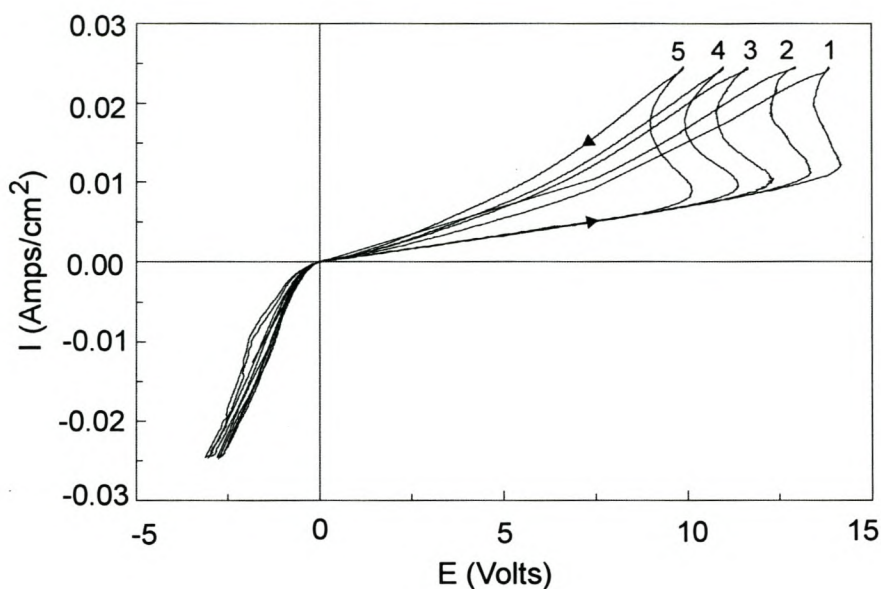


Figure 6.3. Cyclic i - V curves of a membrane modified with EDA on one side for 85 seconds. Arrows on the curves indicate the direction of the current. Curve 1 corresponds to the first cycle and curve 5 corresponds to the last cycle. Curves 2, 3, and 4 show intermediate cycles.

Figure 6.4 shows that when only a cyclic anodic current was applied to membranes, no switching effect was observed on the i - V cyclic curves (curves 1 and 2). However, when the modified layers of the membrane were cathodically polarised, the anodic parts of the i - V cyclic curve exhibited the “switching” effect (Fig. 6.4, curve 3).

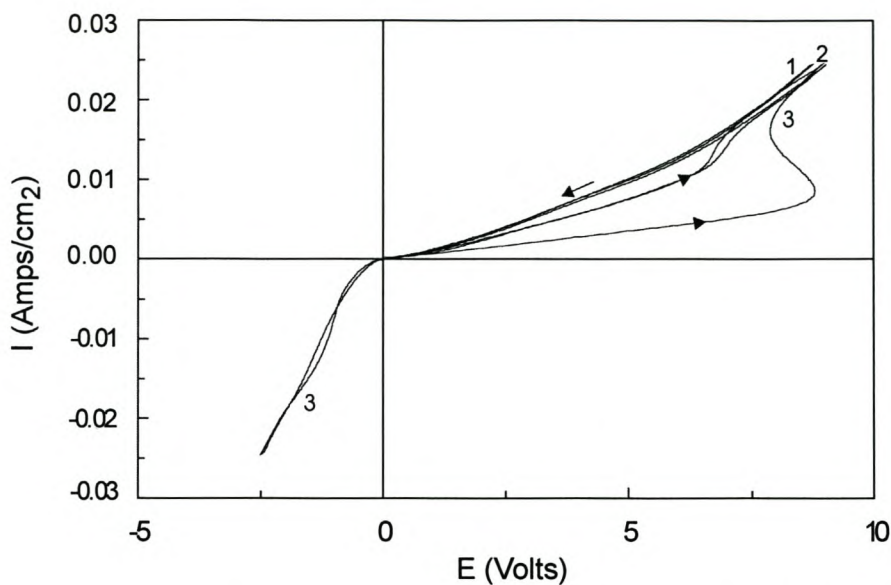


Figure 6.4. Cyclic i - V curves of a membrane modified with EDA for 85 seconds. Anodic cycling was applied to the membrane only (curves 1 and 2). Curve 3 corresponds to the galvanodynamic cycle with both cathodic and anodic waves. Arrows on curve 3 indicate the direction of the current.

6.3.2.3. Membranes modified for 85 and 120 seconds with embedded platinum catalyst

Figure 6.5 show typical i - V cyclic curves obtained for modified membranes in which the aminated layers contained clusters of metallic platinum. The asymmetry of the i - V cyclic curves was reduced considerably with the aminated layers of modified membranes containing embedded microparticles of platinum (compare with Fig. 6.3).

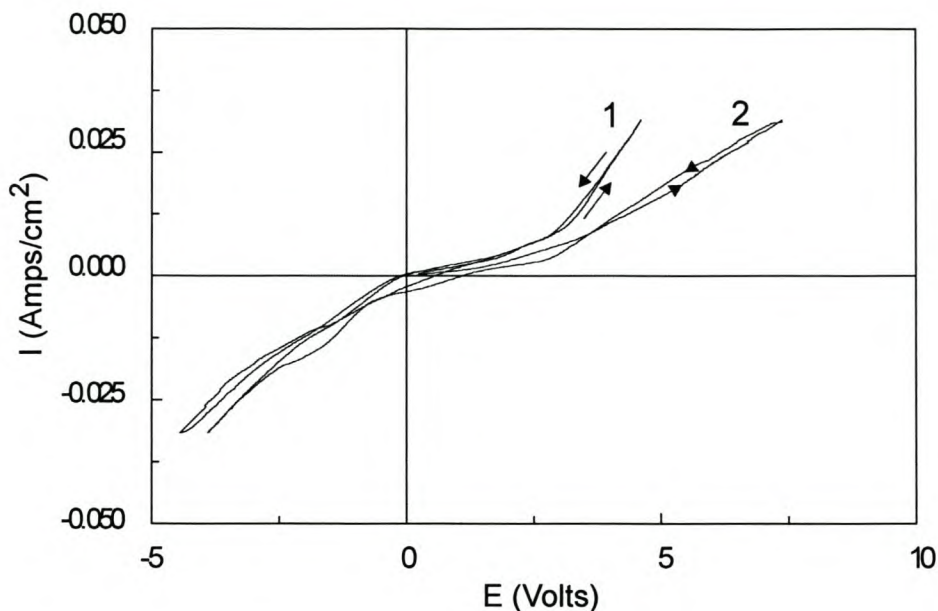
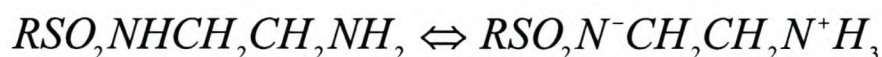


Figure 6.5. Cyclic *i-V* curves of EDA-treated membranes with the aminated layers containing embedded microparticles of platinum. Curve 1 corresponds to 85 sec of EDA treatment, and curve 2 corresponds to 120 seconds of EDA treatment, respectively.

6.4. Discussion

The potential at which the switching effect occurred decreased with an increase in the number of galvanodynamic cycles (Fig. 6.3). This can be explained by the acid-base equilibrium that occurs in the so-called zwitterions of modified membranes equilibrated with neutral solutions of NaCl (Covitch et al., 1982). According to Covitch et al. (1982), the terminal amino group of the EDA sulfonamide is a good leaving group. The zwitterionic nature of this structure promotes displacement even at a neutral pH, which can be represented as follows:



The results showed that *i-V* cyclic curves for unmodified hydrolysed membranes were symmetrical. The *i-V* cyclic curves of membranes that were modified were asymmetrical and exhibited a “negative differential resistance” (NDR) branch. This can be seen in *i-V* cyclic curves obtained for membranes modified with EDA for 45,

60 and 85 seconds in a solution of 0.1 M NaCl (pH \approx 6) (Figure 6.6, curves 1, 2, 3, respectively).

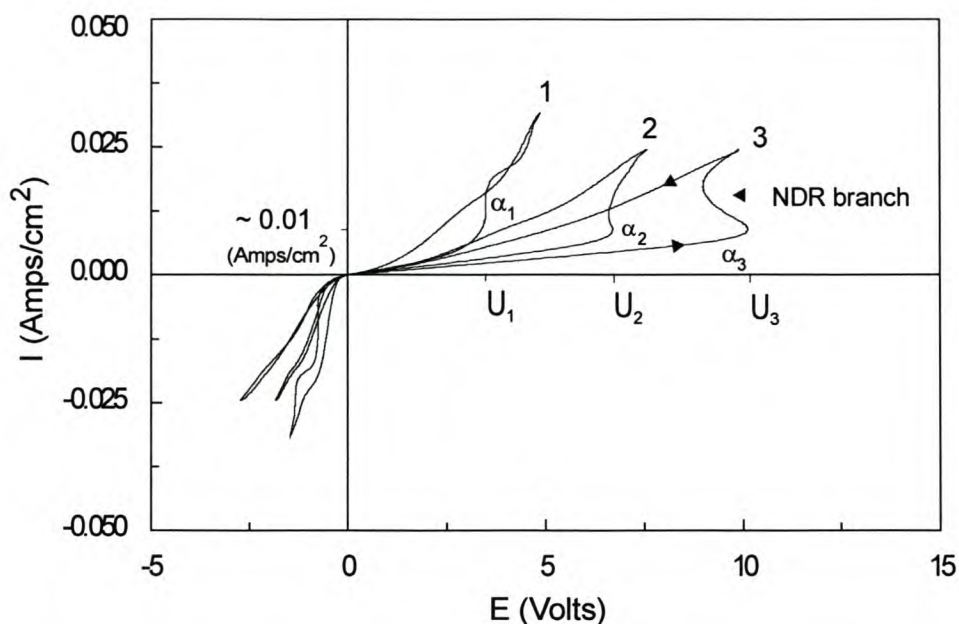
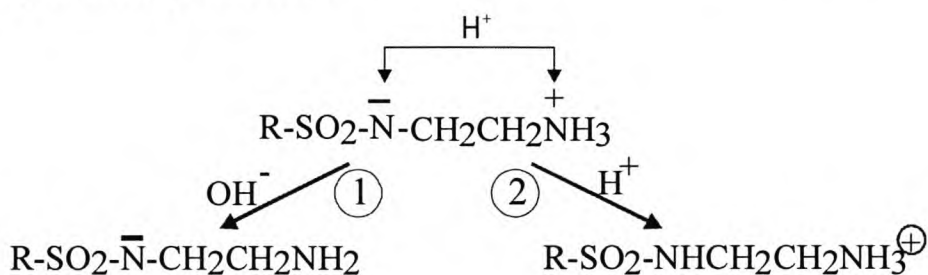


Figure 6.6. Cyclic i - V curves of EDA-treated perfluorinated membranes. Times of modification: 45, 60 and 85 seconds (curves 1, 2, and 3, respectively). The slopes ($\alpha_1=0.166$, $\alpha_2=0.107$ and $\alpha_3=0.072$) of the initial parts of the i - V curves correspond to 45, 60 and 85 seconds of modification with EDA. Steady-state values U_1 , U_2 , and U_3 correspond to 3.5, 6.7 and 10.1 volts, respectively, when the potential of a modified membrane begins to decrease at a current density of approximately 0.01 amps/cm 2 .

Figure 6.6 exhibits two specific characteristics of i - V cyclic curves of membranes modified with EDA. The first is a strong asymmetry between cathodic and anodic branches of the i - V cyclic curve depending on the direction of the current. The membrane resistance was much higher when an anodic current was applied to the aminated layer of the membrane than when a cathodic current was applied. The second feature is that a part of the i - V cyclic curve showing a larger membrane resistance exhibited a “negative differential resistance” (NDR) branch (Fig. 6.6) (Timashev, 1991). The potential of U_1 , U_2 , and U_3 , which were obtained at a constant galvanodynamic rate of 0.1 mA/sec, increased with increasing time of membrane treatment with EDA (Fig. 6.6). An increase in the time of EDA treatment of membranes resulted in the “NDR” branches of i - V cyclic curves becoming more developed (Fig. 6.6).

The switching effect in membranes modified with EDA could be due to the formation of additional fixed-charged groups in the aminated layers of the membranes. However, this does not explain why switching is only observed when the aminated layer of the membrane is initially either neutral or subjected to cathodic polarisation (see the anodic wave immediately following the cathodic one (curve 3), Fig. 6.4). We propose that the difference in the shape of the *i*-*V* cyclic curves (compare curves 3 with 1 and 2, Fig. 6.4) can be explained by the dynamic equilibrium occurring in the membranes during the galvanodynamic cycles, which can be represented by Reaction 1.



Reaction 1. *Zwitterion nature of aminated layer of a membrane modified with EDA in acidic and alkaline conditions.*

When the aminated layer of a membrane is anodically polarised, protons that are formed at the anode of the cell during the galvanodynamic cycle diffuse from chamber IV through the cation-exchange membrane (6, Fig. 1) to chamber III of the cell and react with the aminated layer of the membrane. The reaction is schematically represented by equilibrium 2 (Reaction 1). Thus, the equilibrium shifts towards the positively charged groups. As a result of this process, the main charge carriers in the system (i.e. sodium ions) have to overcome a large electrical barrier. However, when the aminated layer of the membrane is cathodically polarised during the galvanodynamic cycle, the equilibrium 2 (Reaction 1) either does not change or is shifted to equilibrium 1 (Reaction 1). This phenomenon is possible due to permeation of the Donnan electrolyte through the cation-exchange membrane. The latter can explain the sharp increase in the conductivity of the membrane system where charge carriers are mainly sodium ions. This increase in conductivity is observed as an “NDR” branch (Figs. 6.3, 6.4, 6.6).

This proposed definition of the observed switching effect can explain the association that exists between the number of galvanodynamic cycles and the

potential at which the switching effect occurs (Fig. 6.3). Since the equilibrium processes occurring in modified membranes depend on the pH value, the number of cycles has an effect on the equilibrium and eventually results in the steady-state value of the potential.

In the range of membrane potentials measured in this study, it seems that the time of membrane modification with EDA has little effect on the current density at which the switching is observed. The switching effect occurs at a current density value of approximately 0.01 A.cm^{-2} (Fig. 6.6).

In order to investigate the mechanism of the switching phenomenon in membranes modified with EDA, particularly the influence of H^+ and OH^- ions on the switching effect, the modified membranes were platinised (as described in Section 5.1.2). Figure 6.5 shows typical *i*-V cyclic curves obtained for membranes with aminated layers embedded with clusters of metallic platinum. The *i*-V cyclic curves of modified membranes that were platinised were less asymmetrical than *i*-V cyclic curves of modified membranes that were not platinised. The membrane resistance increased when an aminated platinum-containing layer was subjected to a cathode wave of the cycle. However, the membrane resistance decreased considerably when the aminated platinum-containing layer was facing the anode. In Figure 6.5 it can be seen that no “NDR” branch was present in the *i*-V cyclic curves of modified membranes containing platinum catalyst.

The metallic platinum clusters on modified membranes have an effect on the shape of the *i*-V cyclic curves, which can be explained by the platinum clusters acting as bipolar microelectrodes (Fig. 6.7). Small particles of platinum embedded in the polymeric matrix of a membrane, which were placed in a electrical field between the two electrodes of the electrochemical cell, acted as bipolar microelectrodes during reactions of water splitting.

When the bipolar platinum microelectrodes embedded in the EDA-treated layer of the proton-exchange membrane are facing the anode, hydroxyl ions are generated and accumulate in chamber III of the electrochemical cell (Fig. 6.7 and Reaction 1). Simultaneously, protons are generated and diffuse freely through the aminated layer and the bulk of the membrane into chamber II (Fig. 6.7 and Reaction 1).

The hydroxyl ions are neutralised by H^+ ions in the adjacent aminated layer of the membrane (chamber III) (Fig. 6.7 and Reaction 1). Since Na^+ are the main charge

carriers in the system, the potential barrier for their diffusion is reduced. The result is that the overall resistance of the membrane system is also reduced (Figs. 6.5 and 6.6).

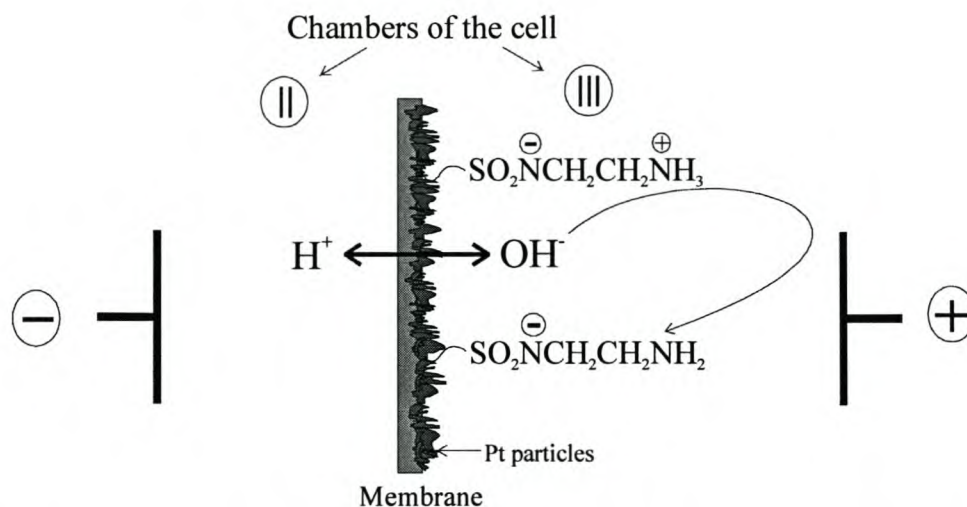


Figure 6.7. Schematic representation of the processes occurring in chambers II and chambers III of the electrochemical cell during anodic polarisation of the aminated layer of the membrane containing platinum particles

The H^+ ions generated when the platinum bipolar microelectrodes embedded into the aminated layer of the membrane is facing the cathode (cathodic wave of the galvanodynamic cycle), diffuse to chamber II of the cell. The presence of these protons in chamber II results in the formation of a zwitterion (Reaction 1), which increases the potential barrier for the diffusion of sodium ions as main charge carriers in the system. In this case the hydroxyl ions are neutralised by H^+ ions in the adjacent aminated layer of the membrane. This explains the increase in membrane resistance, resulting in a decrease in the asymmetry of the i - V curves of the cathodic waves of the galvanodynamic cycles (Fig. 6.5)

6.5. Conclusions

Surfaces of perfluorinated sulfonyl-fluoride cation-exchange flat-sheet membranes were aminated on one-side with EDA. The electrical potential of the aminated membranes was studied in a four-compartment electrochemical cell using galvanodynamic i - V cyclic curves. The membranes that were modified for longer periods of time (e.g. 120, 300, 600 and 3600 seconds) had a very high electrical

resistance. We were unable to obtain similar curves for these membranes using potentiostat Solatron SI 1287 as the membrane potential of these membrane systems exceeded the working range of the potentiostat.

It was found that the conductivity of the aminated membranes switched significantly during galvanodynamic cycles. The *i*-*V* cyclic curves obtained for the aminated membranes were highly asymmetrical. It was also shown that the *i*-*V* cyclic curves contained “NDR” branches. The longer the time of EDA treatment of the membranes, the stronger was the “NDR” effect that was observed. We also observed that the “switching” potential of a single membrane decreased with an increase in the number of the galvanodynamic cycles. The “switching” effect depends on the “history” of a membrane. If a membrane was cathodically polarised, the “switching” effect was observed. However, if a current was cycled between a neutral and a positive value, no “switching” effect was observed. The “switching” effect observed in the EDA-treated membranes is explained by the formation of additional fixed charged groups in the aminated layers of membranes. It was also suggested that the formation of the charged groups was most likely due to the influence of the pH of the electrolyte on the acid-base equilibrium in the aminated layers of the membranes. A simple electrolysis process caused changes in the pH of the electrolyte during galvanodynamic cycling. Generation of additional ions in the aminated layers through water splitting by platinum bipolar microelectrodes, resulted not in the increase of the switching effect but, instead, eliminated it.

A study of the properties of aminated perfluorinated cation-exchange membranes containing platinum catalyst can contribute to additional practical knowledge in the fields, such as the separation of amino-acids, improved relative cationic separations, and vapour and gas transport.

References

1. Bessarabov DG, Michaels W and Sanderson RD, 2000, Preparation and characterisation of chemically-modified perfluorinated cation-exchange platinum-containing membranes, *Journal of Membrane Science*, 179, 1-2, 221
2. Covitch MJ, Lowry SR, Gray CL, Blackford B, 1982, Thermal cross-linking of a chemically-modified ionomer, *Polym. Sci. Technol. (Polym. Sep. Media)*, 16, 257
3. Nidola A, Martelli GN, 1982, US Patent 4,364,803

4. Timashev SF, 1991, Physical Chemistry of Membrane Processes, Ellis Horwood Series in Physical Chemistry, New York

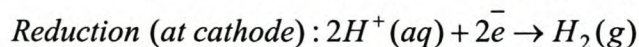
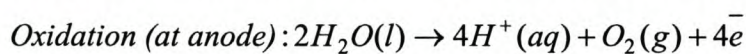
Anodic oxidation of water by electrocatalysis using a electrocatalytic membrane system

Abstract

The application of electrocatalytic membrane systems, such as the anodic oxidation of water, was investigated by the electrochemical methods of galvanostatic and cyclic voltammetric measurements. A novel experimental set-up, using a strip of Nafion for electric contact between the reference electrode and working electrode, was investigated in cyclic voltammetric measurements.

7.1. Theory of water electrolysis in a electrocatalytic cell

The overall reaction of the electrolysis of water can be represented as follows:



The change in enthalpy for the electrochemical decomposition of water is (Ullmann, 1987):

$$\Delta H = \Delta G + T\Delta S = -nFE + nFT\left(\frac{\partial E}{\partial T}\right)_p$$

where H is the enthalpy, G is Gibbs free energy, S is entropy, T is the temperature, n is the number of electrons transferred per formula conversion, F is the Faraday constant, and E is the electrochemical potential. The required electrical energy then becomes (Ullmann, 1987):

$$W = \Delta G = F \times n \times E_{rev}$$

where E_{rev} is the ideal (reversible) decomposition potential. Under standard conditions E_{rev} can be expressed as (Ullmann, 1987):

$$E_{rev} = \frac{\Delta G}{n \cdot F} = 1.228 \text{ V}$$

The actual decomposition potential is always higher than the ideal value due to the irreversible processes on the electrodes and the resistance of the electrolyte. In the ideal case, operation of the cell requires an amount of electrical energy, $W = \Delta G$, and the addition of heat, $Q = T \Delta S$. If both amounts of energy are to be supplied in the electrical form, the potential under standard conditions is increased by thermal potential (ΔE_Q) (Ullmann, 1987). Thermal potential can be represented as follows:

$$\Delta E_Q = \frac{T \Delta S}{n \cdot F} = 0.252 \text{ V}$$

The theoretical minimum decomposition potential at standard conditions is (Ullmann, 1987):

$$E_{th} = E_{rev} + \Delta E_Q = 1.480$$

The cell voltage (U) can be represented as follows (Ullmann, 1987):

$$U = E_1 + E_2 + E_3 + E_4$$

where E_1 is the theoretical voltage (E_{rev}), E_2 and E_3 is the anodic and cathodic overvoltage at the phase boundary electrolyte-electrode, and E_4 is the voltage drop due to electrical resistance of the electrolyte system. The overvoltage of E_2 and E_3 can be influenced by suitable choice of electrode materials and electrode surface conditions. The voltage drop of the electrolyte (E_4) depends on the conductivity of the electrolyte, thickness of the SPE membrane, permeability of the membrane and the current density.

The efficiency of electrolysis is related to the minimum voltage as represented in the following equation (Ullmann, 1987):

$$\eta = \frac{E + \frac{T \Delta S}{nF}}{U}$$

The difference between the open circuit (equilibrium) potential (E_o) and the closed circuit potential (E_c) is the overpotential (η):

$$\eta = E_o - E_c$$

The ohmic overpotential is due to resistance in the cell such, as electronic resistances of electrodes and active materials, as well as the ionic resistance of the electrolyte. The ohmic overpotential can be decreased by increasing the operating temperature of the electrochemical cell and the pressure within the electrochemical cell (Ullmann, 1987). Since increased temperature results in improved electrolyte conductivity, operating an electrochemical cell under high temperatures can decrease the cell resistance. The increase in pressure within a electrochemical cell reduces the accumulation of gas within the cell, which results in the resistance of the electrolyte decreasing.

7.1.1. Determination of cell potential of SPE platinum-containing membranes by galvanostatic measurements

7.1.1.1. Experimental set-up for galvanostatic measurements

Galvanostatic measurements were performed in a reactor as shown in Figure 7.1. The cell consists of titanium electrodes, insulators, cooling compartments, gas and liquid distribution channels, inlets and outlets for water and gas. Flat-sheet cation-exchange membranes were placed between the titanium electrodes. The insulators were placed between the titanium electrodes and the reactor (Fig. 7.2).

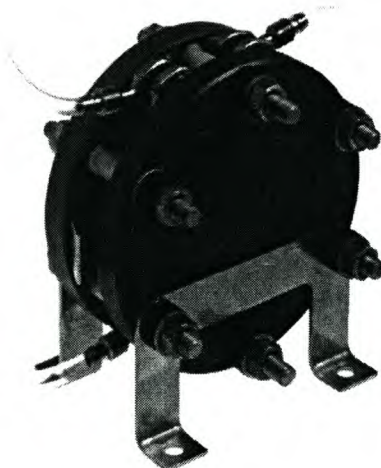


Figure 7.1. *Reactor used in galvanostatic measurements, which consists of titanium electrodes, gas and liquid distribution channels, inlets and outlets for water and gas.¹*

¹ Reactor was provided by DINAX technologies, cc.

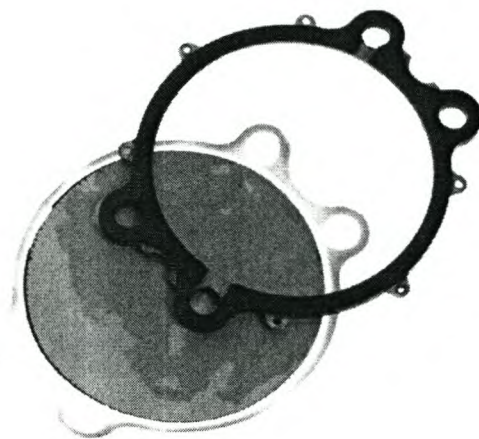


Figure 7.2. *Components of reactor: Gaskets and SPE platinum-containing membrane.*²

Hydrolysed membranes were placed in the reactor and the cell potential at room temperature was measured with a Solartron SI 1280B electrochemical measurement unit. The cell potential was measured for a membrane surface area of 38.5 cm².

7.1.2. Determination of the effect of temperature on the anodic oxidation of water by galvanostatic measurements

7.1.2.1. Preparation of platinum-containing membranes for use in anodic oxidation of water

Hydrolysed membranes were converted to the H⁺-ionic form by boiling in 1N HCl solution. 15ml 0.03M platonic acid solution was poured onto a cation-exchange membrane in a membrane cell. The time of contact of 0.03M platonic acid solution with a membrane was 1 minute. The membrane cell was then submerged in a bath of hydrazine. The platonic acid solution was autocatalytically reduced by hydrazine for 11.5 minutes. 15ml 0.03M platonic acid solution was poured onto the reverse side of the cation-exchange membrane in the membrane cell. The time of contact of 0.03M platonic acid solution with the membrane was 2 minutes. The membrane cell was then submerged in a bath of hydrazine. The platonic acid solution was autocatalytically reduced by hydrazine for 23 minutes. The membrane was washed with distilled water

² Provided by DINAX technologies, cc.

and inserted into a reactor (Fig. 7.3) for the anodic oxidation of water at various temperatures.

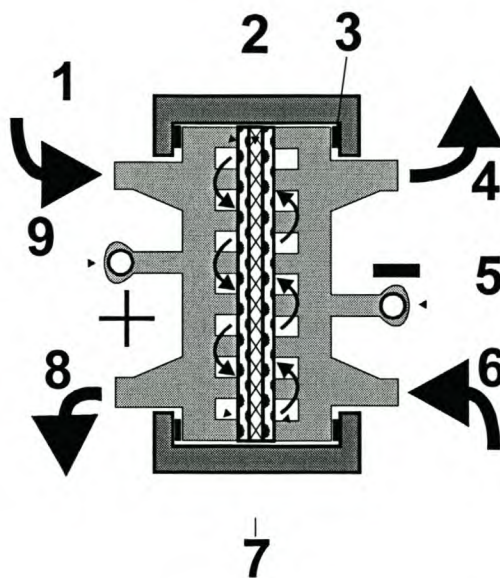


Figure 7.3. Schematic representation of reactor used in anodic oxidation of water. Microporous titanium electrodes (1); proton-exchange membrane (PEM) (2); isolators between titanium electrodes (3) and reactor (5); outlet (for water and hydrogen) (4); cathode side of a reactor (5); cathodic inlet (for water) (6); gas and liquid distribution channels (7); anodic outlet (for water) (8); anode side of the reactor (9) (Bessarabov, 2001).

7.1.2.2. Galvanostatic experimental conditions for anodic oxidation of water

The potential-current density relationship for the anodic oxidation of water was determined at temperatures of 33 °C, 45 °C and 60 °C for a membrane surface area of 38.5 cm². The experiments were run at a low applied current for 7 hours.

7.1.2.3. Results of the anodic oxidation of water with platinum-containing membranes

Figure 7.4 is a typical example of the anodic oxidation of water at an applied current of 0.27A for 7 hours. The maximum cell potential occurs after 24039 seconds. The deflections observed on the curve can be attributed to the evolution of oxygen gas during the anodic oxidation of water (Figure 7.4).

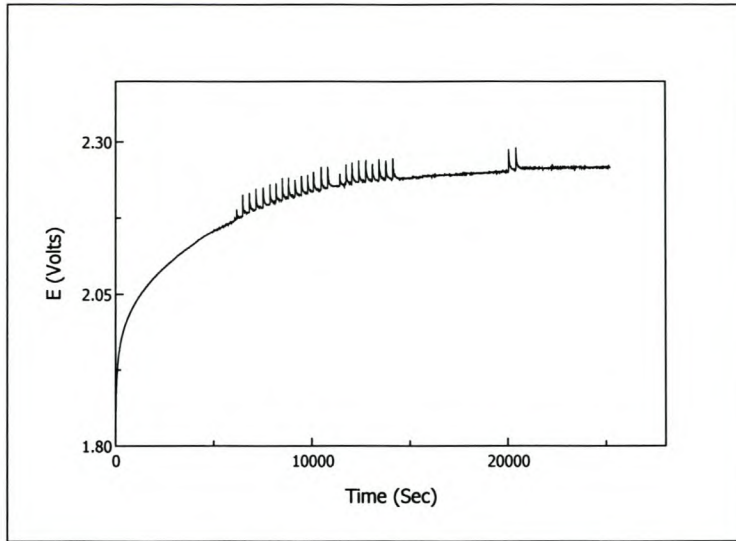


Figure 7.4. Typical plot for the anodic oxidation of water at a temperature of 33 °C for an applied current of 0.270A

The effect of different temperatures on cell potential at specific current densities for the anodic oxidation of water can be seen in Figure 7.5.

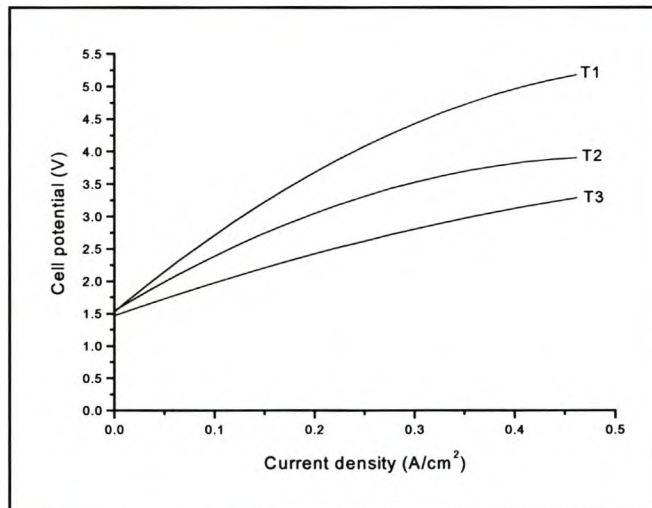


Figure 7.5. The effect of temperature on the anodic oxidation of water at temperatures of 33 °C (T1), 45 °C (T2) and 60 °C (T3)

7.1.3. Final remarks

It can be seen in Figure 7.5 that the cell potential decreases as the temperature in the membrane cell increases. This can be attributed to improved electrolyte conductivity of cation-exchange membranes, since the permeability of the membrane increases at high temperatures (Millet et al., 1990). Therefore, the increase in electrolyte

conductivity results in cell resistance decreasing and cell efficiency increasing. Further, this results in the decrease in electrode overpotentials (Ullmann, 1987).

The difficulty of determining the cell potential in the anodic oxidation of water increases with the increase in applied current. This was due to the continuous evolution of oxygen and hydrogen gas during the anodic oxidation of water (Fig. 7.6). Greater oxygen evolution can be attributed to an increase in the rate of the anodic oxidation of water.

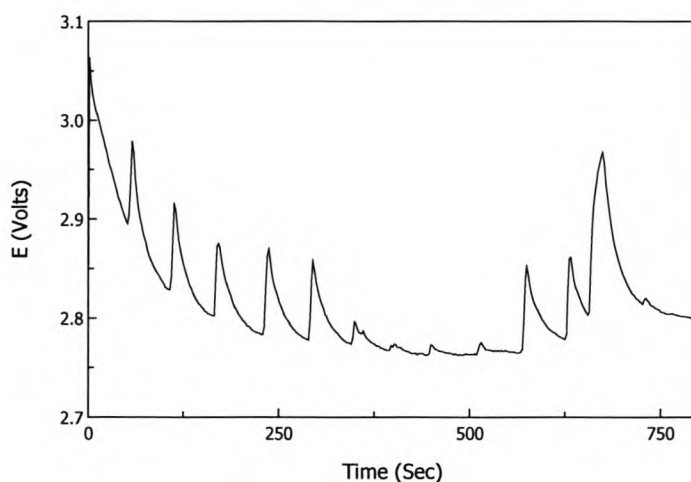


Figure 7.6. *Anodic oxidation of water by galvanostatic measurements with an applied current of 1.9A for 800 seconds at a temperature of 33 °C. The peaks represent the bursts of oxygen evolution.*

Galvanostatic measurements of the anodic oxidation of water showed that an increase in temperature results in a decrease in cell potential. This results in an increase in electrochemical cell efficiency due to increased electrolyte conductivity. Since the applications of electrocatalytic systems need to be economically viable, galvanostatic measurements provide valuable information on the electrochemical cell efficiency during electrocatalytic processes. The galvanostatic measurements of the anodic oxidation of water also showed that platinum-containing membranes are able to function well in the commercial process of oxygen and hydrogen evolution.

7.2. Development and validation of a method to study electrocatalytic reactions on a platinised membrane

This study involves the characterisation of platinised membranes by cyclic voltammetry. Since it is difficult to characterise a platinised membrane in a membrane reactor, a novel method was developed, for the investigation of the anodic oxidation of water. An important aspect of this new method is the use of a strip of Nafion between the reference electrode and the membrane.

7.2.1. Cyclic voltammetry of the anodic oxidation of water in the presence of aqueous sulphuric acid solution on flat platinum electrodes: spatial separation of the reference electrode from the working electrode

Two platinum electrodes were mounted in a beaker containing a solution of water and 10% sulphuric acid. The Ag/AgCl/[KCl(sat)] reference electrode was mounted in a 0.1N HCl solution in a separate container as shown in Figure 7.7. The reference electrode was linked to a potentiostat and coupled to a Luggin capillary. The potentiostat Solartron S1287 was used in the experiments. A strip of Nafion was used for electrical contact between the working electrode and reference electrode (Fig. 7.7). Cyclic sweep voltammograms at a scan rate of 100mV/sec were recorded for the solution of water at 298K.

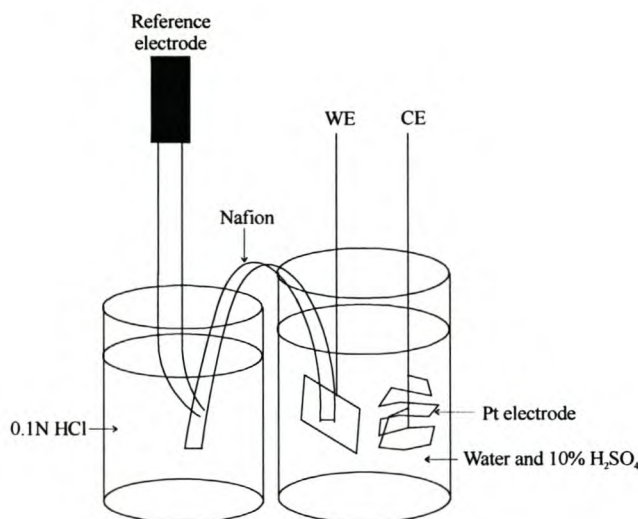


Figure 7.7. Schematic representation of experimental set-up used for cyclic voltammetry measurements in the electrolysis of water using a Ag/AgCl [KCl(sat)] electrode, working electrode (WE) and counter electrode (CE)

Figure 7.8 shows a cyclic voltammogram for the electrolysis of water at room temperature. The cyclic voltammogram exhibits a hydrogen adsorption peak (1), hydrogen evolution peak (2), oxygen reduction peak (3), oxygen evolution peak (4) and double layer charging (5) (Fig. 7.8).

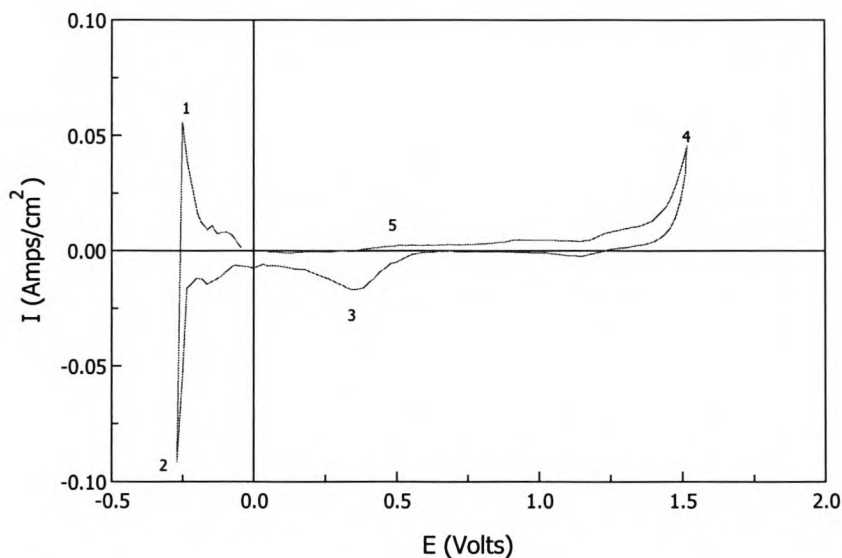
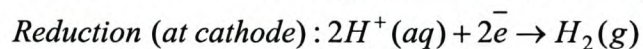
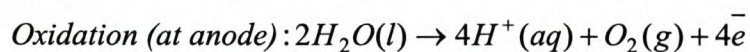


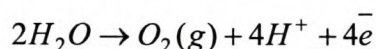
Figure 7.8. Cyclic voltammogram of the electrolysis of water at room temperature of a scan rate of 100mV/sec. Ag/AgCl/[KCl(sat)] was used as the reference electrode

7.2.2. Final remarks

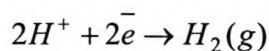
It can be seen in Figure 7.8 that the evolution of hydrogen occurs at potential -0.27V and the evolution of oxygen occurs at a potential of 1.53V. The overall reaction of the electrolysis of water can be represented as follows:



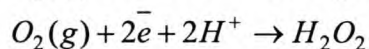
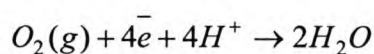
The reaction for the evolution of oxygen (Fig. 7.8_4) is as follows:



The reaction for the evolution of hydrogen (Fig. 7.8_2) is as follows:



The reaction for the reduction of oxygen (formation of PtO) (Fig. 7.8_3) can be represented as follows:



Hydrogen evolution occurs at a potential of 0.0V and oxygen evolution at 1.23V when using a standard hydrogen electrode (SHE). The results of water electrolysis with a Ag/AgCl/[KCl(sat)] reference electrode showed that hydrogen evolution occurs at a potential of -0.27V and oxygen evolution at 1.53V. These results show a potential difference of approximately 0.3V. This can be attributed to the decomposition potential always being higher than the ideal value due to ohmic drop (cell construction). Also, the difference in the potential between the standard hydrogen electrode (SHE) and Ag/AgCl/[KCl(sat.)] electrode is 0.2224 (Laidler et al., 1982). This explains the potential difference of 0.3V obtained.

It can be concluded from these results that cyclic voltammetric measurements can accurately be measured by using a strip of Nafion as an ion conductor. The following section investigates the possibility of reducing the drying of the Nafion strip during cyclic voltammetric measurements.

7.2.3. Characterisation of water electrolysis using SPE membranes at different temperatures by cyclic voltammetry

The SPE electrolysis of water at various temperatures was investigated by cyclic voltammetry. The reactor used in these experiments can be seen in Figure 7.9. The reactor consists of membrane holder, pressure regulator, cooling chambers, inlets and outlets for water and gas. Pumping water through the cooling chambers of the reactor regulated the temperature for the electrolysis of water. Platinum-containing membranes were placed in the membrane holder. The anodic oxidation of water was investigated for a membrane surface area of 5 cm² and a reactor pressure of 10 atm.

The Ag/AgCl/[KCl(sat)] reference electrode was mounted in 0.1N HCl solution. The reference electrode was linked to a potentiostat and coupled to a Luggin capillary. The potentiostat Solartron S1287 was used in the experiments. A strip of Nafion was used for electrical contact between the reference electrode and a platinum-containing membrane. In these experiments, the Nafion strip was encapsulated with a plastic sheath to prevent drying (Figure 7.10). The plastic sheath was moistened with

water, so as to prevent Nafion strip from drying. The platinum-containing membrane was inserted in the membrane cell (Figure 7.10).

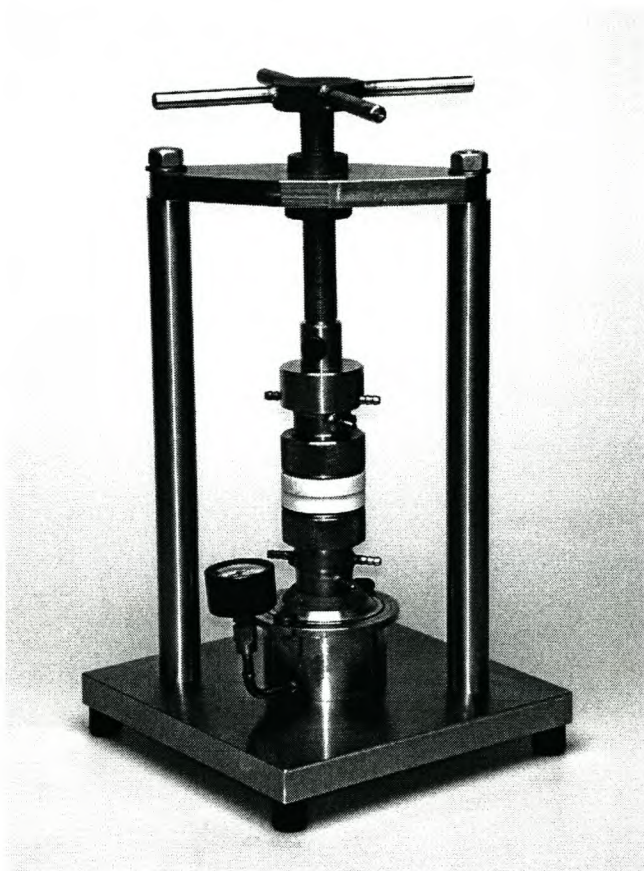


Figure 7.9. Reactor used in cyclic voltammetric measurements, which consists of a pressure regulator, membrane holder, cooling chambers and gas and water inlets and outlets.³

Cyclic sweep voltammograms were recorded at a scan rate of 100mV/sec for the electrolysis of water at temperatures 33 °C and 60 °C (Figure 7.11).

³ Reactor was provided by DINAX technologies, cc.

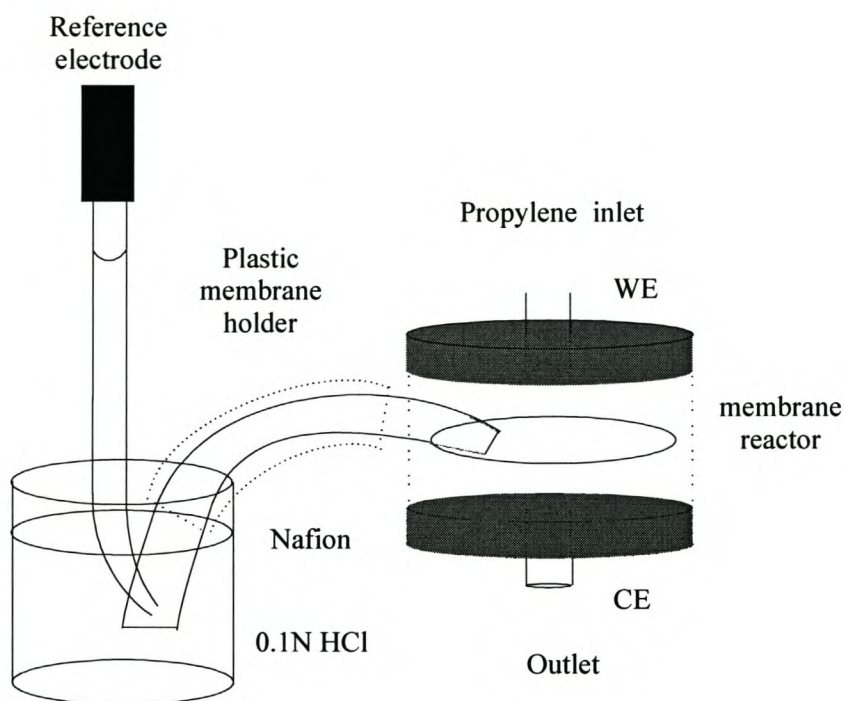


Figure 7.10. Schematic representation of experimental set-up used in electrolysis of water using Nafion. The reaction was investigated by cyclic voltammetric measurements using a Ag/AgCl/[KCl(sat)] electrode, working electrode (WE) and counter electrode (CE)

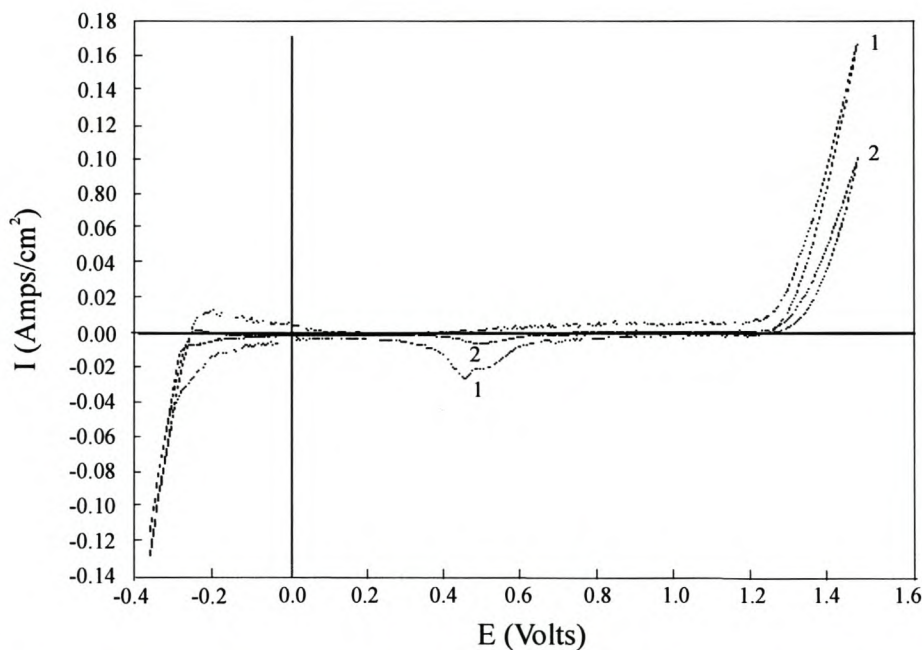


Figure 7.11. Cyclic voltammograms for the electrolysis of water at temperatures of 33 °C (2) and 60 °C (1)

7.2.4. Final remarks

The results of the cyclic voltammetric measurements of the anodic oxidation of water at 60 °C and 33 °C shows that the cyclic voltammograms are narrow. This can be attributed to a low current flow through the Nafion strip, which is due to the drying of Nafion. The results show that the anodic oxidation of water is sensitive to temperature with greater oxygen evolution being observed at higher temperatures (Fig. 7.11). This can be attributed to the increase in the reaction rate for the electrolysis of water with the increase in temperature (Fig. 7.11). The results also show that a lower cell potential is required at higher temperatures for oxygen evolution (Fig. 7.11) (see Section 7.1.2).

Cyclic voltammetry is a useful technique for studying electrocatalytic processes, such as the anodic oxidation of water. Information on the electrocatalytic reaction can be obtained by observing characteristic changes in the anodic and cathodic sweeps of a cyclic voltammogram.

7.3. Conclusions

The application of electrocatalytic membrane systems in processes, such as anodic oxidation of water, was successfully achieved. The efficiency of the electrocatalytic membrane system was investigated by galvanostatic measurements. Increased temperatures result in the increase in cell efficiency, as well as the decrease in cell potential.

The results exhibited potential values that were higher than the theoretical values for anodic oxidation of water. However, actual decomposition potential is always higher than the ideal value due to irreversible processes on the electrodes and ohmic drop (due to cell construction). Also, the difference in the potential of a standard hydrogen electrode (SHE) and a Ag/AgCl/[KCl(sat.)] electrode is 0.2224 (Laidler et al., 1982). This explains the higher potential values obtained for the anodic oxidation of water.

The electrochemical techniques of cyclic voltammetry and galvanostatic measurements provide valuable information for investigating electrocatalysis using electrocatalytic membrane systems.

References

1. Bessarabov DG, 2001, Electrochemically driven heterogeneous catalysis: oxidative strategy for petrochemical industry, 4th Annual UNESCO School and IUPAC Conference on Macromolecules and Materials Science, 7-11 April, Stellenbosch, South Africa
2. Laidler KJ and Meiser JH, Physical Chemistry, 1982, Benjamin/Cummings Publishing Company, Inc, USA
3. Millet P, Durand R and Pineri M, 1990, Preparation of New Solid Polymer Electrolyte Composites for Water Electrolysis, International Journal of Hydrogen Energy, 15, 4, 245-253
4. Nutall, 1977, Conceptual Design of Large Scale Water Electrocatalysis Plant using Solid Polymer Electrolyte Technology, International Journal of Hydrogen Energy, 2, 395-403
5. Ullmann, 1987, Electrochemistry, Ullmann's Encyclopaedia of Industrial Chemistry, Fifth Revised Edition, Vol. A 13, VHC publishers, Germany, p214

Quantification of Atomic Force Microscopy images of membrane surfaces embedded with platinum catalyst by statistical method

Abstract

The effect of various deposition conditions on the roughness profile of a platinum catalyst embedded on membranes was explored. Statistical methods were used for the quantification of the roughness profile using Atomic Force Microscopy images. Statistical analysis of various data sets by the Hurst exponent was investigated. Different approaches to surface roughness quantification were reviewed.

8.1. Introduction

The topographic structure of surfaces can be defined in terms of surface roughness, morphological factors and geometry. Furthermore, knowledge of the topographic structure of a surface can give quantitative insight into processes that produce a particular surface, such as: fracture, cluster aggregation, sputtering, electroless deposition, etc. (Kiely et al., 1997).

Experiments have shown that surface topography cannot be adequately described by means of statistical parameters, and that the corrugation of the surface height may have a broad bandwidth (Sayles et al., 1978; Yan et al., 1998; Herrasti et al., 1992). Non-regularities are inherent in thin film surfaces, which are observed by SEM, AFM and STM analyses as very sharp changes in local membrane surface density and other irregularities. Sharp jumps of local heights of surfaces of membranes and electrodes were obtained, for example, by various metal deposition techniques (Timashev et al., 2000).

It is important to acknowledge that the state of a membrane surface can determine various important characteristics of membranes, such as electrocatalytic activity, wetting behaviour, interface formation and film growth. This also includes the non-uniformity in distribution of hydrophobicity on a membrane surface, which may determine the hydrodynamic instability of the membrane in various membrane processes (such as, ED, UF, MF, etc) or fluctuation in membrane electrical surface resistance (Timashev et al., 2000).

Two factors that must be considered for understanding the electrochemical behaviour of solid electrodes are: the influence of the substrate crystallography and the topography of the electrode surface area on the kinetics of the electrocatalytic processes (Salvarezza et al., 1995). The outwardly observed electrocatalytic activity of metal particles is an aggregate effect of morphological factors (particle size and distribution), geometry (inter-atomic spacing, crystal structure), thermodynamic properties (surface energy, heat of adsorption), as well as the electronic state of the reactive site (valency) (Poirier et al., 1994).

It has been shown that the enhancement of the roughness factor of a SPE catalytic system improves the electrocatalytic activity of the catalyst system (Delime et al., 1998 and Zecevic et al., 1997). Thus, the quantification of the surface profile of electrocatalytic membranes is important. There are different approaches to quantifying the surface roughness of a membrane. Some of these methods will be explored in this chapter.

8.2. Regular and irregular solid surfaces

A surface can be defined as the boundary of an object in a three-dimensional Euclidean space. Regular surfaces consist of smooth surface domains. Irregular surfaces consist of weak and strongly disordered surfaces. Chemical and structural defects cause a solid surface to become irregular. Structural defects, such as pits, kinks and steps, can be formed when surfaces have been carefully prepared (e.g. by polishing or cleaning). Chemical defects are foreign molecules and atoms that are adsorbed onto solid surfaces. An example of this is when sulphur is electro-adsorbed onto highly orientated pyrolytic graphite (HOPG), which results in the electro-adsorbed sulphur atoms introducing a strong disorder to the substrate surface (Salvarezza et al., 1995).

8.3. Development of irregular surfaces

A variety of natural and industrial processes have led to the creation of irregular surfaces. Irregular surfaces can be produced by the addition, removal or re-ordering of material at the solid surface. Different methods used for the creation of irregular metal surfaces by the removal of material, includes, chemical dissolution, corrosion, grinding and polishing. Different methods used for the creation of irregular metal

surfaces by the addition of material include: crystal growth, vapour deposition, electrodeposition, chemical deposition, mechanical deposition, immersion deposition, sputter deposition and evaporation deposition (Salvarezza et al., 1995). The characteristics of metal deposits (e.g. by vapour deposition) depend strongly on the nature of the substrate, growth rate of metal deposits and the reaction temperature. Extensive research on surface roughness phenomena have been investigated on electrochemically deposited metals (Salvarezza et al., 1995).

8.4. Surface growth models

Atomistic and continuous models have been proposed to explain the development of irregular surfaces. In atomistic models, particles arrive at the substrate surface either by “ballistic trajectories” or “random walks”. Continuous models are based on Langevin-type equations (Salvarezza et al., 1995). Growth patterns predicted by these models can be compared with experimental data. The models also provide an explanation for the development of rough surfaces.

8.5. Experimental methods for the characterisation of irregular surfaces

Several methods have been proposed for the characterisation of irregular solid surfaces such as, molecular absorption, x-ray reflectivity, reflection high-energy electron diffraction (RHEED), transmission electron microscopy (TEM), scanning tunneling microscopy (STM), atomic force microscopy (AFM), scanning electron microscopy (SEM) and low-energy ion scattering (LEIS). Surface characterisation of rough surfaces has been attempted with optical microscopy, SEM and TEM images. These images provide only a projection of the surface topography while characterisation of the vertical dimension remains unknown. Atomic force microscopy (AFM), which is a specialised technique of scanning probe microscopy (SPM), has been used to characterise surfaces of brittle and ductile materials, as well as electrocatalytic SPE membranes. The use of AFM in surface roughness analysis provides many advantages, such as the use of AFM data to determine surface roughness by means of root-mean-square roughness (measure of the variation in height), autocovariance (measure of spatial correlation of heights) and power density (measure of wavelengths of periodic features) (Kiely et al., 1997).

In spite of the many advantages that AFM offers in surface roughness analysis, there are disadvantages associated with using AFM, such as inaccurate roughness analyses due to the imaging of artifacts (Kiely et al., 1997). Therefore, alternate methods for the quantitative determination of surface roughness have also been investigated, such as statistical methods for the characterisation of surface roughness.

8.6. Different statistical methods for surface roughness characterisation

8.6.1. Hurst exponent and its significance in the statistical analysis of various data sets¹

Consider an interval, or window, of length w in a trace. Within this window, one can define two quantities:

Firstly, $R(w)$, the range for the values of y in the interval. The range is measured with respect to a trend in the window, where the trend is estimated simply as the line connecting the first and the last points within the window. $R(w)$ subtracts the average trend in the window.

Secondly, $S(w)$, the standard deviation of the first differences delta y (dy) of the values of y within the window. The first differences of the y 's are defined as the differences between the values of y at some location x and y at the previous location on the x -axis (equation 8.1).

$$dy(x) = y(x) - y(x - dx) \quad (8.1)$$

where dx is the sampling interval, i.e. the interval between two consecutive values of x .

A reliable measurement of $S(w)$ requires data with a constant sampling interval dx , because the expected difference between successive values of y is a function of the distance separating them. $S(w)$ in the rescaled range (R/S) method² is used to standardize the range $R(w)$ to allow comparisons of different data sets. If $S(w)$ is not used, the range $R(w)$ can be calculated on data sets that have a non-constant sampling interval.

¹ The description of the method as described by Benoit software.

² The rescaled range was a statistical method invented by Hurst (Feder, 1989).

The rescaled range $R/S(w)$ is defined as:

$$\frac{R}{S}(w) = \left\langle \frac{R(w)}{S(w)} \right\rangle \quad (8.2)$$

where w is the window length and $\langle R(w) \rangle$ denotes the average of a number of values of $R(w)$. Due to the self-affinity, it is expected that the range taken by the values of y in a window of length w is proportional to the window length to a power equal to the Hurst exponent (H) as:

$$\frac{R}{S}(w) = w^H \quad (8.3)$$

In practice, for a given window length w , one subdivides the input series in a number of intervals of length w , measures $R(w)$ and $S(w)$ in each interval, and calculates $R/S(w)$ as the average ratio $R(w)/S(w)$ (equation 8.2). This process is repeated for a number of window lengths, and the logarithms of $R/S(w)$ are plotted versus the logarithms of w . If the trace is self-affine³, this plot should follow a straight line, where the slope equals the Hurst exponent. The fractal dimension of the trace can then be calculated from the relationship between the Hurst exponent (H) and the fractal dimension:

$$D_{rs} = 2 - H \quad (8.4)$$

where D_{rs} denotes the fractal dimension estimated from the rescaled range method.

The Hurst exponent (H) is defined as:

$$H = \log(R/S) / \log(T) \quad (8.5)$$

where T is the duration of the sampling of data, and R/S the corresponding value of rescaled range. In this way Hurst generalised an equation valid for the Brownian motion in order to include a broader class of time series. The generalisation proposed by Hurst is:

$$\frac{R}{S} = k * T^H \quad (8.6)$$

where k is a constant and T is time.

³ A series that scales time and distance by different factors.

Although the Hurst exponent⁴ was originally for application in time series, it is also applicable for energy series and spatial series (i.e. in our study of surface roughness). The Hurst exponent is able to describe the roughness of a surface while also providing spatial information. The Hurst Exponent is a robust statistical tool that is a useful measure of fractal distributions.

The following can be concluded from equation 8.6:

- If $H=0.5$, the behaviour of the time, energy and spatial data set is similar to a random walk (Fig. 8.1). A random walk is defined as the distance covered by a random particle undergoing random collisions from all sides (www.cbi.polimi.it/glossary/Hurst.html).

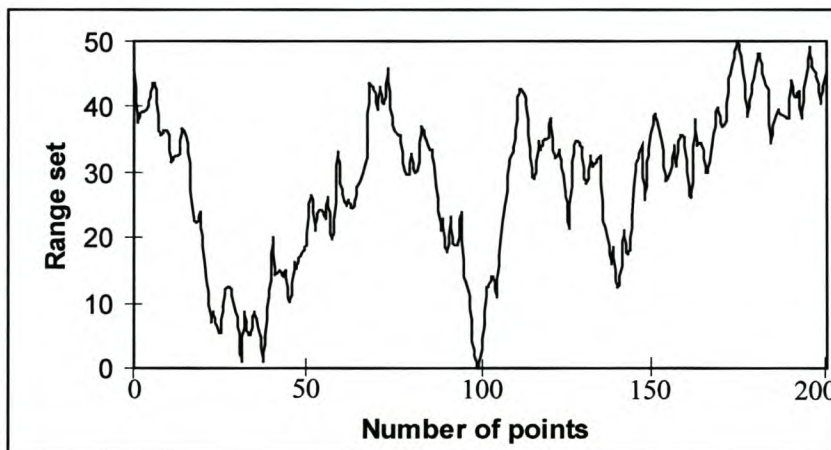


Figure 8.1. A typical curve showing the behaviour of a data set characterised by the Hurst exponent for $H=0.5$.⁵

- If $H<0.5$, the time, energy and spatial series covers less “distance” than a random walk (i.e. if the series increases, it is more probable that it will decrease and vice versa) (Fig. 8.2) (www.cbi.polimi.it/glossary/Hurst.html).

⁴ Hurst spent a lifetime studying the Nile and the problems related to water storage. He developed a new set of statistical tools that examine data that may not have an underlying Gaussian distribution.

⁵ The graph shown in Figure 8.1 was generated by the method used by the Benoit software for the following variables: data points=200, range of set=50 and $H=0.5$

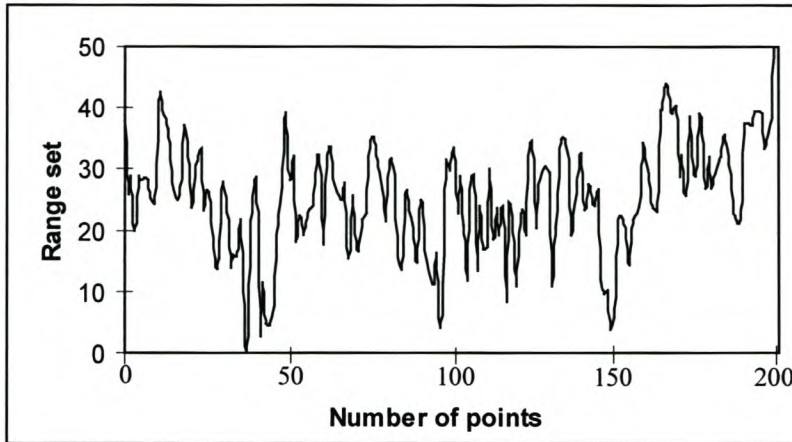


Figure 8.2. A typical curve showing the behaviour of a data set characterised by the Hurst exponent for $H < 0.5$.⁶

- If $H > 0.5$, the time, energy and spatial series covers more “distance” than a random walk (if the series increases, it is more probable that it will continue to increase) (Fig. 8.3) (www.cbi.polimi.it/glossary/Hurst.html).

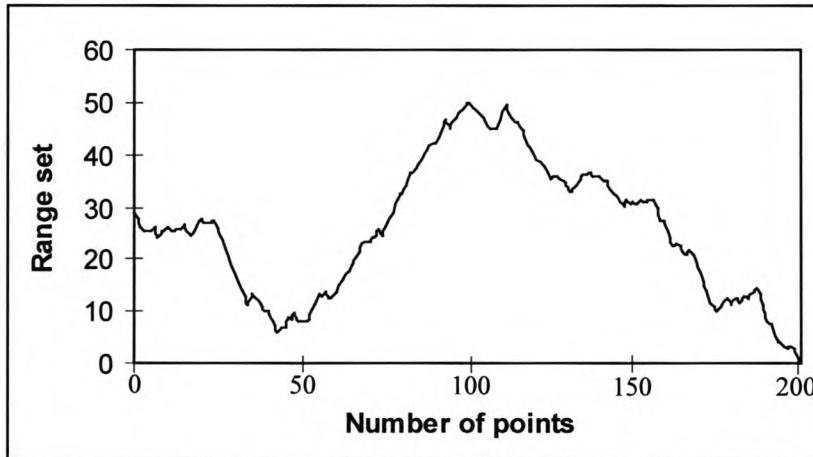


Figure 8.3. A typical curve showing the behaviour of a data set characterised by the Hurst exponent for $H > 0.5$.⁷

Since H is related to the fractal dimension D , the following equation can be formulated:

$$H = E + 1 - D \tag{8.7}$$

⁶ The graph shown in Figures 8.2 was generated by the method used by the Benoit software for the following variables: data points=200, range of set=50 and $H=0.1$

⁷ The graph shown in Figure 8.3 was generated by the method used by the Benoit software for the following variables: data points=200, range of set=50 and $H=0.9$

where E is the Euclidean dimension ($E=0$ for a point, 1 for a line, 2 for a surface). In one-dimensional signals, $H=2-D$.

8.6.2. Fractal description of surface disorders

Ordered surfaces can be described by Euclidean geometry. The dimensions of Euclidean geometrical objects such as, dots, lines, planes or bodies are generally classified according to fractal dimensions 0, 1, 2 and 3, respectively. However, not all natural and artificial geometrical objects fit this classification. These objects need to be assigned intermediate dimensional values. Fractal geometry was therefore developed, since Euclidean geometry is unable to describe disordered surfaces (Mandelbrot, 1982). A definition of a fractal is a shape made of parts similar to the whole in some way. The fractal dimension (Fd) of a surface (Marchese-Ragona et al., 1993):

- is characterised by only one number,
- can be correlated with observable phenomena such as cleanability, corrosion, adsorption, catalysis and degassing, and
- can often distinguish surfaces that other engineering parameters classify as being similar.

The minimum value of the fractal dimension for a line profile is 1.0. This describes a perfectly flat line that fills only a one-dimensional space (Fig. 8.4 A). The maximum value of the fractal dimension for a line profile is 2.0 (Fig. 8.4 B). This is for a line that is so rough that it forms a solid surface and consequently fills a two-dimensional space. In practice, the fractal dimension of a line profile is between 1.0 and 2.0 (Fig. 8.4 C). The minimum value of the fractal dimension for a surface contour is 2.0, which is a perfectly flat surface that fills only a two-dimensional space (Fig. 8.4 B). The maximum value of the fractal dimension for a surface contour is 3.0 (Fig. 8.4 E). In this case, the surface is so rough that it fills a three-dimensional space. In practice, the fractal dimension of a surface is between 2.0 and 3.0 (Fig. 8.4 F) (Marchese-Ragona et al., 1993 and Feder, 1989).

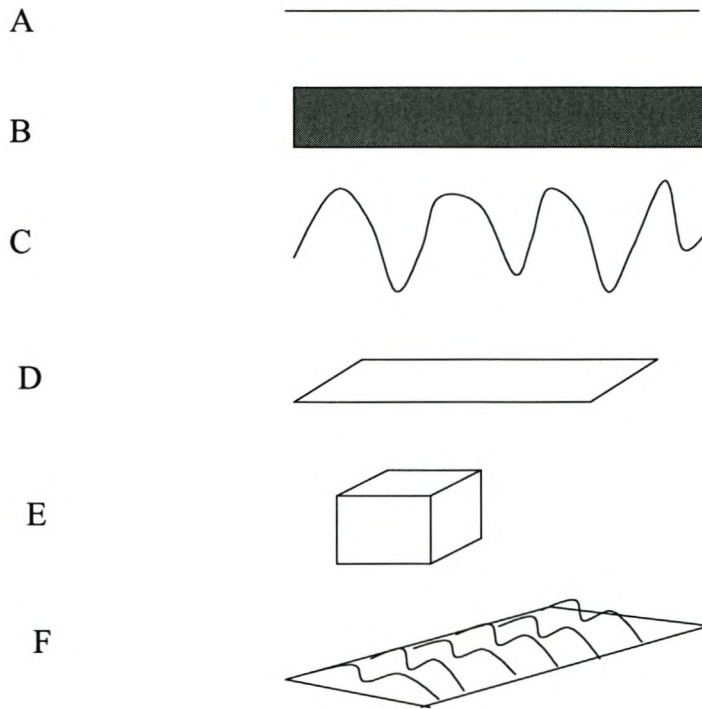


Figure 8.4. Schematic representation of surfaces with different fractal dimensions (F_d). F_d is 1.0 (A); F_d is 2.0 (B); F_d is between 1.0 and 2.0 (C); F_d is 2.0 (D); F_d is 3.0 (E); F_d is between 2.0 and 3.0 (F) (Marchese-Ragona et al., 1993).

According to fractal geometry, strongly disordered systems can be described by three classes of fractals, namely: surface fractal, mass fractal and pore fractal (Fig. 8.5).

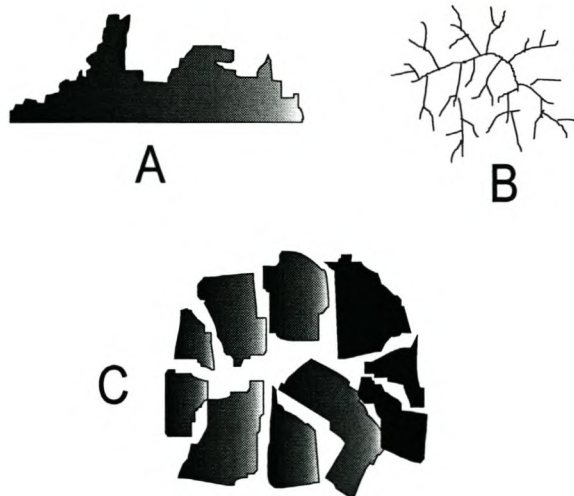


Figure 8.5. Schematic representation of different types of fractals: surface fractal (A), mass fractal (B) and pore fractal (C) (Salvarezza et al., 1995).

The surface of an object may result in a surface fractal (Fig. 8.5 A). Otherwise, the object itself and its surface may behave as fractals, in which case the object will correspond to a mass fractal (Fig. 8.5 B). A dense object that has a distribution of holes (pores) with a fractal structure is a pore fractal (Fig. 8.5 C) (Salvarezza et al., 1995).

There are several mathematical methods to calculate F_d . One of these methods is the perimeter-area method. This method is based on the fact that the intersection of a plane with a self-affine or self-similar fractal will generate self-similar lakes or islands. Lake perimeter and area relationships were established, which resulted in the formulation of the fractal description of a surface as:

$$L = \alpha D' A^{D'/2} \quad (8.8)$$

where L is the perimeter, A is the area, α is a constant and D' is the fractal dimension of the lakes coastlines. The fractal dimension of the three-dimensional surface (D) is related to D' , which can be represented as:

$$D = D' + 1 \quad (8.9)$$

8.6.3. Power spectrum

Jenkins and Watts (1968) defined a time series as a random or non-deterministic function x (i.e. behaviour cannot be predicted exactly) of an independent variable, t , which represents time. Different sections of a time series do not necessarily resemble each other in appearance, but when their average statistical properties are compared they are similar. Thus, it is necessary to describe the time series in terms of random variables and their associated probability distributions. The behaviour of a time series may be described as a set of random variables $\{X(t)\}$ where t can have any value from $-\infty$ to $+\infty$. A stochastic process may be defined as an ordered set of random variables $\{X(t)\}$ and its associated probability distribution. Therefore, an observed series $x(t)$ may be regarded as doubly infinite in that an infinite set of values is possible at each of an infinite number of time points.

In the present study the theory developed for a time series will be used to analyse a spatial series (i.e. platinum-containing membranes), which will provide information on the surface roughness profile of platinum-containing membranes (Pegram et al., 1995).

There are two broad categories of spatial series, namely, stationary and non-stationary series. Statistical properties of a stationary series are constant with time, as opposed to the changing properties of a non-stationary time series. Physical roughness data of platinum-containing membranes constitute a non-stationary spatial series, with the independent variable, l , representing distance in the direction of measurement from some arbitrary datum (Pegram et al., 1995).

Flicker-noise spectroscopy (FNS) is a general phenomenological theory of the analysis of the experimental time, spatial, and energy-dependent series, which allow for obtaining physical, non-model parameters that characterise the time evolution of every open non-linear dissipative system and determines its space or energy structure. Essential part of FNS includes analysis of data sets using power spectrum and structural functions (variograms). The basic assumption of the FNS method is that the sequence of non-regularities (bursts, jumps, discontinuities of derivatives, etc) is the essential elements of the evolution of any complex system. In other words, a generalised intermittency of the dynamic variable $V(t)$ at every temporal (spatial, energetic) level is assumed (Parkhutik et al., 2000(a)).

Applying the generalised function theory to the intermittent signals, power spectra and structural functions of different orders corresponding to the dynamic variable $V(t)$ can be obtained. It is supposed that the evolution process is a quasi-stationary stochastic one and that its statistical characteristics do not change in the course of time shift. This means that the autocorrelation function $\psi(\tau) = \langle V(t)V(t+\tau) \rangle$ depends only on τ and $\psi(\tau) = \psi(-\tau)$. In this case an equation for the Fourier transform $S(f)$ of the autocorrelation function (so-called “power spectrum”), in accordance with the Wiener-Khinchin theorem, was obtained (Timashev et al., 1999).

$$S(f) = 2 \int_0^{\infty} \cos(2\pi f\tau) d\tau \quad (8.10)$$

Another feature parameter of the FNS theory is a structural function (average difference moments) $\Phi_{(p)}(\tau)$ of the order p :

$$\Phi_{(p)}(\tau) = \langle |V(t) - V(t+\tau)|^p \rangle \quad (8.11)$$

The dependencies $S(f)$ and $\Phi_{(p)}(\tau)$ characterise the presence of correlation links in a sequence of individual events contributing to the noise (Parkhutik et al., 2000(a)).

In our study, the Benoit software uses the properties of power spectra of a self-affine trace. An estimate of the fractal dimension is obtained when calculating the power spectrum $P(k)$ (where $k=2p/l$ is the wavenumber, and l is the wavelength) and plotting the logarithm of $P(k)$ versus the logarithms of k . Plot of $\log[\text{power spectrum}]$ versus $\log[\text{frequency}]$ should follow a negative slope. The slope will be more than -1 and less than 1.

$$\text{slope} = 2H + 1 \tag{8.12}$$

The fractal dimension (D_s) can be determined using the slope of the plot as follows:

$$D_s = 2 - H \tag{8.13}$$

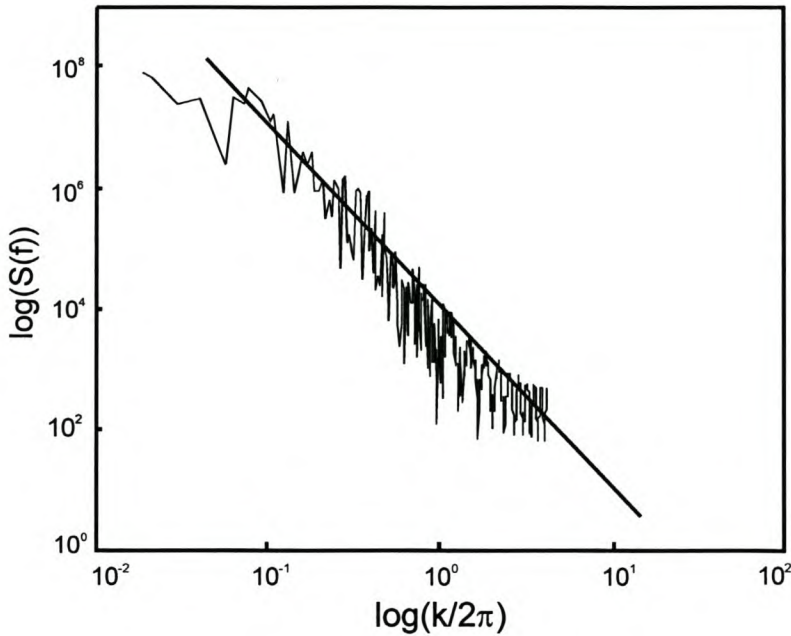


Figure 8.6. Typical power spectrum computed from roughness data of a membrane surface. k is the wavenumber.

8.6.4. Variograms

A variogram, also known as variance of the increments or structure function, is defined as the expected value of the squared difference between two y values in a

trace separated by a distance w . Thus, the sample variogram $V(w)$ of a series $y(x)$ is measured as follows:

$$V(w) = \langle [y(x) - y(x + w)]^2 \rangle \quad (8.14)$$

where, $V(w)$ is the average value of the squared difference between pairs of points at distance w . The distance of separation w is often referred to as the "lag".

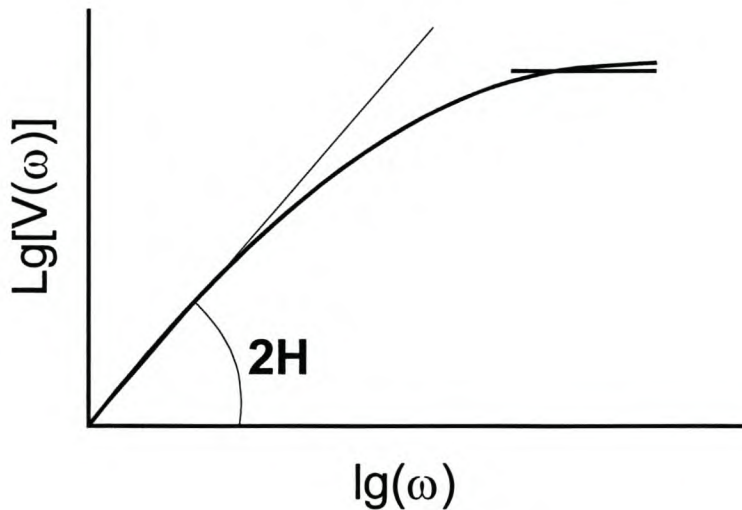


Figure 8.7. Curve representing a variogram of a series with relation to Hurst exponent (H).

If one takes a length span equal to w , the value of the difference between $y(w)$ and $y(0)$ will normally be distributed with a variance $s(w)^2$ (where s is the standard deviation), which is proportional to w^{2H} . The squared difference will result in an expected value of $s(w)^2$, which can be used to formulate an equation that demonstrates the relationship between $V(w)$ and the Hurst exponent (H):

$$V(w) \approx w^{2H} \quad (8.15)$$

In practice, to obtain an estimate of H , the average squared difference between all the pairs of points separated by a distance w is calculated as $V(w)$ in equation 8.15 for a number of window lengths, and the logarithms of $V(w)$ are plotted versus the logarithms of w . If the trace is self-affine, the plot should be a straight line with a slope that is twice the Hurst exponent (H). The fractal dimension of the trace can then be calculated from the relationship between the Hurst exponent (H) and the fractal dimension (D_v):

$$D_v = 2 - H \tag{8.16}$$

where D_v denotes the fractal dimension estimated from the variogram.

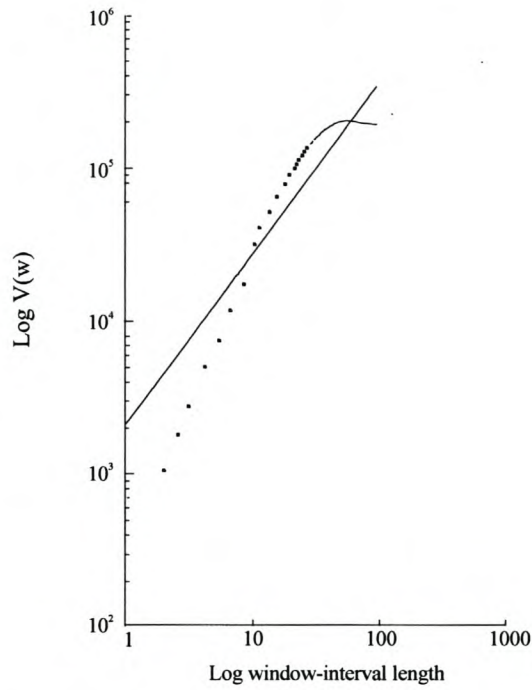


Figure 8.8. Typical curve representing a variogram of a platinum-containing membrane

8.6.5. Wavelets

Wavelet analysis, also known as localized spectral analysis, is a tool for analysing localised variations in power by decomposing a trace into time frequency space to determine both the dominant modes of variability and the extent to which these modes vary in time. Wavelet transform of the signal $V(t)$ with chosen basic function $\varphi(t)$ is given by:

$$W_v(s, \tau) = |a|^{-12} \int_{-x}^x V(t) \varphi\left(\frac{t - \tau}{s}\right) dt \tag{8.17}$$

where $W_v(s, \tau)$ is a wavelet coefficient, s is a scale coefficient (inversely proportional to the frequency) and τ is a shift parameter. A wide range of functions may be used as basic or ‘mother’ wavelets. Most widely used is the second derivative of the Gauss function:

$$\varphi(z) = (1 - z^2) \exp(-z^2 / 2) \tag{8.18}$$

and the Morlet wavelet:

$$\varphi_{k_o}(z) = \exp(ik_o z) \exp(-z^2 / 2) \tag{8.19}$$

where k_o is a specific oscillation parameter (Parkhutik et al., 2000(b)).

This method is appropriate for the analysis of non-stationary traces, which is where the variance does not remain constant with the increasing length of the data set. Fractal properties are present where the wavelet power spectrum is a power law function of frequency. The wavelet method is based on the property that wavelet transforms of the self-affine traces have self-affine properties.

8.6.5.1. Description of Benoit algorithm for calculation of Hurst exponent

Consider n wavelet transforms each with a different scaling coefficient a_i , where S_1, S_2, \dots, S_n are the standard deviations from zero of the respective scaling coefficients a_i .

Define the ratio of the standard deviations G_1, G_2, \dots, G_{n-1} as:

$$G_1=S_1/S_2, G_2=S_2/S_3, \dots, G_{n-1}=S_{n-1}/S_n$$

Estimate the average value of G_i as⁸:

$$G_{avg} = \frac{\sum_{i=1}^{n-1} G_i}{n-1} \tag{8.20}$$

The Hurst exponent is:

$$H = f(G_{avg}) \tag{8.21}$$

where f is a heuristic function which approximates the Hurst exponent by G_{avg} for stochastic self-affine traces. The fractal dimension (D_w) is:

$$D_w = 2 - H \tag{8.22}$$

8.6.6. Standard roughness average (R_a)⁹

The standard roughness average is the arithmetic average of the absolute values of the measured profile height deviations (equation 8.23).

$$R_a = \frac{1}{n} \sum_{i=0}^N |Z_i - \bar{Z}| \dots\dots\dots \tag{8.23}$$

⁸ Benoit sets $n=4$ and $a_i=2i$ for $i=0,1,2,3$. The mother wavelet in Benoit is a step function.

⁹ Description of algorithm is according to method used by AFM software of Topometrix

where n is the total number of points in the image matrix. Z_i is the height of the i -th point, which can be represented as follows:

$$\bar{Z} = \frac{1}{n} \sum_{i=0}^N Z_i \quad (\text{average height}) \quad (8.24)$$

The standard roughness average is used in the AFM software of Topometrix TM×2000 AFM.

8.6.7. Root-mean-square surface roughness (R_{RMS})¹⁰

The root-mean-square surface roughness is based on the concept of the standard deviation of the height, which describes the spread of the height distribution about the mean value (equation 8.25). The root-mean-square surface roughness can be represented as follows:

$$R_{RMS} = \sqrt{\frac{\sum (Z_i - \bar{Z})^2}{L_s}} \quad (8.25)$$

where L_s is the length measured along a AFM scan length containing a pre-determined number of data points (in our case, 1000 data points). Z_i is the height of the i -th point (equation 8.24).

The root-mean-square can also be determined from the power spectral density (PSD) (Topometrix AFM manual).

8.7. Quantification of the surface roughness profile of platinum-containing membranes¹¹

8.7.1. Protocol for the determination of the roughness profile of a platinum-containing membrane

Topometrix AFM software was used to obtain AFM images of the profile of platinum-containing membranes. 10 line profiles of each AFM image was analysed¹². This methodology of using line profiles makes it possible to analyse AFM images containing artifacts, as the parts of the image containing artifacts can manually be avoided. An example of a line profile of an AFM image for a platinum-containing

¹⁰ Description of algorithm is according to method used by AFM software of Topometrix

¹¹ Surface roughness calculations of platinum-containing membranes, which were determined with Benoit software by the analysis of AFM images using Topometrix AFM software.

¹² In chapter 4, the surface roughness data was determined from the total area of the AFM image and not by using the line profile methodology as in this chapter.

membrane can be seen in Figure 8.9. The data was transferred to Excel software as an import file for use by Benoit software. Each of the 10 line profiles was analysed with Benoit software. The average of these 10 line profiles for power spectrum, variograms and wavelet analysis was calculated, as well as the percentage deviation for each analysis.

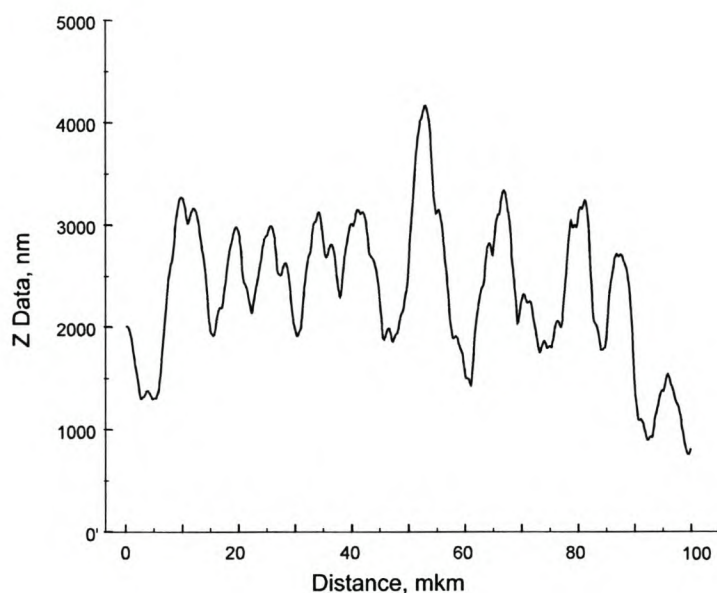


Figure 8.9. *Typical vertical line profile of a membrane sample obtained from an AFM image*

8.7.2. Results of surface roughness quantification of platinum-containing membranes

The results of the surface roughness quantification of platinum-containing membranes for power spectrum, variogram and wavelet analyses are tabulated in Tables 8.1-8.9.¹³ The percentage deviation of power spectrum, variogram and wavelet analyses was calculated to determine the accuracy of the different analysis for surface roughness quantification.

¹³ These results were obtained by using Benoit software.

Table 8.1. Hurst exponent of membranes embedded with platinum when 0.05M platinic acid solution was reduced by hydrazine at various time intervals.¹⁴ The Hurst exponent was determined using AFM images of scan area 20 μ m \times 20 μ m.

Time of reduction of 0.05M platinic acid solution by N ₂ H ₄ (min)	Hurst exponent as determined by power spectrum*	Hurst exponent as determined by variogram*	Hurst exponent as determined by wavelets*
3.5	0.75	0.63	0.74
5.5	0.50	0.90	0.93
7.5	0.44	0.87	0.95
9.5	0.50	0.78	0.80
12.5	0.61	0.75	0.69
15.5	0.63	0.80	0.80

Table 8.2. Percentage deviation of Hurst exponent (of 10 line profiles) of membranes embedded with platinum when 0.05M platinic acid solution was reduced by hydrazine at various time intervals. Results were determined from AFM images of scan areas of 20 μ m \times 20 μ m.

Time of reduction of 0.05M platinic acid solution by N ₂ H ₄ (min)	Percentage deviation of Hurst exponent for power spectrum	Percentage deviation of Hurst exponent for variogram	Percentage deviation of Hurst exponent for wavelet
3.5	22.97	7.45	7.88
5.5	16.71	2.94	6.09
7.5	9.22	3.78	4.87
9.5	13.38	4.46	8.56
12.5	20.65	10.31	10.08
15.5	20.15	6.33	6.94

¹⁴ See section 8.7.1

* Benoit software was used to determine the Hurst exponent by variogram, power spectrum and wavelet analyses.

Table 8.3. Results of surface roughness characterisation of membranes embedded with platinum when 0.05M platinic acid solution was reduced by hydrazine at various time intervals. Results were determined from AFM images of scan areas of $20\mu\text{m}\times 20\mu\text{m}$.¹⁵

Time of reduction of 0.05M platinic acid solution by N_2H_4 (min)	R_a	R_{RMS}	$FD^{PS\#}$	$FD^{vario\#}$	$FD^{wavet\#}$	$FD^{line\spadesuit}$	$FD^{area\vee}$
3.5	99.14	128.24	1.25	1.37	1.26	1.30	2.71
5.5	402.40	484.90	1.50	1.10	1.07	1.20	2.43
7.5	632.87	864.18	0.83	1.51	1.22	1.38	2.78
9.5	288.28	242.31	1.50	1.22	1.2	1.2	2.51
12.5	94.27	118.31	1.39	1.25	1.31	1.22	2.41
15.5	94.43	148.31	1.37	1.20	1.20	1.22	2.34

Table 8.4. Hurst exponent of membranes embedded with platinum when 0.05M platinic acid solution was reduced by sodium borohydride at various time intervals. The Hurst exponent was determined using AFM images of scan area $130\mu\text{m}\times 130\mu\text{m}$.

Time of reduction of 0.05M platinic acid solution by NaBH_4 (min)	Hurst exponent as determined by power spectrum	Hurst exponent as determined by variogram	Hurst exponent as determined by wavelets
3.5	0.72	0.50	0.92
5.5	0.92	0.43	0.88
7.5	0.71	0.31	0.86
9.5	0.87	0.22	0.87
12.5	0.91	0.43	0.88
15.5	0.75	0.50	0.92

¹⁵ See section 8.7.1

[#] Fractal dimension was determined by using the Hurst exponent in the following equation: $FD=2-H$. (PS =power spectrum, $wave$ =wavelet and $vario$ =variogram)

^{*} Fractal dimension was determined by the line profile method, which uses the box-counting method (Topometrix AFM software).

[∨] Fractal dimension of a surface of a membrane embedded with platinum was determined by the lake-filling method (Topometrix AFM software).

Table 8.5. Percentage deviation of Hurst exponent (of 10 line profiles) of membranes embedded with platinum when 0.05M platinic acid solution was reduced by sodium borohydride at various time intervals. Results were determined from AFM images of scan area $130\mu\text{m}\times 130\mu\text{m}$.

Time of reduction of 0.05M platinic acid solution by NaBH_4 (min)	Percentage deviation of Hurst exponent for power spectrum	Percentage deviation of Hurst exponent for variogram	Percentage deviation of Hurst exponent for wavelets
3.5	19.49	8.90	9.02
5.5	22.12	22.98	4.05
7.5	25.30	12.07	10.74
9.5	18.87	10.06	5.16
12.5	20.32	23.76	6.87
15.5	23.07	19.19	6.07

Table 8.6. Results of surface roughness characterisation of membranes embedded with platinum when 0.05M platinic acid solution was reduced by sodium borohydride at various time intervals. Results were determined from AFM images of scan area $130\mu\text{m}\times 130\mu\text{m}$.

Time of reduction of 0.05M platinic acid solution by NaBH_4 (min)	R_a	R_{RMS}	$FD^{PS\#}$	$FD^{vario\#}$	$FD^{wave\#}$	$FD^{line\spadesuit}$	$FD^{area\vee}$
3.5	474.21	474.83	1.38	1.50	1.08	1.42	3.06
5.5	404.04	544.56	1.08	1.57	1.12	1.45	2.86
7.5	94.85	129.05	1.29	1.69	1.14	1.43	3.00
9.5	313.4	413.31	1.13	1.78	1.13	1.55	2.94
12.5	517.9	758.78	1.09	1.57	1.12	1.46	2.76
15.5	474.21	684.78	1.25	1.50	1.08	1.42	2.40

[#] Fractal dimension was determined by using the Hurst exponent in the following equation: $FD=2-H$. (PS =power spectrum, $wave$ =wavelet and $vario$ =variogram)

[♦] Fractal dimension was determined by the line profile method, which uses the box-counting method (Topometrix AFM software).

[∨] Fractal dimension of a surface of a membrane embedded with platinum was determined by the lake-filling method (Topometrix AFM software).

Table 8.7. Hurst exponent of membranes embedded with platinum when 0.03M platinic acid solution was reduced by sodium borohydride at various time intervals. Hurst exponent was determined from AFM images of scan area $130\mu\text{m}\times 130\mu\text{m}$.

Time of reduction of 0.03M platinic acid solution by NaBH_4 (min)	Hurst exponent as determined by power spectrum	Hurst exponent as determined by variogram	Hurst exponent as determined by wavelets
3.5	0.93	0.38	0.90
11.5	0.89	0.55	0.64
15.5	0.86	0.36	0.94
25.5	0.82	0.63	0.58
35.5	0.95	0.62	0.64

Table 8.8. Percentage deviation of Hurst exponent (of 10 line profiles) of membranes embedded with platinum when 0.03M platinic acid solution was reduced by sodium borohydride at various time intervals. Results were determined from AFM images of scan area $130\mu\text{m}\times 130\mu\text{m}$.

Time of reduction of 0.03M platinic acid solution by NaBH_4 (min)	Percentage deviation of Hurst exponent for power spectrum	Percentage deviation of Hurst exponent for variogram	Percentage deviation of Hurst exponent for wavelets
3.5	23.68	13.75	6.42
11.5	31.71	14.92	5.94
15.5	13.25	18.14	5.19
25.5	41.88	8.15	8.05
35.5	24.87	9.46	11.71

Table 8.9. Results of surface roughness characterisation of membranes embedded with platinum when 0.03M platinic acid solution was reduced by sodium borohydride at various time intervals. Results were determined from AFM images of scan area $130\mu\text{m}\times 130\mu\text{m}$.

Time of reduction of 0.03M platinic acid solution by NaBH_4 (min)	R_a	R_{RMS}	$\text{FD}^{\text{PS}\#}$	$\text{FD}^{\text{vario}\#}$	$\text{FD}^{\text{wave}\#}$	$\text{FD}^{\text{line}\diamond}$	$\text{FD}^{\text{area}\vee}$
3.5	344.02	513.49	1.07	1.62	1.10	1.45	2.58
11.5	412.86	536.59	1.11	1.45	1.36	1.38	2.53
15.5	449.13	663.20	1.14	1.64	1.06	1.46	2.71
25.5	962.65	1238.14	1.18	1.37	1.42	1.32	2.72
35.5	754.19	980.35	1.05	1.38	1.36	1.30	2.70

8.8. Discussion

The various analyses used for determining the Hurst exponent, such as variogram, power spectrum and wavelet, exhibited results that were both similar and different. This is attributed to the analyses having different degrees of error (Accuracy of different traces is provided by Benoit software). The determination of the surface roughness profile by wavelet analysis exhibit the greatest accuracy compared with variogram and power spectrum analyses. This can be seen in the percentage deviation results for power spectrum, variogram and wavelet analyses (Tables 8.2, 8.5 and 8.9).

The Hurst exponent (H) for the surface of membranes embedded with platinum when 0.05M platinic acid solution was reduced by hydrazine, as well as sodium borohydride and when 0.03M platinic acid solution was reduced by sodium borohydride, resembles a series that covers more “distance” than a random walk. This can be seen in Tables 8.1, 8.4 and 8.7, which show that $H > 0.5$. Thus, with the increase in height of the platinum catalyst on the surface of the membrane, the greater the probability that it will continue to increase in height (and vice versa) (Fig. 8.3).

[#] Fractal dimension was determined by using the Hurst exponent in the following equation: $FD = 2 - H$. (PS=power spectrum, wave=wavelet and vario=variogram)

[♦] Fractal dimension was determined by the line profile method, which uses the box-counting method (Topometrix AFM software).

[∨] Fractal dimension of a surface of a membrane embedded with platinum was determined by the lake-filling method (Topometrix AFM software).

The R_a and R_{RMS} values for membranes embedded with platinum when 0.05M platinic acid solution was reduced by hydrazine, decreases with an increase in deposition time (Tables 8.3). The decrease in the roughness of the surface of a platinum-containing membrane can be attributed to the smoothing of the platinum catalyst surface with the increase in thickness of the platinum catalyst on the membrane.

The R_a and R_{RMS} values for membranes embedded with platinum when either 0.05M or 0.03M platinic acid solution was reduced by sodium borohydride, fluctuates greatly. However, the trend exhibited by R_a and R_{RMS} is that of a gradual increase with the increase in deposition time (Tables 8.6 and 8.9). Thus, an increase in the roughness of the surface of the platinum catalyst on the membrane is observed.

The fractal dimension values determined by variogram, power spectrum and wavelet analyses are similar to the fractal dimension values determined by the line profile method (Tables 8.3, 8.6 and 8.9). The fractal dimension results obtained by line profile are between 1 and 2. Since a surface with $FD=1$ is featureless and a surface with $FD=2$ is extremely rough, these surfaces with FD values between 1 and 2 can therefore be described as moderately rough (Marchese-Ragona et al., 1993). The fractal dimension results obtained by the Lake-filling method for surfaces of platinum-containing membranes are between 2 and 3 (Tables 8.3, 8.6 and 8.9). Again, these results show that these surfaces are so rough that they fill a three-dimensional space (Marchese-Ragona et al., 1993).

Small scan areas are not an accurate description of a roughness profile of a sample. Larger scan areas are able to provide greater information on the general trend of the roughness profile of a sample. Kiely et al (1997) has showed that surface roughness is scale dependent, since R_{RMS} increases with the increase in scan area. However, in Fig. 8.10 it can be seen that the scan area at which R_{RMS} becomes scale independent can be identified as the largest characteristic measurement length of the surface (L_4) (Kiely et al., 1997). Thus, larger scan areas are able to provide results of greater accuracy as R_{RMS} becomes increasingly scale independent with the increase in the measured length of surface.

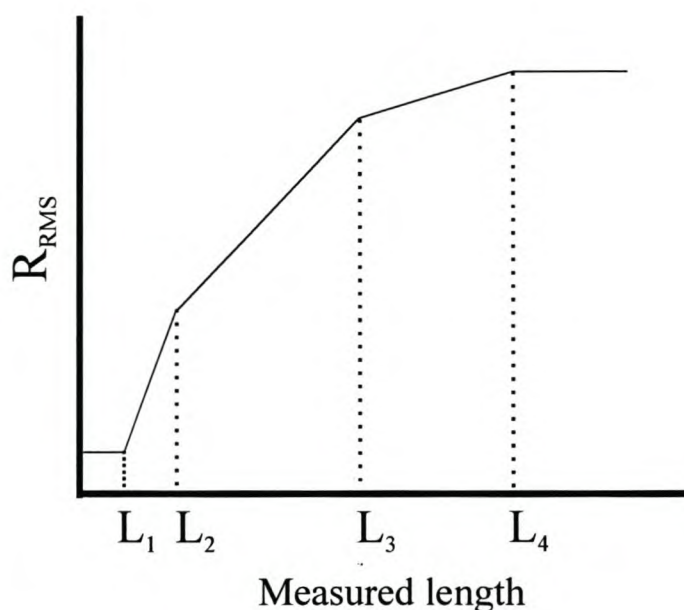


Figure 8.10. Schematic representation of the dependence of R_{RMS} on the measured length (scan area) of a surface (Kiely et al., 1997).

The results of membranes deposited with platinum by the reduction of 0.05M platinum acid with hydrazine was calculated using AFM images of the measured length (scan area) of $20\mu\text{m}\times 20\mu\text{m}$. The AFM images of scan area of $130\mu\text{m}\times 130\mu\text{m}$ could not be used in this case due to the presence of artifacts in these images. Artifacts result when the membrane surface profile is very rough. The results using AFM images of scan area $20\mu\text{m}\times 20\mu\text{m}$ may not be as accurate as with scan areas of $130\mu\text{m}\times 130\mu\text{m}$, since a smaller scan area provides less information on the general trend of the surface roughness profile. However, the results with smaller scan areas are able to provide valuable information on surface roughness although they are largely scale dependent (Kiely et al., 1997).

8.9. Conclusions

The determination of the Hurst exponent, fractal dimension and average roughness provides information on the surface roughness profile of the platinum catalyst embedded on membranes. This information is valuable as it provides a qualitative analysis of the platinum catalyst on the membrane under various deposition conditions.

The Hurst exponent results provide qualitative information on the surface of a platinum catalyst in terms of the distance covered by a random particle undergoing

random collisions from all sides (“random walk”). The R_a and R_{RMS} results show that platinum acid solution reduced by sodium borohydride produces a surface profile that exhibits greater roughness than when using hydrazine. The fractal dimension results determined by the line profile and lake-filling methods show that the surface profile of the platinum catalyst is very rough.

The quantification of the roughness profile of a platinum catalyst surface by various statistical methods is useful for the characterisation of surfaces as it provides a possibility of distinguishing reliably the features of one catalytic membrane surface from another. This method of surface quantification can be valuable for constructing a database of information on the surface roughness profile of a platinum catalyst embedded on a membrane under specific deposition conditions, which can be useful for the preparation of electrocatalytic SPE membranes with specific roughness properties (Timashev et al., 2000).

The mathematical methods used in this chapter are very limited. It could explain the less consistent results obtained. Thus, continued research in this field, such as by Timashev et al. (1999 and 2000) and others, are important for developing an adequate method for the mathematical treatment of such data.

References

1. Chesters S, Wang HC and Kasper G, 1990, A fractal-based method for describing surface roughness and texture, Proceedings of the Institute of Environmental Sciences, USA
2. Delime F, Leger JM and Lamy C, 1998, Optimization of platinum dispersion in Pt-PEM electrodes: Application to the electro-oxidation of ethanol, Journal of Applied Electrochemistry, 27-35
3. Feder J, 1989, Fractals, Plenum Press, New York, 283 pages
4. Herrasti P, Ocon P, Vazquez L, Salvarezza RC, Vara JM and Arvia AJ, 1992, Scanning-tunneling-microscopy study on the growth mode of vapour-deposited gold films, Phys. Rev. A, 45, 7440-7447
5. Kiely JD and Bonnel DA, 1997, Quantification of topographic structure by scanning probe microscopy, Journal of Vacuum Science and Technology B, 15, 4, 1483-1493
6. Mandelbrot BB, 1982, The fractal geometry of nature, WH Freeman, New York

7. Marchese-Ragona SP and Christie B, 1993, Surface characterization using fractal analysis, Topometrix technical notes, No. 2-0493-009
8. Parkhutik V and Timashev S, 2000(a), Kinetics of porous silicon growth studied using flicker-noise spectroscopy, *Journal of Applied Physics*, 87, 10, 7558-7566
9. Parkhutik V, Budnikov E.Yu and Timashev SF, 2000(b), Application of flicker-noise spectroscopy in studies of porous silicon growth and properties, *Materials Science and Engineering*, B69-70, 53-58
10. Pegram GGS and Pennington MS, 1995, A method for estimating the hydraulic roughness of unlined bored tunnels, Report to the Water Research Commission by the Department of Civil Engineering, University of Natal, WRC Report No. 579/1/96
11. Priorier JA and Stoner GE, 1994, Microstructural effects on electrocatalytic oxygen reduction activity of nano-grained thin-film platinum in acid media, *Journal of Electrochemical Society*, 141, 2, 425-430
12. Salvarezza RC and Arvia AJ, 1995, Modern aspects of electrochemistry, No. 28, edited by Conway BE et al., Plenum Press, New York
13. Sayles RS and Thomas TR, 1978, Surface topography as a non-stationary random process, *Nature*, 271, 431-434
14. Timashev SF, Bessarabov DG, Sanderson RD, Marais S and Lakeev SG, 2000, Description of non-regular membrane structures: novel phenomenological approach, *Journal of Membrane Science*, 170, 191-203
15. Timashev SF, Budnikov E.Ya, Klochikhin VI, Kostuchenko IG, Lakeev SG and Maximychev A, 1999, Mathematical models of the non-linear excitations, transfer, dynamics, control in condensed systems and other media, edited by Uvarova, Plenum, New York, 17-50
16. Yan W and Komvopoulos K, 1998, Contact analysis of elastic-plastic fractal surfaces, *Journal of Applied Physics*, 84, 3617-3624
17. Zecevic SK, Wainright JS, Litt MH, Gojkovic S.Li and Savinell RF, 1997, Kinetics of O₂ reduction on a Pt electrode covered with a thin film of solid polymer electrolyte, *Journal of Electrochemical Society*, 144, 9, 2973-2982

Electronic references

1. www.cbi.polimi.it/glossary/Hurst.html, Hurst exponent

2. www.zebra.net/~Idmcjr/dsmcl/FMH/hurst.html, The Hurst exponent and fractal structure

Considerations for future research into the use of solid polymer electrocatalytic membrane systems

Abstract

Examples of electrocatalytic processes using immobilised phosphoric liquid membranes (ILM) are reviewed. The similarity of the catalytic design of ILM with electrocatalytic SPE membranes is discussed. The possibility of using SPE electrocatalytic systems in electrocatalytic processes designed for ILM is discussed. The feasibility of binary catalyst systems, as well as the application of modified membranes embedded with platinum catalyst, is also discussed.

9.1 Electrocatalytic immobilised phosphoric liquid membranes (ILM)

Electrocatalytic SPE membrane systems are similar to immobilised phosphoric liquid membranes in their design. Since electrochemical cell reactions consist of electron transfer or oxidation-reduction reactions between substrates and catalysts, catalytic systems can be designed according to these electrochemical cell reactions (Otsuka, 1997(a)). Thus, both these membrane systems consist of four catalytic elements, namely: (1) oxidation site, (2) reduction site, (3) proton conducting element and (4) electron conducting element. The anode and cathode reactions are electrochemically connected by proton and electron conducting elements (Otsuka, 1997(a)).

Immobilised phosphoric liquid membranes (ILM) have been used in electrocatalytic processes such as: synthesis of aldehydes, selective hydrogenation of nitric oxide, partial oxidation of light alkanes and olefins and epoxidation of olefins during water electrolysis. Since these electrocatalytic processes are important for industrial processes and organic synthesis, these electrocatalytic processes, as well as ILM systems will be reviewed. These applications are of particular importance since they can be extended to electrocatalytic SPE membrane systems, which are similar in design to ILM. This chapter will discuss some of the applications of ILM systems in the light that these applications can be extended to SPE electrocatalytic membranes.

9.1.1. Wacker-type catalytic systems

The Wacker-type oxidation is important industrially because it is used to make approximately 4 million tons of aldehydes from alkenes annually. It has been known for more than a hundred years that PdCl_2 oxidises ethylene to acetaldehyde, but it has only been used as a catalytic reaction since the 1950s. The Wacker process involves, namely, (1) the reaction of ethylene with water to form acetaldehyde, where the Pd(II) complex is converted to the Pd(0) complex and (2) re-oxidation of the Pd(0) complex to Pd(II) to complete the catalytic cycle (Fig. 9.1) (Siegbahn, 1995). The Wacker reaction consists of the following catalytic elements:

1. Catalyst for oxidation: Pd^{2+}
2. Catalyst for reduction: Cu^{2+}
3. H^+ conductor: HCl (aq.)
4. e^- conductor: $\text{Pd}^{2+}/\text{Pd}^0/\text{Cu}^{2+}/\text{Cu}^+$

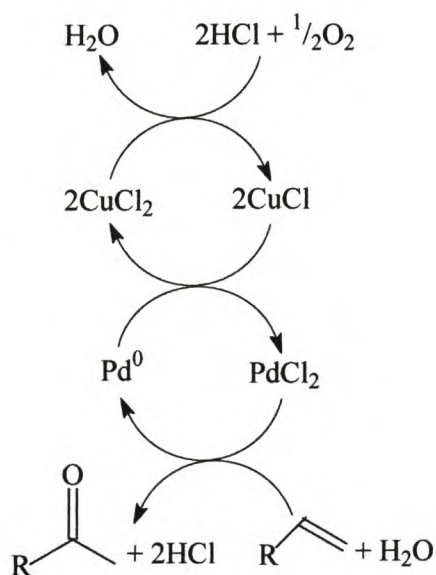
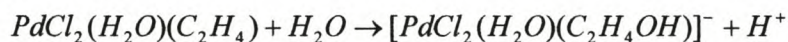
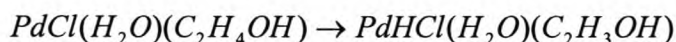


Figure 9.1. Reaction scheme for the Wacker-type oxidation of alkenes (Malleron *et al.*, 1997).

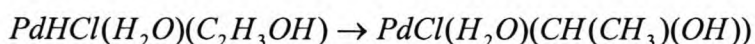
The first step of the Wacker process involves the attack of a hydroxyl anion on an olefin coordinated to the Pd(II) complex, which produces a hydroxyethyl group:



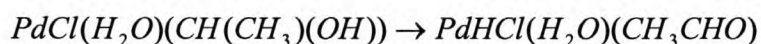
In the second step of the Wacker process, a chloride ligand is removed. This is followed by the elimination of a β -hydrogen to form a π -co-ordinated vinyl alcohol:



The insertion of a vinyl alcohol ligand leads to the formation of another hydroxyl group, as in the first step:

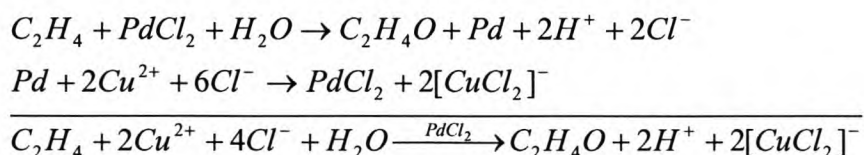


OH bond cleavage of the hydroxyl group leads to a Pd-acetaldehyde complex:



Acetaldehyde is then obtained by ligand dissociation or exchange (Siegbahn, 1995).

The palladium metal is continuously re-oxidised by cupric chloride during the olefin oxidation process (Smidt et al., 1962):



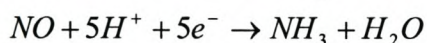
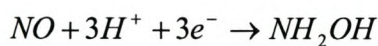
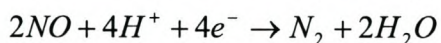
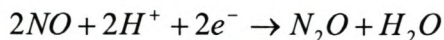
Palladium was found to be the most suitable catalyst of noble metals, such as Pd-black, Pt-black, Ru, Rh, Os and Ir (fine powder), for the Wacker-type oxidation of ethylene to acetaldehyde (Otsuka et al., 1991 and Otsuka 1997(a)).

9.1.2. Selective hydrogenation of nitric oxide

Hydroxylamine is an important intermediate for the production of ϵ -caprolactam, which is the monomer for Nylon 6. The catalytic halogenation of nitric oxide or nitric acid in sulphuric acid with platinum-based catalysts produces hydroxylamine. The design of a catalyst system for the synthesis of hydroxylamine requires (1) electrocatalyst for the reduction of NO in NH_2OH , (2) electrocatalyst for the oxidation of H_2 to $2H^+$ and $2e^-$, (3) proton conductor and (4) electron conductor (Otsuka, 1997(a)). Otsuka (1997(a)) selected Pt black as the catalytic component at the anode for the activation of H_2 into H^+ and $2e^-$, aqueous H_2SO_4 as a proton conductor and a gold lead wire as an electron conductor. Otsuka (1997(a)) showed that Fe-

phthalocyanine (Fe-Pc) had a high selectivity for NH_2OH . The electrochemical reactions at the anode and the cathode for the reduction of nitric oxide can be represented as follows (Otsuka, 1997(a)):

Cathode :



Anode :



9.1.3. Partial oxidation of light alkanes

The one-step partial oxidation of light alkanes to their alcohols and aldehydes, with O_2 as the oxidant, is the most attractive and difficult target in the field of selective oxidation catalysis (Zhang et al., 1997). Zhang et al. (1997) showed that the partial oxidation of light alkanes (methane, ethane and propane) can be achieved by applying an O_2 - H_2 cell at ambient temperature and atmospheric pressure (Fig. 9.2).

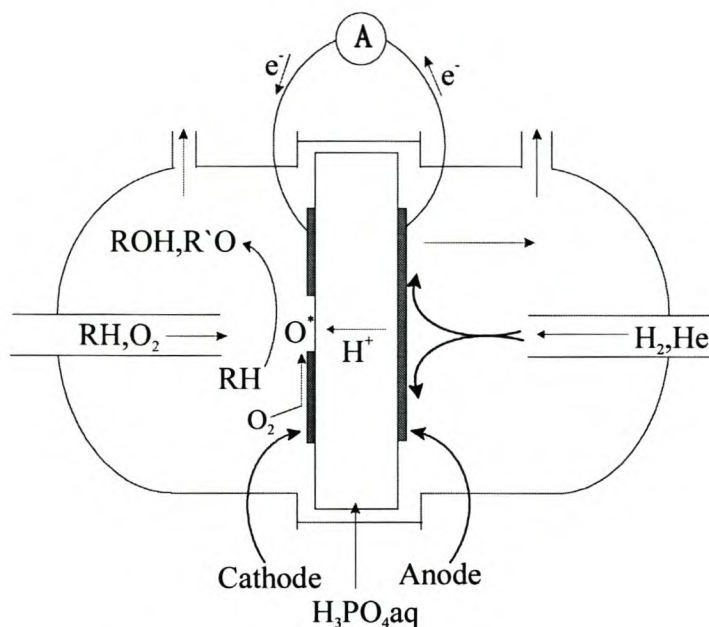
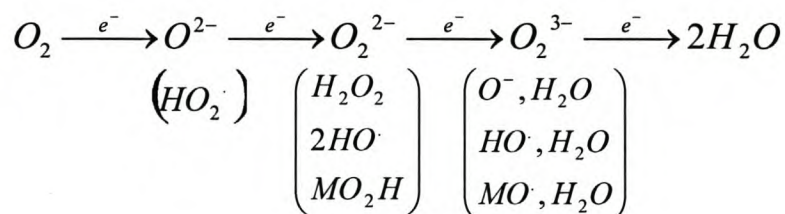


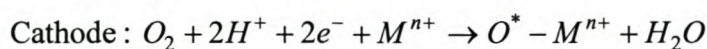
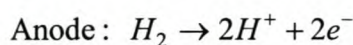
Figure 9.2. Schematic representation of a cell used for the oxidation of light alkanes in the gas phase

Zhang et al. (1997) and Otsuka et al. (1998) suggested that reductively activated oxygen (O^*) on the cathode were responsible for the oxygenation of light alkanes, benzene and hexane. The reduction of O_2 at the cathode can be schematically represented as follows (Zhang et al., 1997 and Otsuka et al., 1998):



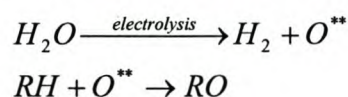
If the reduced oxygen intermediates, including those protonated (in parentheses), have a finite lifetime in the presence of a suitable catalyst (M), these reduced oxygen species can possibly attack the hydrocarbons in the cathode compartment. This will result in the oxygenation of alkanes during the O_2 - H_2 cell reactions (Zhang et al., 1997).

The stoichiometric anode and cathode reactions for the oxygenation of alkanes with an acid electrolyte for the reductive activation of O_2 in a H_2 - O_2 fuel cell can be represented as follows (Zhang et al., 1997):



where, M^{n+} represents the active sites on the cathode.

In contrast to the reductive activation of O_2 during the O_2 - H_2 cell reaction, the reverse reaction (electrolysis of acidic water) can activate the oxygen at the anode as follows (Otsuka, 1997(b)):



The oxidatively activated oxygen can also activate hydrocarbons to produce oxygenated products under mild reaction conditions (Otsuka, 1997(b)).

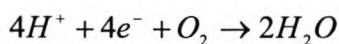
9.1.4. Partial oxidation of olefins

The partial oxidation of ethylene with a fuel cell system produces acetaldehyde in the gas phase. Otsuka et al. (1990) showed that palladium is a unique cathode material capable of catalysing the selective formation of acetaldehyde. The reactions at the anode and cathode for the oxidation of ethylene can be represented as follows (Otsuka et al., 1990):

Anode



Cathode



This single step synthesis of acetaldehyde in the aqueous solution has many advantages compared with the Wacker process, namely (Otsuka et al., 1990):

- The reactants, products and catalysts can easily be separated as the reactions take place in the gas phase,
- Corrosions of reactors can be avoided as no corrosive aqueous solutions such as, $PdCl_2$, $CuCl_2$ and HCl are needed,

- The reactants, ethylene and oxygen, are separated by a silica wool diaphragm filled with H_3PO_4 (aq), which reduces the danger of an explosion and,
- The fuel cell system co-generates electricity and acetaldehyde.

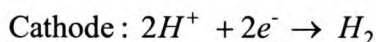
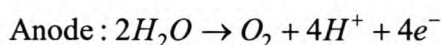
The optimum conditions for the synthesis of acetaldehyde are (Otsuka et al., 1990):

- an anode electrode with Pd black and a cathode with Pt black are most effective for the synthesis of acetaldehyde,
- the increase in pressure of oxygen at the cathode will result in the increase in the synthesis of acetaldehyde (optimum pressure of acetaldehyde at the anode is 30kPa) and,
- the optimum reaction temperature is 373K.

Another example of the oxidation of alkenes is the oxidation of propylene to produce acrolein, acetone and acrylic acid, an π -allyl type oxidation product. The oxidation of propylene was achieved applying the same fuel cell system as used for the oxidation of ethylene (Otsuka et al., 1990).

9.1.5. Epoxidation of olefins during water electrolysis

Epoxides are important for their use as synthetic intermediates. However, all commercial syntheses of epoxides are either indirect or multi-step co-ordinations, except for the synthesis of ethylene oxide (Otsuka et al., 1994). Otsuka et al. (1995) proposed a method for the synthesis of propylene oxide with nascent oxygen, which is produced during the electrolysis of water (Fig. 9.3). The most active and selective anode electrocatalyst amongst the noble metals for the synthesis of epoxides was Pt-black (Otsuka et al., 1995). The electrolysis of water with an acid electrolyte produces oxygen at the anode and hydrogen at the cathode, as represented by the following electrochemical reactions (Otsuka et al., 1995):



Otsuka et al. (1995) suggest that the hydrogen-stripped atomic oxygen atoms (O^*), generated on the platinum black anode, epoxidises propylene to form propylene oxide, with a relatively high selectivity and current efficiency (Otsuka et al., 1995).

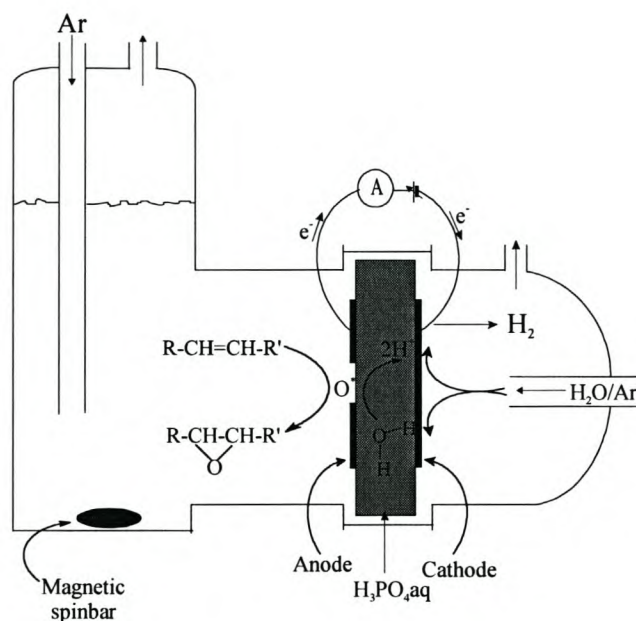


Figure 9.3. Schematic diagram of a reactor for the epoxidation of olefins during water electrolysis

Potential measurements were performed with the instrumental arrangement represented in Figure 9.4 (Otsuka et al., 1995). The formation of propylene oxide and acetone were enhanced at an applied voltage greater than 1.1V (Otsuka et al., 1995). The oxidation occurred at a voltage lower than 1.23 V (the thermodynamically required voltage for the electrolysis of water). The epoxidation of olefins at an applied voltage greater than 1.5V enhanced the formation of by-products ($CO_2 > \text{acetic acid} \geq \text{propionic acid}$).

Otsuka et al. (1995) was able to epoxidise 1-hexene, cis- and trans-2-hexenes to form propylene oxide. However, the oxidation of cyclohexane and benzene using the same method was slow. Otsuka et al. (1995) suggests that this is due to the active oxygen generated in this catalytic system being specific for the epoxidation of olefins.

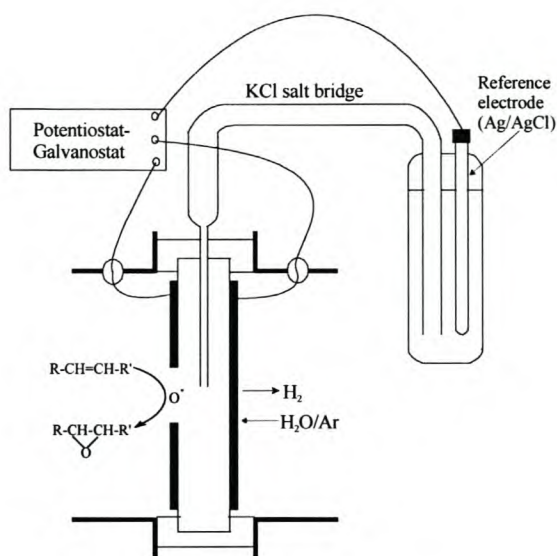


Figure 9.4. Schematic representation of the instrument used for potential measurements (Otsuka et al., 1995)

9.2. Further application of electrocatalytic membrane systems

This study has focussed particularly on the optimisation and characterisation of electrocatalytic membranes. Future work should investigate the catalytic response of modified membranes (EDA and surfactant) with embedded platinum catalyst in various applications, such as water electrolysis.

This study showed that membrane modification affects the morphology, surface roughness and surface area of a platinum catalyst on a membrane. Further research should focus on whether the changes in the platinum particle shape, size, distribution, as well as the roughness of a platinum catalyst, contributes positively to the catalytic response of the electrocatalytic membrane system in applications, such as water electrolysis.

Another interesting area of research would be to compare the surface roughness profile, surface area and morphology of electrocatalytic membrane systems, which result in favourable and unfavourable catalytic responses. This information, together with surface roughness analysis (using the Hurst exponent), is able to provide valuable information on surface roughness profiles of electrocatalytic membrane systems that will contribute to increased catalytic responses.

9.3. Binary catalyst systems

Research has shown that platinum-containing membranes modified by the addition of a second or third metal, such as tin, results in improved electrocatalytic activity in the electrooxidation of ethanol and methanol (Aramata et al., 1988 and Delime et al., 1999). Further research should investigate the feasibility of binary catalyst systems pertaining to their catalytic response in electrocatalytic membrane systems. An advantage of using binary catalyst systems is that the cost of preparing electrocatalytic membrane systems will be reduced. However, a cost-effective electrocatalytic membrane system at the expense of catalytic response is of no avail. Therefore, it would be of interest to investigate binary catalyst systems to ascertain whether their catalytic response in applications, such as water electrolysis, can contribute to a cost effective, as well as an improved electrocatalytic membrane system.

9.4. Conclusions

Current research has demonstrated the endless possibilities of electrocatalytic processes that exist when using electrocatalytic membrane systems. Some of these electrocatalytic processes, with the emphasis on immobilised phosphoric liquid membranes, have been reviewed in this chapter. However, the extension of these electrocatalytic processes to electrocatalytic SPE membrane systems can contribute to greater opportunities in the area of electrocatalysis. This is because of the many advantages offered by SPE membrane systems, such as: significantly elevated operation temperatures and pressures, as well as mechanical stability.

The feasibility of binary catalyst systems is an important consideration due to these catalyst systems being cost effective. Also, the catalytic response of the electrocatalytic membrane system consisting of platinum particles of unique morphology as a result of membrane modification, is an interesting avenue to explore.

Many opportunities exist within the area of research of electrocatalytic SPE membranes, such as novel methods of preparing electrocatalytic membrane systems, improving the catalytic response of electrocatalytic membrane systems and the feasibility of textured platinum catalyst particles in electrocatalysis processes.

References

1. Aramata A, Kodera T and Masuda M, 1988, Electrooxidation of methanol on platinum bonded to the solid polymer electrolyte, Nafion, *Journal of Applied Electrochemistry*, 18, 577-582
2. Delime F, Leger JM and Lamy C, 1999, Enhancement of the electrooxidation of methanol on Pt-PEM electrode modified by tin. Part I: Half cell study, *Journal of Applied Electrochemistry*, 29, 11, 1249-1254
3. Malleron J.-L, Fiaud J.-C and Legros J.-Y, 1997, *Handbook of palladium-catalyzed organic reactions: Synthetic aspects and catalytic cycles*, Academic Press, California
4. Otsuka K and Kobayashi A, 1991, Design of the Catalyst for Partial Oxidation of Ethylene by Applying an Electrochemical Device, *Chemistry Letters*, 1197-1200
5. Otsuka K, 1997(a), Design of Catalysts based on the Electrochemical Microcell Models, *Catalysis Surveys for Japan*, 195-203
6. Otsuka K, 1997(b), Reductive and Oxidative Activation of Oxygen for Selective Oxygenation of Hydrocarbons, 3rd World Congress on Oxidation Catalysis, 93-102
7. Otsuka K, Shimizu Y and Yamanaka I, 1990, Selective Synthesis of Acetaldehyde Applying a Fuel Cell System in the Gas Phase, *Journal of Electrochemical Society*, 137, 7, 2076-2081
8. Otsuka K, Ushiyama, Yamanaka I and Ebitani K, 1995, Electrocatalytic synthesis of propylene oxide during water electrolysis, *Journal of Catalysis*, 157, 450-460
9. Otsuka K, Yamanaka I and Hagiwara M, 1994, Simultaneous Epoxidation of 1-Hexene and Hydroxylation of Benzene during Electrolysis of Water, *Chemistry Letters*, 1861-1864
10. Otsuka K, Yamanaka I and Wang Y, 1998, Reductive Activation of Oxygen for Partial Oxidation of Light Alkanes, *Natural Gas Conversion V: Studies in Surface Science and Catalysis*, 119, 15-24
11. Siegbahn PEM, 1995, A Theoretical Study of Some Steps in the Wacker Process, *Structural Chemistry*, 6, 4/5, 271-279
12. Smitd J, Hafner W, Jira R, Sieber R, Sedlmeier J and Sabel A, 1962, The Oxidation of Olefins with Palladium Chloride Catalysts, *Angewandte Chemie Intl., Edn Engl.*, 1, 2, 80-88

13. Zhang Q and Otsuka K, 1997, Partial Oxidation of Light Alkanes during O₂-H₂ Cell Reactions at Room Temperature, *Chemistry Letters*, 363-364

Conclusions

Detailed discussions and conclusions are included after each chapter. This section will summarise the current study of microheterogeneous SPE membranes for electrocatalysis, as well as emphasise some of the important conclusions.

1. Preparation of platinum-containing perfluorinated cation-exchange membranes, with varying characteristics of the platinum catalyst

Platinum deposition on cation-exchange membranes and modified cation-exchange membranes was successfully achieved by the Takenaka-Torikai method. This method involves the deposition of a thin metallic layer of platinum on a membrane by the autocatalytic reduction of $[\text{PtCl}_6]^{2-}$ complex anions with a reducing agent such as, hydrazine or sodium borohydride. Flat-sheet cation-exchange membranes were platinised under various deposition conditions. These included: type of reducing agent used, total time of platinisation, temperature of reducing agent, concentration of platinumic acid solution and external activation of the platinumic acid solution during the deposition process.

The thickness of the platinum catalyst on a membrane, as well as the platinum catalyst loading, increased with an increase in the time of platinisation, temperature of the reducing agent and concentration of platinumic acid solution.

The use of hydrazine as a reducing agent in the deposition process resulted in greater platinum loading on a membrane as compared with using sodium borohydride. However, the use of sodium borohydride as a reducing agent resulted in the formation of platinum particles that were smaller in size. The sonication of platinumic acid solution during the deposition process also resulted in platinum particles that were small in size.

It was shown that the morphology of a platinum catalyst on a membrane can be controlled through varying the conditions of the electroless deposition process.

2. Characterisation of cation-exchange membranes and platinum catalyst

Microscopy characterisation techniques, such as Scanning Electron Microscopy (SEM) and Atomic Force Microscopy (AFM), were used for the morphological characterisation of the platinum catalyst on membranes. SEM showed that the

platinum catalyst layer occurred predominantly on the surface of a membrane. A platinum layer of greater thickness was achieved when using hydrazine as compared to sodium borohydride. The platinum catalyst layer consisted of platinum particles that were flaky, spherical or semi-spherical in shape.

Infrared spectrometry (IR), Brunauer Emmett Teller adsorption (BET) and dielectric analysis (DEA) were used to analyse the physical and chemical characteristics of membranes, as well as platinum-containing membranes. The SO_3^- oscillations that are characteristic for hydrolysed membranes were observed in IR spectra. Membranes modified with ethylene diamine (EDA) exhibited absorption bands that are characteristic of aminium ion (NH_3^+) groups. Membranes modified with cetyltrimethylammonium bromide surfactant exhibited absorption bands that are characteristic of nitrogen-methyl interaction. DEA analysis showed that the ion and dipole mobility of EDA-modified membranes decreases as the time of membrane treatment with EDA increases.

Electrochemical techniques, cyclic voltammetry and galvanostatic measurements, confirmed the anodic oxidation of water. A new method was developed for characterising membranes within a membrane cell by cyclic voltammetry. The method involves using a strip of Nafion as an ion conductor. Galvanodynamic measurements of EDA-modified membranes showed that the switching conductivity phenomenon in these modified membranes occur.

The various techniques of characterising platinum-containing membranes provided valuable information on the morphological, physical, chemical and electrochemical characteristics.

3. Surface modification of cation-exchange perfluorinated membranes

Chemical modification of cation-exchange membranes was achieved with ethylene diamine (EDA). The formation of an anion-exchange layer can be attributed to the zwitterion nature of the modified layer of the membrane. In membranes modified with EDA, platinum particles were observed deep within the bulk of the membrane. Since the anion-exchange layer offers less resistance to $[\text{PtCl}_6]^{2-}$ ions, easy penetration of these ions into the membrane occurs. The electrical resistance of membranes increases with the increase in treatment with EDA. This is due to the increase in resistance of the anion-exchange layer to cations such as, Na^+ and H^+ .

The modification of membranes with cetyltrimethylammonium bromide surfactant resulted in the synthesis of textured platinum catalysts. The platinum particles were pyramidal in shape and protruded outwards from the membrane surface. Modification of membranes with surfactant results in an increase in electrical resistance. The conductivity of the membrane was restored by the removal of surfactant from the membrane by a process of ion exchange.

A new method for controlling the structure, size and distribution of platinum particles deposited on a modified membrane was demonstrated.

4. Development of a protocol for the quantitative determination of the platinum loading on a cation-exchange membrane by UV spectrophotometry

An experimental protocol was developed for the quantitative determination of platinum loading on a membrane by UV spectrophotometric analysis. It included the use of colorimetric analysis with UV spectrophotometry for the quantitative determination of the platinum loading on membranes.

5. Quantification of membrane surface roughness obtained by means of AFM measurements

The Hurst exponent of platinum-containing membranes was determined using power spectrum, variogram and wavelet analyses. The fractal dimension (FD) and the average roughness (R_a) of platinum-containing membranes were also determined. The average roughness was determined to be greater when using sodium borohydride as the reducing agent during the deposition process. Percentage deviation was calculated for power spectrum, wavelet and variogram analyses, which showed that wavelet analysis was most accurate for surface roughness quantification of platinum-containing membranes.

6. Anodic oxidation of water with platinum-containing membranes

The anodic oxidation of water was successfully achieved with platinum-containing membranes. The anodic oxidation of water was investigated by electrochemical methods of galvanostatic and cyclic voltammetric measurements. The increase in temperature results in a decrease in cell potential, which can be attributed to the increase in the anodic oxidation of water.

A new experimental set-up was developed for the characterisation of the anodic oxidation of water by cyclic voltammetry. This experimental set-up involved the spatial separation of the reference electrode from the working electrode by a strip of Nafion.

List of publications

1. Bessarabov DG, Michaels W and Vermeulen JP, 1999, *Electroless deposition of platinum on proton conductive perfluorinated membranes modified with ethylene diamine*, International Journal of Ionics, No's 1&2, 5, 52-58
2. Bessarabov DG, Michaels W, Sanderson RD, 2000, *Preparation and characterization of chemically-modified perfluorinated cation-exchange platinum containing membranes*, Journal of Membrane Science, 179, 221-229
3. Bessarabov DG, Michaels WC and Popkov YM, 2001, *Galvanodynamic study of the electrochemical switching effect in perfluorinated cation-exchange membranes modified by ethylenediamine*, Journal of Membrane Science, 194, 1, 81-90
4. Bessarabov DG and Michaels WC, 2001, *Solid polyelectrolyte (SPE) membranes containing textured platinum catalyst*, Journal of Membrane Science, 194,1, 141-144
5. Bessarabov DG and Michaels WC, 2001, *Morphological diversity of Pt clusters deposited onto proton-exchange perfluorinated membranes for catalytic applications*, Membrane Technology, 139, 5-9

List of communications

1. Michaels WC and Sanderson RD, Bessarabov DG, Morphological diversity of Pt-based catalyst deposited on cation-exchange perfluorinated membranes (poster presentation), In: Book of Abstracts of 4th Annual UNESCO School and IUPAC Conference on Macromolecules and Materials Science, 7-11 April, Stellenbosch, South Africa, 2001
2. Michaels WC and Bessarabov DG, Electroless deposition of Pt-based catalysts on perfluorinated cation-exchange membranes (poster presentation), In: Symposium Proceedings, 4th WISA-MTD Symposium, Fleurbaix, Stellenbosch, RSA, 26-27 March, 2001, pp 89-92
3. Michaels W, Vermeulen J, Sanderson RD and Bessarabov DG, Platinum deposition of chemically modified perfluorinated cation-exchange membranes (poster presentation), In: Book of Abstracts of 3rd Annual UNESCO School & IUPAC Conference on Macromolecules & Materials Science, 10-12 April 2000, UNESCO School & IUPAC Conference, Stellenbosch, South Africa
4. Bessarabov DG, Sanderson RD, Michaels W, Vermeulen JP, Marais S, Popkov YM, Preparation and characterisation of membranes for electrochemically promoted catalysis and separations (poster presentation), In: Book of Abstracts of the III International Conference on Catalysis in Membrane reactors, P29, Copenhagen, Denmark, September, 1998
5. Bessarabov DG, Michaels W, Popkov YM, Timashev SF, Platinum deposition on chemically modified perfluorinated cation-exchange membranes for electroinduced catalysis and separations (poster presentation), In: Book of Abstracts, 4th International Conference on Catalysis in Membrane Reactors (ICCMR-2000), July 3-5, 2000, Zaragoza, Spain, p 109

6. Bessarabov DG, Michaels W, Popkov YM, Electrochemical switching process in perfluorinated proton-exchange membranes modified by ethylenediamine: effect of embedded platinum catalyst, In: Proceedings of 12th Annual Meeting of North American Membrane Society (NAMS2001), Lexington, Kentucky, USA, pp. 67, 2001
7. Bessarabov DG, Michaels W, Morphological diversity of Pt clusters deposited onto proton-exchange perfluorinated membranes for catalytic applications, In: Proceedings of 12th Annual Meeting of North American Membrane Society (NAMS2001), Lexington, Kentucky, USA, pp. 30, 2001
8. Bessarabov DG, Michaels W, Marais S, Sanderson RD, Prozesky V, Characterisation of Pt-containing proton-exchange membranes by nuclear microprobe (poster presentation), In: Book of Abstracts of the 6th International Conference on Nuclear Microprobe Technology and Applications (ICNMTA'98), P2.3, October, 1998, Stellenbosch, South Africa
9. Bessarabov DG, Michaels W, Marais S, Sanderson RD, Preparation and characterisation of solid polyelectrolyte (SPE) membranes containing nano-phase platinum for electroinduced separations and catalysis (poster presentation), In: Book of Abstracts "The Science of Minerals", 7-8 May, Muldersdrift, Johannesburg, 1998
10. Bessarabov DG, Michaels W, Marais S, Sanderson RD, Preparation and characterisation of Pt-containing solid polyelectrolyte (SPE) membranes for electroinduced separations and catalysis (poster presentation), In: Book of Abstracts of the 7-th International Chemistry Conference in Africa and 34-th Convention of the South African Chemical Institute, P85, 6-10 July, 1998, University of Natal, Durban, RSA
11. Bessarabov DG, Michaels W, Marais S, Sanderson RD, Popkov YM, Timashev SF, Preparation and characterisation of Pt-containing proton-conductive membranes for electrochemically promoted catalysis and separations, In: Book of

Abstracts of the 5th Euroconference on Solid State Ionics, p.15, Andalusia, Spain, September, 1998

12. Bessarabov DG, Michaels W, Marais S, Sanderson RD, Popkov YM, Preparation and characterisation of composite metal-containing ion-exchange membranes for electroinduced catalyses and separations (poster presentation), In: Preprints of ICMST'98, June 9-13, Beijing, China, 1998, 214-215
13. Bessarabov DG, Michaels W, Marais S, Sanderson RD, Popkov YM, Preparation and characterisation of Pt-containing ion-exchange membranes for electroinduced separations and catalysis (poster presentation), In: Proceedings of NAMS'98, Cleveland, USA, 1998, 119